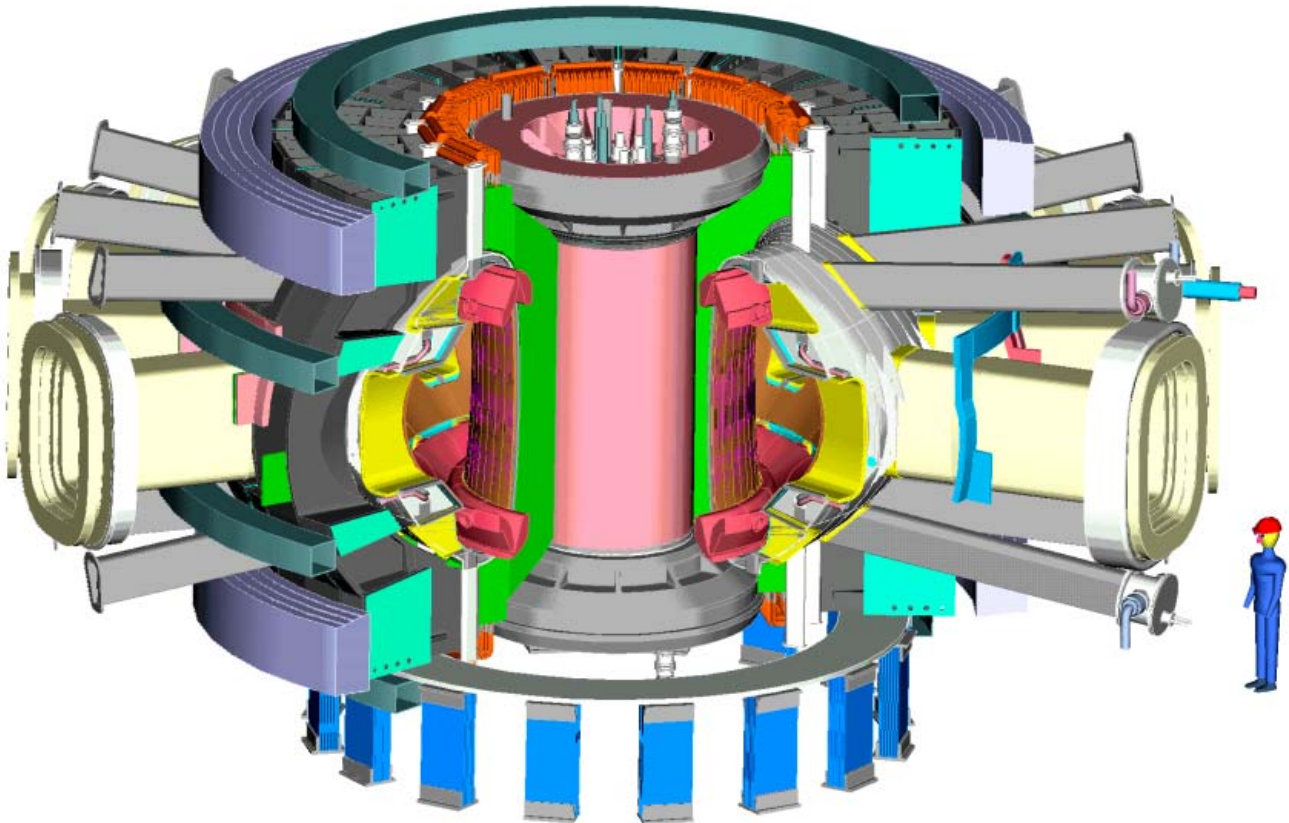


# **Fusion Ignition Research Experiment** **-FIRE-**

## Engineering Status Report For Fiscal Year 2001

Issued January 2002



### **Contributors:**

T. Brown, R. Ellis, H.M. Fan, P. Heitzenroeder, C. Kessel, D. Meade, C. Neumeyer;  
J. Schmidt, R. Woolley, K. Young, I. Zatz (**PPPL**)  
J. Schultz, R. Thome, P. Titus (**MIT**)  
T. Burgess, B. Nelson, D. Swain, M. Gouge, G. Johnson (**ORNL**)  
R. Bulmer (**LLNL**); M. Ulrickson (**SNL**)  
H. Khater, M. Sawan (**UW**); D. Petti, B. Merrill, L. Cadwallader (**INEL**);  
D. Dilling (**Consultant**); D. Driemeyer, F. Cole, L. Waganer (**Boeing**)  
C. Baxi, J. Wesley (**GAT**); V. Christina, E. Peterson, F. Tepes, A. Berger, J. Rathke (**AES**)

**FIRE FY 01 Engineering Report Update  
Table of Contents**

- 1.0 Introduction**
- 2.0 Physics Objectives and Guidelines**
- 3.0 General Design Requirements and Plans for FY 02**
- 4.0 Design Configuration / Integration**
- 5.0 Engineering Systems**
  - 5.1 TF Coils and Structures**
  - 5.2 Central Solenoid and PF coils**
  - 5.3 Vacuum Vessel**
  - 5.4 Plasma Facing Components**
  - 5.5 Thermal Shield**
  - 5.6 Ion Cyclotron Heating**
  - 5.7 Plasma Fueling and Pumping**
  - 5.8 Tritium System**
  - 5.9 Neutronics and Shielding**
  - 5.10 Decay Heat and Radiation Exposure**
  - 5.11 Remote Maintenance**
  - 5.12 Magnet Power Supplies**
  - 5.13 Cryoplant**
  - 5.14 Facilities and Siting**
  - 5.15 Safety**
  - 5.16 Diagnostics**
- 6.0 Evaluation of the FY 01 Design**
- 7.0 Peer Review**
- 8.0 Research and Development (R&D)**

## 1.0 Introduction

The Next Step Options (NSO) study is underway to consider the next steps that might be undertaken in a restructured U. S. Fusion Energy Sciences Program. The findings of this study are periodically provided to the Fusion Energy Science Advisory Committee (FESAC) which advises the DOE Secretary of Energy on fusion research strategy. The NSO study has two major goals:

***(1) Development of research goals and a strategy for burning plasmas in the restructured fusion sciences program.*** An international multi-machine program strategy is evolving which comprises a series of experimental projects that could lead to the development of fusion energy in an environment of limited energy research funding.

***(2) Development of a minimum cost burning plasma research device.***

A compact high field copper coil tokamak has the best prospect for achieving fusion-dominated plasmas at minimum cost. The design concept presently being evaluated is FIRE (Fusion Ignition Research Experiment).

The possibility of constructing a next step experiment in magnetic fusion will depend critically on its cost. Since the U. S. DOE has constructed ~\$1B class facilities such as the Spallation Neutron Source (SNS), Advanced Photon Source (APS) and the National Ignition Facility (NIF), the construction cost target for NSO has been set at ~\$1B.

The NSO study has been organized as an integrated physics/engineering design activity within the Virtual Laboratory for Technology (VLT). A set of preliminary goals and associated requirements were established as a first step in the development of an optimized Burning Plasma Strategy. A burning plasma experiment is one element of a "multi-machine" strategy to accomplish many

of the ITER objectives using separate lower cost facilities. These facilities would focus on physics issues such as: (1) burning plasma physics, (2) long pulse advanced toroidal physics and (3) fusion technology. This strategy reduces the technical risk and would require much smaller cost outlays compared to a single large integrated facility.

The NSO study process involves national and international activities. An NSO Program Advisory Committee (PAC) has been set up to guide the design work on FIRE. The NSO PAC has 15 members from the U. S. and international tokamak community, and reports to the Director of the VLT. An external peer review of the major FIRE engineering systems was undertaken in June 2001. A proactive outreach program was initiated to involve the fusion community and the broader scientific community in determining the mission and direction for FIRE. Technical papers have been presented at all the major fusion conferences. Over 25 presentations have been made over the past year and discussion sessions have been held, including discussions at major international fusion laboratories. The FIRE web site (<http://fire.pppl.gov>) has archived the technical work on FIRE and also serves as a repository of current information on fusion research.

The NSO study has only been underway since the beginning of FY 99 and much work is yet to be done, however, the results are very encouraging. They indicate that a compact burning plasma device can be developed which is responsive to cost issues and could be a practical and important next step in a revitalized modular fusion sciences research program.

## 2.0 Physics Objectives and Guidelines for a Next Step Tokamak Burning Plasma Experiment

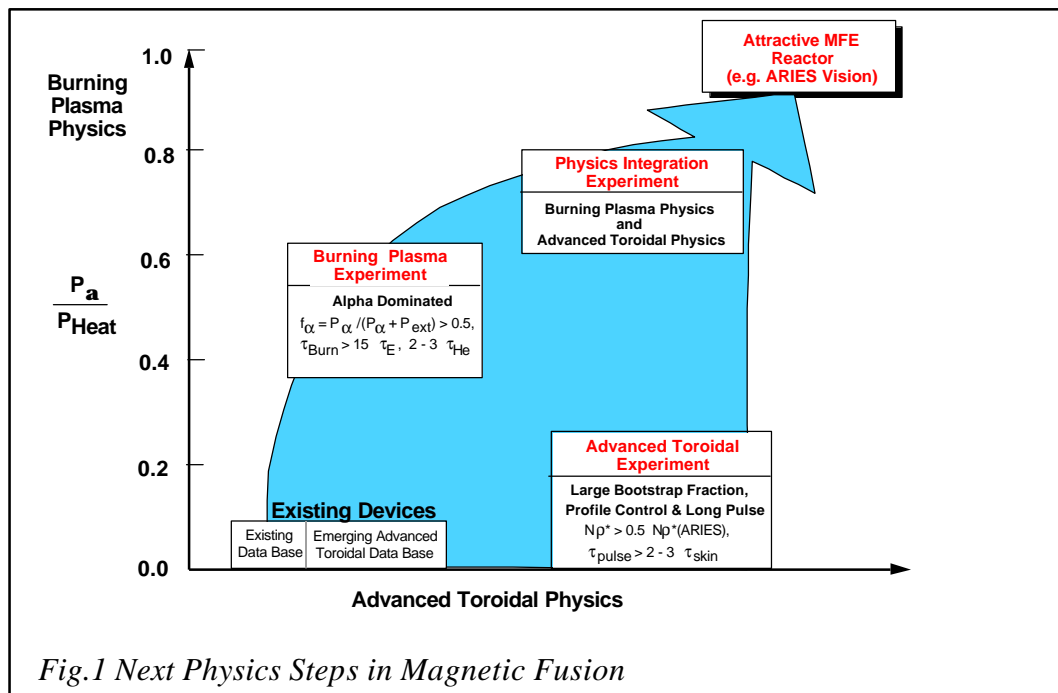
Burning plasma physics is widely accepted as the primary objective for a major next step in magnetic fusion research. The Grunder Panel of FESAC and the Madison Forum endorsed burning plasmas as the next step. The 1999 Snowmass Summer Study endorsed burning plasmas with the Burning Plasma Working Group, the Energy Working Group B and the Magnetic Fusion evening session, all overwhelmingly supporting the burning plasma objective and that the tokamak was technically ready for a high gain burning plasma experiment. The 1999 Secretary of Energy Advisory Board (SEAB) review of fusion noted that "There is general agreement that the next large machine should, at least, be one that allows the scientific exploration of burning plasmas". If Japan and Europe do not proceed with ITER, "the U.S. should pursue a less ambitious machine that will allow the exploration of the relevant science at lower cost." "In any event the preliminary planning for such a

device should proceed now so as to allow the prompt pursuit of this option."

Our present understanding of plasma transport, macroscopic stability, wave particle interactions and boundary physics while improving through experiments on existing facilities will always be incomplete until tested and understood in a "real" fusion plasma.

During summer of 2001, FESAC made several strong recommendations regarding the U.S. Burning Plasma program including:

- *NOW is the time for the U.S. Fusion Energy Sciences Program to take the steps leading to the expeditious construction of a burning plasma experiment.*
- *The U.S. Fusion Energy Sciences Program should establish a proactive U.S. plan on burning plasma experiments and should not assume a default position of waiting to see what the international community may or may not do regarding the construction of a burning plasma experiment. If the opportunity for international*



*collaboration occurs, the U.S. should be ready to act and take advantage of it but should not be dependent upon it.*

The FESAC also recommended that a community workshop be held for the critical scientific and technological examination of proposed burning plasma experimental designs and to provide crucial community input and endorsement to the planning activities undertaken by FESAC. At this workshop, the community would also carry out a uniform technical assessment led by the NSO program of each of the burning plasma experimental options for input into the Snowmass summer study.

With the FESAC recommendations as background, the FIRE project after discussions with the NSO-PAC, adopted the following mission for FIRE:

**to attain, explore understand and optimize magnetically confined fusion-dominated plasmas.**

Understanding the properties of high gain fusion-dominated plasmas in an advanced toroidal configuration is a critical issue that must be addressed to provide the scientific foundation for an attractive magnetic fusion reactor. The functional fusion plasma objectives for major next physics steps in magnetic fusion research can be described as:

Burning Plasma Physics - The achievement and understanding of alpha-dominated plasmas that have characteristics similar to those expected in a fusion energy source, and

Advanced Toroidal Physics - The achievement and understanding of bootstrap-current-dominated plasmas with externally controlled profiles and other characteristics (e.g., confinement and  $\beta$ ) similar to those expected in an attractive fusion system.

These requirements lead naturally to a set of fusion physics Stepping Stones as illustrated in Fig. 1. The ranges of plasma performance and duration to address these issues are shown schematically with the natural time scales for important plasma processes.

A design study of a Fusion Ignition Research Experiment (FIRE) is underway to investigate near term opportunities for advancing the scientific understanding of self-heated fusion plasmas in advanced toroidal configurations. The emphasis is on understanding the behavior of plasmas dominated by alpha heating ( $Q \sim 10$ ) that are sustained sufficiently long compared to most characteristic plasma time scales ( $\sim 20 \tau_E$ ,  $\sim 4\tau_{He}$ ,  $\sim \tau_{skin}$ , where  $\tau_{He}$  is the helium ash confinement time at  $5\tau_E$ , and  $\tau_{skin}$  is the time for the plasma current profile to redistribute at fixed total current) to allow the evolution of alpha defined profiles. The programmatic mission of FIRE is to attain, explore, understand and optimize alpha-dominated plasmas to provide knowledge for the design of attractive magnetic fusion energy systems. The programmatic strategy is to access the alpha-dominated regimes with confidence using the present tokamak data base (e.g., Elmy-H-mode,  $\beta = 0.75$  Greenwald density) while maintaining the flexibility for accessing and exploring advanced tokamak modes at lower magnetic fields and fusion power for longer durations in later stages of the experimental program. A major goal is to develop a design concept that would meet these physics objectives with a tokamak (load assembly) construction cost of  $\sim \$350M$  and a total project cost in the range of  $\sim \$1 B$ .

FIRE Engineering Report  
FY01 Update

The activities have focused on the technical evaluation of a compact, high-field, highly-shaped tokamak with the parameters shown in Table I. The philosophy of FIRE is to challenge, and extend existing physics limits toward the regimes envisioned for a fusion reactor. Confinement projections are uncertain, and one of the major objectives of a next step experiment is to extend the experimental range beyond existing experiments and capability to test projections closer to reactor conditions. The physics issues and physics design guidelines for projecting burning plasma performance in FIRE are similar to those for ITER-FEAT. The operating regime for FIRE is well matched to the existing H-mode database and can access the density range from  $0.3 < n/n_{GW} < 1.0$  through a combination of pellet fueling and divertor pumping. This flexibility is important for investigating the onset of alpha-driven modes at the lower densities and to optimize the edge plasma for confinement studies and optimal divertor operation. The performance of FIRE was projected by selecting JET data with parameters similar to FIRE, namely  $\beta_N = 1.7$ ,  $Z_{eff} < 2.0$ ,  $\kappa > 1.7$  and  $2.7 < q_{95} < 3.5$ . The

average  $H(y, 2)$  and density profile peaking,  $n(0)/\langle n \rangle_V$  for these data was found to be 1.1 and 1.2, respectively. This is consistent with the analysis of JET H-mode data presented by Cordey et al [3]. A 0-D power balance code was used to calculate the Q-value in FIRE as a function of H-factor as shown in Fig. 2. The density profile was assumed to have  $n(0)/\langle n \rangle_V = 1.2$  (x points) or 1.5 (? points) with 3% Be and self-consistent alpha ash accumulation. On this basis, FIRE would be expected to achieve  $Q = 10$  for JET-like H-modes. Physics based models using marginal stability transport models such as GLF23 also predict Q values in the range  $\sim 10$ . These models dependent sensitively on the value of the temperature of the H-mode pedestal which is projected to be higher for plasmas with strong shaping (triangularity) and pedestal density low relative to the Greenwald density. A next step experiment, such as FIRE, would provide a strong test of these models and improve their capability for predicting reactor plasma performance.

A 1 1/2 -D Tokamak Simulation Code (TSC) simulation of this regime with  $H(y,2) = 1.1$  and  $n(0)/\langle n \rangle_V = 1.2$  indicates that FIRE can access the H-

Table I. Design Goals for FIRE

R (m), a (m)	2.14, 0.595
$\kappa_{95}, \delta_{95}$	$\sim 1.8, \sim 0.4$
$q_{95}$	$> 3$
$B_t(R_o)$ (T)	10
Wmag TF (GJ)	5
$I_p$ (MA)	7.7
flattop time (s)	$\sim 20$
alpha heating fraction	$> 0.5$
$\tau_E, \tau_{skin}$ (s)	$\sim 1, \sim 13$
$Z_{eff}$ (3% Be + He ( $5 \tau_E$ ))	1.4
Fusion Power (MW)	$\sim 150$
ICRF Power (MW)	20
Tokamak Cost (\$B)	$\sim 0.35$
Project Cost (\$B)	$\sim 1.2$

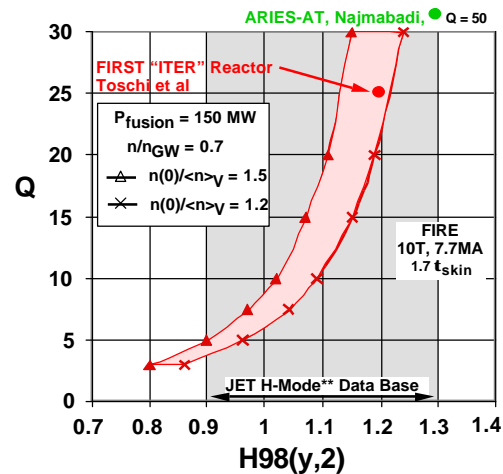


Fig. 2. Fusion Gain for FIRE

FIRE Engineering Report  
FY01 Update

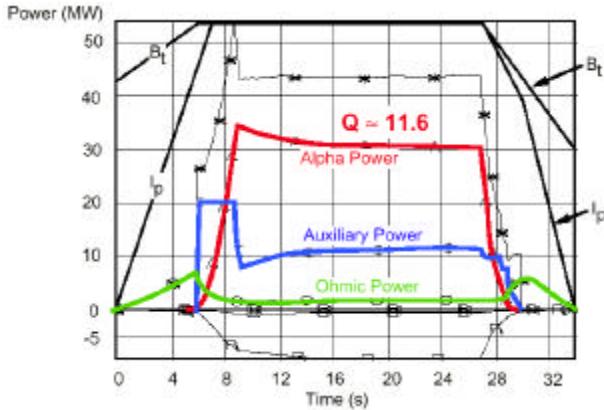


Fig. 3. Evolution of a fusion-dominated plasma.

Mode and sustain alpha-dominated plasmas for  $> 20 \tau_E$ ,  $> 4 \tau_{He}$  and  $\sim 1.5 \tau_{skin}$  as shown in Fig. 3. This example shows the importance of having sufficient magnetic field flattop for plasma startup ( $\sim 4$  s), helium ash evolution ( $\sim 4$  s) prior to achieving a steady burn for experimental studies. In addition, capability must be provided for controlled plasma shutdown without causing a disruption on every pulse. The primary methods of burn control will be to adjust the input power and the D-T fueling rate.

A longer term goal of FIRE is to explore advanced tokamak regimes using pellet injection and current ramps to create reversed shear plasmas (e.g., PEP modes), and then applying lower hybrid current drive to sustain the AT mode at high fusion gain ( $Q > 5$ ) for a duration of 1 to 3 current redistribution times. Simulations using TSC with self-consistent lower hybrid current drive modeling show that 100% non-inductively driven burning plasmas could be sustained at  $\beta_N \sim 3$ , 64% bootstrap current with  $Q \sim 7.5$ , fusion powers of 150 MW if confinement enhancements  $H(y,2) \sim 1.6$  were attained at  $B = 8.5T$  and  $I_p = 5.5$  MA. An important feature of the FIRE cryogenic

copper alloy magnets is that the pulse length increases rapidly as the field is reduced with flattops of  $\sim 40$  s at 8 T and  $\sim 90$  s at 6 T. The primary limitation to exploiting this long pulse capability is the generic problem of handling the plasma exhaust power under reactor relevant conditions.

The baseline magnetic fields and pulse lengths can be provided with BeCu /OFHC (Oxygen Free High Conductivity) copper toroidal field (TF) coils and OFHC poloidal field (PF) coils that are pre-cooled to 77 °K prior to the pulse and allowed to warm up to 373 °K at the end of the pulse. The cross-section of FIRE is shown schematically in Figure 4. The key “advanced tokamak” features are: strong plasma shaping, double null poloidal divertors, low TF ripple ( $\sim 0.34\%$  @ outer midplane), internal control coils and space for yet to

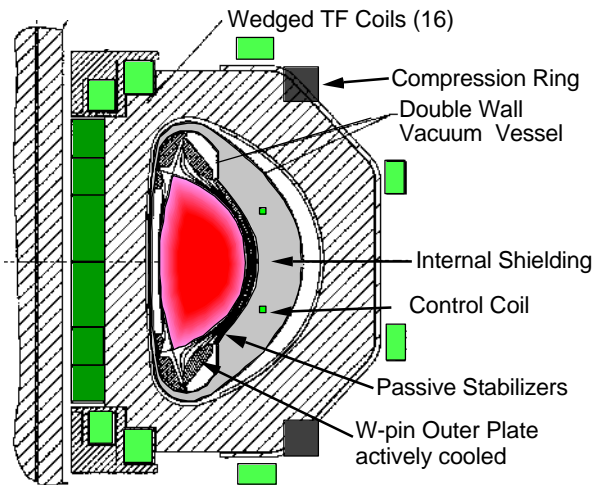


Fig. 4. Cross-section of FIRE

be determined wall stabilization capabilities. The 16 TF coil system is wedged with a compression ring to resist de-wedging at the top and bottom of the inner TF leg. Shielding is added between the walls of a double wall vacuum vessel to reduce nuclear heating of the coils, limit insulation dose and allow hands-on maintenance outside the envelope of the

## FIRE Engineering Report FY01 Update

TF coils within a few hours after a full power D-T shot. Large (1.3 m by 0.7 m) midplane ports provide access for remote manipulators and diagnostics, while 32 angled ports provide access to the divertor regions for utilities and diagnostics. FIRE is being designed mechanically to accommodate 3,000 full field, full power pulses and 30,000 pulses at 2/3 field. The repetition time at full field and full pulse length will be < 3 hr, with shorter times at reduced parameters. The fusion energy production of 5 TJ (similar to BPX) produces a lifetime neutron dose to the TF insulating material at the inboard midplane of  $\sim 1.5 \times 10^{10}$  Rads which is consistent with the polyimide insulation being considered.

The power densities on the divertor plates are  $\sim 5 \text{ MWm}^{-2}$  for detached operation and  $\sim 25 \text{ MWm}^{-2}$  for attached operation. The divertor plasma-facing components are tungsten “brush” targets mounted on copper backing plates, similar to a concept developed by the ITER R&D activity. The outer divertor plate is water-cooled, while the baffle and inner divertor targets are inertially cooled. The first wall is comprised of Be plasma-sprayed onto copper tiles which do not need active cooling for pulses < 15 s. The large neutron wall loading ( $3 \text{ MWm}^{-2}$ ) at fusion power of 200 MW contributes significantly to the first wall and vacuum vessel heating. Either a modest reduction in fusion power due to lower H-mode threshold assumptions, or improved cooling will be required for a 20 s pulse length. The plasma facing materials were chosen to reduce the tritium inventory in the first wall. Sixteen cryopumps – closely coupled to the divertor chambers, but behind sufficient neutron shielding – provide pumping ( $=100 \text{ Pa m}^3/\text{s}$ ) for D-T and He ash during the pulse. Pellet

injection scenarios using direct injection inside the magnetic axis and guided inside launch will be incorporated, and are expected to provide a modest increase in fusion reactivity due to density profile peaking while minimizing tritium consumption. The in-device tritium inventory will be determined primarily by the cycle time of the divertor cryopumps, and can range from < 2 g for regeneration overnight to  $\sim 20$  g for monthly regeneration.

The possibility of using only high conductivity (OFHC) copper in the TF coil in a bucked and wedged configuration was investigated. The limitation on burn time for both BeCu and OFHC designs is the power handling capability of plasma facing components and the vacuum vessel. The wedged design with BeCu was chosen as the baseline design mainly for its simplicity and robustness.

A number of important physics issues remaining to be addressed during the design phase, and then resolved during the experimental program. These include generic issues such as: mitigation and avoidance of disruptions and vertical displacement events, H-mode power threshold, effects of neoclassical tearing modes, detached divertor operation with good confinement, and divertor/edge plasma modeling under high power conditions.

FIRE, coupled with a non-burning steady-state superconducting advanced tokamak in an international multi-machine strategy, would address essentially all of the objectives identified for Next Physics Steps in Magnetic Fusion (Fig. 1).

FIRE Engineering Report  
FY01 Update

### 3.0 General Design Requirements

The basic set of machine parameters and features given in Table 3.0-1 were adopted by FIRE in late FY 2001 after an study of possible variations around the initial design point in the FY 2000 study, and discussion with the NS)-PAC. The table will ultimately serve as the basis of the formal General Design Requirements Document (GDRD) which will be completed prior to a Conceptual Design Review (CDR).

Table 3.0-1. Basic Parameters and Features of FIRE.

<u>Parameter</u>	<u>Value</u>
R, major radius, m	2.14
a, Minor radius, m	0.595
B <sub>t</sub> , Tesla	10
No. TF coils	16
Q	~10
Fusion power, MW	150
Max. TF ripple	0.3% (edge)
Pulse rep. Time, hr.	~3 at full power
TF and PF coil type	LN <sub>2</sub> cooled copper and BeCu
Plasma current	7.7 MA
Flat top, s	~ 20
Triangularity, $\delta_{95}$	~0.4
$\delta_x$	~0.7
Elongation, $\kappa_{95}$ ,	~1.8
$\kappa_x$	~2.0
Neutral beam Power	None planned
ICRF Power, (MW)	20
FWCD	None in baseline-possible later option.
LHCD	None in baseline-possible later option.
Vacuum level	10 <sup>-8</sup> torr
Bake out temp.	350? C
Life pulses at full field	3000 (min.)

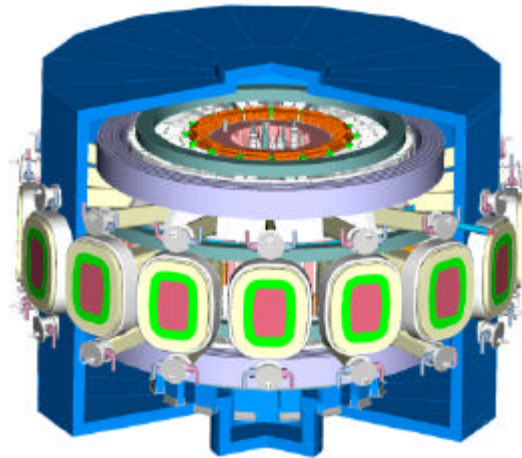
Coil initial temp.	80 °K
Coil max. temp.	373 °K
First wall materials	Beryllium
First wall replacement/maint. times	Single unit: 3wks; limiter: 6wks.; entire system 12 mos.
Total Fusion Energy	5 terajoules
Limiters	For start up
First wall life	Machine lifetime
VV pressure suppression system	No
FW heat flux	TBD
First wall cooling	Inertial
VV operating temp.	100 °C
Divertors	Double null; actively cooled outer W plate, inertially cooled elsewhere, possible upgrade to active cooling for longer pulses
In-vessel RH requirements.	Must be able to replace/repair all components
Ex-vessel RH requirements	Classification system & maintenance similar to ITER.
TF support arrangement	Wedged with compression rings

[1] ITER Physics Basis, Nucl. Fusion **39** (1999) 2208

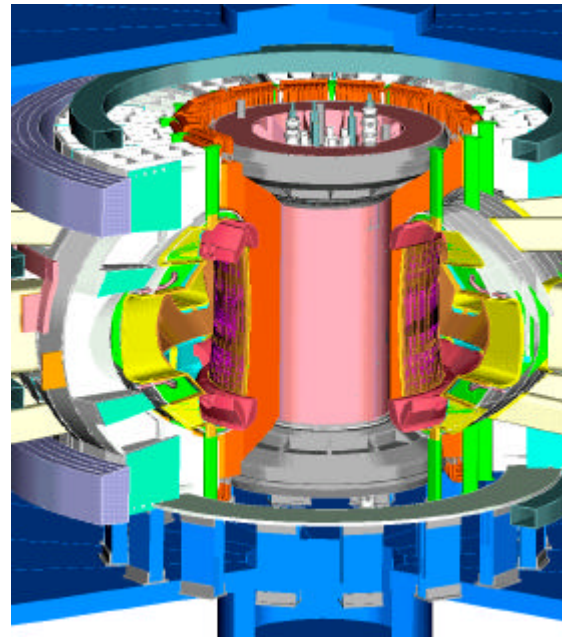
#### 4.0 Design Configuration/Integration

At the end of FY 01, the device has been altered in size (slightly), increasing the major radius to 2.14 m from its reference baseline dimension of 2.0 m. The general arrangement and details of the components are not expected to change, but there will be some subtle alterations to address the change in the radial build dimensions of a lower aspect ratio device. The reference 2.0 m device is shown in Fig. 4.0-1 (a) and (b). The main design features include:

- *High plasma triangularity ( $0.4 d_{95}$ ) is provided for improved performance.*
- *Double null gaseous divertors.* Gaseous divertors have been shown to be effective in radiating most of the power going to the divertor regions throughout the first wall rather than depositing it in a localized toroidal stripe in the divertor. They are also easier to engineer.
- *Divertor module maintenance through horizontal ports.* This enables the extraction of larger divertor components and fewer pieces.
- *A double walled vacuum vessel with integral shielding.* This design approach provides improved vessel structural stiffness and makes double use of the cooling jacket as nuclear shielding. Locating shielding between the walls reduces nuclear heating in the TF coils and the dose level external to the vessel. The reduced nuclear heating permits longer flat top times and higher current densities than would otherwise be possible. This "close in" shielding arrangement reduces the dose outside the vessel and



(a) Cross-Sectional View of FIRE Through Its Insulation Enclosure



(b) Cross Section View of the FIRE Tokamak

**Fig 4.0-1 Isometric Views of FIRE**

activation of nitrogen that is in the thermal shield.

- *Wedged TF coils aided by a pair of large compression rings to support torsional shear at the inner corners of the TF*

It is expected that some configurational benefits will be achieved in the increased machine size; somewhat wider ports, additional space for magnetic diagnostics and added (CS side) coolant of the TF inner leg. Also the integration of the pellet injection system into the base configuration will be developed, adding details to show injection from low and high field side of the plasma and from the top using different sets of guidetubes.

#### 4.1 Design Features

Figures 4.0 (a) and (b) illustrate the design features of the reference design. The major components and features are:

- 16 wedged TF coils, inertially LN<sub>2</sub> cooled with coil windings located in a partial coil case. High strength BeCu C17510 is used in the inner legs and OFHC copper in the remainder of the coil. Compression rings girdle the TF coils to suppress "dewedging" in the upper and lower inside corners of the coils.
- Two pairs of divertor coils (up-down symmetric). These coils are inertially LN<sub>2</sub> cooled, strip wound OFHC copper coils.
- Two pairs of external ring coils (up-down symmetric). These are similar in construction to the divertor coils.
- A free standing segmented central solenoid (CS) that will be made of LN<sub>2</sub> cooled, oxygen free, high conductivity copper (OFHC) water jet cut discs.
- A double wall vacuum vessel. The inner space is filled with steel and water for nuclear shielding.
- Internal plasma facing components (shown in Fig. 4.1-1). The Be coated

Cu first wall and *tungsten pin-type* inner divertor module is inertially cooled through the vacuum vessel; the tungsten pin-type outer divertor module and baffle is actively cooled. The divertor is designed for a high triangularity, double-null plasma with a short inner null point-to-wall distance and a near vertical outer divertor flux line.

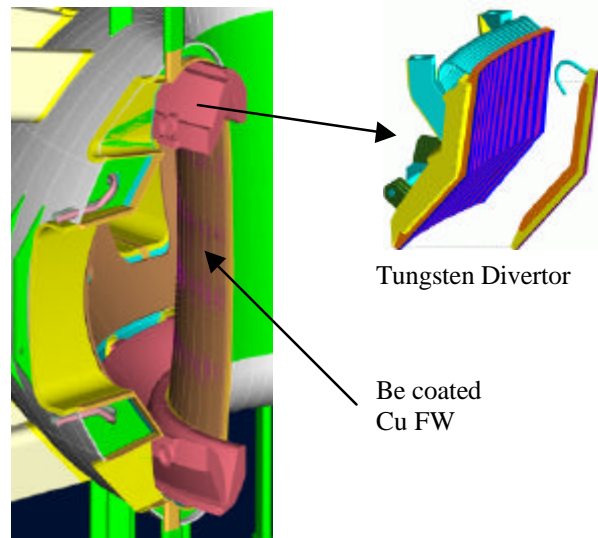


Fig. 4.1-1. FIRE Plasma Facing Components

- Two outboard poloidal limiters, spaced 90 degrees apart, enclose the ICRH quadrant.
- A passive stabilization system consisting of an inboard pair of ring coils and an outboard saddle coil.
- An active control coil system consisting of a pair of coils located within the outboard vessel jacket.
- A thermal enclosure similar to the design used for C-Mod (i.e., polyimide foam insulation with fiberglass inner and outer protective/structural skins).

## 4.2 Design Choices

Sixteen TF coils were selected as the number of coils to provide reasonably large openings between coils for in-vessel access. The radial position of the coil back leg is set by a number of considerations, including access, ripple, and shield thickness requirements; FIRE's design has good balance between these considerations. The inner leg of the TF coil, where the stress is highest, is made of high strength, high conductivity variant of C17510 BeCu. This alloy was developed for BPX, and commercialized since then by its developer, Brush-Welman. The variant we propose to use has a 0.2% yield strength of 720 Mpa and an electrical conductivity of 68% IACS. The stress in the outer regions of the coil is low enough to permit less costly oxygen free copper (C102) to be used. Large rings located outside the TF coils are used to obtain a load balance between wedging of the intercoil case structure and wedging at the upper/lower inboard corners of the TF coil winding.

The design of the baffle and outboard divertor was revised by integrating the two components into a single module. This was done to increase the baffle heat load capacity by providing coolant to the baffle, a component not actively cooled in the earlier design. The reconfigured baffle-outboard divertor module can be extracted through the horizontal ports in a maintenance scheme that provides for component rotation and a vertical lift.

## 4.3 Machine Assembly

The assembly sequence is illustrated in Fig. 4.3-1. FIRE is assembled in four 90-degree sectors built up from two TF

coils and a 90-degree vacuum vessel quadrant.

A vacuum vessel quadrant is rotated into the bore of a two TF coils at assembly. Sixteen large, "straight-in" view ports are equally distributed along the vacuum vessel mid-plane. Sixteen upper and lower auxiliary ports are provided, angled in a position to allow diagnostic view of the divertor region. Small circular ports are also located at the top and bottom of the vacuum vessel, passing through the region between the TF coil windings.

The horizontal ports will provide access to the ancillary systems outside the device. Three ports are assigned to RF

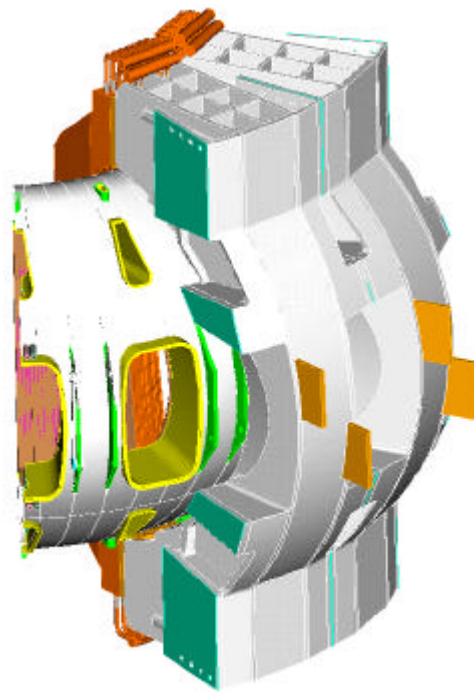


Fig. 4.3-1 90-degree Sector Assembly

heating, and the remaining ports allocated between diagnostics, vacuum pumping and a pellet injection system.

FIRE Engineering Report  
FY01 Update

Some port space will also be used for in-vessel PFC coolant routings. The electrical feed connection to internal control coils are located above/below two horizontal ports located 180° apart. The angled auxiliary ports located in the upper and lower vessel regions accommodate cryopumps, the divertor cooling lines and diagnostics.

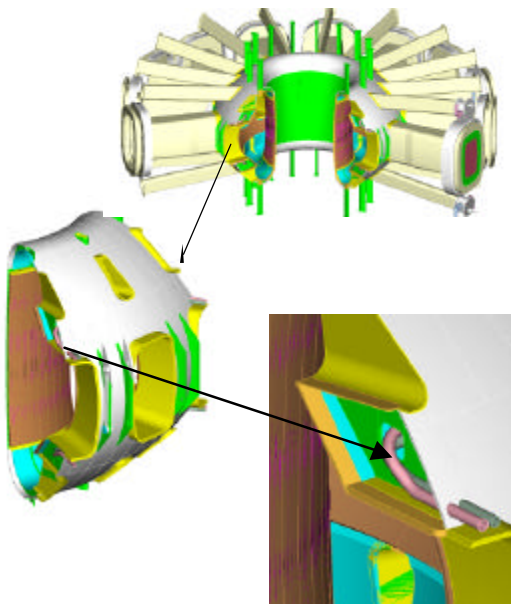


Fig. 4.3-2. The FIRE Vacuum Vessel is assembled from 90-degree Sectors

**Table 4.3-1 FIRE Radial Builds**

	<b>COMP BUILD</b>	<b>COMP</b>	<b>TOTAL</b>
	Mm	Dim	Dim
	Machine Center		0.0
	Gap	440	440.0
<b>CS</b>	turn insul + ground wrap	5.0	
	Nom winding thk	410	
	Insulation outside	2.0	
	gas plenum	8.0	
	CS shell	5	430.0
	Gap	8	878.0
<b>TF</b>	turn insulation	1.0	879.0
	plate thickness	486.0	1365.0
	Plasma side tube	0.0	
	turn insul + ground wrap	5.0	492.0
	Trapezoidal Effect	0.0	
	TF TPT	5.0	
	Minimum TF/VV gap	5.0	
	VV TPT	5.0	
	Thermal Shield	12.0	27.0
<b>VV</b>	VV shell thk	15.0	
	Water	20.0	
	VV shell thk	15.0	50.0
<b>PFC</b>	Cu Heat Sink	25.0	
	FW	38.0	63.0
	Plasma SO	35.0	
	Plasma minor radii	595.0	
<b>R0</b>			<b>2140.0</b>

The radial build dimensions for the 2.14 m device are listed in Table 4.3-1, identifying the space allocated to the components in the confined region inboard of the plasma center.

FIRE Engineering Report  
FY01 Update

**5.0 Engineering Systems**

Sections 5.1 to 5.16 which follow describe the engineering systems of the FIRE device. This includes the TF coils and Structure, the Central Solenoid and PF coils, the Vacuum Vessel, Plasma Facing Components, Thermal Shield which encloses the LN<sub>2</sub> cooled device, the Ion Cyclotron Heating System,

Fueling and Pumping System, Tritium System, Neutronics and Shielding, evaluation of Activation, Decay Heat and Radiation Exposure, Remote Maintenance Systems, Magnet Power Supplies, Diagnostics, the Cryoplant, Facilities and Siting, and Safety evaluation.

# FIRE Engineering Report FY01 Update

## 5.1 TF Coils & Global Structure

### 5.1.1 TF Coils and Stress Conditions

Characteristics of the TF coil pertinent to its mechanical design are listed in the table below.

Table 5.1.1-1

Number of TF Coils	16
Bt, Tesla	10
Flat-top, s	21 (minimum)
Life Pulses at Full Field	3000 (minimum)
Time between Pulses,hr	3
Coil Initial Temp, K	80
Coil Max Temp, K	373

The toroidal field coil system of the FIRE tokamak utilizes LN<sub>2</sub> cooled, copper alloy Bitter plate type magnets. A wedged or vaulted configuration with a free-standing CS is the baseline structural concept for the project. A high strength, high conductivity beryllium copper alloy that was developed for an earlier Tokamak study, the Burning Plasma Experiment (BPX), is proposed for the conductor. A number of alternative structural concepts have been reviewed and continue to be reviewed, each with advantages and disadvantages relating to FIRE's mission. These have been summarized in table Tables 5.1.1-2, and 3. TF wedging pressures and CS hoop tensions have determined the basic sizing of the machine, but support of torsional shear in the inner legs has had an important influence on the evolution of the FIRE structural design. To support this shear, friction between the wedged segments of the coil is all that is available. With torsional shears between 30 and 50 MPa, and friction coefficients of .3, 160 MPa wedge compression is needed on the plasma side of the TF where the torsional shear is at a maximum. Wedge pressures from a pair of large compression rings, provides this in the upper and lower inner leg corners. Centering forces supply the wedge pressure at the equatorial plane.

	FIRE Baseline Design W (wedged TF)	FIRE BW (bucked and wedged TF)
TF Inner Leg Mat	BeCu	OFHC
R (m), a (m)	2.0, 0.525	2.0, 0.525
B <sub>(Ro)</sub> (T), baseline (upgrade)	10(12)	10(12)
flattop time (s)	~20(12)*	31(23)
TF Allowable(MPa)	700	300
TF Von Mises Stress	466(666)	230(326)
Min. TF stress Factor of Safety (FS) (allowable/actual) <sup>1</sup>	1.5 (1.05)	1.3 (.92)
Wmag TF (GJ)	3.7(5.328)	3.7(5.328)
I <sub>p</sub> (MA)	6.44(7.7)	6.44(7.7)
CS Peak Stress at PRE	294(354)	(228 <sup>1</sup> )
CS Temp at PRE	83(85)	83(85)
CS allowable at Pre <sup>1</sup>	345(347)	345(347)
CS F.S at Pre	1.15(.98)	2.1(1.5)
CS Peak Stress at EOB	182(332)	(30)
CS Peak Temp (EOB)	159 (176)	159 (176)
CS Allowable (EOB)	313(305)	313(305)
CS F.S at EOB	1.7(.92)	>10(10)
CS flattop time (s)	21(15)	21(15)
Fusion Power (MW)	~ 200	~ 200

**Table 5.1.1-3 Comparison of Ro=1.24m  
machines**

	FIRE*	
	W (wedged TF) <sup>1</sup>	BW (bucked and wedged TF) <sup>1</sup>
TF Inner Leg Mat	BeCu	OFHC
R (m), a (m)	2.14, 0.595	2.14, 0.595
B <sub>(Ro)</sub> (T), baseline (upgrade)	10 (12)	10(12)
flattop time (s)	~20(12)	~31(23)
TF Allowable(MPa)	700	300
TF Von Mises Stress	529 (762)	230(326)
Min. TF stress Factor of Safety (FS) (allowable/actual) <sup>1</sup>	1.3 (.92)	1.3 (.92)
Wmag TF (GJ)	5.08(7.32)	5.08(7.32)
I <sub>p</sub> (MA)	7.7 (8.25)	7.7 (8.25)
CS Peak Stress at PRE	322(322)	(228 <sup>1</sup> )
CS Temp at PRE	88?(88)	88(88)
CS allowable at Pre <sup>1</sup>	344(344)	344(344)
CS F.S at Pre	1.07(1.07)	2.1(1.5)
CS Peak Stress at EOB	190(279)	(30)
CS Peak Temp (EOB)	177(227)	177(227)
CS Allowable (EOB)	304(280)	304(280)
CS F.S at EOB	1.6(1.0)	>9(9)
CS flattop time (s)	17.5(32??)	17.5(32??)
Fusion Power (MW)	150	150

**Table 5.1.1-2 Comparison of Ro=2.0m Versions  
of FIRE**

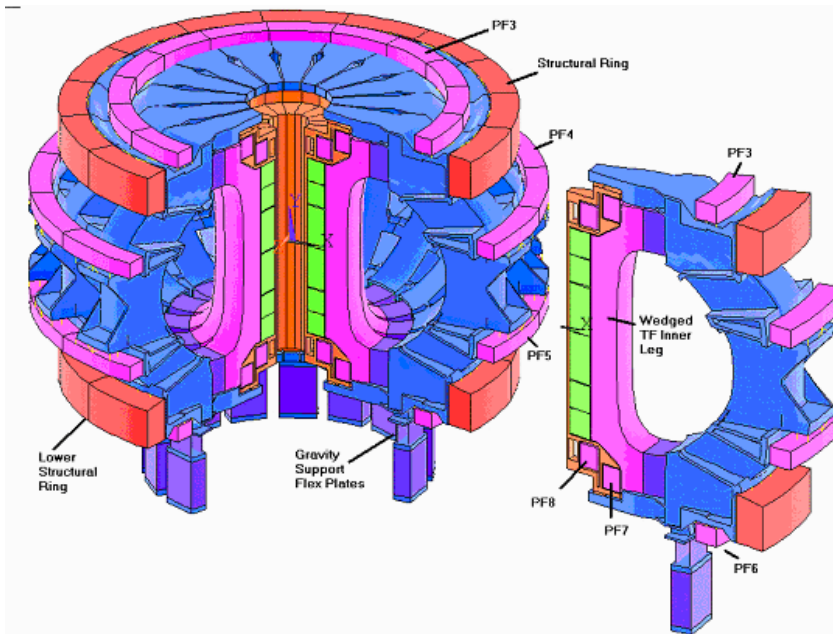


Figure 5.1.1-1, Twelve Segment Symmetry Expansion (left) of 1/16 cyclic symmetry model (right)

**Stress Criteria**

A variety of Beryllium Copper is the present material of choice for FIRE. Peak stress in the FIRE TF is about 469 MPa. at the CS side of the inner leg for 10 T operation, at precharge. The stress in the bucked and wedged configuration is about half this and allows the use of cold worked copper.

These monotonic primary stress limits are to be applied to stresses resulting from a primary load. 1.5 Sm is allowed for primary plus, bending and for primary plus discontinuity; and 3.0 Sm is allowed for primary plus secondary. Appropriate

**Table 5.1.1-4 Primary Membrane Stress**

Conductor:	Structure:
Sm=2/3 Yield	Sm=Lesser of 2/3 Yield or 1/2 Ult
And Adequate Ductility	And Adequate Ductility

**Table 5.1.1-5 Primary Stress Allowables**

68% IACS	60% CW	Cast 304SST	50%CW
BeCu Cond	OFHC Cond		304 SST
Sm=483 Mpa at RT	Sm=200 Mpa at RT	Sm=154 Mpa at RT	Sm=620Mpa a at RT
Sm=497 Mpa at 77K	Sm=233 Mpa at 77K	Sm=188 Mpa at 77K	Sm=834Mpa a at 80K

multipliers are used for upset and faulted loads. Where multiply redundant structures make it difficult to decompose the stress state into these stress categories, the FIRE criteria document, in paragraph I-3.1.1 allows a limit analysis. The limit load is that load which represents the onset of a failure to satisfy the normal operating condition, and this limit load is to be twice the normal operating load.

It is not clear which of the inner leg stresses being discussed are primary stresses given that the primary vertical support is from the external structure. For the wedged machine, an attempt is made to assign the stress components to appropriate elements of the coil and structure. The wedge stress supports the primary inner leg

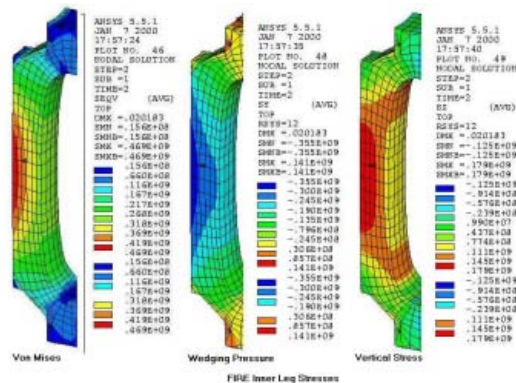


**Figure 5.1.1-2 10T Precharge Inner Leg Stresses**

# FIRE Engineering Report FY01 Update

centering load, and should meet the primary membrane allowable. The peak stress at the nose is 469 MPa at precharge for the 10 T configuration with the tierod removed. With a pretensioned tierod, the peak stress was 433. If the inboard leg supports only the wedge pressure, The outboard leg and case structure must be shown capable of supporting the vertical separating force as a primary load.

Use of the large rings improves the wedge pressures in the inner corners of the TF coils, but has only a small effect on the largest Von Mises stress in the coil which is at the equatorial plane of the inner leg.

“Smeared” stresses presented in the table above have been found to vary little with the application of the effects of a packing fraction=.9 or Stress multiplier=1.11 because the predominant stress component is wedge pressure to which the multiplier does not apply.

**Table 5.1.1-7 Wedged BeCu Machine Monotonic Stress Check**

	Material	TF Field	Primary Stress (1)	Allowable	F.S
Inner Leg	BeCu	10	249(2)	480	1.9
Inner Leg	BeCu	12	358(2)	480	1.3
Outer Leg	OFHC	10	155[2]	233	1.5
Outer Leg	OFHC	12	223[2]	233	1.0
Case at Outer Leg			200	188	

(1)(Average Wedge Pressure, Vertical load assumed supported by the Outer TF and Case)

(2) Hand Calculations with the case contributing 200 MPa.

**Table 5.1.1-8 Wedged BeCu Machine Inner Leg Bending Stress Check**

	Cu Type	B <sub>TF</sub> (T)	Mem. + Bend	Allowable	F.S
Inner Leg	BeCu	10	469	724	1.5
Inner Leg	BeCu	12	689	724	1.05

To satisfy the "adequate ductility criteria" the BeCu wedged machine was analyzed with a 13T TF field with elastic-plastic TF material properties. A stress-strain curve with a 600 MPa

elastic limit was used for the inner leg. This conservatively brackets the properties of the BeCu conductor which has a .2% offset yield of 724 MPa. A .6% strain resulted from the 13T loading, and the structural response remained bounded for this over-loaded condition. The .6% strain was conservatively imposed on the insulation as though it all was in-plane in the turn to turn insulation. The resulting stress was within the allowable tensile stress for the insulator.

During the BPX design effort, cyclic fatigue for the Higher strength BeCu limited the allowed tensile stress to 60 ksi (413 MPa). Fracture mechanics calculations were the basis for this. Paris Law constants were measured for BeCu as a part of the CIT/BPX projects. The design number of full field pulses for FIRE is 3000 (as a min). This is much less than BPX. TF stresses are predominantly compressive. The vertical tensile component in the inner leg is about 120 MPa. This indicates margin in the fatigue behavior at the equatorial plane of the inner leg. In the inner upper and lower corners, on the plasma side where the coil build is reduced to make room for

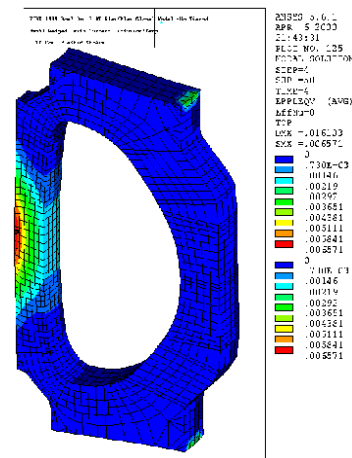


**Figure 5.1.1-3 Plastic Strain after 13 T loading**

PF1 and the divertor, there is some imposed strain from the inner leg motion due to the centering force, and subsequently, the thermal expansion of the central column when the coil is turned off. Evaluation of the strain controlled fatigue for the 3000 full power pulses is acceptable. A local strain absorbing insulation detail will be needed, such as kapton sheets interleaved with epoxy glass.

A central tierod had been used in FIRE, but the improvement in inner leg stresses was only about 30 MPa, and the complexity of the tierod and

# FIRE Engineering Report FY01 Update

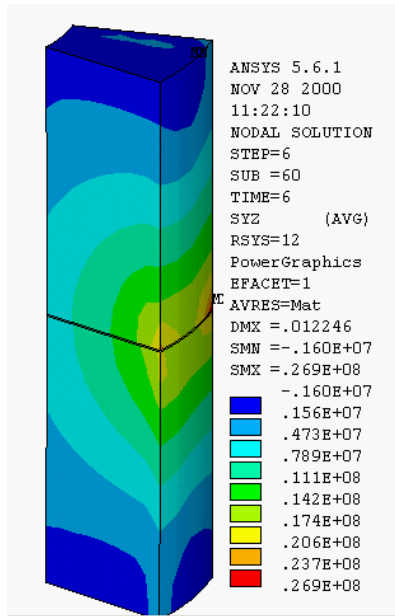


**Figure 5.1.1-4 SOF CS1 Torsional Shear** - About 20 MPa at Mid-Plane OD. - The Bucked and wedged design loads the CS in torsional shear, but there is About -70 MPa vertical compression at this point in CS1 to improve shear capacity.

interference with the CS leads and coolant lines in the bore made removal of the tierod attractive.

### The Bucked and Wedged Design

The bucked and wedged version of the FIRE model was run for a number of different fit-up tolerances, and friction coefficients. The following observations resulted:

- TF wedge pressures are approximately half the pressures of the wedged only design, allowing the use of OFHC copper, and reducing insulator compressive stress
- The TF must bear on full height of CS.
- CS1 Heat-up causes bending in inner leg. Solution is to "preheat" CS2
- CS stresses are limited by a compressive maximum at Nul (the inversion, or zero CS1 current point in the pulse)
- CS currents can be increased above that for the TF wedged-only design, allowing more freedom in selection of CS bias, but would then require the TF be on to limit hoop stress.
- Unlike the wedged TF design, CS segment differential radial motion is near zero during the pulse. Provision must be made for radial displacements after the pulse. When the TF is

off and does not press against and align the CS

- Fractional mm Fit-Up Tolerances are OK
- Off Normal Fit-Ups > 1.0mm Produce Small Plastic Strains, Well within The Plastic Capacity of the Conductor Materials.
- 1.25mm Gap Yields the TF, 1.25mm Interference Yields the CS. 1.25mm Gap or Interference produce a One-Time Plastic Strain (Self Fitting?)

### Limit Load Analysis

Starting with 11.5T, the bucked and wedged configuration was analyzed with increasing toroidal field, and the behavior was monitored. At 14T the radially inward displacements started to grow, and a bucking cylinder was added to the bore of the CS. Results of the last two runs are tabulated below.

**Table 5.1.1-9 Bucked & Wedged 16T TF Elastic-Plastic Limit Load Analysis**

Bo	15T	16T
Run	#73	#74
Buck Cyl VM	1270	1600
Buck Cyl Hoop	-836	-1130
Buck Cyl vert	639	859
TF VM		389 (432 w /.9 PF)
TF εp VM	.008	.0142
TF Hoop	-325	
TF Vert	+277	+346 (plasma side)
CS Von Mises	284	320
CS Hoop	-300	-307
CS εp VM	.006	.012
Case VM at EQ PL		699
Case UY Max	+0.0002	.007
Case UY Min	-.013	-.016

All Stress are "Smeared" and in MPa, The bucking cylinder was added at 14T, Bucking along CS1,2,and 3 ,

**Table 5.1.1-10 Ultimate Stress of Cold Worked OFHC Copper**

80%CW	420MPa RT	500 MPa at 77°K
60%CW	350MPa RT	474 MPa at 77°K

At 16T, the vertical displacements, shown in Figure 5.1.1-5 are predominantly in the inner leg illustrating the shift of vertical load from the inner leg to the outboard structures. This is a characteristic also claimed for the wedged configuration, in which the primary structure supporting the vertical separating force is the outboard structures. The torsional displacements after two shots, and with the coils turned off are interesting. These are shown in Figure 5.1.1-6 and show that the tokamak central column has taken a permanent twist, however the displacements were the same after the first and second pulses. The machine could continue 16T shots, but possibly

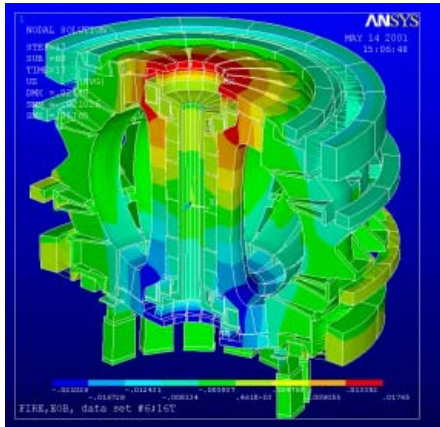


**Figure 5.1.1-5 Buckled and Wedged 16T Limit Analysis, EOB Vertical Displacements, Including Cool-down.**

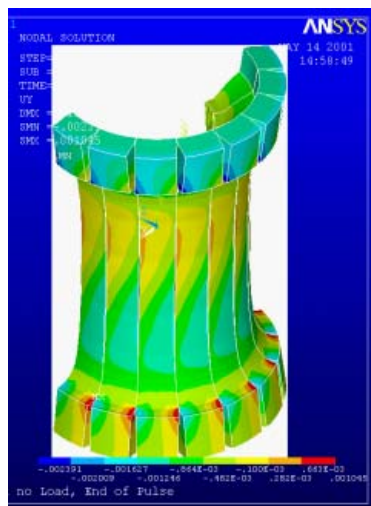


**Figure 5.1.1-6 Toroidal Displacements, Locked-In Twist, After two Shots with 16T TF. Light Blue is - 1.6mm and Brown is 3mm**

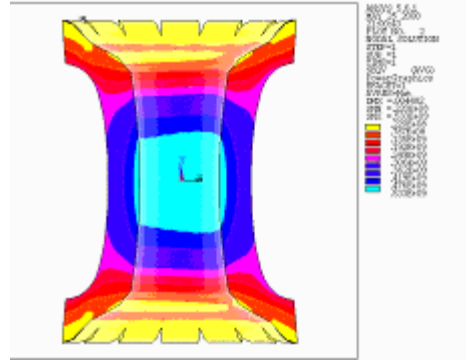


**Figure 5.1.1-7 Single Coil 10% over Nominal 10T Current - 533 MPa Von Mises Stress**

not lesser fields because the inner leg has yielded in the toroidal direction. Wedge pressure needed for OOP support would be diminished for lower field operation.

- From Elastic Analysis, Major Stresses In CS and TF Remain below 1.5 Sm for ranges in fit-up, Friction behavior, and preload. The Elastic-Plastic Analyses show the Limit Load to be Above 16T TF - Twice Operating Loads
- A Bucking Cylinder is Needed to Demonstrate 16 Tesla Limit Load. 14cm thick Cylinder is Modeled, Lead Cut-Outs and Coolant Passages will require added build.

Survivability in off-normal or faulted loading also is a measure of design margin a 180 degree model was built to begin investigating the sensitivity of the TF system to these unusual loads.

### Preliminary Fault Analysis

At this time the faults are postulated based on ITER experience and are not the result of power supply behavior or a FMEA.

Table 5.1.1-11 Preliminary Fault Analysis

Model and Current/Loading	Peak TF Stress
Nominal 10T No Tierod Detailed Model	469 MPa
Fault Model, Nominal 10T	522 MPa
Fault Model, Single Coil 10% Over Nominal	533 MPa
Fault Model Single Coil 20% Over Nominal- the Rest 20% Under	441 MPa

### FIRE Pulse Lengths

# FIRE Engineering Report FY01 Update

A simple zero D integration scheme was used to estimate the flat top times for various toroidal fields and nuclear heats. This was done in parallel with a more rigorous ANSYS coupled thermal-current diffusion analysis. The analyses agree.

**Table 5.1.1-12 TF Flat Top Times for FIRE**

**Options.**

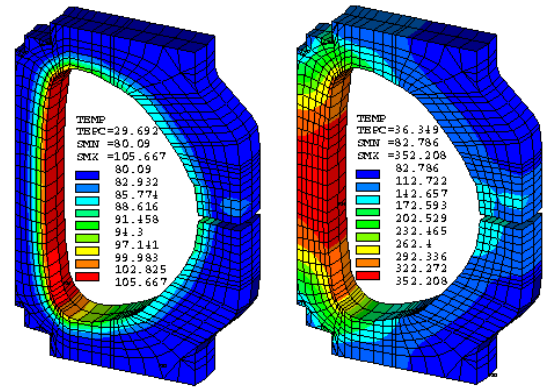
68% IACS BeCu TF (Feb 3 Dimensions, TF Central Column OR=1.308,IR=.820),Simplified Calculations using Packing Fraction=0.9 Nonuniformity=1.0, 80° Start, 370°K Limit

TF Field	4T	8T	8T	10T	10T	12T	12 T
Nuc Heat MW/m <sup>3</sup>	0	7.5	0	11	0	11	0.0
Time sec	214	31	46	18.5	26	12	15

**Table 5.1.1-13 Thermal Energy of 16 coils after each Pulse, 80° Start.** (Energy to be removed during cool-down)

Peak Temp after Pulse	292°	313°	370°
TF Coil Thermal Energy	9.958GJ	11.054 3 GJ	14.079GJ

Sub cooling of the coils to 65 °K does not offer substantial improvement. The more rigorous analysis of the current and thermal diffusion behavior was performed using ANSYS, and does not include nuclear heating. An 80 ° K start was used. A 10T pulse was simulated and the point at which the temperature neared the 370° limit was noted as the end of flat top. 28 sec was obtained for 77%IACS material which can be compared with the simpler analysis which produced 26 sec for the one-D solution and 68% IACS material. Temperature contours for this benchmark are shown below.



5 Sec. Early in Ramp-Up  
48 sec. End of Flat-Top  
FIRE TF Current/Thermal Diffusion Analysis Results. 77% IACS Material

**Figure 5.1.1-8 Temperature Distributions in the FIRE TF, 77% IACS., Packing Fraction=.9,~28 sec Flattop**

## Global Structural Modeling

Both linear and non-linear models have been used. The linear global structural model employs links convertible to gap elements at interfaces between the model components. The ANSYS computer code is used. The winding pack is connected to the external case with links or gaps. Tensions develop in the links when gaps would have opened. This is adjusted at some locations

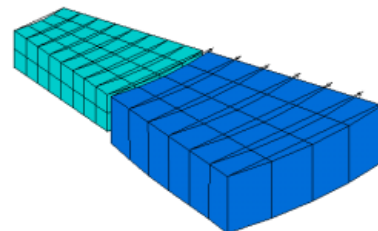


**Figure 5.1.1-9 Section Through CS and TF coils at the Equatorial plane.** In the Non-Linear Model, Gaps are used at the wedged face. Cyclic symmetry is obtained by coupling the gaps across to the opposite face.

by removing the gaps/links which open, for the load cases where this is necessary.

# FIRE Engineering Report FY01 Update

The non-linear model used gaps at the wedge face and simulates the frictional capacity of the inner leg to resist out-of-plane torsion. Gaps also are used at the case segment to segment interface. It is intended that the case to case mechanical connections be minimized, as these must sustain large local pressures, but be insulated. The non-linear analysis has confirmed that the present sizing of the ring (.5m X .75 m), stressed to an average hoop stress of 500 MPa, provides adequate centering force for frictional restraint of the TF inner leg and of the case segments.

The connection between the current-thermal diffusion analysis and the structural calculation is done outside ANSYS. An algorithm assigns temperatures to the structural model from the current/thermal diffusion model by proximity and averaging. There is a separate CS/PF model which has been maintained current and is fully structurally non-linear. This has been used to investigate support structures for the CS and PF1

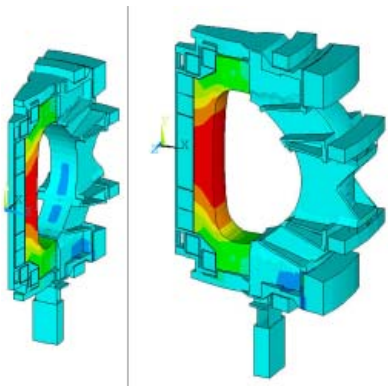


**Figure 5.1.1-10 Typical temperature distribution input to the structural model**

and 2. For the wedged TF, the CS stack can be modeled independently.

The TF Von Mises stress is primarily due to in-plane loading. The largest Von Mises Stress predicted by the model, is used to select a copper alloy with maximum conductivity, and adequate tensile strength. The in-plane stress reduction using bucking and wedging is sufficient to allow the use of copper coils. The Von Mises stress is 240 for bucking and wedging vs. 450 for wedged case. This appears as an attractive alternative, but the mechanisms available to support TF inner leg torsional shear need to be considered in the choice of structural concept.

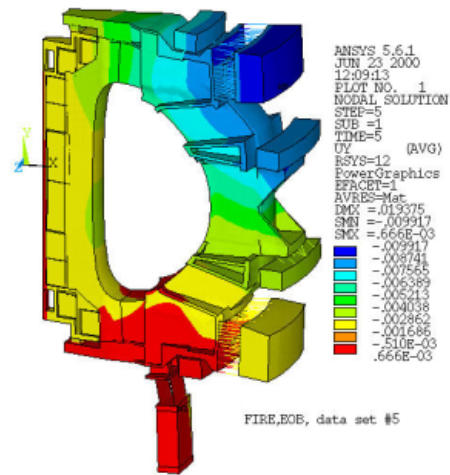


**Figure 5.1.1-12 Out-of-Plane Displacements of the FIRE Structural Model**

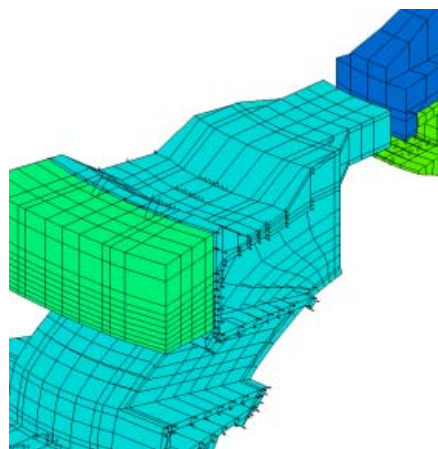


**Figure 5.1.1-11 Case Model with Gap elements at the Parting Plane. Friction is the only shear transmission mechanism.**

## TF and Global Structural Support of Out-of-Plane (OOP) Loads

An evolution of models has been employed to investigate various means of supporting the out-of-plane (OOP) loads, and changing PF builds. Support of the OOP loads is statically indeterminate and changing structural support concepts changes the magnitude and location of the torsional shear in the inner leg of the TF. The wedged configuration has better performance with respect to the out-of-plane shear than the bucked and wedged concept, which gives up some wedge pressures in resisting the outward loads from the CS. Difficulties arise from OOP support for all of the in-plane load carrying concepts. The upper and lower inner corners of the TF de-wedge from the tension in the horizontal legs, and the

differential heat-up of the inner leg. A few concepts were investigated to relieve the OOP torsional shear:

- Thermally loaded Aluminum Shrink Ring
- Stiffened Outer Structure
- Flex Region to isolate the TF central column from the outer OOP structure
- Thermal Contouring of the TF to heat the de-wedge corners

None of which fully solve the problem. For the “flex”, the torsional shear concentrates near the equatorial plane of the inner leg, and the de-wedged regions must “flex” to allow the relative motion of the central column and the outer coil structure. Bending stresses of the “flexing” coils must be accommodated. Dividing the Bitter plates into multiple thin sections that flex easily with OOP displacements was investigated. These sections could not be too thin or too wide or the local OOP Lorentz forces would induce load controlled bending stresses. This “flexure” approach requires that there be no net torque on the central column, which, for nominal loading is not a problem. Off-Normal conditions, and disruptions, could, however produce net loads and torques on the central column. The Aluminum ring proved to weak to solve the problem. Thermal contouring could improve wedging pressures by radially thinning sections needing

outward in-plane loads, rather than to offset vertical tension in the inner leg, as in IGNITOR.

In Figure 5.1.1-13 , the TF corner stresses at assembly are shown. The wedging pressure achieved with the rings in the corner is between 60 and 90 Mpa at assembly. This increased to 150 MPa compression when the coil is energized, which is sufficient to support the 45 MPa peak torsional shear. These figures are from the linear models and some localized slippage is likely, but the non-linear model showed this to be small.

The results of shear margin calculations show the improvement in the region that can frictionally

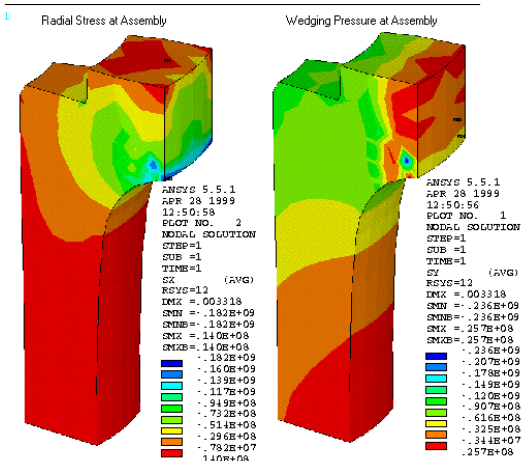


Figure 5.1.1-13 TF Inner-Upper Corner Stress Results for the “With-Ring” Model

more wedge compression, or by allowing inter-pulse temperatures to build where wedge pressures were needed, but this was judged troublesome. The next approach considered was to add a large ring to offset the horizontal leg tension. This is similar in concept to the large static ring used in IGNITOR, but the positioning of the ring in FIRE is intended to offset radially

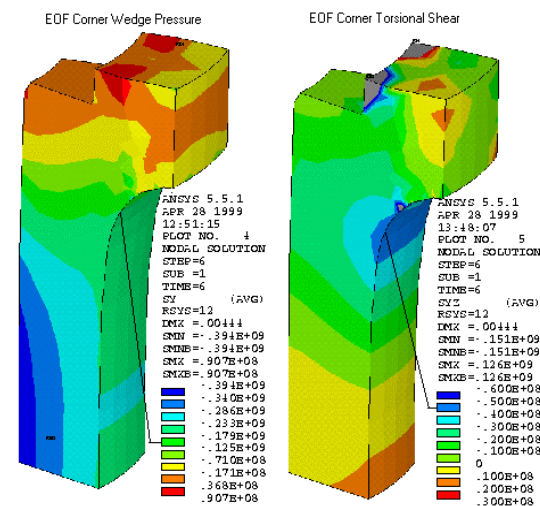


Figure 5.1.1-14 TF Inner-Upper Corner Stress Results for the “With-Ring” Model

support the torsional shear at the wedge faces. In the shear margin plot , figure 5.1.1-15, the region having adequate frictional support of the OOP loads is shown in red. There is a small difference in extent of this region between the “with ring” and “without ring” models, but the added area is important because it includes the area of largest torsional shear.

Ring loads are quite large. At assembly the average ring hoop stress is about 500 MPa This goes up about another 100 Mpa at EOF. Initial ring loading can be applied with a number of mechanisms. In the history of this concept, which is used on IGNITOR and was used on early CIT designs, Hydraulic jacks and mechanical jack systems have been employed. IGNITOR currently uses a mechanical system which has been prototyped, and supports similar pressures as would be required for FIRE It is an opposed wedge design, with a thermal assist to tighten the

# FIRE Engineering Report FY01 Update

stud. This, or possibly a freezable fluid filled jack would be used for FIRE

strip wound and are sized to provide wedge pressure for both the TF and Case.

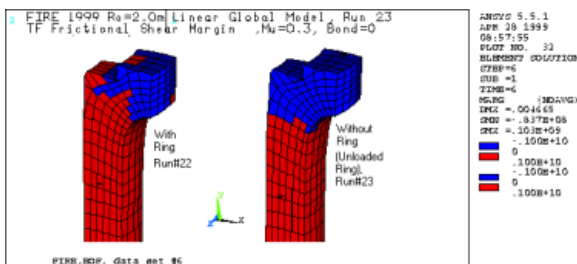


**Figure 5.1.1-15 Effect of TF Preload Ring on Frictional Shear Margin**

**Table 5.1.1-14 Case Equatorial Plane Stresses, 12T Run#52 Results:**

Time	Peak Stress (MPa)
PRE	228
SOF	448

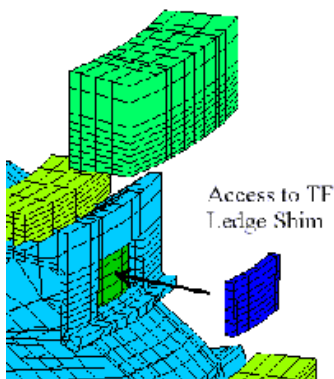


**Figure 5.1.1-16 TF Ledge Shims .** The preload structure will apply loads to the TF coil turns via this load path.

EOB	585
Eof	617
EOP Hot	362

Case stresses are highest near the local bearing locations of the ring. Elsewhere, case stresses are below 675 Mpa shown in Figure 5.1.1-18. Much of the case stress at the equatorial plane relates to thermal expansion of the TF, and occurs later in the pulse. Even though the largest fraction is thermal, a high strength material is needed to eliminate the possibility of plastic strains in the case.. Equatorial plane stresses are too high for cast material. (80K Yield=282 MPa,41 ksi). There is about 228 MPa from Lorentz loading and 362 MPa from thermal. Cold worked plate is suggested for the case sidewalls. The rings are

This requires a predictable load share between these two load paths, and some additional effort to shim or individually load the ledge will be needed. . The rings bear through the case against a

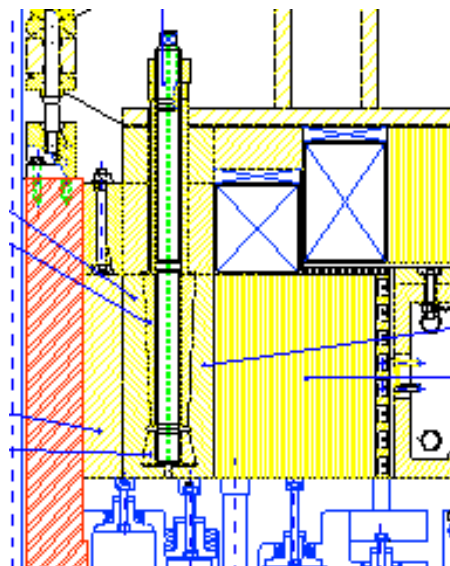


**Figure 5.1.1-17 IGNITOR Mechanical Jack.**

ledge added to the TF coil. The chamfer on the ring is intended to increase the area of the ring without encroaching on the slanted port detail. In the current design, the PF3 coil has been moved from under the ring to the top and bottom of the case structure, leaving space for the preloading wedges or jacks that will be needed. The case was modeled as a closed box around the coil. The top plate of the case reinforcement was not wedged or toroidally connected. Wedging pressures at the joint plane of the case sectors is about 300 MPa in the present model. The webs have been increased in thickness to allow the use

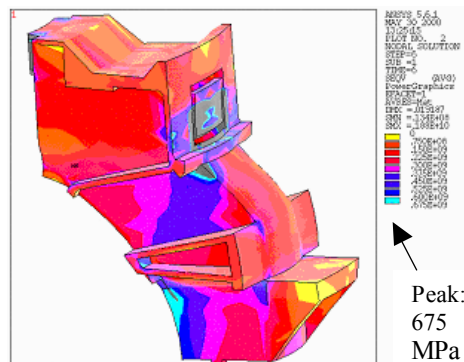


**Figure 5.1.1-18 Coil Case Von Mises Stresses**

# FIRE Engineering Report FY01 Update

of cast material for the complex web and flange geometry of the intercoil structures.

## TF Joints

A "Wrapped" terminal concept equilibrates poloidal (hoop) tension and improves the thermal anomaly at the eyebrow cut-out. The details of its penetration through the case need to be worked out, but it does not interfere with the poloidal coils, and is in the same area as the present lead layout.

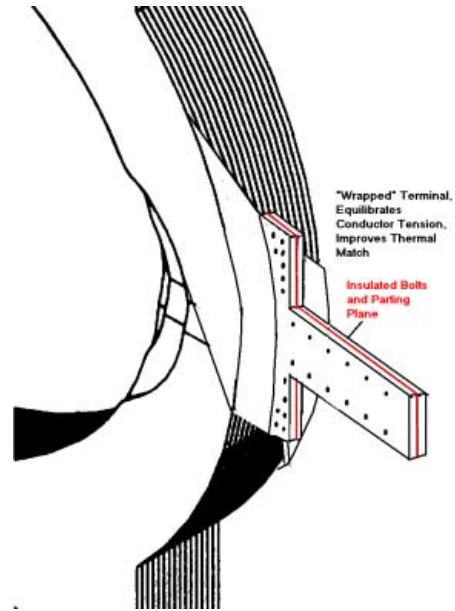


Figure 5.1.1-19 "Wrapped" Terminal Concept

## 5.2 Central Solenoid & PF Coils

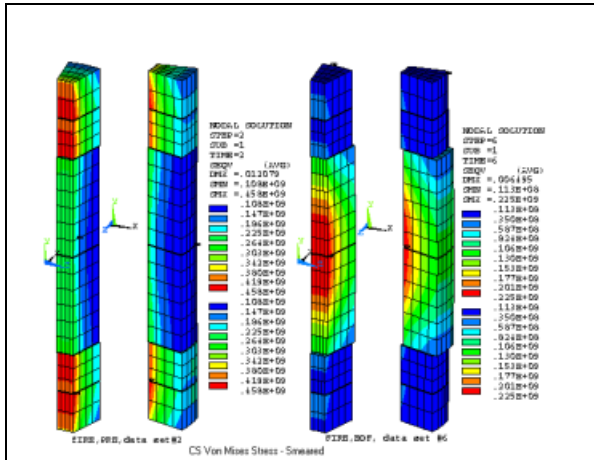


Figure 5.2-1 Typical CS Stress Results from the Global Model

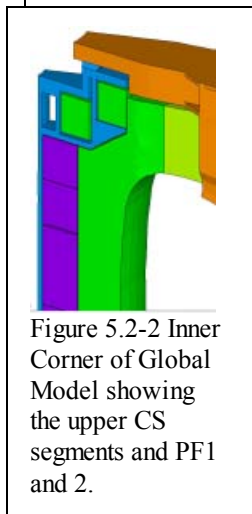


Figure 5.2-2 Inner Corner of Global Model showing the upper CS segments and PF1 and 2.

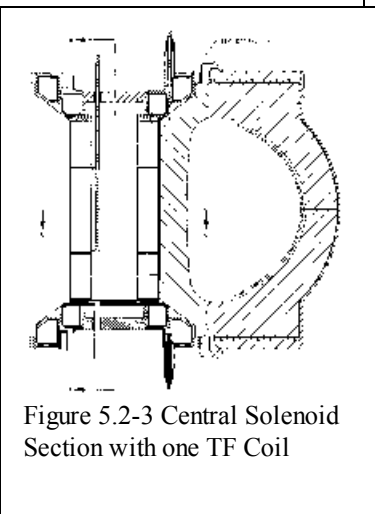


Figure 5.2-3 Central Solenoid Section with one TF Coil

current densities vary among the coils in the CS assembly, and thus the coil segments experience different Lorentz forces, Temperatures, and resulting radial strains. Radial grooved plates at the interfaces between coil segments maintain concentricity.

The CS and PF coils are analyzed in both the global model and in a more detailed model of the free-standing CS/PF1 and PF2 coil system with their case/structure. Because of the evolution in the PF scenarios it has been easier to keep up with the evaluations using the separate model.

This model can use up-down symmetry because the OOP forces do not load the poloidal coil system.

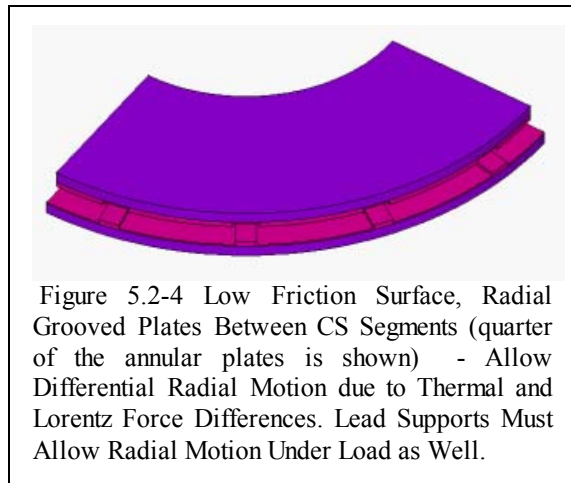
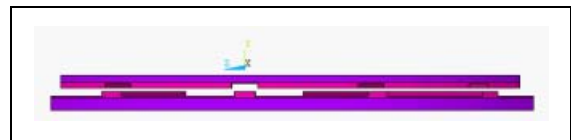


Figure 5.2-4 Low Friction Surface, Radial Grooved Plates Between CS Segments (quarter of the annular plates is shown) - Allow Differential Radial Motion due to Thermal and Lorentz Force Differences. Lead Supports Must Allow Radial Motion Under Load as Well.

The Central Solenoid (CS) is an OFHC copper coil. It is a free standing coil in the baseline design. A bucked and wedged arrangement was investigated as an alternate. Two machine sizes have been investigated. Machines with  $R_o=2.0m$  and an  $R_o=2.14m$  have been considered. The larger machine, designated FIRE\* is basically a scale-up of the smaller machine, but the central column space has been reallocated to provide more space for the CS to support a larger plasma current.

The CS is a pancake wound coil with turns water jet cut from plate. Radial coolant grooves are used between double pancake assemblies. The central solenoid coil is segmented into 5 coils with a large mid section coil, CS1, and two smaller coils on each end of the stack. Coil

### FIRE\*CS and PF Coil Builds ( $R_o=2.14m$ Machine, Lower Half is Symmetric with Upper Half)

Coil	Real	R	Z	DR	DZ
CS1U	1	0.68	0.452	0.39	0.894
CS2U	2	0.68	1.158	0.39	0.4986
CS3U	3	0.68	1.6668	0.39	0.4986
PF1	4	.8557	2.2385	0.325	0.37
PF2	5	1.291	2.5060	0.325	0.37
PF3	6	3.304	3.120	0.39	0.39
PF4	7	4.766	1.200	0.39	0.39

### FIRE CS and PF Coil Builds ( $R_o=2.0m$ Machine, Lower Half is Symmetric with Upper Half)

Coil	Real	R	Z	DR	DZ
------	------	---	---	----	----

## FIRE Engineering Report FY01 Update

CS1U	1	.61	.398	.39	.791
CS2U	2	.61	1.035	.39	.44
CS3U	3	.61	1.475	.39	.43
PF1	4	0.786	1.975	0.325	0.380
PF2	5	1.211	2.211	0.325	0.380
PF3	6	3.00	2.646	.4	.3
PF4	7	4.400	1.000	0.400	0.300
Plasma	15	2.0	0.0	1.0	2.0

### CS Joints

Sizing of a reactor during the conceptual phase needs to include allowance for the local details of the coil design. Stress analysis of this is based on “smeared” properties to which multipliers are applied to account for insulation, cooling and joint details. In the evaluation of FIRE

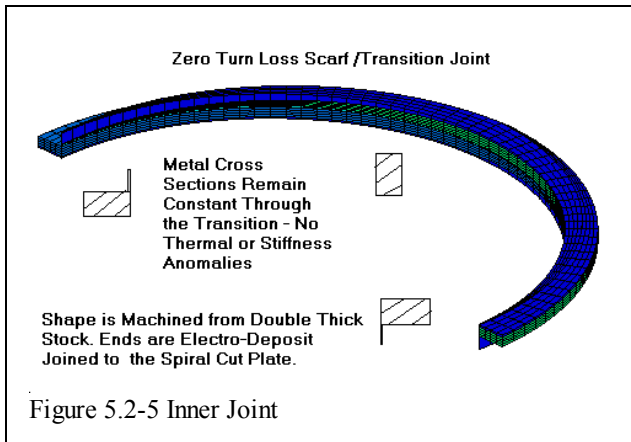


Figure 5.2-5 Inner Joint

“smeared” CS and PF stresses, the packing fraction due to insulation and cooling channels is taken as .85 and the stress multiplier for the inner joint is taken as 1.0, and it is important to achieve these factors for the sizing of FIRE to be realized. Pancake to pancake joints have a stress multiplier associated with them which is usually quite a bit larger than 1.0. There are two major sources of the multiplier. The geometry of the connection including the effects of the offset adds local stresses at the mechanical connection details. This usually requires addition of material to bring the stresses within the levels experienced by the rest of the turn. The increase in metal produces a stiffer region embedded in the coil and picks up more load than a single turn would normally take, adding further stresses to the mechanical details of the joint. The increase in metal also causes the second source of stress increase. Because the larger masses of metal run cooler in an inertially cooled coil, they don’t

expand with the rest of the coil. The result is additional tensile stresses in the vicinity of the joint.

A shape similar to that shown in figures 5.2.5 and 6 was developed for BPX after investigating many pinned or bolted or hooked joint concepts. The scarf/transition joint proposed for FIRE is a constant cross section design that eliminates both the stiffness and thermal anomaly. There is no void left by the joint, and no turn loss. In BPX, the joint was to be soft soldered over large lapped areas. A better connection results using electro-formed joints at the butt ends of the scarf. Use of this detail means that the stress in the joint is the same as that computed by the larger models of the coil. This is especially advantageous at the ID of the coil. If some other joint concept is chosen, the coil stress allowable must be de-rated by the stress multiplier for the ID joint. This joint concept has similar advantages when used on the OD, but because the OD stresses in the CS are much lower than the ID, more conventional mechanical joints might be considered. For example, the double pancakes could be made an assembly with the scarf at the ID, then stacked and assembled mechanically at the OD. Since the coil segments are small enough, the scarf could be used at the

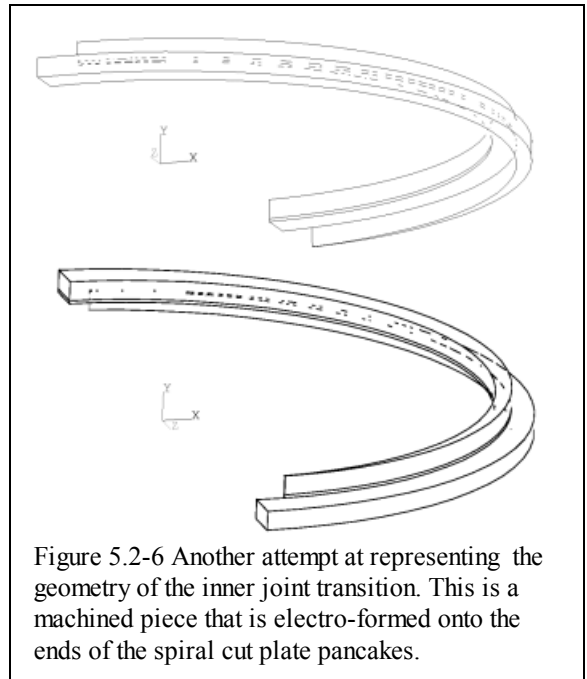


Figure 5.2-6 Another attempt at representing the geometry of the inner joint transition. This is a machined piece that is electro-formed onto the ends of the spiral cut plate pancakes.

OD as well. This would require electro-forming at the coil assembly, but C-Mod has shown that this is feasible.



Figure 5.2-7 Electroforming the terminal flag onto one of C-Mod's strip wound poloidal field coils. The process of forming the inner joint of FIRE's CS double pancake assembly would be very similar, with the spiral cut pancakes expanded to allow access for a plating tank. Rubber sealed slots to allow the inner turn to be inserted in the tank. (Ed. Fitzgerald C-Mod Photo)

### CS/PF Stress Analysis

Three analysis models have been used, the global model, an axisymmetric model and a 3D model derived from the global structural model. There are significant stresses in the PF 1 coil.

structural over-hang of PFs 1 and 2. A stiffer structure will improve this. Other significant stresses typically occur in CS1 and CS2. These are contributed to by self loads appearing as

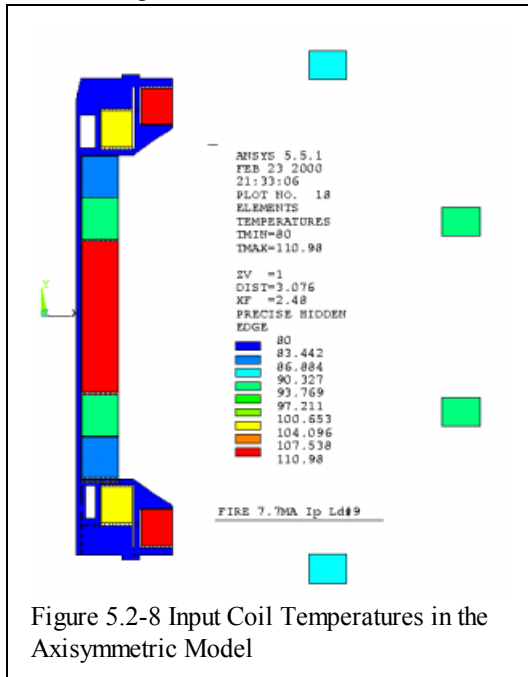


Figure 5.2-8 Input Coil Temperatures in the Axisymmetric Model

This stress however has a large component relating to "roll-over" resulting from the

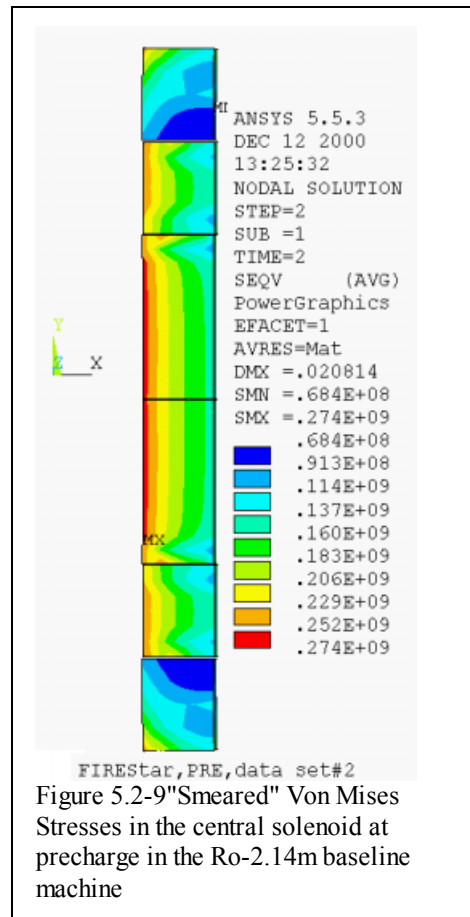


Figure 5.2-9 "Smeared" Von Mises Stresses in the central solenoid at precharge in the Ro-2.14m baseline machine

## FIRE Engineering Report FY01 Update

hoop stresses. The worst stresses should be biased to earlier in the pulse, when the temperatures are low, and the physical properties of the candidate materials are best. Based on the project criteria document, average coil stresses have to meet primary membrane stresses, and the peak stresses in these coarse analyses of the coils have to meet the bending allowable. A similar approach is used the TF coil. The CS and PF coils are a little different in that these are made up from wound, not bitter plate conductors and if 1.5 Sm is allowed for these, the ID turns will be operating close to yield. If the CS/PF1,2 assembly can be removed from the machine with manageable difficulty, high stress regions at the ID could be inspected periodically in the life of the tokamak. The CS ID is accessible for instrumentation if inspection is not feasible.

A rigorous stress evaluation needs to consider a packing fraction (taken as 85% to allow for cooling channels), and temperature effects on the stress allowable. The FIRE criteria document sets the primary membrane allowable at 2/3 yield for conductor, For a conductor that is also it's primary structure. the calculation of Sm should be the lesser of 1/2 ult or 2/3 yield. For 60%CW OFHC the ultimate stress check governs, and the Sm values are 235 at 80K and 167 at RT. The peak stress of the FEM analyses has been compared with 1.5 Sm, as being similar to a bending stress. This assumes the distribution of stress in the coil is linear from ID to OD. In actuality it is peaked at the ID, and the linearized "bending" stress that should be compared with 1.5 Sm, will be somewhat lower than the peak stress from the FEM analysis. – Although this effect is only about 10 MPa. It is claimed that for 3000 full power pulses, fatigue is not a problem. But this will need further confirmation. Stress states in the coils are acceptable for all the PF scenarios proposed for FIRE, but with no margin (actually a slight negative margin) for the 12T 7.7 MA scenario. In the Ro=2.0m machine

### FIRE Scenario Summary

All supplied by C. Kessel unless noted

# & Notes	Date	Ro	Ip	Bt	EOB-SOD (Sec)
15(a)		2.14	8.25?	12?	?
14	12/19/00	2.14	7.7	10	27
13	12/17/00	2.14	7.7	10	27
12	12/02/00	2.14	7.7	10	27
11(b)		2.0	7.6	11.5	28
10(b)	10/19/00	2.0	7.25	11.5	28
9(a)		2.0	7.7	12	19
8	06/22/00	2.0	7.7	12	19
7	06/21/00	2.0	7.7	12	19
6		2.0	2.0	4	250
5	06/09/99	2.0	6.44	10	27

4	06/08/99	2.0	6.44	10	27
3		2.0	6.44	10	17
2	06/03/99	2.0	6.44	10	17
1		2.0	6.44	10	

(a) Titus Average of #13 and #14

(b) Bucked and Wedged specific

### Scenario #12, FIRE\* Ro=2.14m, 10 T 7.7 MA Packing Fraction=.85

CS1 Currents, MAT	PRE stresses	EOB stresses
PRE 11.68 EOB: -11.82	CS1 PRE VM=322.3 MPa F.S.=1.07	CS1 EOB VM=190 MPa F.S.=1.6

In this scenario for the 10T 7.7 MA Ro=2.14m machine, stresses are acceptable at the beginning and the end of the pulse, and the margin at the end of pulse should allow a re-bias to obtain some volt-sec margin if needed. In these results, CS1 is limiting at both time points.

### 12T TF, 7.7 MA 15 second PF Scenario Ro=2.0m

This is the highest set of performance parameters considered for the Ro=2.0 machine. The scenarios available for this case produce stresses that are either too large early in the pulse or too large later in the pulse. Estimates of an intermediate flux still produce stresses slightly above the allowable. Typically in these scenarios, either CS2 is highly stressed at precharge or CS1 is highly stressed at EOB. Temperature effects on the allowable favor higher precharge currents.

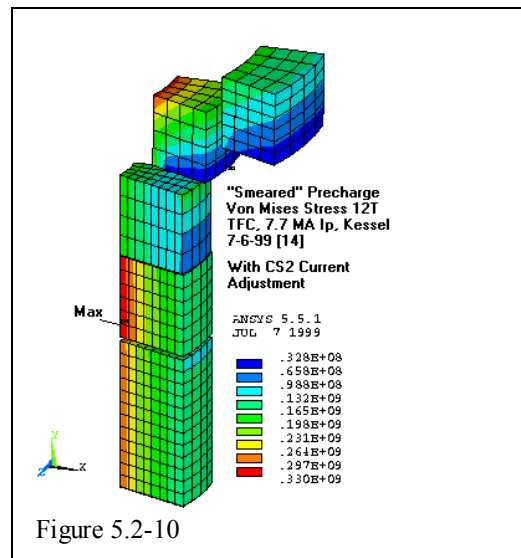


Figure 5.2-10

# FIRE Engineering Report FY01 Update

To evaluate the potential for a workable scenario, the effects of the optimum flux shifts were estimated by weighting the stress states of

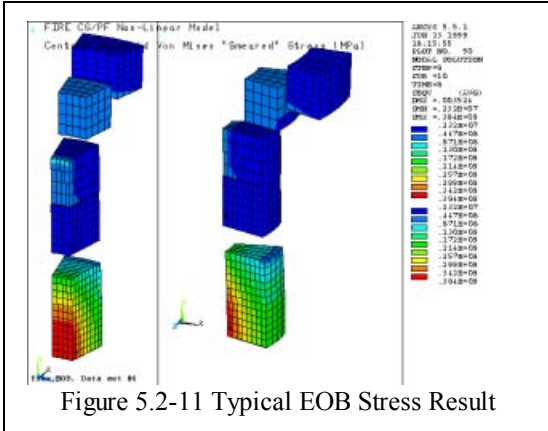


Figure 5.2-11 Typical EOB Stress Result

the last two 12T 7.7 MA scenarios. The thermal effect on the allowable is:  $1.5S_m = 350 - 100 * (T - 80) / 212$ .

Results of Weighted Scenarios 12 T 7.7 MA scenarios, Packing fraction=.85

Weight New - shifted, flux, state, everywhere, back by,5,V with CS2 Precharge adjustment	Weight Old 12 T 7.7 MA scenario	PRE	EOB
3/4	1/4	CS2 PRE VM=354 Temp=85 1.5Sm=347 F.S.=98	CS1 EOB VM=332 Temp=176 1.5Sm=305 F.S.=92

## Results for Supplied 12 T 7.7 MA Scenarios

These are presented as the basis for the estimated re-bias presented in the previous paragraph.

CS/PF Von Mises Stresses MPa, Kessel 12T TF, 7.7 MA 15 second PF Scenario, with shifted, flux,state, , back by,5,V , Upper Number is "Smeared", Lower Number is for Packing Fraction=.85 (Stress Multiplier=1.17),

	PRE	SOD	SOF	SOB	EOB	EOC
CS1	294 346	241 284	232 273	220 259	249 293	121 142
CS2	369	303	46	60	50.4	72.3
CS3	173	145	160	184	151	147
PF1	258	216	321	192	174	200
PF2	185	157	76	97	93	98.2
PF3	1.2	1.2	140	33	35	52.5
PF4	1.4	0	91	171	170	62.4

CS/PF Von Mises Stresses MPa, Kessel 12T TF, 7.7 MA 15 second PF Scenario, with shifted,

flux,state, , back by,5,V , First Number is "Smeared", from the Axisymmetric Model, and the Second, in ( ), is the "smeared" result from the 3D Model,

	PRE	SOF	SOB	EOB	EOC
	ld#3	ld#4			
CS1	250,(294)	250,(232)	(220)	(249)	(121)
CS2	314,(369)	60,(46)	(60)	50.4	72.3
CS3	150,(173)	148,(160)	(184)	151	147
PF1	160,(258)	325,(321)	(192)	174)	200)
PF2	128,(185)	20,(76)	(97)	93)	98.2)

CS/PF Von Mises Stresses MPa, Kessel 12T TF, 7.7 MA 15 second PF Scenario, kcs6, Upper Number is "Smeared", Lower Number is for Packing Fraction=.85 (Stress Multiplier=1.17),

	PRE	SOD	SOF	SOB	EOB	EOC
CS1	169 199	130 153	131 154	346 407	384 452	219 257
CS2	215 253	165 194	166 195	24 28	29 34	33 39
CS3	110 129	84 99	85 100	129 151	93 109	134 157
PF1	136 160	104 122	107 126	109 128	79 93	100 118
PF2	111 131	84 99	102 120	71 84	60 71	66 78
PF3	.9 1.	.7 .82	.7 .82	42 49	44 51	72 85
PF4	.4 .5	.3 .35	.33 .39	170 200	170 200	62 73

CS/PF Von Mises Stresses MPa, Kessel 12T TF, 7.7 MA 15 second PF Scenario, Upper Number is "Smeared", Lower Number is is for Packing Fraction=.85 (Stress Multiplier=1.17),

	PRE	SOD	SO F	SO B	EO B	EOC
CS1	169 199	130 153	131 154	346 407	384 452	219 257
CS2	215 253	165 194	166 195	24 28	29 34	33 39
CS3	110 129	84 99	85 100	129 151	93 109	134 157
PF1	136 160	104 122	107 126	109 128	79 93	100 118
PF2	111 131	84 99	102 120	71 84	60 71	66 78
PF3	.9 1.	.7 .82	.7 .82	42 49	44 51	72 85
PF4	.4 .5	.3 .35	.33 .39	170 200	170 200	62 73

## FIRE Engineering Report FY01 Update

CS/PF Peak Stresses, MPa, Kessel with 15 second 12T TF, 7.7 MA PF Scenario, kcs6.pic Scenario, Upper Number is "Smeared" Hoop Stress, Lower Number is "Smeared" Von Mises No Preload

	PRE	SOD	SOF	SOB	EOB	EOC
CS1	163 169	126 130	126 131	274 346	310 384	165 219
CS2	208 215	160 165	160 166	4.8 24	10.7 29	20 33
CS3	109 110	84 84	84 85	38 129	34 93	42 134
PF1	136 136	1094 104	107 107	107 109	74 79	92 100
PF2	108 111	82 84	100 102	312 71	17 60	29 66
PF3	.8 .9	.6 .7	.6 .7	41 42	43 44	60 72
PF4	.06 .4	.06 .3	.06 .33	164 170	164 170	60 62

### 21 second 10T 6.6MA PF Scenario

The PF stress analysis results for the updated 21s flattop are presented here. Stresses are acceptable for this longer pulse. The peak stress for all coils and all time is 294 MPa which is less than the 1.5 Sm allowable of 350 Mpa for work hardened OFHC Copper. The peak temperature is 182°K in PF2 ( for a packing fraction of .8)

CS/PF Peak Von Mises, MPa, Kessel with 21 second PF Scenario#4, Ip=6.44 MA Upper Number is "Smeared", Lower Number is for Packing Fraction=.85 ,No Preload

	PRE	SOD	SOF	SOB	EOB	EOC
CS1	209 246	164 192	164 182	127 149	164 214	109 128
CS2	265 311	208 244	208 244	28.7 33.7	164 193	50.9 60
CS3	133 156	107 126	105 120	101 119	56 66	131 154
PF1	180 212	131 154	144 170	169 199	132 155	86 101
PF2	135 159	107 126	127 149	90 106	71 84	45 53
PF3	1.07 1.26	.84 .98	.8 .94	36 42	39 46	20 24
PF4	.5 .65	.4 .47	.4 .47	120 141	120 141	54 64

### CS and PF Coil Temperatures

CS and PF coil Temperatures, 15 second 12T TF, 7.7 MA PF Flux Shifted 5V  
Copper IACS=100%, Packing Fraction=.85

Time (sec)	CS1	CS2	CS3	PF1	PF2	PF3	PF4
0	80	80	80	80	80		
4.637	84.	87.	82.	82.	86.	80.	80.
5.00.	85.	89.	82.	82.	87.	80.	80.
12.00	93.	99.1	87.	103.	114.	85.	84.
14.5	101	101	88.	112.	125.	87.	90.
24	142.	108.	95.	144.	163.9	89.	120.
27	155.	110.	98.	157.	177.	90.	127.
31	160.	111.	98.	161.	182.	91.	128.
35	160.	112	98.	161.	182.	91.	128.

CS and PF coil Temperatures, 250 second 4T TF, 2MA PF Scenario  
Copper IACS=100% Packing fraction = .85

Time (sec)	CS1	CS2	CS3	PF1	PF2	PF3	PF4
0	80	80	80	80	80	80	80
4.6	80.8	81.4	80.4	80.42	81.2	80.0	80
5	81.0	81.6	80.4	80.49	81.4	80.	80.0
7	81.2	82.2	80.6	80.82	81.9	80.	80.2
10	81.6	82.6	80.9	81.56	82.6	80.	81
255	144	86.8	87.9	119.3	125	80.2	170
257	145	86.8	87.9	119.4	125	80.2	170
260	144	86.8	87.9	119.4	125.	80.2	170

Coil Temperatures, °K, Kessel June 8 1999 21 second PF Scenario, 6.44 MA, 10T, Copper IACS=100%, Packing Fraction=.85

Time (sec)	CS1	CS2	CS3	PF1	PF2	PF3	PF4
0	80	80	80	80	80	80	80
4.6	83	85.52	81	81	84	80.	80
	84	86.48	81	82	85	80.	80.
10	88	91.99	83	92	98	82.	82
12.5	93	92.84	84	99	105	84.	86.
31	140	96.84	88	151	161	90.	128.
34	150	98.12	90	158	170	90.	134.
38	152	99.36	91	161	173	91	135.
42	152	99.44	91	161	173	91	135.

### Reduction in the Vertical Build of PF1 and PF2

Reducing the build of PF1 and 2 from .38 to .3 increased the temperature from 161 to 253 in PF1 and from 182 to 308 deg K in PF2. These temperatures were for the 12T TF, 7.7 MA Ip Flux Shifted 5v scenario.

# FIRE Engineering Report FY01 Update

PF 1&2 Von Mises Stresses MPa, Kessel 12T TF, 7.7 MA 15 second PF Scenario, with shifted, flux, state, , back by, 5, V, , First Number is "Smearred", from the Axisymmetric Model, and the Second in ( ) is the "smearred" result from the 3D Model,

	PRE	SOF	SOB	EOB	EOC
	ld#3	ld#4			
PF1	160 (258)	325 (321)	(192)	(174)	(200)
PF2	128 (185)	20 (76)	(97)	(93)	(98.2)

PF2 is not stress or thermally limited, and could be reduced in size if the coil case requires more strength.

## CS Shear Stresses

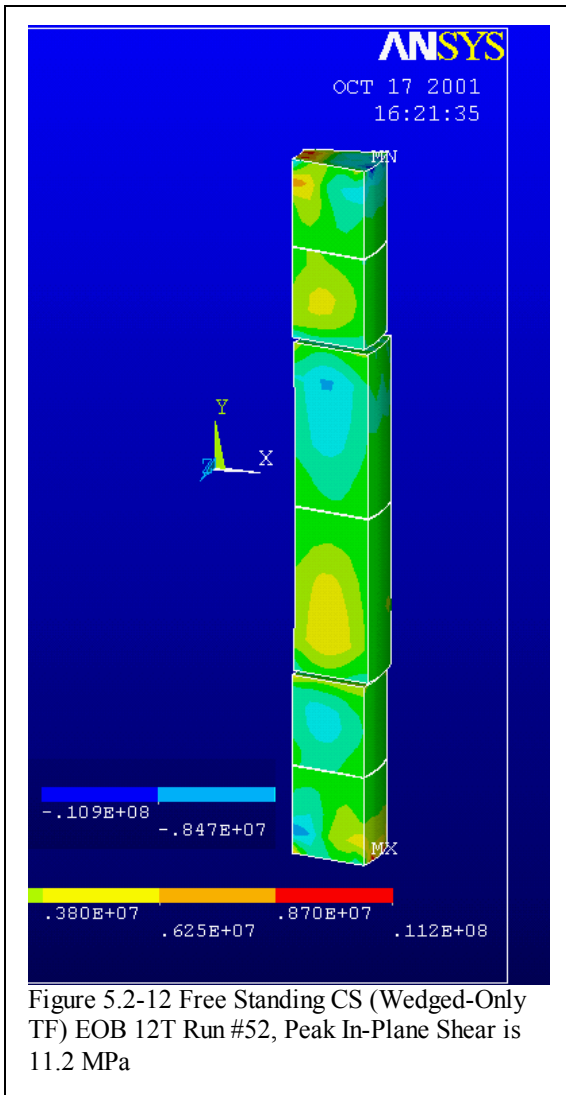


Figure 5.2-12 Free Standing CS (Wedged-Only TF) EOB 12T Run #52, Peak In-Plane Shear is 11.2 MPa

In-plane or r-z shear is low in the freestanding CS coil. These are shown for one of the more

severe time points in figure 5.2-12. Torsional shear in the CS for the bucked and wedged

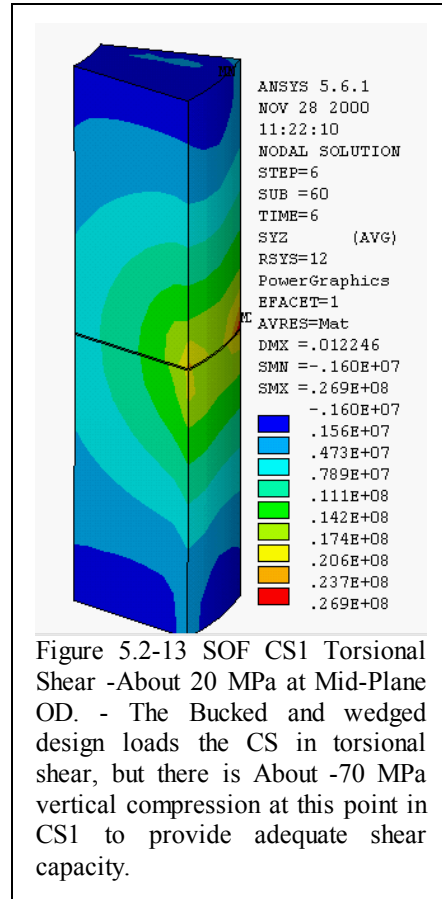


Figure 5.2-13 SOF CS1 Torsional Shear -About 20 MPa at Mid-Plane OD. - The Bucked and wedged design loads the CS in torsional shear, but there is About -70 MPa vertical compression at this point in CS1 to provide adequate shear capacity.

configuration is shown in figure 5.2-12. This shear component, which is not present for the wedged-only case, is one of the drawbacks of the bucked and wedged concept.

## CS/PF Case/Mandrel Stresses

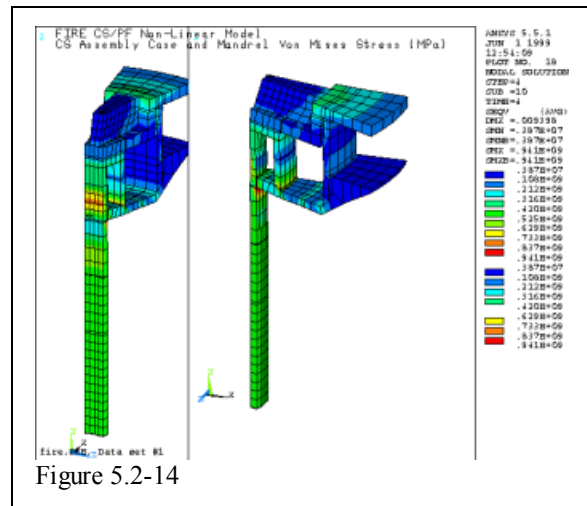


Figure 5.2-14

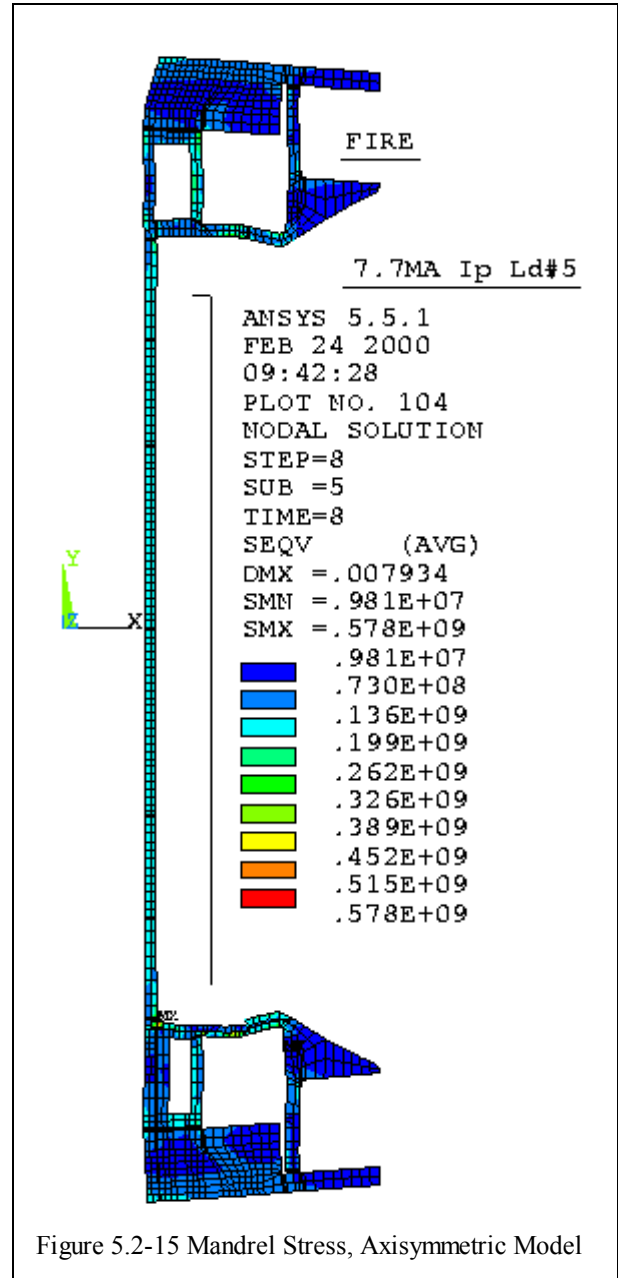
# FIRE Engineering Report FY01 Update

The analysis is based on use of an inner shell to take the vertical separating forces in the coils. The shell has been replaced with studs, and the large tierod intended for TF loads has been removed, allowing whatever area is needed for the stud cross section. Peak stresses in the available model are in the mandrel/inner cylinder at the intersection with the PF1 and 2 case assembly. This results from rotations of this assembly added to the tensions due to thermal expansion of the coils and coil separating forces.

CS/PF,Case Von Mises Stess, MPa, Kessel  
Scenario, No Preload, 1/32 symmetry model

CD	PRE	SOD	SOF	SOB	EOB	EOC
225	941	830	867	825	859*	802

\*(578 from the Axisymmetric model)



acceptable as a faulted load. The current design

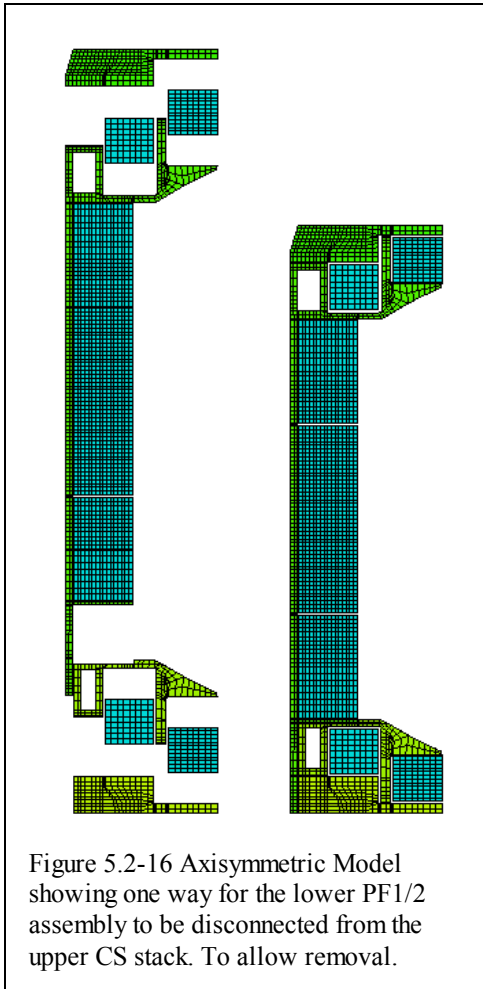


Figure 5.2-16 Axisymmetric Model showing one way for the lower PF1/2 assembly to be disconnected from the upper CS stack. To allow removal.

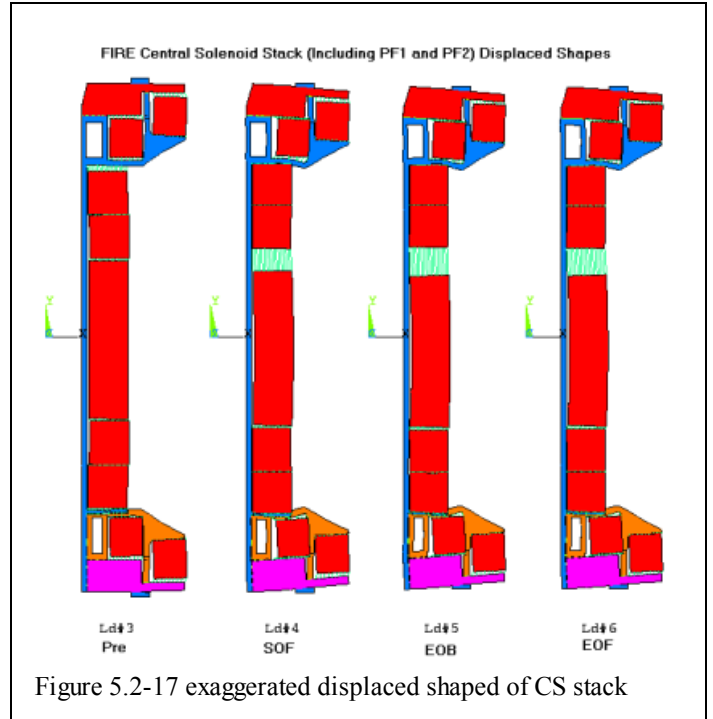


Figure 5.2-17 exaggerated displaced shaped of CS stack

allows for some vertical preload of studs which have replaced the shell in the model shown in Figure 5.2-16. The degree of preload compression, and its effect on the radial sliding grooves at the segment interfaces will be a subject of FY2002 study.

### Vertical Disruption Effects on FIRE CS/PF Coils

#### Effect of CS Segment to Segment Gaps

The possibility of not using a vertical preload of the CS stack has been investigated. The concern is that the mechanisms that allow individual radial growth of the coil segments would be less effective with a large vertical compression in the CS assembly which introduces frictional constraint. A "loose" vertical assembly raises the possibility of gaps between coil segments. In the analysis Figure 5.2-17, Lorentz forces are up-down symmetric. CS1 falls due to gravity. During normal operation. Small gaps of about 1mm would have little consequence. During a disruption, net vertical Lorentz forces develop, and could cause coils to impact one another. This effect was estimated, and found to produce impact factors of 1.2 for expected gap sizes. Vertical net loads on the coils due to disruptions have only been estimated, but these are

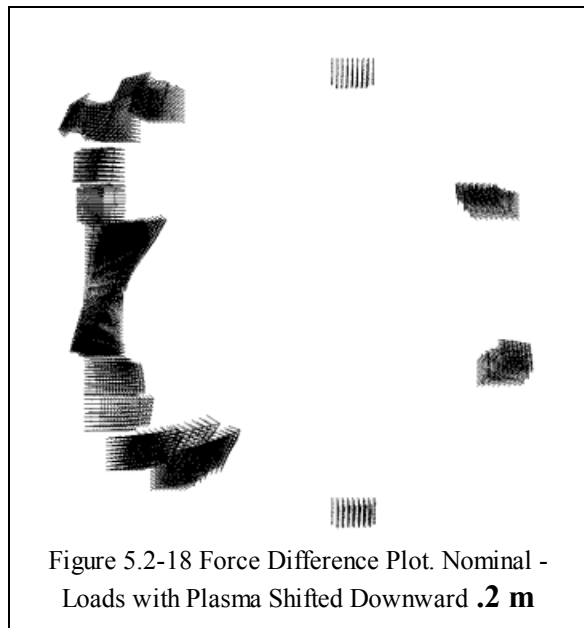


Figure 5.2-18 Force Difference Plot. Nominal - Loads with Plasma Shifted Downward .2 m

# FIRE Engineering Report FY01 Update

Net loads on vacuum vessels have been seen on operating tokamaks. In FIRE, An electromagnetic simulation of disruption loads on the TF coils has been performed, and is presented in section 5.1. The forces shown in Figure 5.2-18 and the analyses presented here for the CS should be conservative due to the shielding effect of the vessel. The vertical impact of segments of the CS stack gaps is a concern. Net vertical loads on the CS assembly may develop, and lateral loads on radial grooves between CS coil segments are a possibility. These radial grooves are shallow cuts in thin G-10 end caps on the windings, and are shown in Figure 5.2-4. The net vertical load on the CS assembly is presently intended to be transferred to the TF coil at the inclined ledge of the inner leg of the TF.

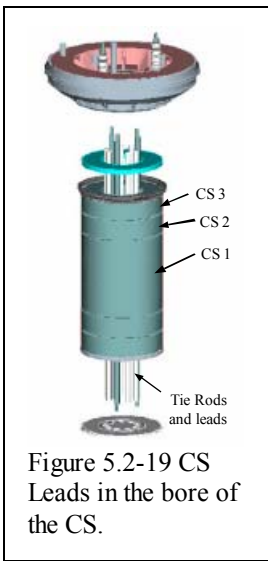


Figure 5.2-19 CS Leads in the bore of the CS.

### Inner Break-Outs and Leads

Detailed design of these components has not yet been performed, but the field distribution of the segmented solenoid will produce challenging lateral loads on uncompensated lengths of the coil break-outs and leads.

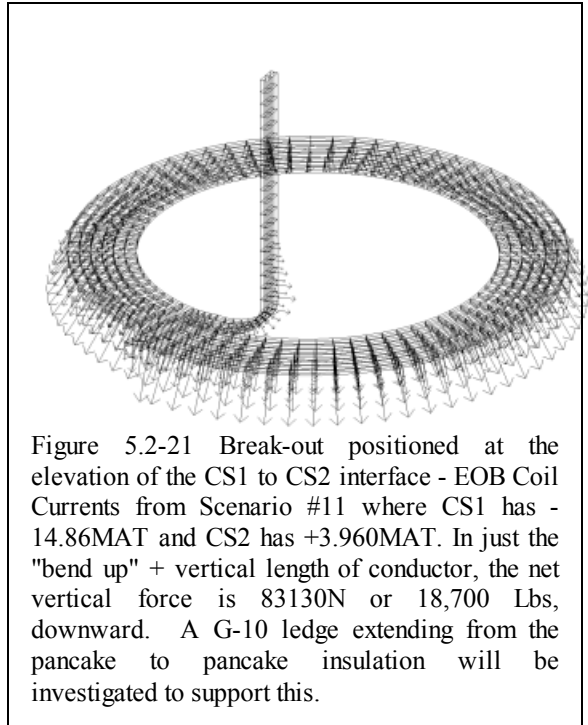


Figure 5.2-21 Break-out positioned at the elevation of the CS1 to CS2 interface - EOB Coil Currents from Scenario #11 where CS1 has -14.86MAT and CS2 has +3.960MAT. In just the "bend up" + vertical length of conductor, the net vertical force is 83130N or 18,700 Lbs, downward. A G-10 ledge extending from the pancake to pancake insulation will be investigated to support this.

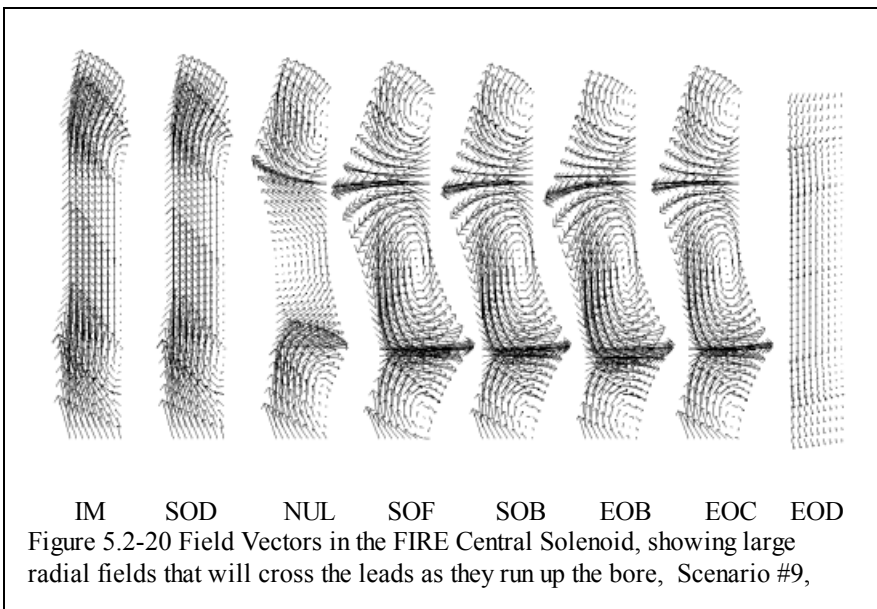


Figure 5.2-20 Field Vectors in the FIRE Central Solenoid, showing large radial fields that will cross the leads as they run up the bore, Scenario #9,

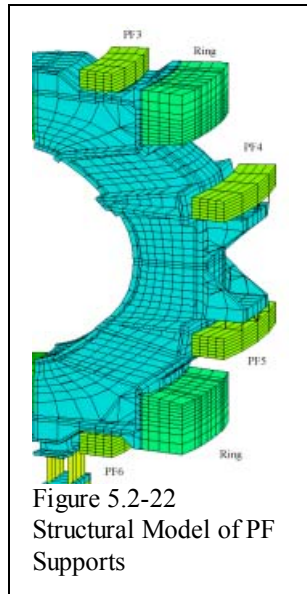
# FIRE Engineering Report FY01 Update

## PF Supports

The PF coils are self supporting with respect to their radial Lorentz Loads. The coil must be allowed to grow thermally and elastically in the radial direction. The coils must be constrained to move concentrically with respect to the machine centerline. Vertical loads must be supported against the case in some fashion. In ITER and TFTR flex plates are used. In CIT and BPX the coils were to bear on G-10 pads which in turn bore on case structures. The G-10 pads were to have radial grooves which imposed concentricity. Fibreslip or similar material was to lubricate the groove. In FIRE, PF1 and 2 are included in the CS stack. PF3 and 4 (and 5 and 6) are the only coils needing support details. Flex plates are more complex, and would require space needed for port clearance, compression ring and TF leads. Radius rods and radial grooved plates have been looked at in some detail. The capacity of the rods is too small to expect them to be able to slide the coil and maintain concentricity while the large ring coils are energized. And, like the flexplates they would add hardware to regions intended for ports and leads.

## Concentricity Maintenance

The radial grooves used in the CIT/BPX arrangement may be subject to binding and alignment problems. This was the motivation for considering the use of a system of radius rods. This type of support was used for the GEM detector, and is used for support of large superconducting solenoids. In this concept there would be as a minimum, one unidirectional tangential radius rod in the shadow of each TF coil.



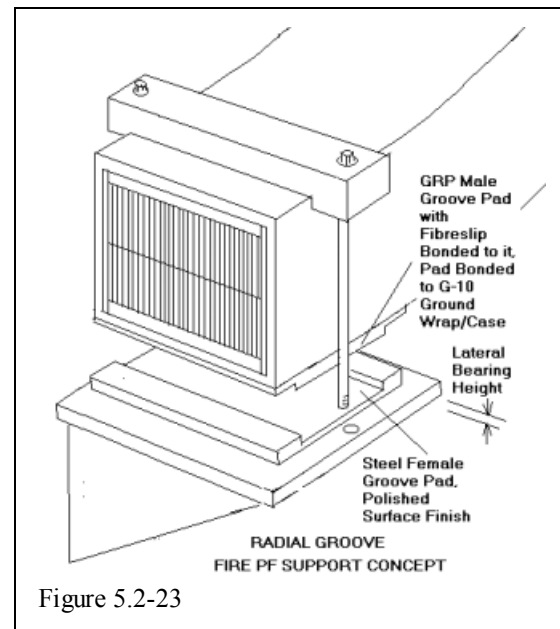
## Vertical Support

In the table below, the vertical forces are tabulated by coil for the time points analyzed in the scenario. This is a 12 T 7.7 MA scenario. The

last two rows are the maxima and minima. For PF3 and 4 all loads are downward throughout the pulse. (Upward for PF5 and PF6) For normal operation the coils could simply bear on the case, or a shelf welded to the case. There are conceivably faulted scenarios that would induce separating loads. Until these are identified, it is assumed that normal and faulted loads are all in compression against the case or support shelf. The lower coils will have to be held against gravity. Upper and lower coils will have to be supported against seismic loads.

## Vertical Coil Loads(N), per 1/16th Sector 12T 7.6MA Scenario

Pf1	pf2	pf3	pf4
4	5	6	7
0	0	0	0
-890667	-2888490	-169868	-14611
-733348	-2371378	-142979	-12500.57
848910	-3122466	-346222.3	-656026.2



-23708.3	-1917265	-271646.7	-2382266
140324.5	-1676956	-308246.8	-2381972
-332456.3	-2051565	-118894.1	-554218.6
-42897.82	-163117.2	-10953.3	-1733.525
848910	0	0	0
-890667	-3122466	-346222	-2382266

pf5	pf6	pf7	pf8
8	9	10	11
14612	169867.6	2888505	890662.5
12501.15	142978	2371372	733350.1
656046.4	346221.1	3122475	-848911
2382261	271647.2	1917262	23705.97
2381967	308245.8	1676957	-140328.7

FIRE Engineering Report  
FY01 Update

554205.2	118893	2051566	332453.7
1733.258	10953.28	163116.6	42898.2
2382261	346221	3122475	890663
0	0	0	-848911

**PF3 and PF4 Radial Elastic and Thermal Expansion, 15 second 12T TF, 7.7 MA PF Flux Shifted 5V  
Copper IACS=100%, Packing Fraction=.85  
(pfk7.inp) Rc for PF3=3.0m, and Rc for**

**PF3, Shifted .05m in X -  
Whole Coil Net Loads -N**

Fradial(N)	Fvert(N)
0.0	0.0
14649.75	-2664954.
11639.56	-2243081.
-267092.6	-5932666.
-76344.37	-4461685.
-80688.23	-5049134.
-105129.1	-2090346.
1059.042	-172087.4

**PF4, Shifted .05m in X -  
Whole Coil Net Loads (N)**

Fradial(N)	Fvert(N)
0.0	0.0
1313.466	-230567.4
1166.676	-197225.1
-707847.6	-1.0511955E+07
-1060524.	-3.7704796E+07
-1059671.	-3.7701856E+07
-440641.4	-8827741.
-108.5507	-27405.71

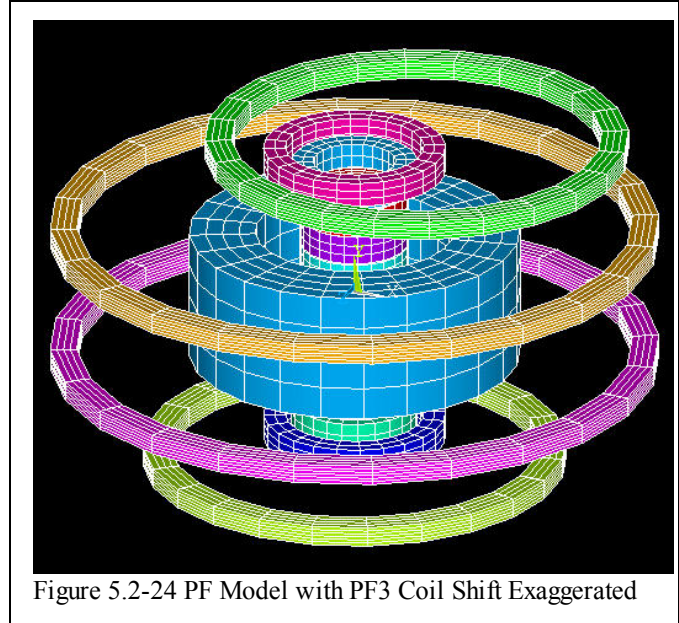


Figure 5.2-24 PF Model with PF3 Coil Shift Exaggerated

**Coil Weights, and Lateral Loads for 1g  
horizontal Seismic Load**

Coil	Total Volume	Volume*8906 kg/m <sup>3</sup>	Mass*9.8 m/sec <sup>2</sup>
PF3	2.236m <sup>3</sup>	19914kg	195155N
PF4	3.279m <sup>3</sup>	29202kg	286187N

The magnetic loads with the coils shifted, for the most part are restoring forces, so magnetic stability of the elastic restraints is not an issue

CS/PF Von Mises Stresses MPa, Kessel 12T TF, 7.7 MA 15 second PF Scenario, kcs6, Upper Number is "Smeared", Lower Number is is for Packing Fraction=.85 (Stress Multiplier=1.17),

	PRE	SOD	SOF	SOB	EOB	EOC
PF3	.9 1.	.7 .82	.7 .82	42 49	44 51	72 85
PF4	.4 .5	.3 .35	.33 .39	170 200	170 200	62 73

The coil centerline radius, Rc for PF3=3.0m, and Rc for PF4=4.4m

The Radial elastic growth of PF3 is 72 MPa/120 Gpa\*3.0m=.0018m

The Radial elastic growth of PF4 is 200 MPa/120 Gpa\*4.4m=.00733m

**PF4=4.4m**

Coil	Final Temp K	Rc*(14.4e-6-13.3e-6)*80 (Cooldown)	Rc*14.4e-6*(T-80) (Heat-Up)	Elastic Growth when Energized	Total Radial Differential Growth
PF3	91.7	-.69mm	.5mm	1.8mm	1.61mm
PF4	128.9	-1.012mm	3mm	7.33	9.318mm

The vertical tierods are not intended to be tensioned at installation. When the radial growth occurs, the coils are bearing against case in compression, and the vertical tierods would be unloaded, and the coil would grow under the clamp bar. For additional insurance the bolts could be provided with a loose fit and spherical washers.

**Allowable Stresses for Rods and Fibreslip Bearing Pads**

**Tensile Properties for Stainless Steels**

Material	Yield, 80 deg. K (MPa)	Ultimate, 80 deg. K (MPa)	Yield, 292 deg. K (MPa)	Ultimate, 292 deg. K (MPa)
304 SST 50% CW	1344	1669	1089	1241
304 Stainless Steel (Bar, annealed)	282	1522	234	640

## FIRE Engineering Report FY01 Update

The PF Supports should always be at LN2 temperatures under the limiting loads. The allowable for a cold worked or Drawn Rod =  $1669/3=556\text{MPa}$ . There is good data for fibreslip at JET for 30 MPa, ITER to 90 MPa and for the CIT study, up to 200 MPa. Fibreslip as a specific product may be unavailable, but similar materials are currently supplied by Dupont.

load and be stiff enough to develop the required force.

2cm Deep Groove edge Bearing Stresses  
Ten Effective Areas, Each Groove Bearing Area  
is  $800*10=8000\text{sq. mm}$

### Vertical Rod Loads and Stresses

PF	DW+ 1g Seismic Vertical Load per Rod, 32 effective	1/2 in-12.7mm Stress Area	Stress
PF5	17887N	$126.7\text{mm}^2$	141 MPa

Magnetic Offset 1060524 N (PF4)	1 g Seismic Lateral Load 286187N (PF4)	Re-Centering After Shot 42930N	Re-Centering during Shot 3.8MN
13 MPa	4 MPa	.5 MPa	47.5 MPa

The sliding grooves are the preferred solution.

The lateral force capacity is related to a summation of sine theta components around the circumference of the coil. The radial groove design has bi-directional capacity, and all 16 would contribute to the summation. This produced an effective groove bearing area of 10 times the individual bearing area, or  $8000\text{mm}^2$  for a 2 cm deep groove. The radial build of PF3 and PF4 is .4 m. The 16 unidirectional radius rods behave as though only five are fully effective.

### Re-Centering Friction Loads

If the coil finds itself offset on its support pads or shelves, the grooves or radius rods need to be strong enough and stiff enough to re-center the coil. The dead weight of PF4 is 286,187N. With the coil resting on the teflon pads, or a fibreslip groove, with friction coefficients of .15, the lateral load needed to slide the coil would be 42930N. If rods were used there would be an equivalent of 5 one inch diameter radius rods effective. The rod stress would be  $42930/5/506=17\text{ MPa}$ . The Groove bearing stress would be  $42930/10/8000=.5\text{MPa}$  for the 2cm groove. Both concepts will be able to center the coil between shots.

It should also be shown that during a shot, that the grooved pads or radius rods can overcome friction and center the coil. For PF4, the largest vertical load is 2.38MN per sector or 38.08 MN for the whole coil. For a friction coefficient of .1, the re-centering load could be 3.8 MN and this would produce  $3.8\text{e}6/5/506=1501\text{ MPa}$  for the one inch rod, and 48 MPa for the 2cm deep groove. At the force needed to center the coil, the rods would be over-stressed. Rod diameters would have to increase to support the centering

## 5.3 Vacuum Vessel

### 5.3.1 Introduction

The vacuum vessel, shown in Fig. 5.3.1-1, provides the vacuum environment for the plasma as well as the first confinement barrier for radioactive materials. The vessel also serves as the support structure for all in-vessel components, provides the first level of nuclear shielding, and helps provide for the passive stabilization of the plasma. The vessel system includes the torus, the ports and port extensions, the gravity supports, the supports for internal components, the passive stability plates, the internal control coils, and the integrated coolant/bake-out lines.

### 5.3.2 Vessel Concept

The vessel torus is a double wall sandwich structure consisting of 15 mm thick inner and outer face-sheets attached to poloidal ribs. The space between the face-sheets, which varies from 20 mm on the inboard side to 540 mm on the outboard side, is filled with radiation shielding material and coolant. Water at 20-50 C and 1 MPa is used to remove nuclear heating during normal operation. The water temperature is raised to 150C for heating the vessel and internals during bake-out. The shielding material can be single sized stainless steel balls with a packing fraction of about 60% or stacked plates with a

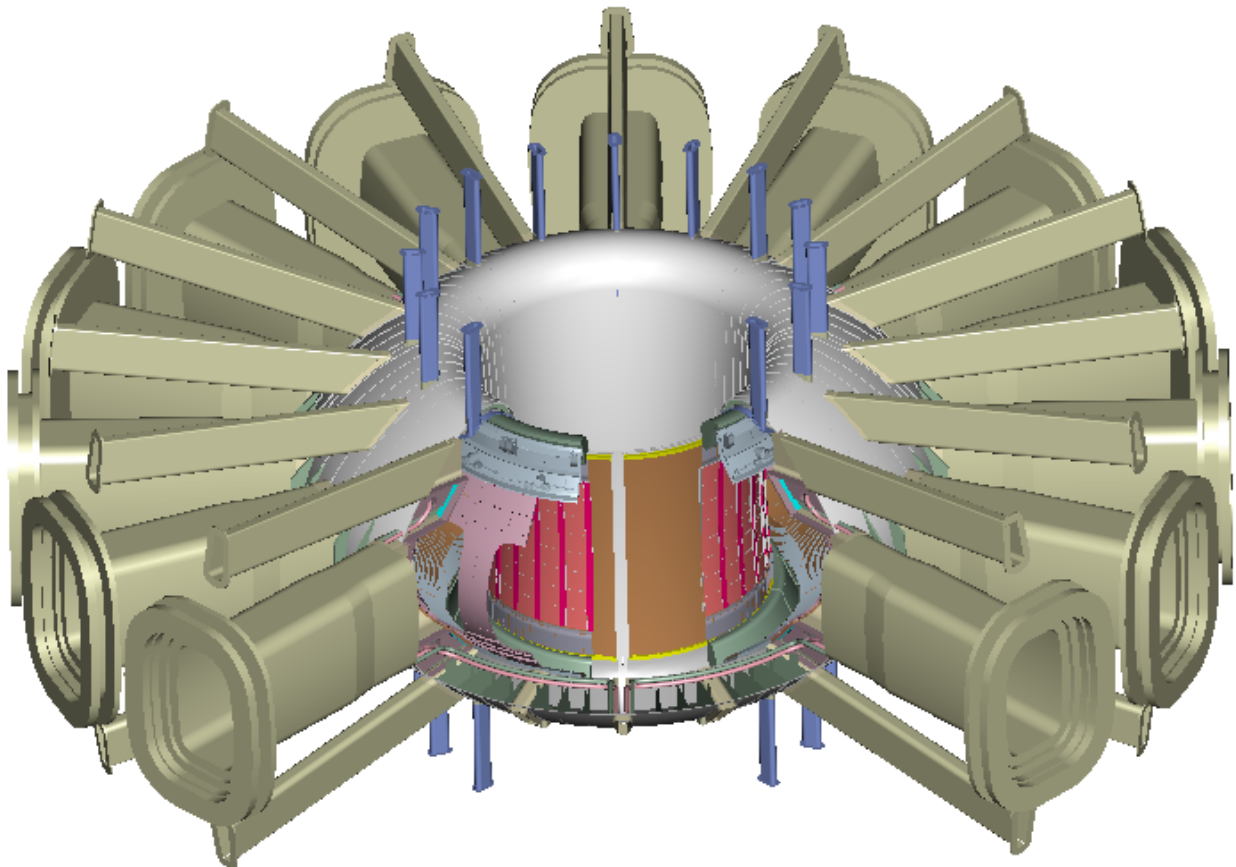


**Figure 5.3.1-1 Vacuum vessel with port extensions and internal components**

FIRE Engineering Report  
FY01 Update

similar packing fraction. The vessel parameters are summarized in Table 5.3.2-1.

The primary advantages of the double wall structure include higher bending stiffness (for a given total material thickness) and better integration of cooling and shielding. Most vacuum vessel designs in use (JET, JT60, DIII-D) and most designs on the drawing board (ITER, KSTAR) use full or partial double wall vacuum vessels. Figure 5.3.2-2 shows a cutaway of the vessel and pertinent dimensions.

There are 16 sets of access ports around the torus, which are used for RF heating, remote maintenance, diagnostics, internal cooling, fueling, and pumping. There are large, 1.3 x 0.7 m midplane ports, upper and lower trapezoidal ports approximately 0.15 x 0.5 m, and upper and lower oblong vertical ports

**Table 5.3.2-1 Vacuum Vessel Parameters**

**Dimensions and Weights**

Vol. of torus interior	35 m <sup>3</sup>
Surf. area of torus interior	89 m <sup>2</sup>
Facesheet thickness	15 mm
Rib thickness	15 to 30 mm
Wt. of structure incl ports	50 tonnes
Wt. of torus shielding	80 tonnes

**Power**

Direct neutron heating:	~200 MW
Indirect first wall load	< 40 MW

**Cooling**

Coolant	Water
Pressure	~ 1 Mpa
Normal oper. temp.	< 100C
Bake-out temp.	~150C

**Materials**

Torus, ports and structure	316L ss
Shielding	304L ss

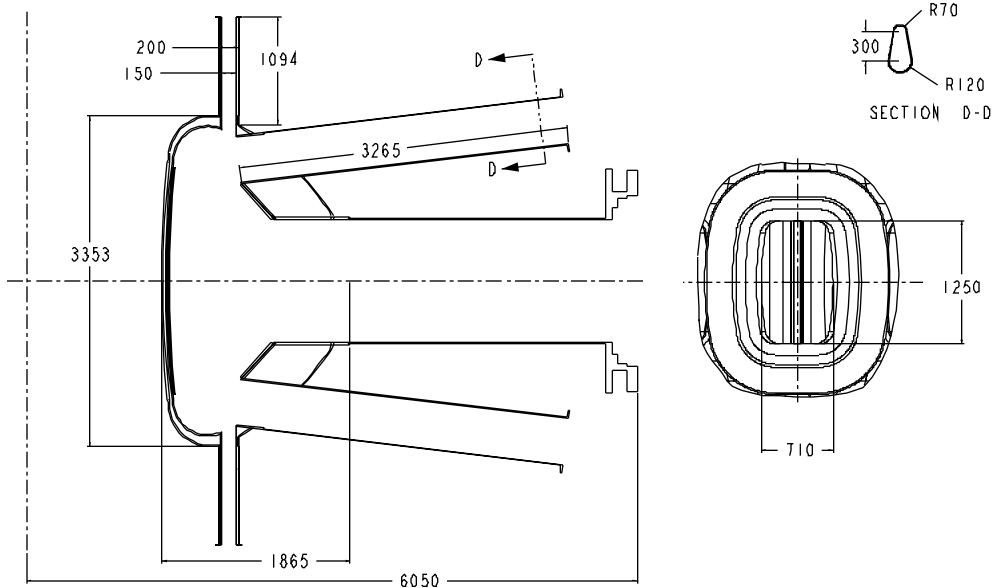


**Figure 5.3.2-2 Vessel and port dimensions**

FIRE Engineering Report  
FY01 Update

approximately .08 x 0.15 m in size. The sets of port openings are identical at each toroidal location to provide structural and design symmetry, but the port extensions may be varied to match their specific purpose. The port extensions are required to extend the vacuum boundary past the TF coil legs and through the cryostat region.

### 5.3.3 Vessel loading and analysis

The vessel is subjected to large gravity, seismic and electromagnetic loads, as summarized in Table 5.3.3-1. The total vertical load is estimated to be about 20 MN, while the net lateral load is about 7 MN. To react these loads, the vessel is

supported near the midplane on the outboard side via vertical and lateral links to the TF coil structure. The vertical links are attached to the radial ribs to spread the applied loads vertically into the vessel. This minimizes the local bending stresses in the vessel and provides a means for adjusting the vessel location globally relative to the TF coils. Lateral supports are located near the vertical links, and are tied to the top of the midplane ports.

The vessel must support all internal components, including the divertor assemblies, the passive stability structure, and the first wall tiles. The outboard divertor modules are actively cooled via pipes at each of the upper and

**Table 5.3.3-1 Vacuum Vessel Loading Conditions**

<b>Load</b>	<b>Value</b>	<b>Unit</b>	<b>Comment</b>
<i>Gravity load</i>	~ 3.5	MN	Vacuum vessel = ~130 tons FW tiles and divertor= ~35 ton Port mounted equip = ~100 - 150 tons
VDE load Vertical Lateral, net	16-32 6-11	MN MN	[ref. J. Wesley, "Disruption, VDE, and runaway electron conversion: physics basis and issues for FIRE", May 1, 2000]
Seismic load Vertical acceleration. Lateral acceleration	0.2 (tbd) 0.2 (tbd)	g g	
Max total vertical load	~ 22 - 42	MN	Gravity + VDE*1.2 dyn. factor
Max total lateral load	~ 8 - 14	MN	VDE*1.2 dyn factor + seismic
<i>Max local EM load</i> Local pressure on vv From internal components	~ 4 - 7	MPa	Local pressure on inboard wall due to halo currents, peaking factor ~ .75 Ip
EM load from TF field ramp	~ 0.75	MPa	Assumes 20 s ramp to or from full field Max load at inboard midplane
Coolant pressure Normal operation Bake-out	< 10 < 10	atm atm	Water assumed as coolant and for bake-out

FIRE Engineering Report  
FY01 Update

lower auxiliary ports. The passive stabilizing structure is actively cooled with imbedded cooling tubes. The first wall tiles and inboard divertor are cooled by conduction to the passive structure. All components must have robust supports to react the electromagnetic loads from a plasma disruption.

Preliminary structural analysis of the vessel indicates that the present dimensions are acceptable to support the various loads. A finite element model was developed for an earlier version of the vessel geometry, and the stresses and deflections obtained are summarized in Table 5.3.3-2. As seen in the table, there are some peak stresses around the divertor supports at the top of the vessel that must be mitigated with additional structure. Details of the stress and

deflection analysis are contained in Appendix D of this report.

### 5.3.4 Passive plates and internal coils

As indicated in Section 2, Physics, a system of highly conducting and actively cooled passive plates and a set of internal control coils must be incorporated into the vacuum vessel. The passive plates consist of 25 mm thick copper sheets that are bonded directly to the surface of the vacuum vessel. The sheets are actively cooled via internal water passages connected

**Table 5.3.3-2 Preliminary Stress Analysis Summary for the FIRE Vacuum Vessel**

Load condition	Torus and support points		Ports and (Support points)	
	General stress <sup>a</sup> (allowable stress = 195 MPa)	Peak local stress <sup>a</sup> (allowable = 390 MPa)	General stress (allowable = 195 MPa)	Peak local stress <sup>a</sup> (allowable = 260 MPa)
1. Gravity (w/ internals)	15	23	(24)	(45)
2. Vacuum load	~10	~25	TBD	TBD
3. Coolant pressure <sup>b</sup> (1 MPa)	~100	~230	TBD	TBD
4. Simulated VDE <sup>c</sup>	<100	~240	(~ 300)	(~400)
5. Halo Loads on divertor	120	170	(~150)	(>400)
6. Thermal stress from nuclear heating <sup>d</sup>	170	300	<200	~330
7. TF ramp-up <sup>e</sup>	~ 25	~ 32	TBD	TBD
Combined, 1,2,3,7	83	124		
Combined 1,2,3,6		240		400

<sup>a</sup>Estimated demarcation between general and peak local stress, peak primary + secondary = 3 × S<sub>m</sub>.

<sup>b</sup>Stress values estimated from previous analysis.

<sup>c</sup>VDE loads applied in simplified manner as body force, supports on outside.

<sup>d</sup>Temperature gradient of ~90°C based on 20-s full-power pulse, simulated temperature distribution.

<sup>e</sup>Stress estimate based on 20 s current ramps in TF coils.

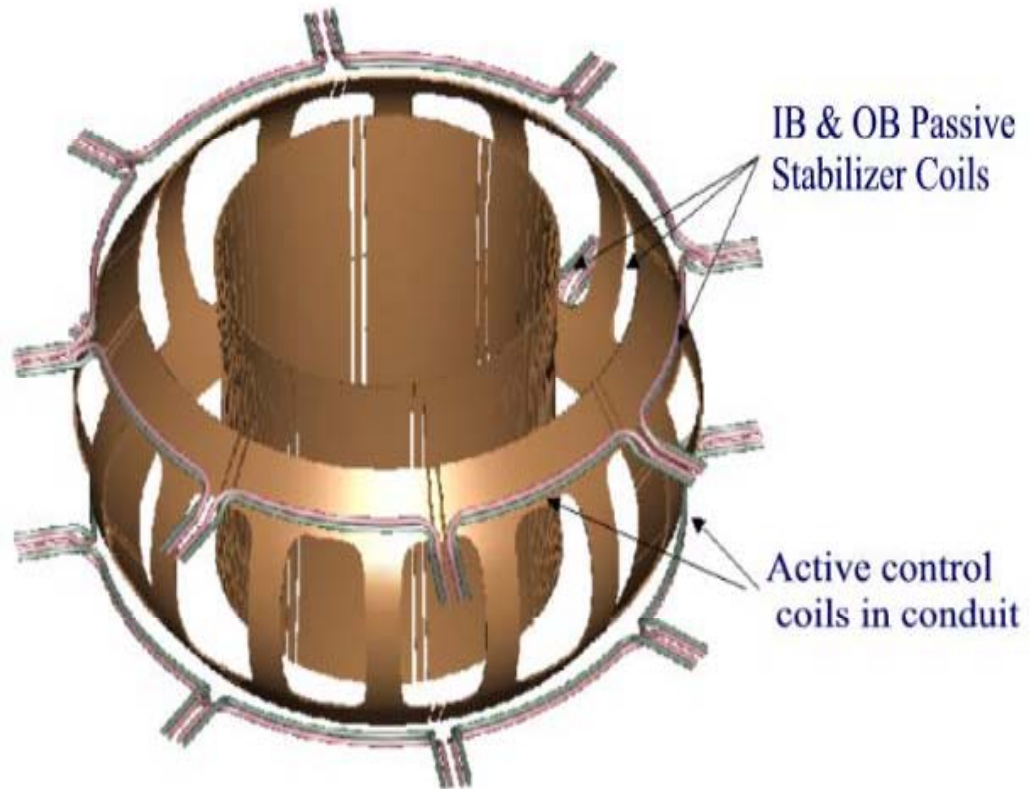


**Figure 5.3.4-1 Active control coils and passive stabilizing system**

through manifolds into the vessel cooling system. A bonded connection is thought to be the most straightforward approach, since cooling can be provided directly by the copper plates to both the

first wall tiles and the vessel, and continuous structural support can be provided to the passive plates by the vessel. The method of bonding has not been decided, but hot isostatic pressing (hipping) is one possibility. The geometry of the passive plate system is shown in Figure 5.3.4-1.

In addition to the passive plates there are a pair of control coils located between the outboard walls of the vessel above and below the midplane ports. Multiple turns of conductors are run in permanent pairs of conduits that are routed directly

through the outboard wall. The conductor will receive a moderately high radiation dose ( $>10^9$  Rad) and will be insulated with either MgO or a polyimide insulation system. Redundant turns are being considered to mitigate one of the failure modes. Each coil is designed to carry up to 75 kA.

### 5.3.5 Fabrication and assembly

The vessel is fabricated in octants, as shown in Figure 5.3.5-1. Each octant consists of the torus, associated gravity and internal supports, short reinforcing stubs around the major port openings and the active and passive stabilizer systems. At assembly, each vessel octant is rotated into the bore of a pre-assembled TF coil pair and connected via the support links. The TF/VV

FIRE Engineering Report  
FY01 Update

subassemblies are then positioned relative to each other with the mating joints located at radial planes between TF coils, through the center of the ports.

using remote welding equipment as part of the ITER R&D program. After the vessel is welded, the gaps in the passive stabilizers are filled with plasma sprayed copper to complete the upper and lower

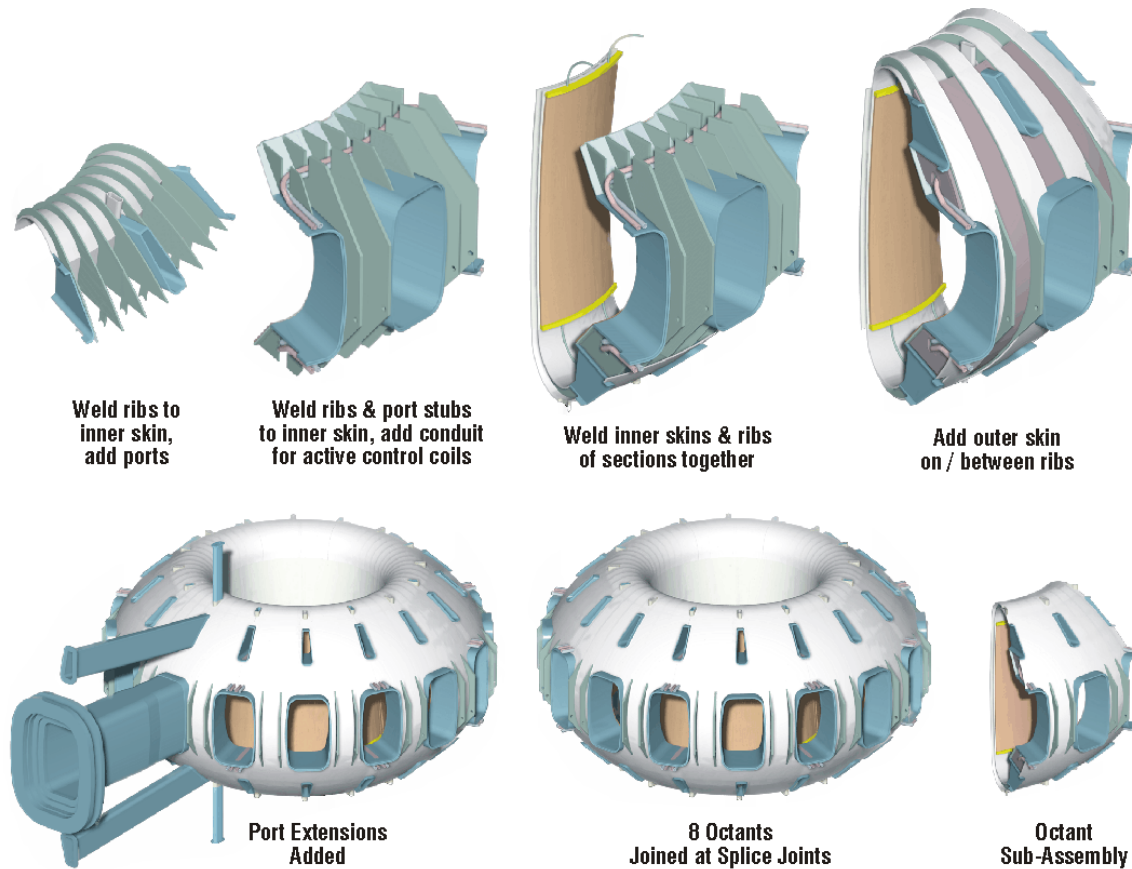


**Figure 5.3.5-1 Vacuum Vessel Assembly Via TF/VV Octants**

When all the octants are in place and positioned, they are welded together from the plasma side of the torus. The field joint for the double wall structure uses splice plates on the plasma side to provide a means for accessing the coil-side facesheet from the plasma side of the torus. This type of joint has undergone significant, full scale testing

stabilizing circuits. After the torus is welded, the port extensions are fitted and welded to the port stubs. This completes the vessel assembly.

## 5.4 Plasma Facing Components (PFC) Design Description

### 5.4.1 Introduction

The FIRE device is designed for high power density and advanced physics operating modes. The divertor must accommodate the high elongation and high triangularity plasma needed for advanced physics modes. This section describes the initial divertor design based on the baseline plasma shape. Additional plasma shapes and operating conditions will be specified during later design phases. The divertor geometry is forced to be quite open due to the short distances from the x-point to the plate and the spreading of the field lines. The connection lengths are short and the scrape-off layer (SOL) thickness is small. Without

a radiative divertor the heat loads are high ( $\sim 25 \text{ MW/m}^2$ ). The intrinsic impurity content of the plasma (2% He and 3% Be) is sufficient to reduce the outer divertor heat loads to about  $20 \text{ MW/m}^2$ . Addition of small amounts of neon can cause complete detachment of the outer divertor.

The divertor plate geometry is shown in Figure 5.4.1-1. The outer divertor plate is at an angle of  $30^\circ$  with respect to the flux lines. This is driven by the flux surface spreading close to the X-point. The inner divertor plate is nearly normal to the field lines. The inner divertor is relatively open, but easily detaches due to the low power load in the double null conditions in FIRE. The slot between the outer divertor plate and the baffle provides for pumping plasma exhaust particles.

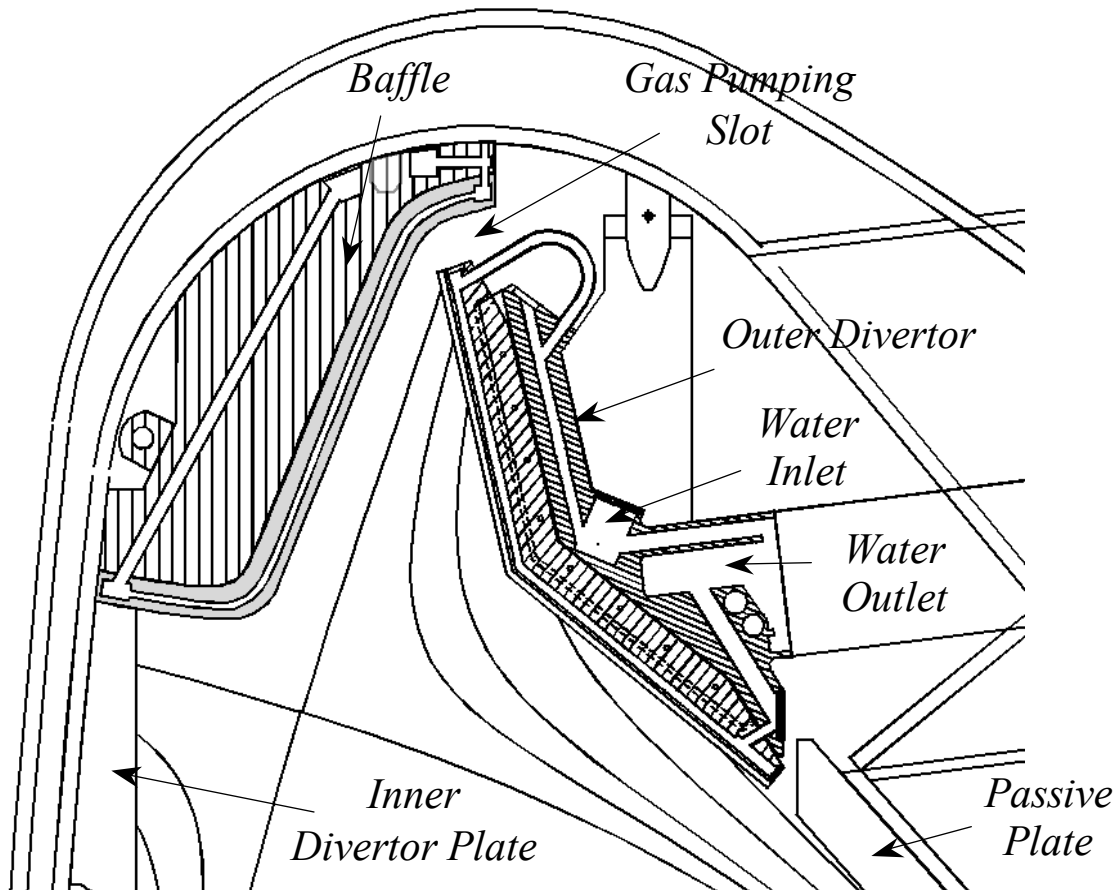


Figure 5.4.1-1. Cross-section through the actively cooled outer divertor module and baffle.

## 5.4.2 Physics Basis For PFC Design

### 5.4.2.1 Operating Conditions

Four cases have been assessed for FIRE operation: (1) the baseline D-T operating mode (10 T, 6.6 MA, 18 s) with a plasma exhaust power of 52 MW; (2) a high field operating mode (12 T, 66 MW, 12 s), (3) an advanced physics D-D operating mode (4 T, 2 MA, 215 s) with a plasma exhaust power of 17 MW; and (4) a long-burn D-T mode (8 T, 5.5 MA, 31 s) with a plasma exhaust of 44 MW. The following assumptions are made concerning the distribution of these total exhaust powers: 20% is radiated from the main plasma deposited on the main wall, 20% is radiated from the scrape off layer with all being deposited on the baffle and divertor throat, 20% is deposited on the inner divertor plate, and the remainder goes to the outer divertor plate.

### 5.4.2.2 Edge Plasma Modeling For Attached Divertor Conditions

The UEDGE code was used to calculate the expected edge conditions in FIRE. For all

cases considered the power into the scrape-off layer was 28 MW and the separatrix density was  $1.5 \times 10^{20} / \text{m}^3$  with a wall recycling coefficient of 1.0. Three different values of the particle and heat diffusivity were considered. The parameters in Case C duplicate edge plasma data from existing machines the best and were the conditions used for the ITER design. The divertor plate was kept perpendicular to the field lines for most cases. Case D is the same as Case C with the divertor plate tilted as in the baseline design and with  $10^{21}$  particles/sec pumping. The conditions for the various cases are shown in Table 5.4.2.2-1.

The results are shown in Table 5.4.2.2-2. The peak heat flux is less than  $25 \text{ MW}/\text{m}^2$  for all cases. The outer divertor is not detached under any of the conditions considered. Additional gas will have to be added to the model to get the outer divertor to detach. Table 5.4.2.2-3 shows the ratio of the power to the divertor plates to the power in the scrape-off layer. The power radiated to the first wall ( $P_{\text{wall}}$ ) and the power radiated by hydrogen are also shown. It can be seen that the inner divertor is detached for all cases considered.

Table 5.4.2.2-1 Plasma transport parameters used for modeling the FIRE edge plasma.

Case	Description	Thermal diffusivity ( $\text{m}^2/\text{s}$ )	Particle diffusivity ( $\text{m}^2/\text{s}$ )
A	High Conductivity	1.5	1.0
B	ITER Conductivity	0.5	1.0
C	Bohm like diffusivity	0.5	$D_{\text{bohm}} + 0.1$
D	Tilted plates and pumping	0.5	$D_{\text{bohm}} + 0.1$

Note:  $D_{\text{bohm}} = T_e/16 \text{ eB}$

Table 5.4.2.2-2 Results of UEDGE modeling of the FIRE edge plasma

Case	$T_{e_m}$ (eV)	$\lambda_m$ (cm)	$T_{e_p}$ (eV)	$n_{e_p}$ ( $10^{21}/\text{m}^3$ )	$Q_p$ ( $\text{MW}/\text{m}^2$ )	$\lambda_p$ (cm)
A	106	0.8	1.5	61	5.7	6.5
B	152	0.6	15	44	25	1.8
C	138	0.7	14	43	23	2.3
D	138	0.7	13	52	19	2.5

FIRE Engineering Report  
FY01 Update

Table 5.4.2.2-3 The ratio of power to the divertor plates and the wall to the power in the scrape-off layer for the various cases.

Case	$P_{in}/P_{sol}$	$P_{out}/P_{sol}$	$P_{wall}/P_{sol}$	$P_{hrad}/P_{sol}$
A	0.003	0.24	0.34	0.42
B	0.002	0.53	0.12	0.35
C	0.005	0.58	0.11	0.31
D	0.09	0.57	0.10	0.24

**5.4.2.3 Edge Plasma Modeling for Detached Divertor Conditions**

The UEDGE Code has been used to study the effect of adding Beryllium and Neon to the edge plasma to stimulate detachment of the plasma in the outer divertor channel. The divertor plates were placed at the proper angle relative to the field lines for these calculations. The particle diffusivity and thermal conductivity had to be reduced on the small radius side of the plasma to achieve a single solution. One expects that the transport will be reduced on the small radius side of the plasma because of the good curvature in that region (this is consistent with the observations of less power transport to the inner divertor in a double null configuration).

The inner divertor is easily detached from the plate. With no impurity addition to the inner divertor the heat flux to the plate is about 1 MW/m<sup>2</sup> from particle transport and 1.8 MW/m<sup>2</sup> from hydrogen radiation. We

used 3 MW/m<sup>2</sup> for the heat flux on the inner divertor.

The results for the outer divertor with the angled plates are very similar to the results for the plate normal to the field lines (26 MW/m<sup>2</sup>). When Be is added to the divertor region, the peak heat flux is reduced to 20 MW/m<sup>2</sup> with about 5 MW/m<sup>2</sup> of radiated power located at a different location from the peak particle heat flux. There was no detachment with the addition of Be alone. With Neon injection, the plasma could be detached from the divertor plate. For 4.1 Pa m<sup>3</sup>/s (31 Torr l/s) Ne injection there was no detachment but the peak heat flux was reduced to 15 MW/m<sup>2</sup>. With 4.7 Pa m<sup>3</sup>/s (35 Torr l/s) Ne injection, the plasma did detach from the divertor plate but the solution evolved toward an x-point MARFE (see Figure 5.4.2.3-1. Note that the radiated power is 80 MW/m<sup>3</sup> in the MARFE region. It is clear that the amount of Ne injected into the divertor needs to be controlled, but the range of injection that is needed is TBD. A scheme for feedback control of the Ne injection will have to be developed.

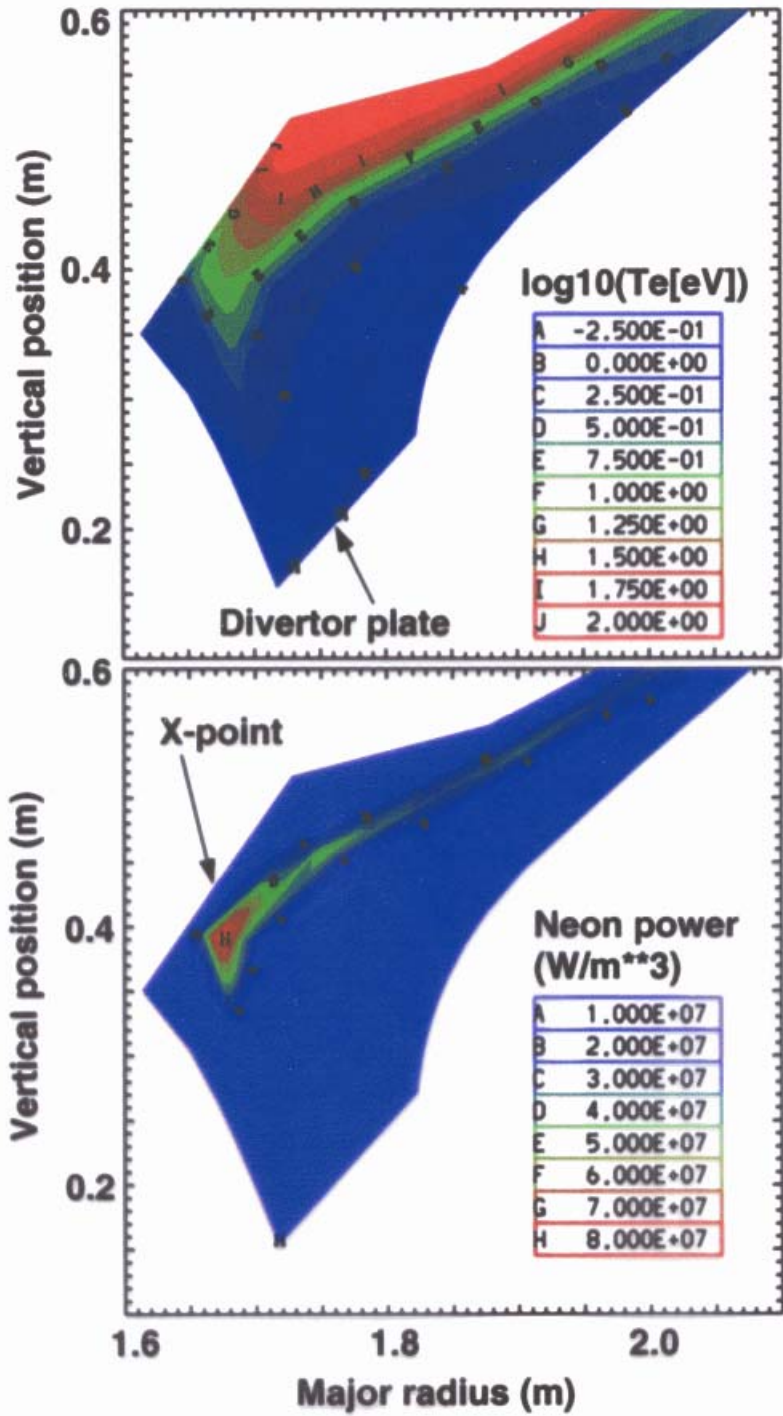


Figure 5.4.2.3-1 Detached outer divertor solution calculated by the UEDGE code

**5.4.2.4 Erosion Due to Normal Plasma Operation**

The erosion of the W and Be plasma facing materials due to normal plasma operation has been assessed using a combination of the DEGAS2, REDEP/WBC and BPHI codes. The plasma conditions calculated by UEDGE, were used as input to the DEGAS2 code to determine the charged and neutral particle fluxes to the divertor plates. An example of the results of the DEGAS2 modeling for the attached outer divertor case is shown in Figure 5.4.2.4-1. The plasma temperature and density profiles from UEDGE were then used to calculate the detailed characteristics of sputtered tungsten transport using the WBC code. The code includes the sputtered atom velocity distribution, electron impact ionization, Lorentz force motion, magnetic and Debye dual structure sheath, impurity-plasma

charge changing and velocity changing collisions.

The WBC redeposition parameters were used as input to the REDEP code that computes self-consistent gross and net erosion rates over the entire outer divertor region. The results predict zero net erosion of the divertor plate and no plasma contamination (see Figure 5.4.2.4-2). This is mostly due to the short mean-free path for ionization for W ( $2.4 \times 10^{-5}$  m). The gross sputtering is mostly due to impurity sputtering (due to 0.1% O impurity) and self-sputtering. The effect of Be and Ne impurities in the edge plasma need to be added to the calculation. The detached plasma solution will also have to be analyzed.

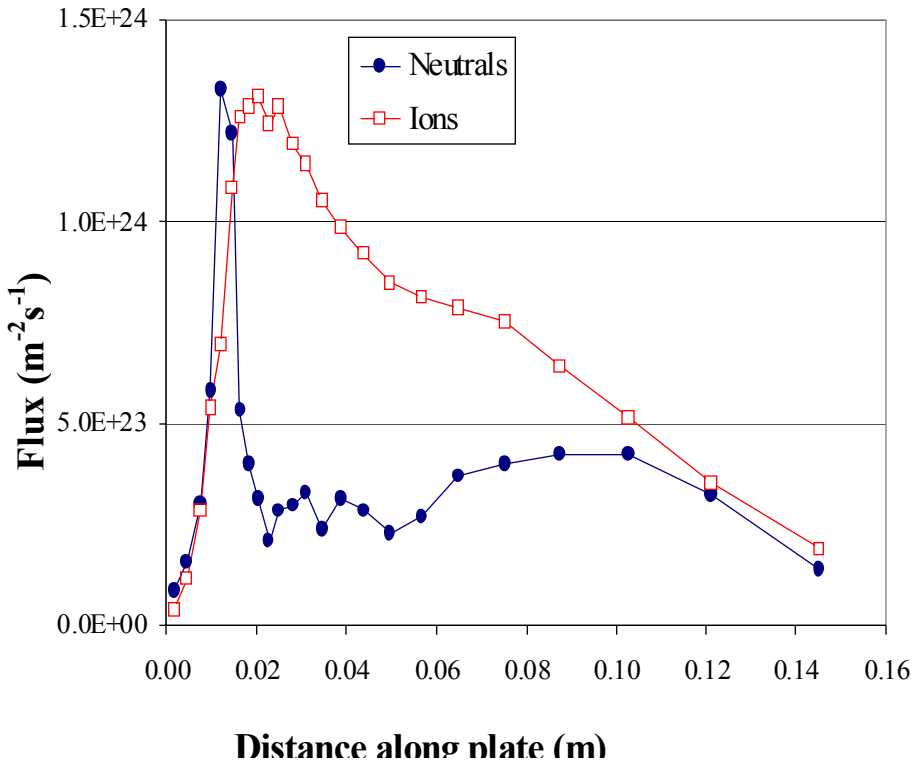


Fig. 5.4.2.4-1. Particle flux on the outer divertor plate from DEGAS2

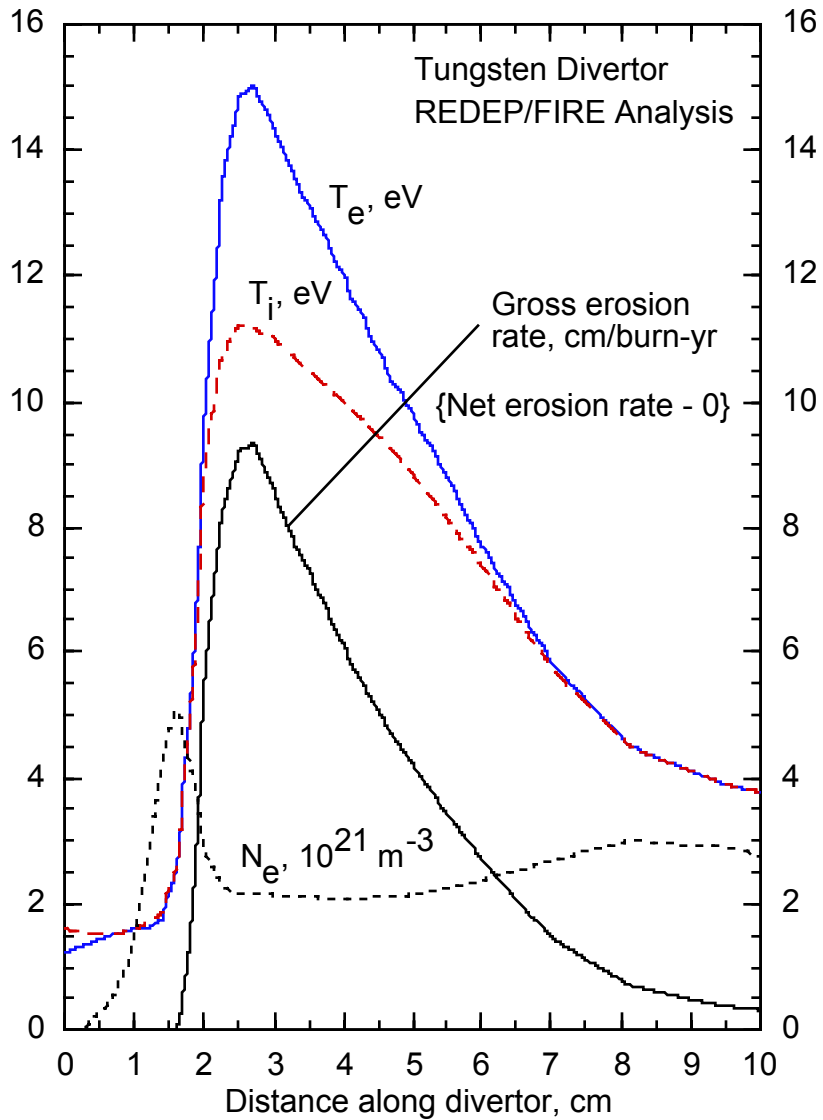


Figure 5.4.2.4-2. Results of the REDEP/WBC analysis of gross and net erosion on the outer divertor

**5.4.2.5 Particle Pumping Requirements**

The loss of particles from the plasma can be estimated by considering the total number of particles in the plasma and the particle confinement time. The total number of particles in the plasma ( $NV$ ) is  $1 \times 10^{22}$ . The energy confinement time is 0.5-0.8 s (we will use 0.65 s). Typically we take the particle confinement time to be 2-10  $\tau_E$ . This

yields a required fueling rate of  $3.1 \times 10^{21}/s$  ( $1.25-10 \times 10^{21}/s$ ). If we assume the fueling efficiency is 50%, the required fueling rate is  $6.2 \times 10^{21}/s$  ( $23 \text{ Pa m}^3/s$ ; range 10-75  $\text{Pa m}^3/s$ ). We recommend 75  $\text{Pa m}^3/s$  as the maximum fueling rate (net with equal D and T).

We have also estimated the particle-pumping rate required for He removal. The fusion burn rate (helium generation rate) is  $1 \times 10^{20}/s$  (200 MW). If we assume the He

fraction in the divertor is 0.02 and the wall recycling coefficient 0.5, the required divertor pumping is  $1.4\text{-}2.7 \times 10^{22}/\text{s}$  ( $50\text{-}100 \text{ Pa m}^3/\text{s}$ ). This result is very similar to the previous estimate of fueling required. In order to have some excess capacity in the pumping system, we recommend providing pumping for up to  $100 \text{ Pa m}^3/\text{s}$ .

**5.4.2.6 Disruption Heat Loads**

Using the disruption conditions specified in the Physics Design Document, the energy deposition on the divertor plates and first wall can be estimated. Two phases have been identified for disruptions; the thermal quench phase when the plasma stored energy is lost to the divertor and the current quench phase when the plasma current decays and the magnetic stored energy is lost to the first wall. We have assumed a plasma-stored energy of 33 MJ. There is a wide range of possible parameters describing disruption energy deposition, so the energy deposition is specified as a range of possible values. The wide range arises because of incomplete understanding of disruption deposition on existing devices, variation in the deposition observed, and uncertainties in the extrapolation to FIRE conditions. The values specified for the disruption analysis are shown in Table 5.4.2.6-1.

During the current quench phase of a disruption, the plasma is very cold and highly radiative. The magnetic stored energy is radiated to the first wall during the current decay. The stored magnetic energy in the FIRE reference plasma is 35 MJ. The expected minimum current decay time is 2-6

ms. The average energy deposition on the first wall is  $0.5 \text{ MJ}/\text{m}^2$ . If we assume a toroidal peaking factor of 2:1, the peak energy deposition is  $0.67 \text{ MJ}/\text{m}^2$ . This is enough energy to melt 0.12 mm of Be if all the energy goes into melting. Thermal conduction and radiation will reduce the amount of melting. This should give an adequate lifetime for the first wall but further modeling is required.

**5.4.2.7 Assessment of Disruption Damage to the Divertor Plasma Facing Surfaces**

The HEIGHTS computer code package was used to model the damage of plasma facing components due to disruption energy deposition. The code package includes the effect of plasma-target interactions, plasma-debris interactions, photon radiation and transport, and plasma-melt layer interaction. A typical result for  $10 \text{ MJ}/\text{m}^2$  deposition in 1 ms is shown in Figure 5.4.2.7-1. It can be seen that melting starts about  $10 \mu\text{s}$  after the disruption thermal quench starts. Vaporization starts about  $20 \mu\text{s}$  later. Once vaporization starts there is a strong reduction in the heat flux because of interaction between the plasma and the atoms in the vapor (vapor shielding). Because of vapor shielding, the amount of melted and eroded material is only weakly dependent on the energy deposited. A comparison of  $100 \text{ MJ}/\text{m}^2$  and  $10 \text{ MJ}/\text{m}^2$  is shown in Figure 5.4.2.7-2. It can be seen that the amount of vaporized material increases by about a factor of two due to the ten-fold increase in energy deposition. This insensitivity of the amount of melted or vaporized material to the energy deposition eliminates much of the

Table 5.4.2.6-1 Disruption energy deposition on the divertor plates

	Low End	Most Likely	Reference	High End
Inner Divertor	$8 \text{ MJ}/\text{m}^2$	$31 \text{ MJ}/\text{m}^2$	$13.4 \text{ MJ}/\text{m}^2$	$96 \text{ MJ}/\text{m}^2$
Outer Divertor	$4 \text{ MJ}/\text{m}^2$	$16 \text{ MJ}/\text{m}^2$	$6.8 \text{ MJ}/\text{m}^2$	$48 \text{ MJ}/\text{m}^2$

FIRE Engineering Report  
FY01 Update

variation due to the uncertainty in the disruption energy deposition. The analysis of divertor lifetime is therefore easier to estimate. The melt layer is predicted to be

150 to 200  $\mu\text{m}$  thick and 2-4  $\mu\text{m}$  is predicted to evaporate due to a disruption.

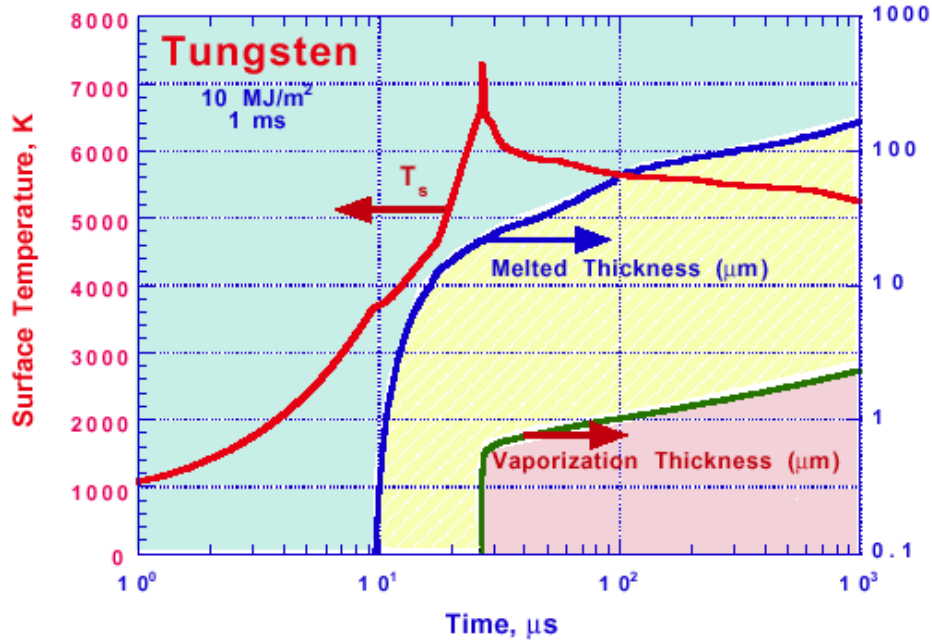


Figure 5.4.2.7-1. Calculation of the effects of disruption energy deposition on the divertor.

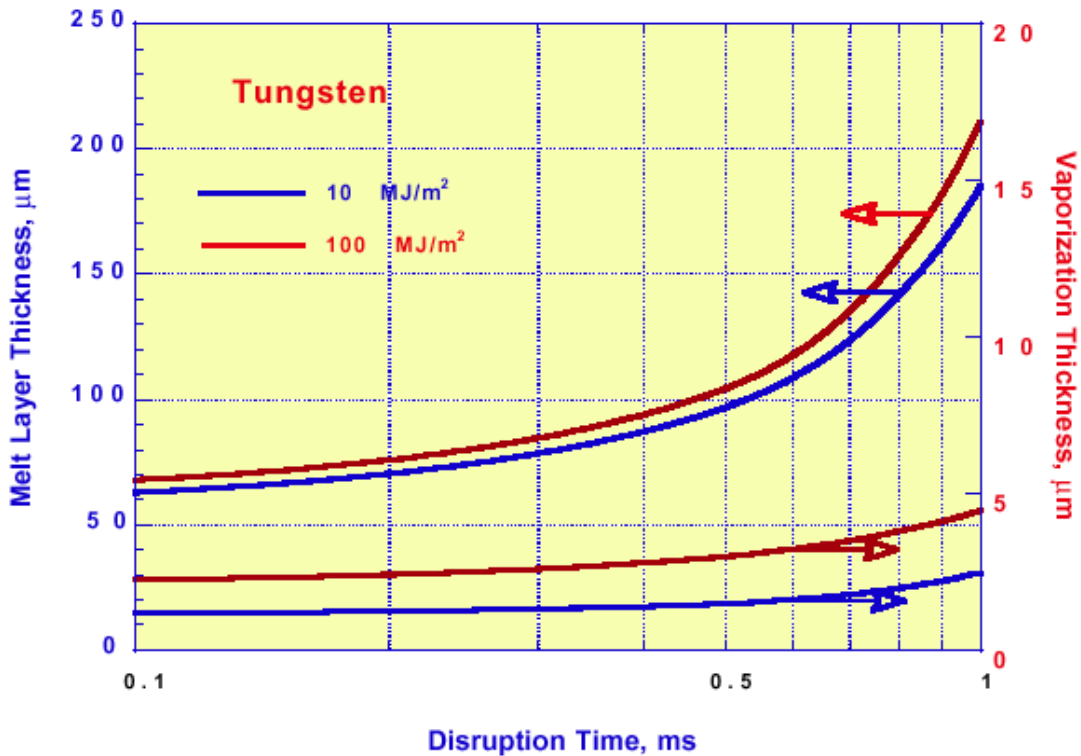


Figure 5.4.2.6-2. The effect of the size of the energy deposition on the amounts of material melted and vaporized in a disruption.

Sudden melting of a tungsten surface can cause splashing of the melted layer. Analysis of the amount of splashing has started. The droplets of splashed material will also interact with the incoming plasma (droplet shielding). The lifetime of the divertor depends strongly on the fraction of the melt layer that is lost on each disruption. If no melted material is lost, the lifetime of the divertor tungsten is a few thousand disruptions (or nearly the life of the machine since only 3000 full power pulses are planned). Loss of the melt layer (or even as little as a quarter of the layer) will result in a lifetime of only a few hundred disruptions. Replacement of the divertor a few times during the life of the machine is expected if part of the melt layer is lost.

#### **5.4.2.8 Possibility of Disruption Mitigation**

Experiments conducted on the DIII-D tokamak have shown that injection of massive amounts of gas can dissipate the plasma stored energy to a majority of the first wall, reduce halo currents, reduced the current decay rate, and does not cause runaway electron generation. Other work on ASDEX-U, JET, and DIII-D on neural networks has shown that, with proper training, a neural network can provide a highly reliable (>95%) warning about 50 ms before a disruption with a very small false alarm rate (<5%). Continued efforts along these lines are likely to improve the usefulness of such techniques to mitigate disruptions. It is very likely that these predictions are conservative.

#### **5.4.2.9 Halo Current Loads**

The halo current specifications from the Physics Design Document were used to estimate the halo currents flowing through the divertor and first wall components. Since the product of the maximum halo current fraction and the toroidal peaking factor is a constant for the worst-case halo currents, the halo current in the worst location is constant. The maximum current flowing through a divertor module is 200 kA. The longest current path through the outer divertor is 0.4 m and the longest path through the inner divertor is 0.14 m. The calculated force on the outer divertor is 0.77 MN while that on the inner divertor is 0.3 MN. These forces are one of the requirements for sizing the supports for the divertor and the thickness of the support plates.

#### **5.4.2.10 Disruption Eddy Current Loads**

The duration of the current disruption specified in the Physics Design Document implies a maximum current decay rate of 3 MA/ms. This implies that a 6.5 MA plasma will decay in 2.2 ms. The Tokamak Simulation Code (TSC) has been used to simulate three disruption cases; 1) stationary disruption where the plasma stays fixed in the machine; 2) a vertical disruption event (VDE) where the plasma moves vertically for several hundred milliseconds before disrupting; and 3) a radially inward moving disruption. The VDE case is shown in Figure 5.4.2.10-1a-c. Approximately 900 filaments are used in the TSC disruption simulations.

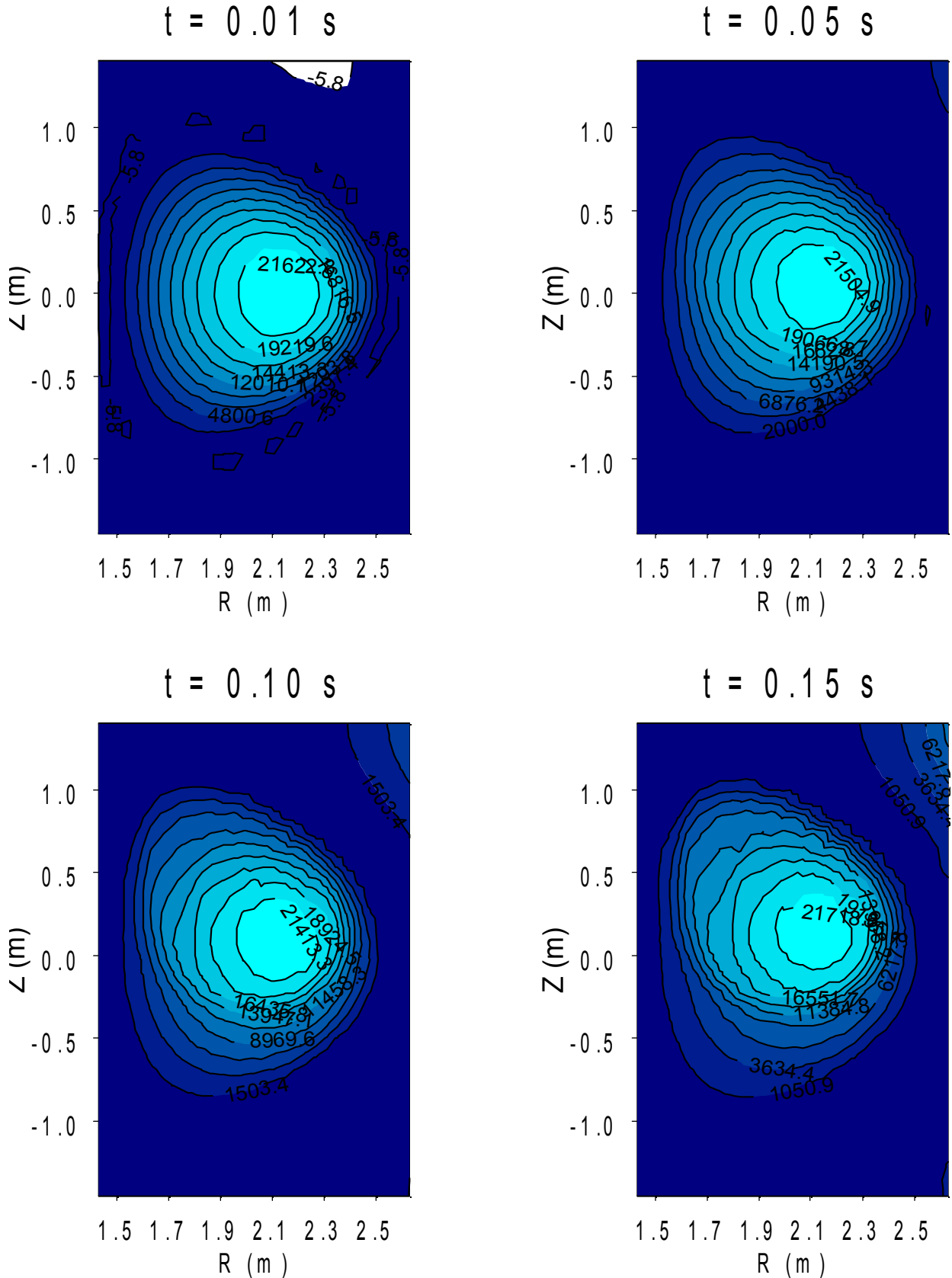


Figure 5.4.2.10-1a Contour plots of the plasma current density during a VDE from the TSC output.



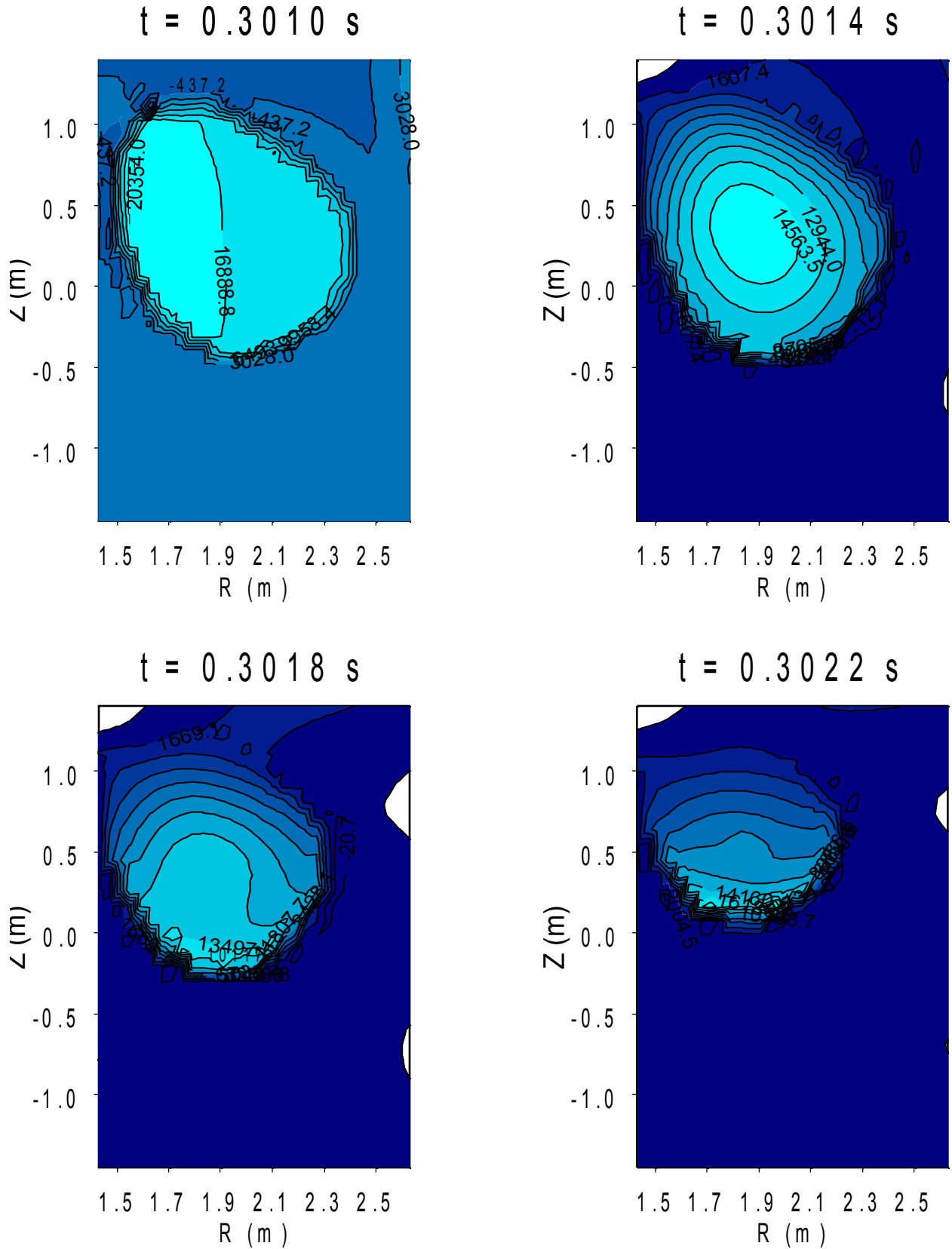


Figure 5.4.2.10-1a Contour plots of the plasma current density during a VDE from the TSC output.

The time variation of the current in the filaments is used as input to the calculation of eddy currents induced in the vacuum vessel and plasma facing components. The PC-Opera code (Vector Fields) has been used to calculate the induced eddy currents. The Opera model of the coils (solenoid, PF coils, and plasma current filaments) together with the vacuum vessel and plasma facing components is shown in Figure 5.4.2.10-2.

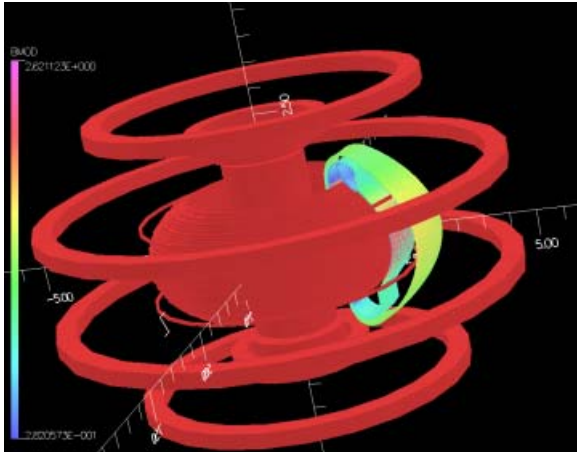


Figure 5.4.2.10-2 PC-Opera model of the FIRE coils, plasma and vacuum vessel segment used for disruption eddy current analysis.

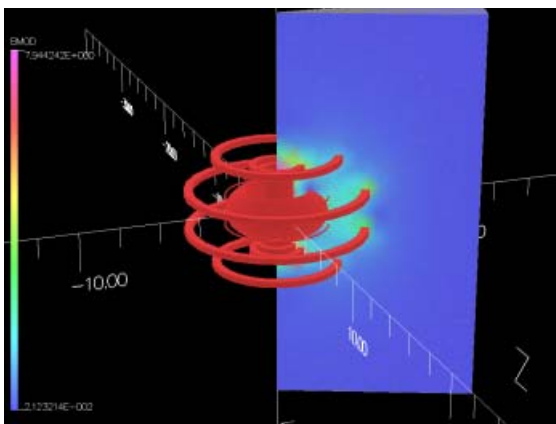


Figure 5.4.2.10-3 The blue wedge shows the limits of the computational region used for the PC-Opera analysis.

Only a 1/16 section of the machine structures needed to be modeled because of the symmetry. Time varying currents were

applied to each conductor based on the TSC data. A full vector potential calculation over the region shown in Figure 5.4.2.10-3 was completed for the entire duration of the disruption.

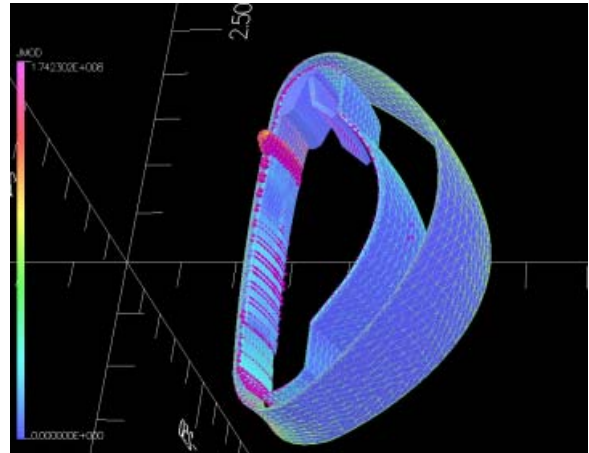


Figure 5.4.2.10-4 A vector plot of the currents induced in the passive plates during a VDE.

Figure 5.4.2.10-4 shows the eddy currents induced in the vacuum vessel and passive plates just before the current decay phase of a VDE. The passive plates carry very large eddy currents because they are toroidally continuous. A substantial reduction of the eddy currents in the divertor plates is realized because of the currents in the passive plates.

Figure 5.4.2.10-5 shows the eddy currents induced in the outer divertor plate at the time of maximum induced current. A similar plot for the baffle and inner divertor is shown in Figure 5.4.2.10-6.

The force on the PFCs is calculated by evaluating

$$F = \vec{J} \times \vec{B}$$

over the volume of the PFC where J is the induced current and B is the total magnetic field. This force information is the basis for

the stress analysis of the divertor plates and their mounts.

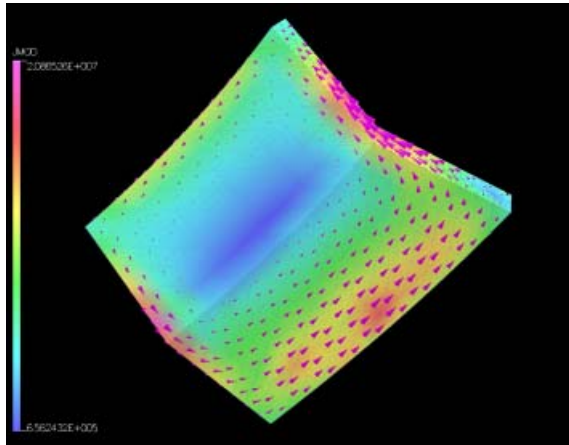


Figure 5.4.2.10-5 The eddy currents induced in the outer divertor plate during a VDE.

Analysis of the static and radial disruptions is still in progress. Based on past experience we expect the VDE to be the worst case for the PFCs.

### 5.4.3 Engineering Design

#### 5.4.3.1 Power Flows and General Thermal-hydraulic Design

Divertor component power flows are summarized in Table 5.4.3.1-1. There are 32 modules of each type (16 upper and 16 lower). For a uniform power distribution over these modules, each must handle the average power loads given in row two of the table. Assumptions used to arrive at the peak module power loads summarized in row three of the table include: (1) 1.2 for roof-tile shadowing of the module leading

edges, (2) 1.2 / 1.5 for toroidal asymmetries

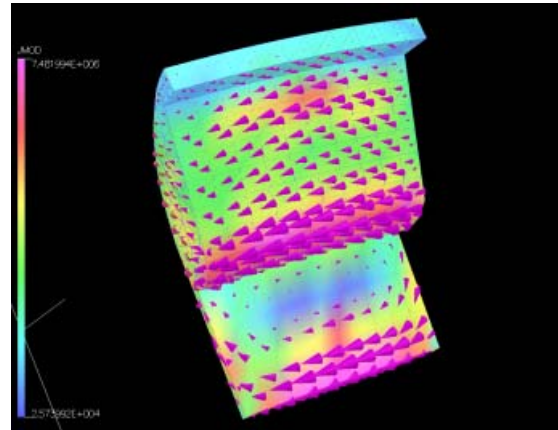


Figure 5.4.2.10-6 The eddy currents induced in the baffle and inner divertor during a VDE.

in exhaust power on the inner plate and baffle / outer plate, and (3) 1.2 for up-down asymmetries in exhaust power distribution. Based on proposed pulse lengths, the total energy that must be dissipated in each component is calculated in row 5 of the table. This shows that the most challenging of the three cases for the passively cooled inner plate and baffle is the long pulse D-D mode. Passively cooled component temperatures at the end of the pulse are estimated in the last two rows of the table, based on proposed module sizes and weights. This highlights that it is advantageous to combine the inner plate and baffle into a single component, assuming that both are copper, which provides a good thermal conduction path. The large mass of the baffle helps dissipate the inner plate power deposition and keeps final temperatures at a more manageable level.

FIRE Engineering Report  
FY01 Update

Table 5.4.3.1-1 Divertor Module Power Flow Summary.

Divertor Module Parameter	10 T Baseline (52 MW, 18 sec)			12 T Mode (66 MW, 12 sec)		
	Inner	Baffle	Outer	Inner	Baffle	Outer
Total Power Distribution (MW)	8.3	10.4	33.3	10.6	13.2	42.2
Avg Power to Module (MW)	0.26	0.33	1.04	0.33	0.41	1.32
Peak Power to Module (MW)	0.45	0.56	2.25	0.57	0.71	2.85
Pulse Length (sec)	18	18	18	12	12	12
Max Total Energy Input (MJ)	8.1	10.1	40.4	6.8	8.6	34.2
Module Volume (m <sup>3</sup> )	0.0076	0.0476	0.0437	0.0076	0.0476	0.0437
Module Mass (kg)	67.7	339.2	388.5	67.7	339.2	388.5
Initial Temperature (°C)	30	30	30	30	30	30
Average Final Temp (°C)	122	105	–	101	93	–
Front (W) Surface Temp (°C)	220	250	–	193	193	–
Rear Surface Temp (°C)	92	–	–	75	–	–

Divertor Module Parameter	Long Pulse (17 MW, 215 sec)			Long Burn (44 MW, 31 sec)		
	Inner	Baffle	Outer	Inner	Baffle	Outer
Total Power Distribution (MW)	2.7	3.4	11.0	7.0	8.8	28.2
Avg Power to Module (MW)	0.09	0.11	0.34	0.22	0.28	0.88
Peak Power to Module (MW)	0.15	0.18	0.74	0.38	0.48	1.90
Pulse Length (sec)	215	215	215	31	31	31
Max Total Energy Input (MJ)	31.8	39.8	159.1	11.8	14.7	58.9
Module Volume (m <sup>3</sup> )	0.0076	0.0476	0.0437	0.0076	0.0476	0.0437
Module Mass (kg)	67.7	339.2	388.5	67.7	339.2	388.5
Initial Temperature (°C)	30	30	30	30	30	30
Average Final Temp (°C)	100	325	–	146	139	–
Front (W) Surface Temp (°C)	153	>700	–	251	350	–
Rear Surface Temp (°C)	80	–	–	112	–	–

Using the same power loading conditions, module cooling channel design parameters and flow rates have been estimated. The results of this are summarized in Table 5.4.3.1-2. Based on the ITER vertical target design and manufacturing development, the FIRE divertor modules are divided into 24 copper “finger” plates across the front surface. This modular design configuration is described in the next section. It provides a simple part for initial fabrication and tungsten-armor joining / acceptance testing, and reduces electromagnetic loads by breaking up eddy current loops in the front, copper structure. The Critical Heat Flux (CHF) margin is provided by 10-m/s flow in the 8-mm-diameter cooling channels with swirl-tape inserts. Each copper finger

includes 2 cooling channels for a total of 48 across the heated surface. All channels are supplied in parallel giving an 18 liter/s inlet flow rate for each module and an estimated 0.4 MPa pressure drop in the module. The recommended inlet water conditions of 30°C and 1.5 MPa pressure give a minimum exit subcooling of 124°C for the peak heat loading condition. Remote cutting and welding operations for module removal are simplified by using a coaxial supply pipe layout. The inner coaxial pipe diameter of 80-mm accommodates insertion of remote cutting / welding equipment down the supply pipe, and also gives a supply pipe flow velocity of 3.6 m/s, which keeps pressure drops manageable in this portion of the cooling system.

Table 5.4.3.1-2 Outer Divertor Module  
Thermal-Hydraulic Design Summary.

Divertor Module Parameter	Value
Avg Power to Module (MW)	1.07
Peak Power to Module (MW)	2.32
Number Cooling Channels	48
Cooling Channel Dia (mm)	8.0
Flow Area, 25% SWT (mm <sup>2</sup> )	37.7
Water Flow Velocity (m/s)	10.0
Module Flow Rate (liter/s)	18.1
Water Inlet Temperature (°C)	30
Inlet Pressure (MPa)	1.5
Pressure Drop (MPa)	0.4
Exit Pressure (MPa)	1.1
Exit Saturation Temp (°C)	184.3
Nominal Temp Rise (°C)	14.2
Nominal Exit Temp (°C)	44.2
Nominal Exit Subcooling (°C)	140.1
Maximum Temp Rise (°C)	30.7
Maximum Exit Temp (°C)	60.7
Min Exit Subcooling (°C)	123.6
Inlet pipe flow velocity (m/s)	3.6
Inlet pipe ID (mm)	80.0
Coaxial pipe OD (mm)	122.7

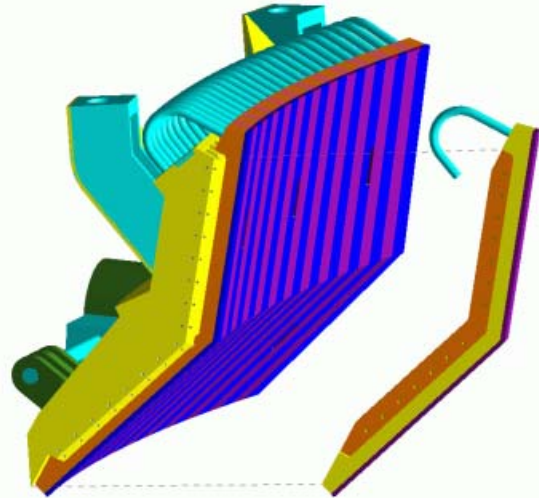


Figure 5.4.3.2.1-1. Outer Divertor Module Design. Alternating colors denote copper-alloy finger plates. Left-most plate is separated from backing plate for clarity.

### 5.4.3.2 Outer Divertor Module Design

#### 5.4.3.2.1 Design Description and Tungsten Armor Concept

The actively-cooled, outer divertor module design is shown in Figure 5.4.3.2.1-1 which can be used in conjunction with the Figure 5.4.1.1-1 cross-section to describe the module design features. The design concept builds on fabrication technologies developed for the ITER divertor and consists of 24, modular, copper-alloy “finger” plates that are mechanically attached to a stainless-steel support structure that spans the toroidal width of the module. The support structure includes machined distribution and collection manifolds that route coolant to the individual finger plates and features for remotely attaching the modules to the vacuum vessel.

The Figure 5.4.1.1-1 cross-section depicts the coolant flow path in the module. Coolant enters through the outer annulus of the coaxial supply pipe. It is distributed across the module toroidal width in the upper supply manifold and then flows upward through gun-drilled holes in the steel backing plate to curved, welded pipes that feed the front copper finger plates. Flow then passes down each finger plate in two parallel 8-mm-diameter channels, and exits at the bottom into the lower return manifold. A machined slot at the toroidal center of the return manifold routes coolant back to the inner return pipe. The 8-mm front-plate channels include swirl-tape inserts over the upper straight section for heat transfer enhancement.

#### 5.4.3.2.2 Module Fabrication and Assembly

Figure 5.4.3.2.2-1 illustrates further design features of the module using a toroidal section view. The copper alloy finger plates have a T-shaped back surface that fits into machined slots in the stainless structure as

FIRE Engineering Report  
FY01 Update

indicated. Press-fit pins are then inserted into angled holes to attach the copper front plates to the support structure. Over the upper section of the plate, where surface heat fluxes are highest, machined slots are used in place of the angled holes to allow the pins to slide axially relieving some of the stress build-up from thermal expansion in the highly heated copper front plate. The upper looped-pipes provide a flexible cooling attachment to the backing structure to accommodate this motion. These features

are not needed at the lower end of the target where surface heat fluxes are much lower. Finger plates are identical except at three locations in each module where one of the two axial holes is eliminated. This provides poloidal slots, as indicated in Figure 5.4.3.2.2-1, for insertion of remote handling grippers near the module outer edges and diagnostic access at the module centerline.

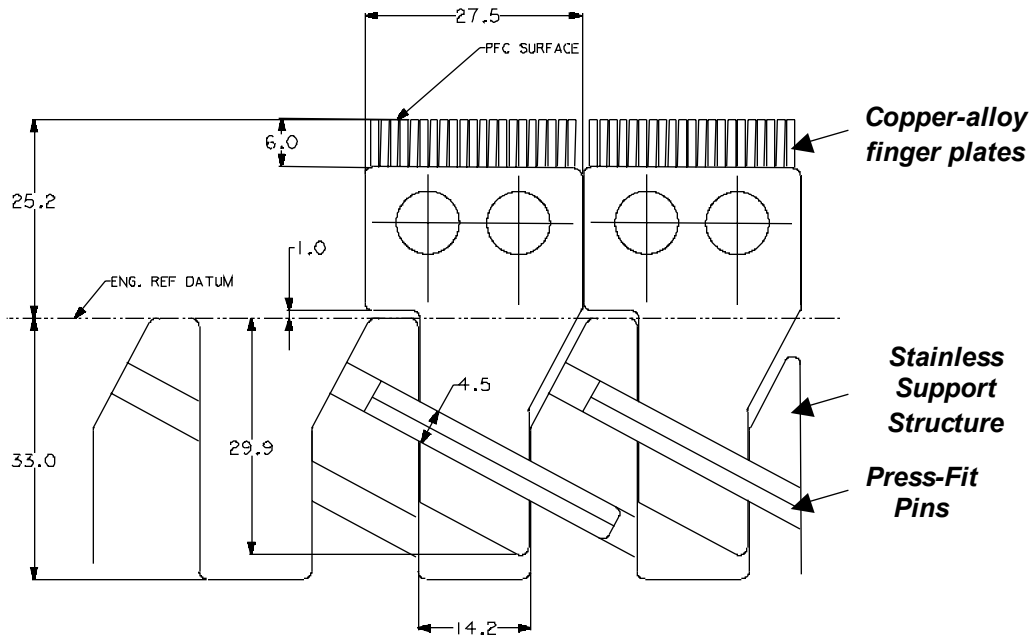


Figure 5.4.3.2.2-1. Angled Press-Fit Pins Attach Finger Plates to Stainless-Steel Backing Structure.

The copper fingerplates include tungsten-brush armor similar to the mock-ups depicted in Figure 5.4.3.2.2-2. This armor geometry has been shown to survive incident heat fluxes of 25 MW/m<sup>2</sup> for 1,000 cycles in testing at Sandia Labs using several different joining procedures. All of the brush armors use small-diameter tungsten (W) weld electrodes (3-mm preferred based on testing) that are fixtured in thin welded metal honeycomb for joining to the heat sink. The rod assembly can be direct-bonded (vacuum hot press or Hot Isostatic Press – HIP) to the heat sink or embedded in a layer of plasma sprayed

copper and then HIP-bonded or e-beam welded. Work is currently planned to down-select two of the W-brush-armor joining approaches for the fabrication of armored copper finger plates that are comparable in size to those proposed for the FIRE divertor. These mock-ups will include a heat-transfer enhancement mechanism in the cooling channel (swirl tape or helical wire insert) and be HHF tested under similar exit CHF conditions. This will complete a full-scale demonstration of critical heat sink fabrication and armor joining procedures for advanced, actively cooled divertor concepts like FIRE.

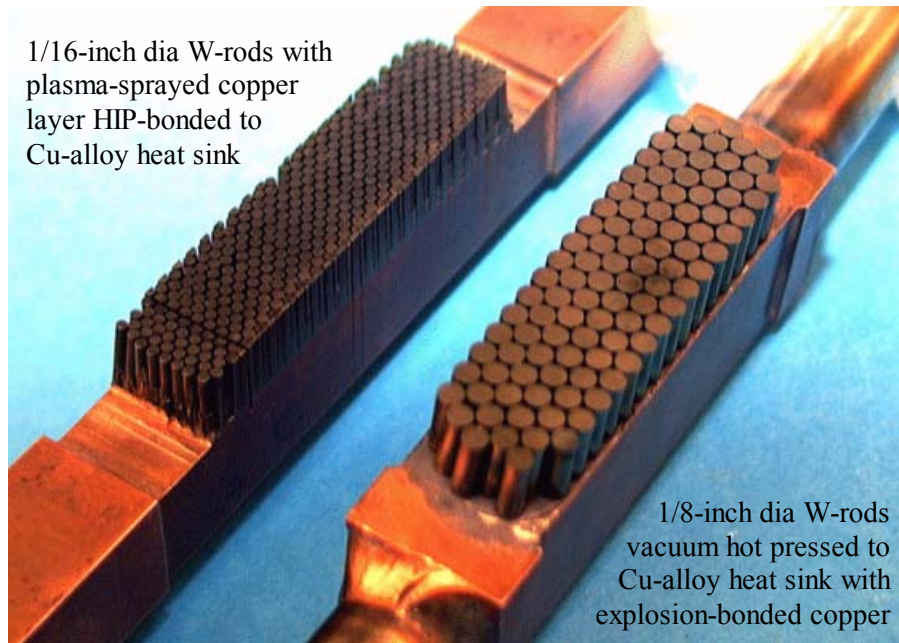


Figure 5.4.3.2.2-2. Two of the Tungsten Brush Armor Configurations Tested at 25 MW/m<sup>2</sup>.

#### 5.4.3.2.3 *Vessel Attachment and Remote Handling*

The divertor modules are mounted to the vessel using the lug and shear-pin arrangement indicated in Figure 5.4.3.2.3-1. To accommodate remote insertion and removal operations, the primary module-positioning feature involves two 42-mm-diameter vertical pins that are attached to the vessel as shown in Figure 5.4.3.2.3-2. The large mounting brackets shown in Figure 5.4.3.2.3-1 engage these conical-ended pins as the modules are raised or lowered into position by the in-vessel handling system. Final mounting holes in the modules are individually machined based on an in-vessel survey of the pin locations so the plasma-facing surface is correctly positioned in the magnetic field geometry. The upper section of these large pins are cylindrical allowing the module vertical position to be adjusted until the lower, locking pins can be inserted. The two locking pins are activated by radial

drive shafts that extend out the vacuum port adjacent to the cooling pipe as indicated. These pins are offset so each can retract into the solid lower portion of the inlet piping interface connection.

The module mounting hardware shown in Figure 5.4.3.2.3-1 was sized based on preliminary guidelines for halo current loading conditions. These guidelines assumed 240 kA for the maximum current. For the reference toroidal field strength of 10 T, and module poloidal length of 0.63 m, this implies a peak module halo current loading of 1.5 MN that must be reacted in the support structure. Assuming this load is distributed among the four module attach points with a peaking factor of 1.5, the design load on any one attachment is 0.56 MN. Using Inconel 718 pins, which have a structural allowable of 393 MPa at 200°C, the pin diameter must be 42 mm for a single shear-interface attachment. The lower locking pins use multiple shear interfaces to

reduce the pin diameter to 20-mm. These halo currents are slightly larger than the physics specification (see Sections 1.1.3 and 1.1.4), but the range of disruption eddy current loads, yet to be analyzed will likely require a larger pin.

Additional divertor module design and handling constraints are illustrated in the Figure 5.4.1.1-1 cross section view. Copper passive plates are required near the X-point for plasma stability, as indicated in the figure. These plates are mounted to the

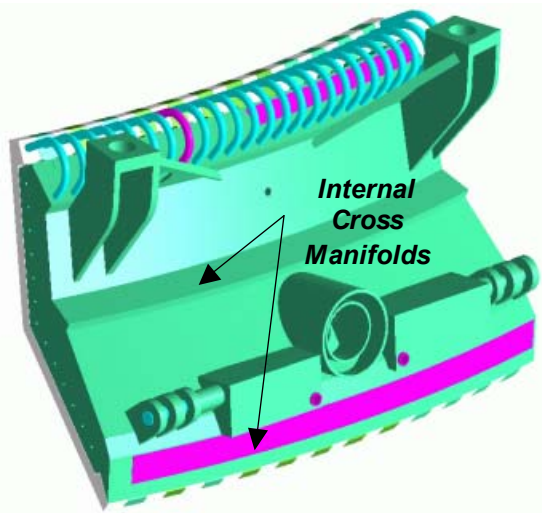


Figure 5.4.3.2.3-1 Outer Module Vessel Attachment and Remote Handling Features.



Figure 5.4.3.2.3-2 Divertor Module In-Position to Engage Vessel Attachment Hardware.

vacuum vessel for cooling and form a low-resistance toroidal loop. The outer divertor modules must clear the upper end of these passive plates during vertical installation and removal operations. This severely limits the space envelope for attachment and cooling interface structure at the lower end of the module. The cooling interface must remain at its present elevation in the vacuum port envelope because the upper section of the ports is reserved for cryo-pumps and diagnostic access. Finally, the attachment structure must not interfere with the finger plate cooling supply tubes and manifold channel cover plates, yet be stiff enough to react disruption electromagnetic loads. Detailed loading conditions have not yet been calculated for the FIRE modules, but it appears that the general attachment layout shown in Fig. 5.4.3.2.3-1 can be adapted to meet these design constraints.

#### 5.4.3.2.4 *Stress Analysis of Divertor Components*

The forces from the disruption eddy currents were used to evaluate the stresses in the divertor components. A typical stress distribution on the outer divertor is shown in Figure 5.4.3.2.4-1. Stresses slightly exceed the allowables for 316 type stainless steel, but we are investigating ways to reduce the stress to make 316 acceptable. Until those attempts succeed, our baseline material for the divertor supports is Inconel 718. Further design work is needed on the mounting fixtures because local stresses are too high. This work will continue in FY02.

#### 5.4.3.3 *Inner Module, Baffle and First Wall Design*

##### 5.4.3.3.1 *Inner Plate and Baffle Design and Armor Concept*

The inner divertor plate and baffle are expected to require minimal cooling for the

reference FIRE power loads and pulse lengths. The baffle structures are cooled elements that fill the flux space between the inner and outer divertor channels. The baffle configuration is shown in Figure 5.4.3.3.1-1 for reference.

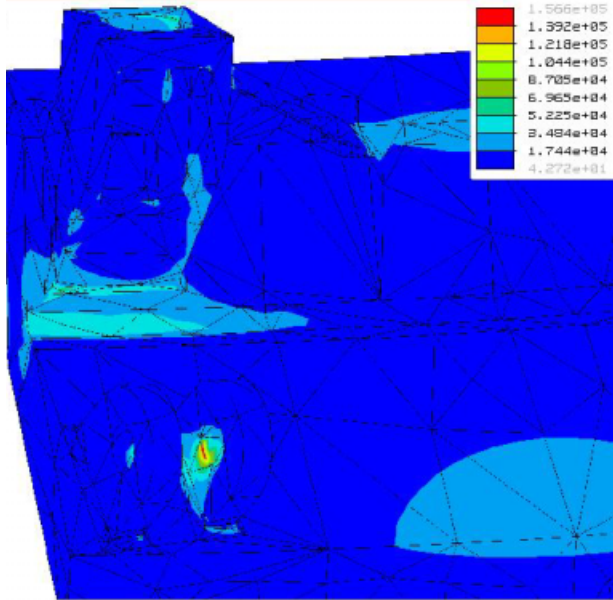


Figure 5.4.3.2.3-1 Results of stress analysis of the outer divertor plate due to the forces from eddy currents during a VDE.

The first wall consists of passively cooled, mechanically attached tiles that line the inner and outer vessel surface between mid-plane ports. They are made from 40-mm thick formed/machined CuCrZr plate covered with 5-mm of plasma-sprayed Be armor. The plates fit between wedge-shaped vertical rails that are bolted to the vacuum vessel as indicated in Fig. 5.4.3.3.1-2. The rails are segmented to facilitate local tile removal. The gaps allow for easy insertion and differential tile thermal growth during operation. Armored copper cover plates secured by washer-loaded quarter-turn fasteners hold the tiles against the vessel during normal operation.

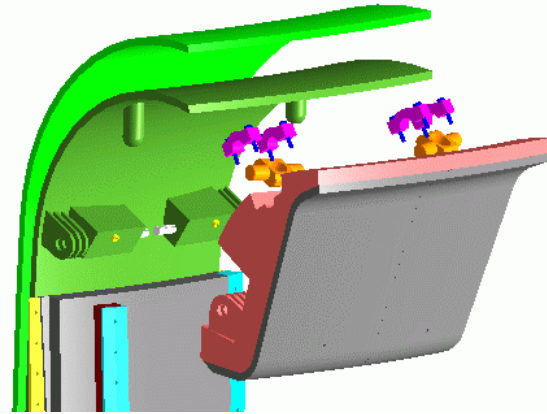


Figure 5.4.3.3.1-1. Baffle configuration and attachment concept.

Passive inner plate and baffle temperature excursions for the proposed FIRE operating conditions are summarized in Table 5.4.3.1-1. This table shows that the low field, long pulse operating mode is the most challenging one for passive cooling. As is summarized in Table 5.4.3.1-1, these plates appear to have sufficient energy storage to survive anticipated heat loads without excessive temperature excursions. They are then slowly cooled between pulses by conduction to the vacuum vessel. When more definitive power flow distributions and design concepts are available, 2-D thermal models will be developed to determine temperature distributions in these components and verify that temperature excursions are acceptable for all operating modes.

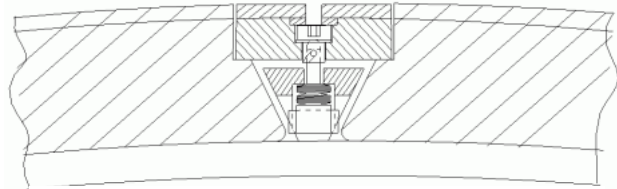


Figure 5.4.3.3.1-2 First-wall tile attachment

The design requirements call for a 10 sec pulse length. Since the heat soaks into the plasma-facing component during the pulse, the back surface temperature where the

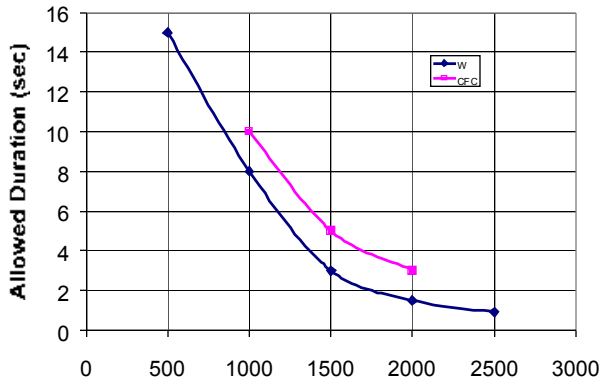


Figure 5.4.3.3.1-3 Allowed pulse duration to not exceed 700°C on the back face of a 3 cm thick tile.

material is attached to the heat sink will likely be the most limiting factor (not the surface temperature). Figure 5.4.3.3.1-3 shows the allowed pulse duration for various heat fluxes assuming the temperature at the connection does not exceed 700°C. Heat loads on the first wall are low compared to the divertor. Beryllium on the first wall can be used up to about 3 MW/m<sup>2</sup> for 10 sec.

5.4.3.3.2 *First Wall Design Considerations*

Figure 5.4.3.3.2-1 shows the temperature increase a 5-mm tungsten / 30-mm copper first wall structure experiences, under 30 W/cm<sup>2</sup> incident heat flux, for different thermal cooling assumptions at the rear surface. The upper curves assume no rear surface cooling. The middle curves assume a 0.14 W/cm<sup>2</sup>-K interface conductance at the rear surface, which is representative of limited-area mechanical attachments. The lower curves assume a 1.4 W/cm<sup>2</sup>-K interface conductance at the rear surface, which is representative of active cooling over ~10% of the rear surface area. The 30 W/cm<sup>2</sup> incident flux is derived for the long pulse D-D operating mode assuming that all 21 MW of exhaust power is radiated uniformly to the first wall. Figure 5.4.3.2-1 shows that active cooling is likely to be required for the long pulse operating modes.

Mechanical attachments could possibly accommodate a 2-min pulse, but the vessel must provide a 30°C heat sink at the mechanical attach points. This would require special cooling of these attachments to assure that large temperature gradients are not induced in the 15-mm thick, stainless steel vessel shell.

It therefore appears that active cooling of the first wall should be considered to provide more robust long-pulse operation. This could be accommodated by incorporating a cooling header between the two vessel shells at the top and bottom of the machine that feeds water to the baffle. The water would then flow through the first wall modules in a limited number of cooling channels to keep the copper temperatures under control and exhaust into the vessel at the mid-plane. Non-uniform radiative loading effects must also be evaluated to determine appropriate local peaking factors for the 30 W/cm<sup>2</sup> incident flux.

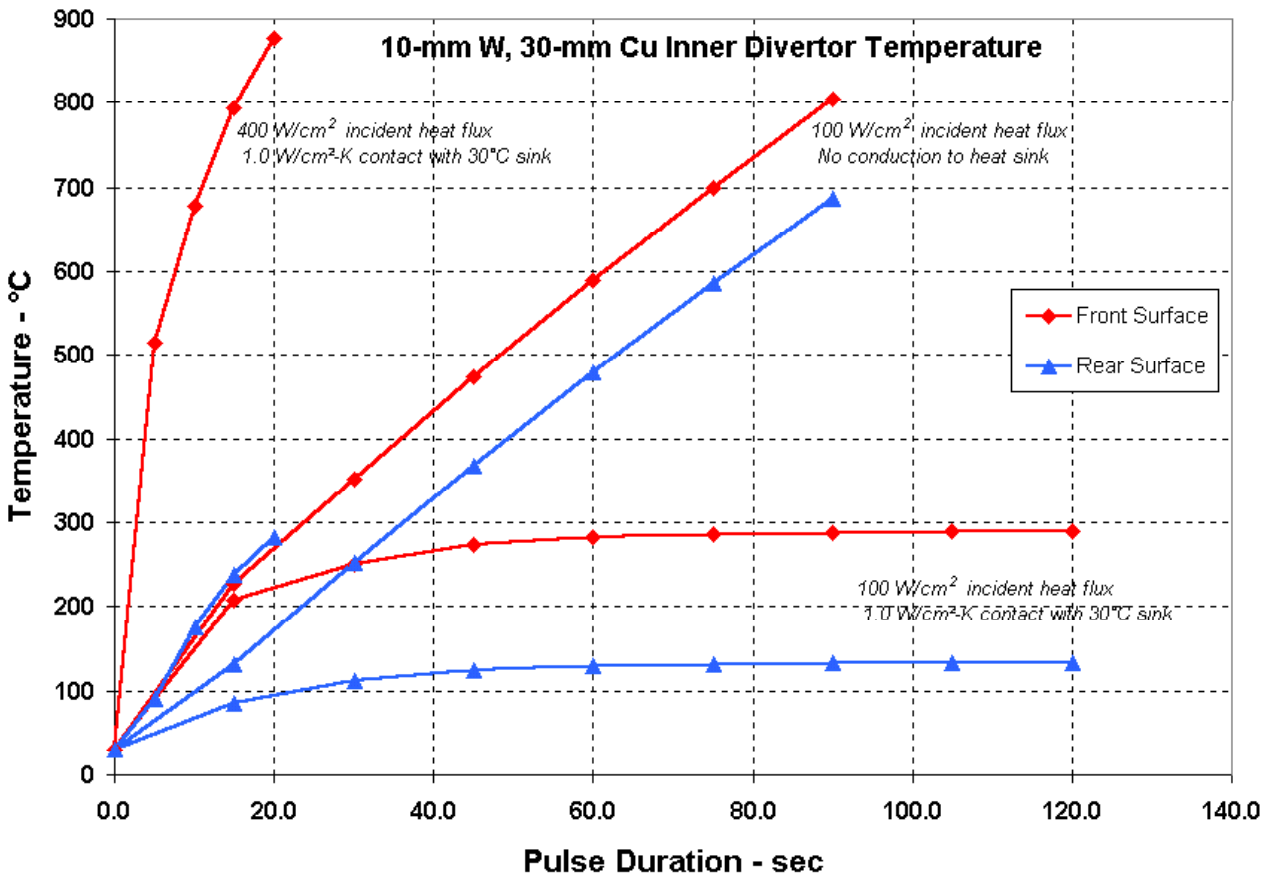


Figure 5.4.3.3.2-1. Predicted Wall CHF for the Proposed FIRE Divertor Module Cooling Channel Design Concept and Exit Coolant Conditions.

5.4.3.3.3 CHF Assessment

As described in Section 5.4.2, each outer divertor module consists of 24 segments, 28 mm in width and 550 mm in length. There are two coolant channels of 8 mm ID per segment. The flow direction is poloidal so that power input to each channel is equal. The maximum power flow to a divertor module is 2.32 MW. Since the peak heat flux is estimated to be 20 to 25 MW/m<sup>2</sup>, a heat transfer enhancement method will be used to achieve the necessary critical heat flux (CHF) with moderate velocities and flows. A review of enhancement methods shows that a swirl tape insert is an attractive option due to available performance data

and extensive fabrication experience for this geometry.

Figure 5.4.3.3.3-1 shows CHF at the coolant channel wall (WCHF) calculated for the divertor module at three different inlet pressures and a range of inlet flow velocities for an inlet temperature of 30 C. This plot includes the effect of coolant temperature rise and pressure drop and calculates the CHF at the worst location, *i.e.*, the exit where the pressure is lowest and coolant temperature is highest.

For the conditions described above, an inlet pressure of 1.5 MPa and a flow velocity of 10 m/s should be adequate for the divertor cooling. The ratio of the incident heat flux to wall heat flux for a 28 mm wide Cu-Cr-Zr

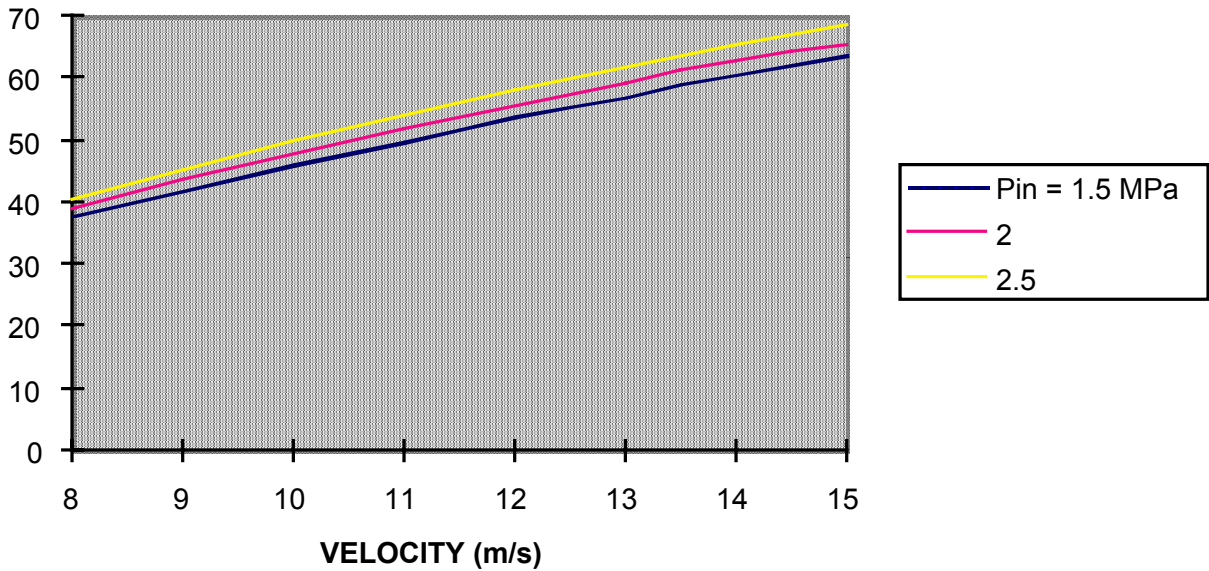


Figure 5.4.3.3-1 First Wall Temperature Increase at 1.0-4.0 MW/m<sup>2</sup> Incident Heat Flux with and without 1 W/cm<sup>2</sup> °C heat transfer at the Rear Surface.

module with two 8 mm channels is estimated to be 1.33, based on previous analysis done for ITER. Thus, the cooling will permit an incident critical heat flux of 34.6 MW/m<sup>2</sup>, allowing a sufficient safety margin. The estimated pressure drop in the module is 0.45 MPa, including the effect of the swirl-tape insert.

A 3-D finite element analysis with axial heat flux profile will be undertaken in the future.

#### 5.4.3.3.4 Thermal Analysis of Divertor Components

Temperature distributions for the divertor components have been calculated with a thermal analysis code for normal operation. The analysis assumed a CuCrZr heat sink with 5 mm W rods on the surface. The water inlet temperature was 30°C at a pressure of

1.5 MPa. Both the outer divertor plate and the baffle plate were analyzed. The peak heat flux was 20 MW/m<sup>2</sup> on the outer divertor (attached plasma case) and 6 MW/m<sup>2</sup> on the baffle plate (detached plasma case). The effect of 13-16 W/cm<sup>3</sup> nuclear heating was included. The outer divertor heat sink was assumed to have a swirl tape in the coolant channel to enhance the heat removal while the baffle plate was assumed to have smooth tubes. The flow velocity in the outer divertor was 10 m/s while the baffle was 3 m/s. The coolant exit temperatures were 95 and 73°C, respectively. The temperature profiles are shown in Figure 5.4.3.3.4-1 and Figure 5.4.3.3.4-2.

FIRE Engineering Report  
FY01 Update

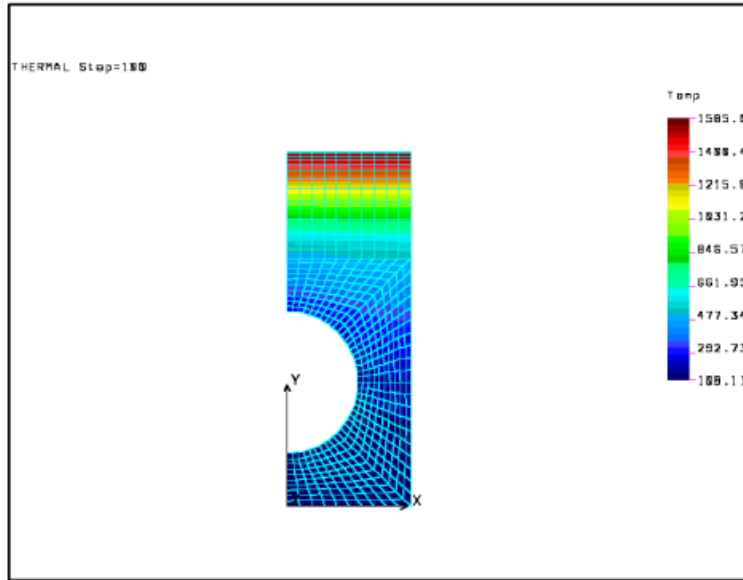


Figure 5.4.3.3.4-1. Temperature distribution in the actively cooled outer divertor plate with 20 MW/m<sup>2</sup> heat flux.

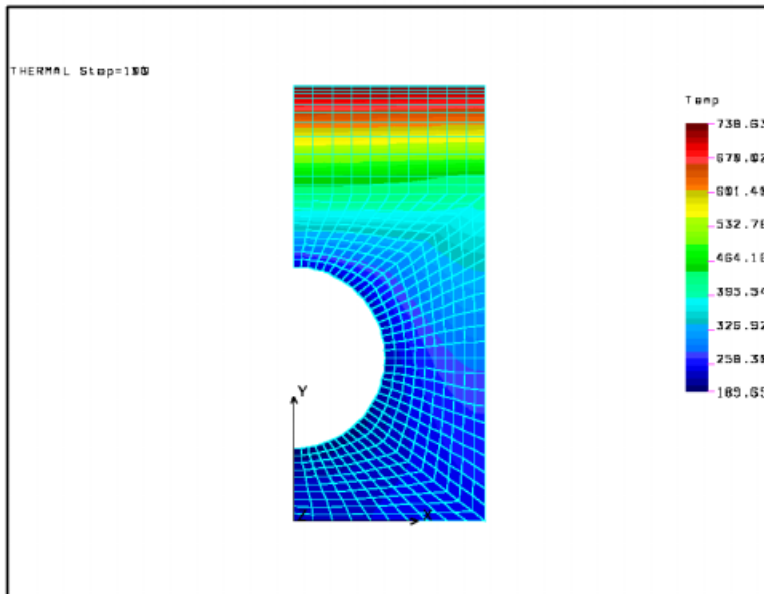


Figure 5.4.3.3.4-2 Temperature Distribution in the actively cooled baffle plate with 6 MW/m<sup>2</sup> heat flux.

#### 5.4.4 Materials Selection

We recommend the following selection of materials for the plasma facing components:

Divertor high heat flux areas: tungsten rods 3 mm in diameter attached to actively cooled copper alloy heat sinks.

Divertor heat-sink structure: CuCrZr alloy, Elbrodur-G for copper-alloy heat sinks based on ITER fabrication experience.

First wall: plasma sprayed beryllium 10 mm thick attached to copper heat sinks that are passively cooled.

Tritium retention in redeposited carbon material has been identified as a major R&D issue to be investigated in the extension of the ITER project. This is due to the experimental data from both JET and TFTR that showed the retention to be approximately 50% of all the tritium injected into the machine. There is no satisfactory method for removing this trapped tritium from the machine. This issue argues strongly for avoiding carbon-based materials in a burning plasma device.

#### **5.4.5 On-going Design and Fabrication Issues**

Active cooling of the first-wall, inner divertor plate and baffle components will be needed for the longer pulse lengths proposed. More detailed designs and 2-D analyses are needed to verify design concepts and establish pulse limits for these parts.

Finite element analyses of the proposed PFC designs are needed under projected disruption and thermal loading conditions to assure that the structures and attachments are sufficient. Proposed sliding pin concepts for relieving thermal stress must also be evaluated.

Mitigation of the eddy current loads on the divertor plates may require that a toroidally conductive path be provided between the outer divertor modules. This would significantly complicate the module design and associated remote installation and removal operations.

In general, reliable, yet easily detachable electrical contact must be provided between

the plasma facing components and the vacuum vessel. Grounding straps and Multilam® contacts were proposed for this in ITER, since each of these can accommodate thermal cycling and relative motion. Similar design concepts must be developed and tested for FIRE.

When design analyses are completed, armored, medium-scale hardware needs to be fabricated and tested to verify the module manufacturing / assembly operations and performance models.

#### **5.4.6 R&D Plans**

The W-brush fabrication process development and scale-up needs to be completed and HHF testing must be conducted to validate performance and yields. The outer divertor fabrication process development and scale-up must be carried through prototype development and testing. The baffle fabrication process development and scale-up must be carried through prototype development and testing. We will fabricate and test electrical connectors to validate performance in case they are needed. We will fabricate dummy elements to use for validating remote handling interfaces and procedures.

## 5.5 Thermal Shield

### 5.5.1 Introduction

The main function of the thermal shield system is to provide the required thermal environment around the coils, which operate at cryogenic temperatures. To maintain this environment, the nitrogen gas inside the shield must be contained (not allowed to leak out) and the air on the outside of the shield must not be allowed to leak into the shield. The main reason to exclude air from the inside of the enclosure is to prevent the accumulation of ice on the cold surfaces. In addition to maintaining the required thermal environment on the inside of the shield, it is also important to maintain the exterior surfaces of the shield at a high enough temperature to prevent water condensation, which can result in corrosion and operational and safety problems.

The basic design concept for the thermal shield is to have a stainless steel structure (channel beams) on the inside of the shield that can support panels made of insulating materials (Figure 5.5.1-1). The SS structure will be covered with a thin SS shell, which will form part of the sealed boundary for the shield. Insulation will be sprayed directly onto this shell. Penetrations will be sealed with rubber or fabric bellows that accommodate the relative motion between the VV and thermal shield.

### 5.5.2 Requirements

The most important requirements for the thermal shield relate to maintaining the 80 K thermal environment inside the shield. To do this efficiently, the maximum heat loss through the shield has been set at 15 kW. To prevent

condensation on the exterior of the shield, the surface temperature must be maintained above the dew point for air with a relative humidity of 50%. In addition, the constraint has been imposed to maintain the shield exterior within 10 °C of the test cell ambient temperature.

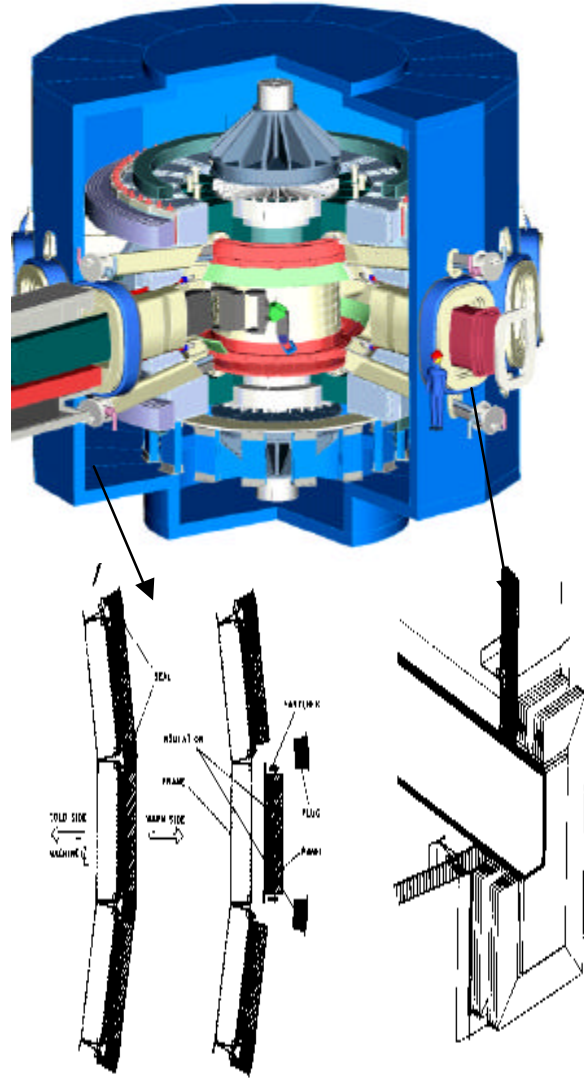


**Figure 5.5.1-1 Thermal Shield Design Concept**

Another important requirement pertains to pressure loads on the shield. If we have an open LN<sub>2</sub> system, interior

FIRE Engineering Report  
FY01 Update

pressure will be due to N<sub>2</sub> gas flow through the system and out the vent. The maximum Δp across shield wall (maximum pressure on inside) has been set at 0.8 kPa (0.12 psi or 3 inches of H<sub>2</sub>O). A higher pressure on the outside of the system could occur during cool down of the system if N<sub>2</sub> flow is not maintained. In this case, the maximum Δp across the shield wall (maximum pressure on outside) has been set at 0.1 kPa.

Requirements related to the flexible joints that accommodate the relative motion between the VV and thermal shield include a maximum integrated leak rate for all seals of 1 l/s (at 1 atm exterior pressure) with a Δp across the joint of 0.8 kPa. The joints must accommodate relative motions between the components up to ± 25 mm.

The requirements for the thermal shield are summarized in Table 5.5.2-1.

The radiological inventories have been estimated to be modest for the FIRE facility and lead to a requirement for the vacuum vessel to be a highly reliable primary confinement barrier for the in-vessel inventories, and the thermal shield to serve as a moderately reliable secondary barrier (see Section 5.15).

In FY01, preliminary accident scenarios were defined for the FIRE cryostat as:

- Failure to completely purge the magnet coolant channels before a full power pulse
- Divertor coolant leak into thermal shield leads to ice accumulation over an operating campaign

- Nitrogen coolant leak into thermal shield accumulates nitrogen over an operating campaign

Preliminary analyses have started and will continue in FY02 to determine the bounds on material available for activation and the impact of an accident of this type.

### 5.5.3 Description

The thermal shield has three basic parts, (1) the SS structure and shell which support the insulation and form part of the sealed boundary for the shield, (2) the insulation itself, and (3) the flexible joints that accommodate the relative motion between the VV and thermal shield. The shield is semi-cylindrical in shape (formed by 16 flat facets) with a flat top and bottom. Its OD and height are 11.2 and 11.5 m, respectively. The total wall thickness of the structure and insulation is 0.65 m.

**Table 5.5.2-1 Thermal Shield Design Requirements – Summary**

Design Parameter	Value
<b>Thermal</b>	
1. Condensation on surfaces of the shield.	None
2. Max. temp. difference between shield exterior and test cell temp.	10 °C
3. Max. heat flow through the shield assembly	15 kW
4. Minimum gas temp. contained by the shield	80 K
5. Max. gas temp. contained by the shield (during VV baking)	150 °C
6. Max. temp. around feedthroughs	200 °C
<b>Structural</b>	
1. Max. Δp across shield wall (max. pressure on inside)	0.8 kPa (0.12 psi)
2. Max. Δp across shield wall (max. pressure on outside)	0.1 kPa
<b>Mechanical</b>	
1. Max. integrated leak rate of all seals (between penetrations and thermal shield wall panels)	1 l/s at 1 atm (Δp- 0.8 kPa)
2. Seals must accommodate relative motion between penetrations and thermal	Vertical - ± 25 mm Toroidal - ± 10 mm

FIRE Engineering Report  
FY01 Update

shield panels (Initial Design Values)	Radial - $\pm 18$ mm
---------------------------------------	----------------------

Sixteen (16) flat panels that are centered on each row of ports form the vertical sides of the thermal shield. Bolting the panels together forms the complete cylinder (each panel spans 22.5 degrees). Each panel consists of a perimeter frame, which is made with 10-inch channels. A thin SS skin is welded to the frame to form part of the barrier for the shield. Insulation is sprayed directly onto this skin. Holes are provided through the skin and insulation where the vacuum vessel ports, buswork, cooling and other services pass through. Clearance is provided between the ports and the hole in the thermal shield to allow for the relative motions of the VV and the shield. The maximum relative motion ( $\pm 25$  mm) results from the condition when the VV and thermal shield are at normal operational temperatures and simultaneously are under seismic conditions.

The seal around the ports is provided by a flexible joint (similar to a bellows) that is attached to the VV port and the SS sheet part of the structure. The joint is a single layer of silicone rubber on a fabric base that is  $\sim 12$  inches long (in the direction of the port axis). It can flex and buckle to accommodate the relative motion.

The insulation is the most important part of the shield. Several types were considered and compared before making a selection. The candidates are shown in Table 5.5.3-1. As can be seen, the thermal conductivity and cost of the cryo-lite and the polyurethane foam are similar. The solimide polyimide foam has a higher thermal conductivity and

cost. Due to the ease of application of the polyurethane foam, (which is sprayed on) this insulation has been selected for the thermal shield. This material can be sprayed directly onto stainless steel to any desired thickness. A rubber vapor barrier can then be sprayed onto the exposed surface, which also enhances its abrasion resistance.

**Table 5.5.3-1 Insulation Comparison**

Mtl Name	k (W/m-K)	Cost (\$/m <sup>3</sup> )
Polyurethane Foam (Manufactured by Foam Enterprises) (Spray foam for tank insulation.)	0.033	$\sim 400$
Cryo-Lite (Manufactured by Johns Manville) (Used to insulate LN <sub>2</sub> over-the-road tanks.	0.033	$\sim 320$
Solimide Polyimide Foam (TA-301) (Manufactured by Laporte plc)	0.042	$\sim 1150$

The top and bottom of the TS are the same basic construction as the vertical sides. The structural frame consists of 10 inch channels positioned side by side and spaced  $\sim 0.5$  m apart. The thin SS skin will be welded to the frame and insulation will be sprayed on as described above.

Several important thermal characteristics of the shield have been estimated. These include the total heat loss through the shield and the inner and outer surface temperatures. The nitrogen gas temperature in the shield was assumed to be 90 K and the air temperature in the room was assumed to be 300 K (27 °C). Given these temperatures, the natural convection heat transfer coefficients were estimated for both the inside and

FIRE Engineering Report  
FY01 Update

outside of the shield. The insulation thickness was adjusted so that the outside surface temperature would be high enough to avoid condensation during operation. The resulting inner and outer surface temperatures are 100 K and 290 K (17 °C) respectively, for an insulation thickness of 0.4 m. The outer surface temperature is comfortably above the dew point of 283 K (10 °C) (for air at 21 °C with a relative humidity of 50 %), so condensation is not expected. The total heat flow through the insulation is ~11 kW which is below the requirement limit of 15 kW.

The basic parameters for the thermal shield are shown in Table 5.5.3-2.

**Table 5.5.3-2 Thermal Shield Design Parameters**

Parameter	Value
Size	
Outside Diameter	11.2 m
Outside Height	11.5 m
Total Wall Thickness	
Structure	0.25 m
Insulation	0.4 m
Inside Surface Area	375 m <sup>2</sup>
Weight	
Insulation (0.4 m thick)	2400 kg
SS Structural Frame (10 inch channels)	24000 kg
SS Shell Around Insulation (0.5 mm thick)	7100 kg
Thermal Characteristics	
Nitrogen Gas Temp. Inside Thermal Shield (assumed)	90 K
Shield Inside Surface Temp. (with natural conv.)	~100 K
Shield Outside Surface Temp. (with natural conv.)	~290 K
Air Temp. in Room Outside of Thermal Shield (assumed)	300 K
Dew Point for Air at 21 C (75 F) and 50 % humidity	283 K
Condensation Expected	None
Total Heat Flow Through Shield	~11 kW

## 5.6 Ion Cyclotron Heating

Ion cyclotron waves will be used to heat the plasma. Based on calculations of plasma transport, 20 MW of heating power will be required.

A design that can deliver this power has been obtained. It consists of four two-strap antennas mounted in main horizontal ports, as shown in **Fig. 5.6-1**.

The amount of power that can be delivered to the plasma depends on a number of things that are not yet well-quantified, such as:

- Distance between the first wall and the plasma separatrix at the outer midplane – a smaller distance allows higher power per antenna.
- Maximum voltages that can be

sustained in the antenna and transmission line – 30 kV is a relatively conservative number; 40 kV has been used on some experiments and would provide considerably higher power per antenna ( $P \sim V_{\max}^2$ ).

- The density and density profiles (both inside the separatrix and in the scrape-off region) of the plasma.

We have concentrated on the antenna configuration and the coupling of the antenna to the plasma, as these are the most critical parameters for initial system design. Power sources, along with tuning and matching equipment and concepts, should follow reasonably conventional (although state-of-the-art) designs. While optimizing the parts of the system external to the vacuum vessel is necessary, we do not regard it as critical.

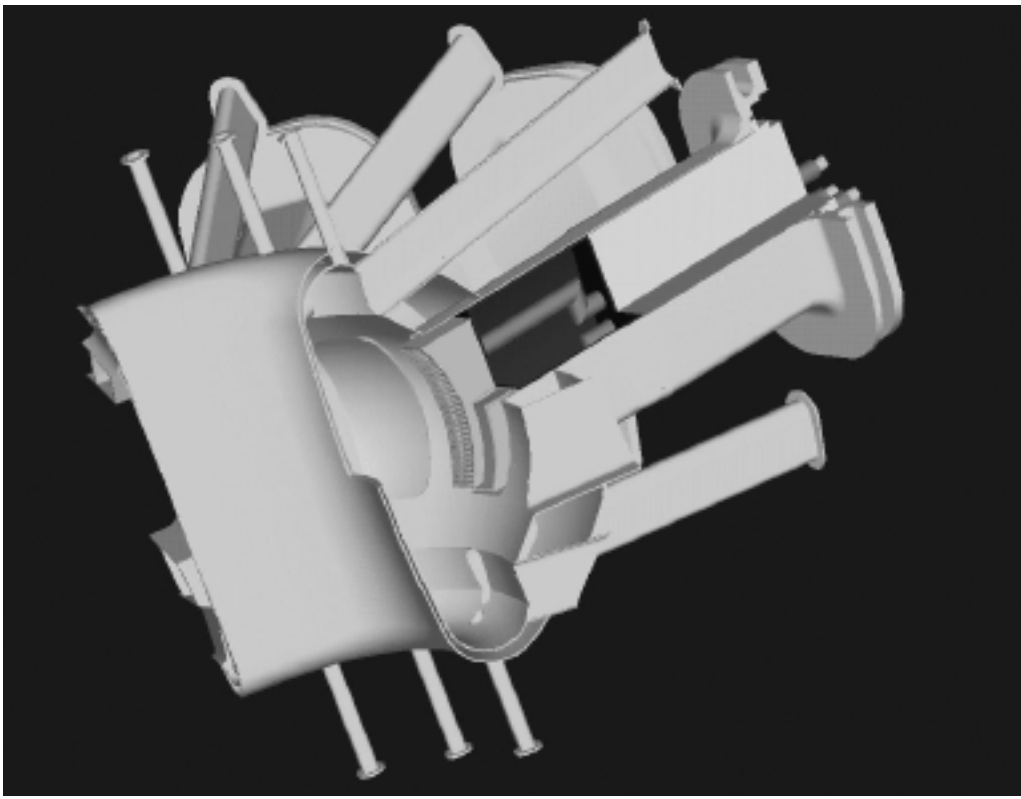


Fig. 5.6-1 – Cutaway view of one two-strap antenna in main horizontal port.

**Heating scenarios**

The rf system is being designed to operate at frequencies from 80 to 120 MHz. **Figure 5.6-2** shows a plot of resonant frequencies of various ion species as a function of major radius. Based on this plot, operation at 10 T will use the second-harmonic T resonance at 100 MHz. For initial non-tritium operation, minority He<sup>3</sup> can be used for effective heating at the same frequency. For lower (e.g., 7 T) operation, second-harmonic D heating (or H minority heating) can be used at  $f \sim 105$  MHz.

**Antenna geometry**

**Figure 5.6-3** shows a proposed antenna configuration that fits into a main horizontal port and that can operate at the frequencies chosen above .

The antenna consists of two current straps, each strap about 15 cm wide and 117 cm tall. Each strap is grounded to the case at both ends, with a 20-cm long stub at each end to increase the electrical length of the strap. The straps are grounded at the center point also for increased mechanical strength. This results in a very strong strap arrangement that can resist the disruption-induced forces. For reasonable assumptions about the strap electrical properties, the electrical length of the straps is near one wavelength in the 80 – 120 MHz frequency range, making this configuration feasible.

Each strap is driven by two coax feeds at the locations shown in **Fig. 5.6-3** (by the dashed circles). The two feeds on each strap are driven out of phase. We assume that there is  $\pi$  phasing between adjacent

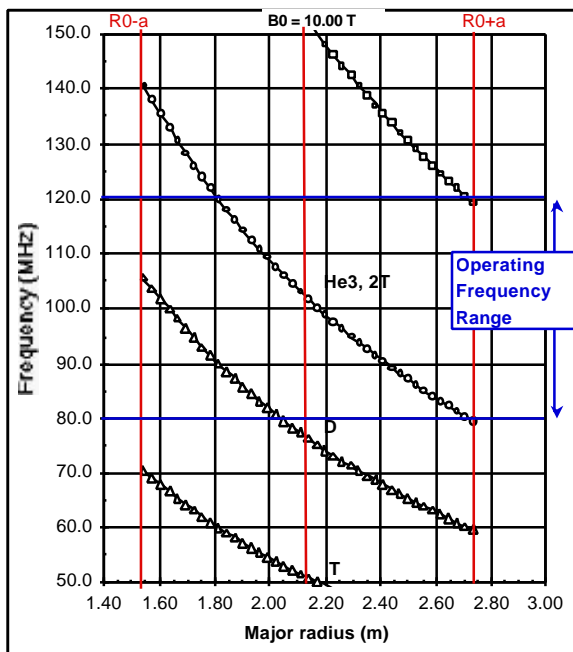


Fig. 5.6-2. Resonant frequencies vs. major radius, for  $B_0 = 10$  T.

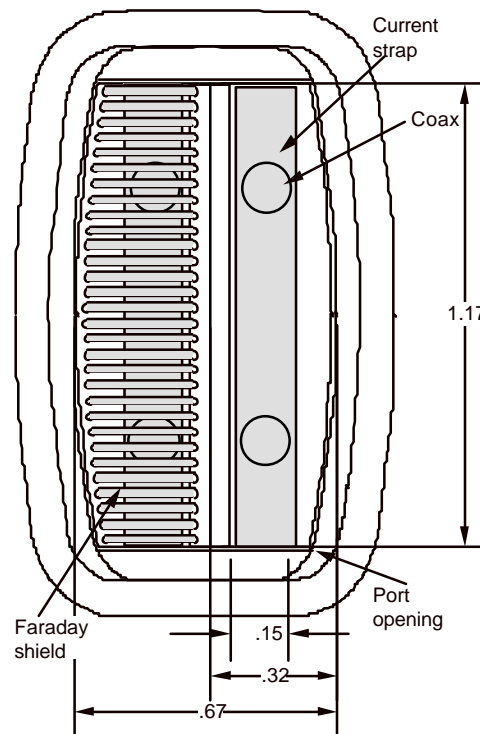


Fig. 5.6-3. View of antenna from the plasma. One Faraday shield removed. Dimensions in m

straps, since there is no current-drive requirement on the IC system.

The antenna is covered by a Faraday shield consisting of a number of metal tubes. Active cooling of these tubes will be required during a shot for pulse lengths of 10 s or greater.

**Power to the plasma**

Figure 5.6-4 shows the maximum voltage in the rf system vs. gap (distance from the outer separatrix to the antenna surface) , with the constraint that the IC system must deliver 20 MW of power to the plasma using four antennas. The line at 35 kV indicates a nominal value of limiting voltage. A conservative design choice would set this value at 30 kV, while a more aggressive design would increase it to 40 kV. These curves were calculated for the nominal density profiles (parabolic-to-a-power) with  $\langle n \rangle = 4.5 \times 10^{20} \text{ m}^{-3}$  and  $\alpha_v = 0.5$  and 0.2.

Based on these results, a four-port system can deliver 20 MW to the plasma at 100 MHz for up to a 6-cm gap, provided it can operate at 35 kV and  $\alpha_n = 0.5$ . For the steeper edge profile with  $\alpha_n = 0.2$ , a 4.5 cm gap would be needed. The present design value for this gap is in the 3 to 4 cm range, so a four-port system should be able to supply the needed power.

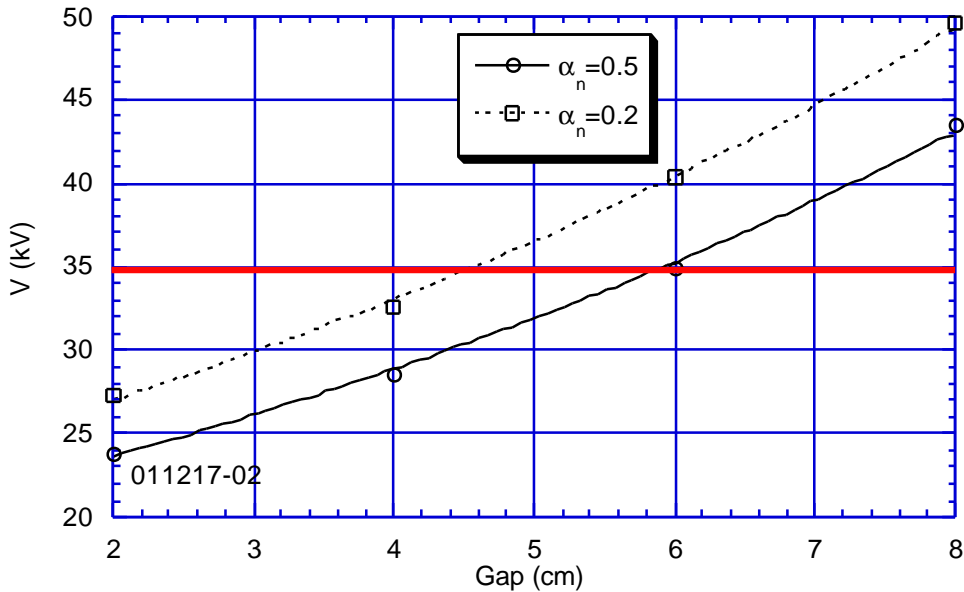


Fig. 5.6-4. Maximum voltage in the IC system needed to deliver 20 MW to the plasma vs. gap, for antennas in four ports and two density profile shapes.

## 5.7 Plasma Fueling and Pumping

### 5.7.1 Introduction

Tritium pellet injection will be utilized on FIRE for efficient tritium fueling and to optimize the density profile for high fusion power. Conventional pellet injectors coupled with a guide tube system to launch pellets into the plasma from the high field side, low field side, and vertically will be provided for fueling along with gas puffing for plasma edge density control. Recent experiments on ASDEX Upgrade and DIII-D indicate that these pellets will penetrate a sufficient distance into FIRE plasmas to provide peaked profiles. About  $1-2 \times 10^{21}$  tritons/s are required to sustain the plasma density in FIRE which is a modest extrapolation of existing pellet injection technology. About 0.2 g of tritium must be injected during each 20 s pulse. The tritium and deuterium will be exhausted into the divertor. The double null divertor will have 16 cryogenic pumps located near the divertor chamber to provide the required high pumping speed of 200 torr-l/s. The tritium from the regenerated cryopumps will be directed to gas holding tanks and fed into a cryogenic distillation system that will separate hydrogen isotopes and purify the tritium for return to the fueling system.

The plasma fueling system design for FIRE is based on previous designs for CIT, BPX and ITER as well as more recent developments and plasma physics results in the area of pellet launch from multiple locations relative to the magnetic axis. The goal is to produce a flexible fueling system that would require minimum change in the progression from FIRE to ITER or a fusion demonstration (DEMO) plant. In the past, tokamaks have generally used gas puffing for establishing and maintaining the plasma density. With this method, the sources of plasma particles are located at the plasma surface. There is general consensus, however, that gas puffing alone will not be sufficient to fuel the next generation of large, long-pulse fusion devices with thick, dense, scrape-off layers, and that core fueling, where the particle sources are located

well inside the plasma edge, will be necessary.

A pellet fueling system (PFS) is provided for core fueling and a gas fueling system (GFS) for edge fueling. The FIRE fueling system provides plasma fueling from all sources (D, T, impurity gases) at a rate of 200 torr-liter/s for 20 s to support all fueling functions. The fuel rate to replace the D-T ions consumed by the fusion reaction is quite modest, about 2 torr-liter/s for a fusion power of 200 MW; the resulting burn fraction is thus only 1% of the steady-state fueling rate. Such low burn fractions result in large vacuum pumping and fuel processing systems with associated tritium inventories and were not anticipated in early (1,2) and even more recent (3) fusion power plant assessments, which had burn fractions in the 10-40 % range. The low burn fraction is only partially due to the finite fueling efficiency (see next section). The fueling system (4,5) must also maintain the required plasma density (near the empirical Greenwald density limit), establish a density gradient for plasma particle (especially helium ash) flow to the edge, and also supply hydrogenic edge fueling for increased scrape-off layer flow for optimum divertor operation. Still another function is to inject impurity gases at lower flow rates (25 torr-l/s or less) for divertor plasma radiative cooling and wall conditioning. Finally, the plasma fueling system provides for plasma discharge termination on demand via massive gas puffing or injection of cryogenic mass via pellets or liquid jets. A concept called isotopic fueling (6) can be used to improve the tritium burn fraction above the nominal 1% level described above by frugal use of tritium fuel to those functions only related to the fusion burn and using deuterium for edge fueling. This can reduce in-vessel tritium inventories and the required tritium-breeding ratio for fusion reactors.

The tritium inventory inside the FIRE vacuum vessel is a major consideration. Due to the large retention of tritium observed in carbon plasma facing components and in co-deposited carbon layers on TFTR and JET, carbon PFCs will not be allowed in FIRE. The divertor plates will be tungsten and the first wall protection will use Be tiles.

### 5.7.2 Fueling Efficiency

The fueling efficiency of tokamaks has been studied since the early 1980's. For gas fueling, the determination of fueling efficiency of short pulse tokamaks has been difficult to quantify because of an outgassing source of hydrogenic fuel from the plasma facing components that can be of the same magnitude as the external gas fueling. Pellet fueling is easier to quantify in terms of fueling efficiency due to the rapid deposition of the fuel (100's of  $\mu$ s) and its deposition beyond the last closed flux surface, which avoids most atomic physics complications in fuel transport to the plasma. In contemporary tokamaks, fueling provides the required density level for a particular plasma experiment. There is incentive to maximize the tritium plasma fueling efficiency due to the cost and safety implications of a large tritium throughput and the complexity of reprocessing large torus exhaust gas loads (6). Fueling efficiency of gas and pellet injection are summarized in Table 5.7.1 and Figure 5.7.1

Device	Gas Fueling Efficiency (%)	Pellet Fueling Efficiency (%)	Remarks
ASDEX	20	30-100	high density
PDX	10-15		high density
Tore Supra	1	30-100	ergodic divertor for gas fuelling
JET	2-10	20-90	active divertor
TFTR	15		low density DT
ASDEX-U		8-50	
DIII-D	10	40-100	active divertor

Table 5.7.1. Tokamak fueling efficiency.

(7,8). Generally, in diverted discharges of the larger tokamaks, gas fueling efficiency is in the range 1-10 % and pellet fueling efficiency is an order of magnitude larger. Recent results from ASDEX-Upgrade (9) are also shown in Figure

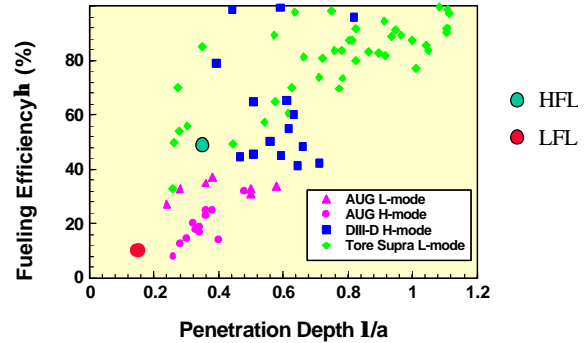


Figure 5.7.1. Pellet fueling efficiency for several experiments. (Also shown are recent results from high field launch (HFL) and low field launch (LFL) on ASDEX Upgrade.)

5.7.1 which compares the penetration and fueling efficiency of pellets launched into the same plasma conditions from the high magnetic field side and low magnetic field side; improvements in pellet penetration and fueling efficiency for high field launch are substantial.

Deuterium pellet injection from four different poloidal locations has been used in experiments on the DIII-D tokamak (10, 11, 12) to investigate several aspects of plasma confinement and density control (see Figure 5.7.2). Pellets can be injected in four locations: outside midplane, vertically inside the major radius, inside launch at  $\sim 45$  degree angle and inside midplane. Pellets injected from the outer horizontal midplane (low field side) show a large discrepancy in the measured fueling efficiency and mass deposition profiles from pellet ablation theory, while the penetration depth compares favorably with theory. An apparent outward displacement of the deposited pellet mass is observed and hypothesized to occur from  $\tilde{N}B$  and curvature induced drift effects. Injection of pellets inside the magnetic axis from a vertical port and inner wall ports using curved guide tubes has been employed on DIII-D to investigate these effects.

## FIRE Engineering Report FY01 Update

The resulting density profiles show pellet mass deposition well inside the expected penetration

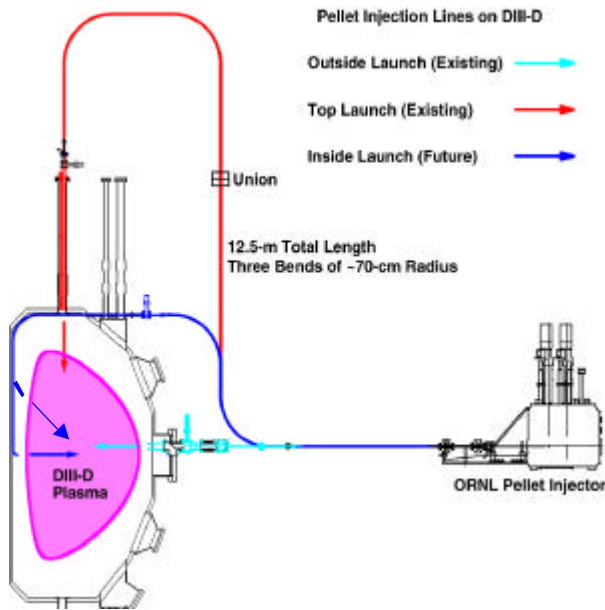


Figure 5.7.2. Pellet launch locations on DIII-D.

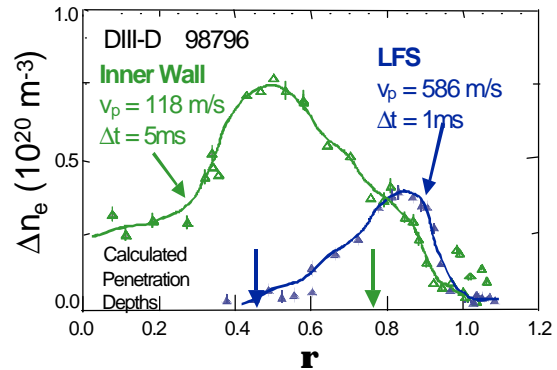
radius, suggesting that a drift of the pellet ablatant is occurring toward the low field side (LFS) edge of the plasma (Figure 5.7.3). The formation of highly peaked density profiles with pellets injected from the high field side is possible at higher heating power than is possible from pellets injected from the low field side.

On FIRE, pellet injection will be possible from the outside midplane, vertically and from the inside lower quadrant aimed towards the plasma center. This will be accomplished by three sets of guidetubes.

Recently, there has been interest in repetitive impurity pellets or impurity gas puffing to foster enhanced radiation in the outer plasma and divertor regions and large (“killer”) pellets for a controlled, preemptive plasma shutdown in anticipation of a major disruption or vertical displacement event (VDE). These systems typically operate at room temperature or higher cryogenic temperatures, but require similar technology for pellet feed and acceleration as are used on H/D/T pellet fueling systems. Major issues for impurity pellet injection include

development of pellet production and feed hardware optimized for the pellet material (i.e.

Figure 5.7.3. Plasma density increase from a pellet launched from the inner wall (high field side) launch compared with launch from the outer wall (low field side).



lithium, carbon, nitrogen, argon) and, for killer pellet injectors, high reliability for a single large pellet or liquid jet on demand. Impurity pellet injection systems (typically small lithium or carbon pellets) have been developed for wall conditioning and plasma diagnostics.

### 5.7.3 FIRE Fueling System Overview

The FIRE fueling system will use a combination of gas puffing and pellet injection to achieve and maintain burning plasmas. This combination will provide a flexible fueling source with D-T pellets penetrating beyond the separatrix to sustain the burning fusion plasma and deuterium-rich gas fueling the edge region to meet divertor requirements in a process called isotopic fueling (6). The isotopic fueling concept was developed to allow independent control of the plasma deuterium and tritium density profiles which can lead to reduced (by factors of 2-4) tritium inventory in plasma facing components. The higher tritium burn fraction allows a significant reduction in tritium gas flows into and out of the vacuum vessel and, for fusion reactors, implies lower required tritium breeding ratios. The fueling system includes; a conventional gas puffing system, using all-metal electromagnetic dosing valves, (four toroidal stations at two poloidal locations at each divertor level), and a pellet injection system.

FIRE Engineering Report  
FY01 Update

The FIRE pellet fueling system (PFS) design includes a long pulse pneumatic pellet injector capable of injecting D-T or tritium. It will be a repeating pneumatic injector using an extruder-based hydrogenic feed system. It will be configured to inject pellets using propellant gas for pellet acceleration (up to 1.5 km/s pellets) or a mechanical punch accelerator (up to 100 m/s for pellet injection into curved guidetubes for vertical or high field side launch) or a combination of these two drivers. The mechanical punch operating alone or with a small amount of propellant gas would reduce considerably the need for differential pumping of the pellet injection line and the reprocessing requirements for propellant gas. The PFS comprises a pneumatic pellet injector with three separate pellet extruders/guns, installed in a containment area in the basement below the torus. The PFS and GFS manifolds are also

located in a basement area below the FIRE torus. Pellet injection will be possible via curved guidetubes from the outside midplane, vertically and from the inside lower quadrant aimed towards the plasma center. This will be accomplished by three sets of guidetubes. The pellets will be injected to the high magnetic field side of the machine through a curved flight tube routed through the lower divertor region. The hydrogenic feed for the injector is provided by a conventional linear piston hydrogen extruder (sized for a 20 s supply of pellets) or by a continuously rotating screw extruder. Deuterium and tritium pellets up to 10 mm in size have been extruded at rates up to 0.26 grams/sec (for short pulses only); this pellet size and feed rate is sufficient for fueling fusion reactors at the gigawatt power level. Table 5.7.2 below shows preliminary parameters for the FIRE hydrogenic fueling system.

Parameter	Gas Fueling System	Pellet Fueling System	Remarks
Design fueling rate	200 torr-l/s for 20 s	200 torr-l/s for 20 s	Torus pumping capacity is 200 torr-l/s
Operational fuel rate	100-175 torr-l/s	100-25 torr-l/s	Isotopic fueling
Normal fuel isotope	D (95-99%) T,H (5-1%)	T (40-99 %) D(60-1%)	D-rich in edge, T-rich in core
Impurity fuel rate	25 torr-l/s	TBD (prefer gas for impurity injection)	25 torr-l/s reduces DT fuel rate due to fixed pumping capacity
Impurity species	Ne, Ar, N <sub>2</sub> , other?	TBD	TBD
Rapid shutdown system	Massive gas puff	“killer” pellet or liquid D jet	For disruption/VDE mitigation
Pellet sizes (cyl. diameter)	N/A	3, 4, 4 mm	3 mm for density rampup, 4 mm for flat-top

Table 5.7.2. Preliminary FIRE fueling system parameters.

#### 5.7.4 FIRE Fueling System R&D

The screw extruder concept has been demonstrated by a Russian Federation prototype system which ran for 1-hour pulses using hydrogen feed gas producing ~2 mm extrudant. This needs to be extrapolated to deuterium and

tritium feed and larger pellet sizes using this technology or variants such as gear or double-screw extruders. ITER-scale (10-mm) pure tritium and D-T pellets have been extruded with a piston-type linear extruder and accelerated to about 1 km/s (see Figure 5.7.4) in the Tritium-Proof-of-Principle Phase II (TPOP-II)

## FIRE Engineering Report FY01 Update

experiment at the Tritium Systems Test Assembly (13)

The technology to deliver intact pellets at the highest possible speeds around curved surfaces (guide tubes) is under development (11, 12). This is a complex issue and depends on the pellet speed and temperature (strength) as well as the guide-tube radius of curvature, its diameter relative to the pellet size, and its cross-sectional shape. The speed dependence of penetration for high field side or vertical launched pellets is not known.

### 5.7.5 FIRE Pumping System

The current baseline design is a set of refrigerated duct D-T cryocondensation/diffusion pumps backed by turbo/drag pumps. This system is designed to pump in both the free-molecular and viscous flow regimes. Water is pumped on the inside diameter of the 160 mm diameter by 1 meter long 30 K entrance duct which connects the divertor to the cryocondensation pump. Other impurity gases and hydrogen are pumped by cryocondensation on a 1/2" O.D. x 0.035 wall stainless steel tubing coil refrigerated by liquid helium. The 2 torr-l/s helium gas produced by the D-T fusion reaction is compressed by viscous drag in the entrance duct by a factor of up to 100. The compressed helium gas is carried from the cryopump to a turbo/drag pump located outside the biological shield through the divertor duct. The design D-T throughput is 200 torr-liter/s for the 20 s pulse

length. The partial pressures prior to a discharge are  $10^{-7}$  torr for fuel gases (H, D, T) and  $10^{-9}$  torr for impurities. There will be a total of 16 cryopumps with 8 each top and bottom (at alternate divertor ports) located 1 meter into the pump duct from the double-null divertor. The duct behind the cryopump will be constructed with transverse optically opaque shielding baffles which will allow 200 l/s helium gas conductance per port to the turbo/drag pumps located outside the biological shield. There are no moving parts inside the torus.

A layout of the cryopumps is shown in Figure 5.7.5. The cryopumps are designed to have a low mass and active helium gas cooling. Between shots the helium flow will be stopped to allow the pumps to regenerate into the compound turbo/drag pumps. This will limit the tritium contained on the cryopumps to less than 1 gram for a 20 sec. discharge. Gas will be returned to the tritium system where it will be processed through an impurity removal step and a cryogenic distillation system that will separate the hydrogen isotopes and purify the deuterium and tritium for return to the fueling system.

The cryogenic cooling requirement for the 16 pumps for the design pumping rate of 200 torr-l/s and the nuclear heating loading which is estimated at  $0.03 \text{ watt/cm}^3$  at the proposed cryopump location 1 meter from the divertor is 3 watts per pump. The liquid helium cooling rate required during a shot is 64 l/h for the 16 pumps.

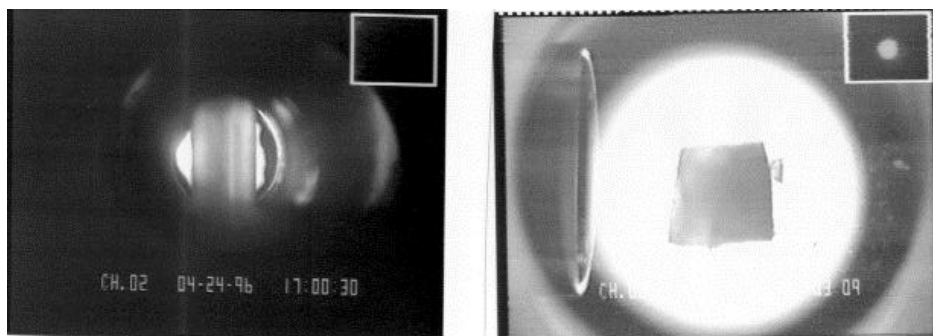


Figure 5.7.4. Pure tritium extrusion and pellet.

## FIRE Engineering Report FY01 Update

The maximum divertor pressure during the pulse is  $\sim 0.02$  torr. At this pressure and the design duct size the Knudsen number is 0.01 so the gas transport is in the viscous flow regime dominated by gas-gas interaction. In this case the minority gas species such as helium and impurities will be carried by viscous drag to the cryopump. This effect can be used to achieve a helium compression of 100 in the inlet duct so that the required helium pumping speed can be reduced and still maintain a high effective helium pumping speed at the divertor.

During the tokamak discharge, the effective pumping speed for 200 torr-l/s flow is 2,000 l/s per duct (32,000 l/s total) at the divertor for D-T, He, and impurities. For each shot,  $\sim 4,000$  torr-l of D-T will be deposited which is a small fraction of the capacity of the 16 pumps. Periodically, the pumps will be warmed and regenerated. Prior to the discharge, with the pumps cold, in the free molecular flow regime, the pump set will have an effective speed of 16,000 l/s for  $D_2$ , 6,400 l/s for air, 46,000 l/s for water vapor, and 3,200 l/s for helium.

The sixteen evacuation locations will be grouped in four sets of four. Each set will have its own cryogenic control system. Liquid helium will flow in series through the four cryocondensation pumps and will go through a heat exchanger to completely flash it before it is sent in parallel through the four cooled ducts. The four turbo/drag pumps in the group will be backed by a single 3.3 l/s scroll pump that is backed with a metal diaphragm pump.

A large pumping speed is desirable for initial pumpdown or during vessel bakeout. For this purpose, a  $\sim 500$  mm diameter duct will be used off a single mid-plane port. This duct, with a large turbopump, will provide a minimum pumping speed of 2000 l/s in the molecular flow regime to achieve to  $10^{-7}$  torr or lower base pressure.

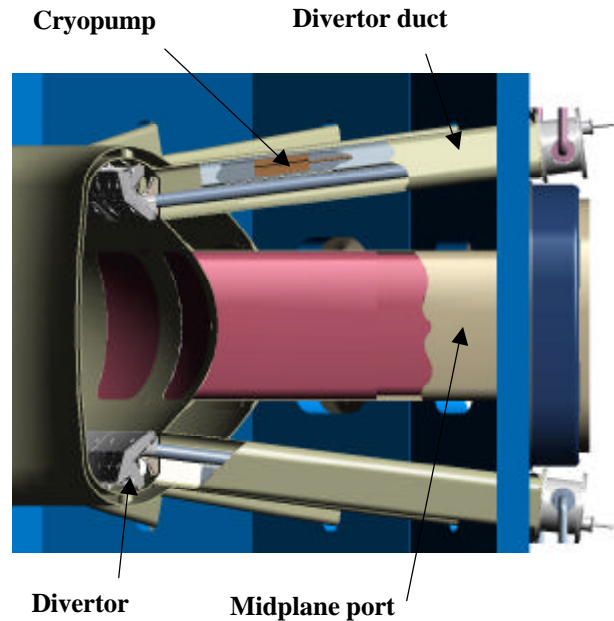


Figure 5.7.5. Elevation view of FIRE torus showing divertor duct and cryopump.

### REFERENCES

1. C. C. Baker, M. A. Abdou, *et al.*, "STARFIRE-A Commercial Fusion Power Plant Study," Argonne National Laboratory Report ANL/FPP-80-1 (1980).
2. M. A. Abdou, *et al.*, "A Demonstration Tokamak Power Plant Study (DEMO)," Argonne National Laboratory Report ANL/FPP-82-1 (1982).
3. The ARIES Team., "The ARIES-1 Tokamak Reactor Study, University of California at Los Angeles report UCLA-PPG-1323 (1991).
4. Gouge, M. J., *et al.*, "The CIT Pellet Injection System: Description and Supporting R&D," *Proceedings of the 13th Symposium on Fusion Engineering*, Vol. II, p.1240, IEEE 1990.
5. M. J. Gouge, "Fuelling of ITER-Scale Fusion Plasmas," *Fusion Technology*, **34**, 435 (1998).
6. Gouge, M. J., *et al.*, "Fuel Source Isotopic Tailoring and Its Impact on ITER Design, Operation and Safety," *Fus. Tech.* **28**, 1644 (1995).

FIRE Engineering Report  
FY01 Update

7. L. R. Baylor, et al., "Deposition of Pellets into Tokamak Plasmas," *Fusion Technology*, **34**, 425 (1998).
8. L. R. Baylor, et al., "Pellet Injection into H-mode Plasmas on DIII-D," *to be published in 26<sup>th</sup> Europ. Conf. on Contr. Fusion and Plasma Physics* (1999).
9. P. T. Lang, et al, "High-efficiency Plasma Refueling by Pellet Injection from the High-Field Side Asdex Upgrade," *Phys. Rev. Lett.* **79**, 1478 (1997).
10. S. K. Combs, et al., "Experimental Study of Curved Guide Tubes for Pellet Injection," *Proc. 1997 IEEE/NPSS 17<sup>th</sup> Symp. Fusion Eng., San Diago*, 1102 (1998).
11. S. K. Combs, et al., "High-Field-Side Pellet Injection Technology," *Fusion Technology*, **34**, 419 (1998).
12. S. K. Combs, et al., "New Pellet Injection Schemes on DIII-D," *to be published in the proceedings of this conference*.
13. P. W. Fisher and M. J. Gouge, "TPOP-II: Tritium Fueling at a Reactor Scale," *Fusion Technology*, **34**, 515 (1998).

## 5.8 Tritium System Requirements

### 5.8.1 Introduction

The tritium system is a key system for FIRE operations, as well as providing development information and operating experience for the fusion program. The development of a safe, low-inventory tritium system is an important project goal.

### 5.8.2 Tritium Injection Requirements

Pellet injection will be the primary plasma system for fueling the core of the FIRE plasma utilizing both high speed pellets and guided lower speed pellets. Gas injection systems will also be provided for edge fueling. The total number of tritons in the nominal FIRE plasma is:

$$N_e = \langle n_e \rangle V_p / 2 \sim 2.25 \times 10^{20} \text{ m}^{-3} \times 18 \text{ m}^3 \sim 5 \times 10^{21} \text{ tritons}$$

The particle confinement in tokamaks is described by  $D \sim \chi$ , or  $\tau_p \sim \tau_E$  which translates into  $\tau_p \sim 0.5$  to  $0.8$  s in FIRE. A fueling rate of  $\sim 0.5 - 1 \times 10^{22}$  particles/s would be required to sustain the density with zero recycling. The standard assumption for FIRE and ITER-RC is that  $\tau_{He} \sim 5 \tau_E$  which suggests an 80% recycling of helium. We make the additional reasonable assumption that the same recycling applies to the hydrogenic species. Therefore, a net rate  $\sim 0.1 - 0.2 \times 10^{22}$  particles/sec would be required to sustain the nominal FIRE plasma.

In present experiments with outer mid-plane pellet fueling, the efficiency is low  $\sim 20\%$ . FIRE will be employing vertical launch of high-speed pellets aimed inside the magnetic axis or slower pellets guided by tubes to near the inside mid-plane. The injection geometry will be updated, as more information becomes available from ongoing experiments. A

pellet fueling efficiency of 50% is assumed for FIRE. The gross tritium fueling rate for the plasma core is then  $\sim 0.2 - 0.4 \times 10^{22}$  particles/s.

### 5.8.3 Requirements for Potential Pulse Sequences

The total number of injected tritons required for various scenarios involving 10 second long pulses is:

$$2 - 4 \times 10^{22} \text{ T/pulse ; } 0.8 - 1.6 \text{ kCi } (\sim 0.1\text{g}) / \text{pulse; } 10 \text{ s pulse}$$

$$2 - 4 \times 10^{23} \text{ T/day ; } 8 - 16 \text{ kCi } (\sim 1\text{g})/\text{day; } 10 \text{ pulses/day}$$

$$1 - 2 \times 10^{24} \text{ T/week; } 40 - 80 \text{ kCi } (\sim 5\text{g})/\text{week; } 50 \text{ pulses/week}$$

$$\text{(where } 2.09 \times 10^{19} \text{ T atoms} = 1 \text{ Ci, } 10^4 \text{ Ci} = 1 \text{ g, pulses are 10 seconds long)}$$

The total number of DT pulses in FIRE is limited to  $< 5\text{TJ}$  of fusion energy, or 2,500 pulses at 200 MW for 10 s, or a tritium fueling throughput of 2 - 4 MCi. There will also be many partial power pulses that will consume tritium while not producing optimal fusion power, therefore the lifetime throughput of tritium is assumed to be increased by  $\sim 5$  to a total throughput of 10 - 20 MCi. Assuming that this program takes place over 5 years would require a tritium throughput capability of 2 - 4 MCi/year.

The fractional tritium burn-up of  $\sim 5\%$  does not affect these estimates significantly.

### 5.8.4 Tritium Retention and Inventory

## FIRE Engineering Report FY01 Update

The provisional limit for the tritium site inventory has been set at =30 g (~0.3 MCi). According to DOE STD 1027, FIRE would be classified as a Low Hazard Nuclear Facility. Similar to the TFTR tritium management strategy, the maximum tritium in any on-site tritium system is set at 15 g, 1/2 the site limit. The D-T experiments on TFTR and JET have shown that the use of carbon plasma facing components produced an effective tritium retention rate of ~ 40%. Assuming the annual tritium throughput of 2 - 4 MiCi, this level of retention would cause the FIRE system limit to be exceeded in 1 to 2 months. Therefore, the use of carbon will not be allowed in the FIRE vacuum vessel. The initial materials for plasma facing components and divertor plates will be Be and W.

Cryogenic pumps will be installed in the behind the divertors of FIRE to provide adequate pumping during the pulse. Essentially all of the injected tritium will end up on the cryopumps. The schedule for regenerating the cryopumps will be determined to maintain the tritium inventory < 30g. The tritium inventory for several regeneration schedules is:

1. weekly regeneration: < 5g of tritium on the cryopumps would be transferred to the tritium handling system. The tritium separation systems described below would be able to easily separate the tritium from the deuterium and other exhaust gases in < 2 days, so that tritium could be ready for experiments the following week. Need to estimate the number of deuterium only shots in a run sequence to estimate the total number of torr-liters of gas on the cryopumps to see if this is a reasonable sequence.
2. daily regeneration: < 1g inventory on the pumps, probably not worth the hassle of the regeneration procedure.

3. monthly regeneration: < 20g of tritium on the cryopumps if running continuously with tritium. This level is also expected to satisfy the explosive limits.

A monthly regeneration of the divertor cryopumps would fit naturally with the anticipated experimental schedule.

### 5.8.5 Tritium Systems for FIRE

The tritium systems will be similar to those used successfully at TFTR, and will include Tritium Storage and Delivery, plasma exhaust cleanup, tritium purification system (for reprocessing the on-site inventory), appropriate room air cleanup systems, tritium exhaust gas processing systems, and tritium monitoring for process control and personnel protection. The block diagram for the tritium system is shown in Fig 5.8.5-1.

The FIRE tritium delivery system will be capable of supplying tritium with a purity > 98%. Tritium will be received from a DOE supplier in hydride transport vessels (HTVs) in quantities up to 25 grams. Tritium inventory will be loaded into the tritium storage and delivery system (TSDS) and will be available upon demand (within 6 hours of when required). The FIRE TSDS will be capable of supplying quantities of tritium up to 3 kCi per pulse via direct gas injection. This capability could be upgraded for the long pulse (~ 40s) pulses in the advanced tokamak phase.

FIRE exhaust gas will be collected in a plasma exhaust tank where it will be stored until processed by the on-site tritium purification system (cryogenic distillation). On-site tritium processing will separate non hydrogen isotopes from the plasma exhaust effluent and cryogenically separate tritium from deuterium and protium, thus producing tritium with a purity of > 98 % purity. Plasma exhaust processing will require ~

FIRE Engineering Report  
FY01 Update

24 hours to be recycled back to the tritium storage and delivery system.

The on-site tritium purification system for FIRE will have a resident tritium inventory of ~ 10 grams of tritium with a throughput of (up to) 50 kCi (5 grams) / day. ITER had planned to reprocess 164 g of tritium during the 40 minute cycle period for an ITER pulse[1].

Tritium residual gases (in glove boxes and in other small volumes) will be processed, oxidized, and deposited on disposal molecular sieve beds for disposal at an off-site facility.

**5.8.6 Options to the Tritium Inventory**

The tritium inventory has been set at 30g (~0.3 MCi), to allow sufficient operational flexibility without introducing additional restrictions. However, there is the potential for reducing the inventory to even lower levels. If a tritium reprocessing system is

used which is able to recycle the working tritium on a daily basis, then the daily working inventory is = 20 kCi (2g).

As noted above, ITER was planning on reprocessing tritium at the rate of >4 g/minute. If FIRE had a system capable of processing 1g/120 minutes, then the working inventory could be reduced by an order of magnitude to 2kCi(0.2g). The main contributions to the inventory would now be in residual holdup in various systems including the vacuum vessel. There should be a follow-up study to look at the minimum tritium inventory case.

[1] D. K. Murdoch, "Tritium Inventory Issues for Future Reactors"; Choices, Parameters, Limits. Proc., SOFT 1998

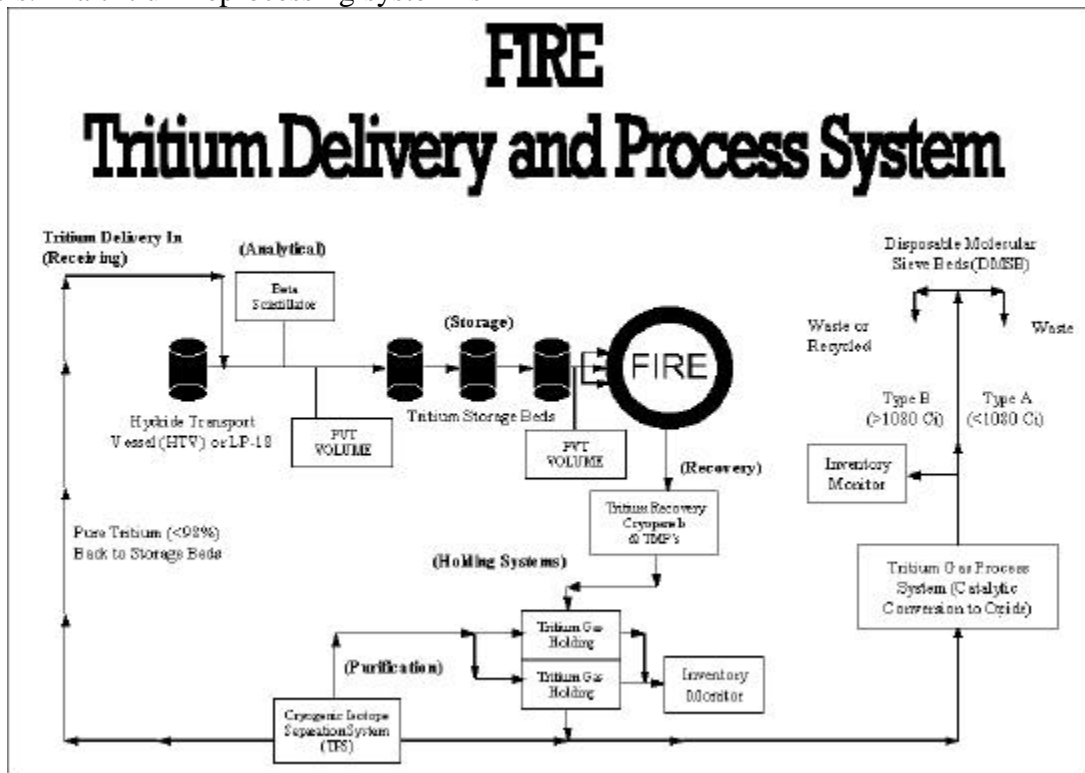


Fig. 5.8.5-1 Tritium System Piping and Instrumentation Diagram (P&ID) for FIRE

## 5.9 Neutronics and Shielding

### 5.9.1 Introduction

The design is in the preconceptual design phase where many different design options and operating scenarios are being considered. DT pulses with widths up to 20 s and fusion powers up to 200 MW producing a total of 5 TJ of fusion energy are planned. In addition, DD pulses with different widths and fusion powers up to 1 MW yield total fusion energy of 0.5 TJ. The baseline design has a major radius of about 2 m and an aspect ratio of 3.8. The average neutron wall loading during the 200 MW DT pulses is 3 MW/m<sup>2</sup>. The corresponding values at the outboard (OB) midplane, inboard (IB) midplane, and divertor are 3.6 MW/m<sup>2</sup>, 2.7 MW/m<sup>2</sup>, and 1.8 MW/m<sup>2</sup>, respectively. It utilizes 16 wedged Cu TF magnets. A double walled vacuum vessel (VV) with integral shielding has been adopted. The plasma facing components include Be coated Cu first wall (FW) and divertor plates made of tungsten rods mounted on water-cooled Cu heat sink.

### 5.9.2 Calculation Models

Nuclear analysis has been performed to evaluate the impact of design options and assess if the major performance objectives of the project can be met without jeopardizing performance of the radiation sensitive components. The neutronics and shielding calculations were performed using the ONEDANT module of the DANTSYS 3.0 discrete ordinates particle transport code system [1] with the most recent FENDL-2 nuclear evaluated data [2].

Two design options were considered for the FW/tiles with passive cooling

(Option 1) and active water-cooling of vessel cladding (Option 2). The FW/tiles on the IB side for Option 1 consist of a 0.5 cm plasma facing component (PFC) (90% Be), followed by 4.3 cm Cu tiles (80% CuCrZr alloy) and a 0.2 cm gasket (50% SiC). In Option 2, the IB FW/tiles consist of 0.5 cm Be PFC (90% Be), 1.8 cm Cu tiles (80% CuCrZr) and 0.2 cm gasket (50% Cu). A 2.5 cm water-cooled Cu (80% CuCrZr, 15% water) vessel cladding is employed behind the tiles. For the OB side, the same radial build is used except that the total thickness is increased to 10 cm in Option 1. The impact of these design options on nuclear heating in the different components and the VV and magnet shielding was assessed. Option 2 was chosen as the baseline design to reduce VV thermal stresses.

Detailed neutronics calculations were performed for the outer divertor that is exposed to the most severe conditions in the divertor region. The front layer is a 0.5 cm W Brush (90% W) followed by a 0.1 cm region (84% W, 14% CuCrZr, 2% void) where the W rods are joined to the Cu heat sink. The 1.9 cm heat sink is made of Cu finger plates (78% CuCrZr, 20% water, 2% void). A 3 cm region (47% CuCrZr, 48% SS316, 5% void) represents the mechanical attachment between the Cu finger plates and the 7 cm thick backing plate (84% SS316, 16% water).

The VV consists of 1.5 cm thick inner and outer facesheets made of 316SS. The space between the VV facesheets (VV shielding zone) includes 60% 304SS and 40% water except in the IB region where 11% 316SS and 89% water is used because of the small thickness. The thicknesses of the VV at the IB midplane, OB midplane, and divertor

FIRE Engineering Report  
FY01 Update

region are 5, 54, and 12 cm, respectively. A 1.5 cm thick layer of thermal insulation (10% Microtherm insulation) is attached to the back of the coil-side VV facesheet. The Cu TF coils are included in the model with 90% packing factor. While beryllium copper is used in the inner legs, OFHC copper is utilized in the rest of the TF coils. A 316SS coil case is used in the OB region with 4 cm front thickness and 6 cm back thickness. Both the IB and OB regions were modeled simultaneously to account for the toroidal effects.

### 5.9.3 Nuclear Heating

Nuclear heating deposited in the different components was determined and used in the thermal analysis. The calculations were performed for the DT pulses with 200 MW of DT fusion power to determine the largest nuclear heating generated. Nuclear heating results can be modified for lower power pulses by scaling linearly with the fusion power. For the DD pulses with the largest fusion power (1 MW), nuclear heating values are at least two orders of magnitude lower than the values for the 200 MW DT pulses.

Table 5.9.1 gives the peak power density values in the different components at the chamber midplane for the two FW/tiles design options. The peak nuclear heating values in the FW/tiles are comparable for the two design options. The IB VV and magnet heating values decrease by ~15% in the baseline design (Option 2)

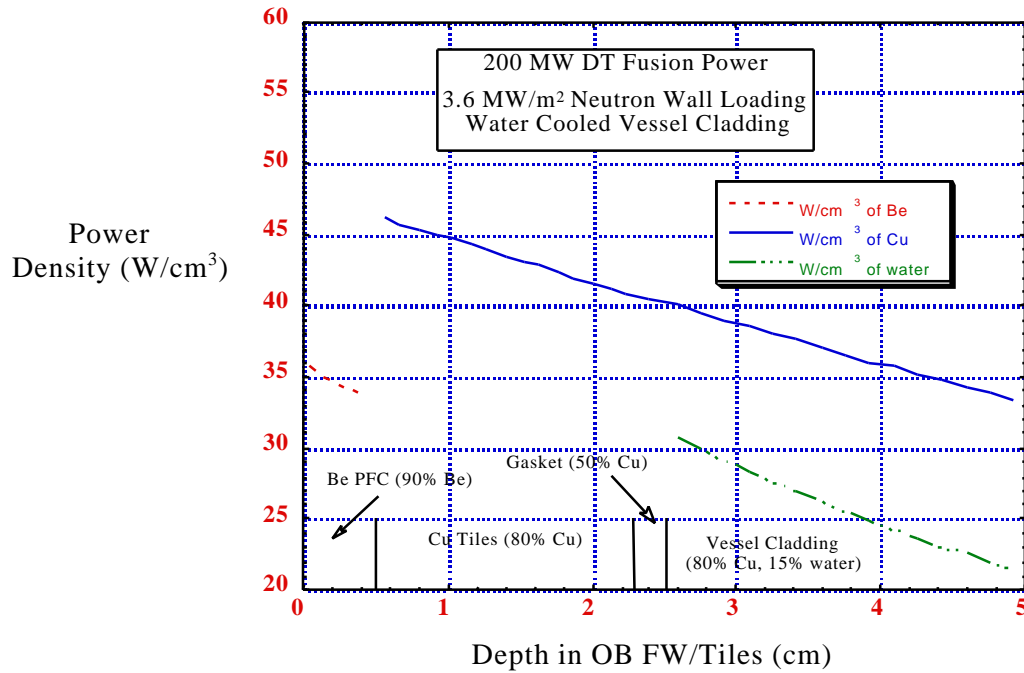
because of the added water coolant in the FW and using Cu in the gasket in place of SiC. The OB VV and magnet heating values increase by a factor of 1.5-2 in Option 2, primarily due to the 5 cm reduction in the FW/tiles thickness. The largest power density values in the magnet occur in the IB region at midplane. The IB VV and magnet heating values decrease by ~15% in Option 2 because of the added water coolant in the FW and using Cu in the gasket in place of SiC. The OB VV and magnet heating values increase by a factor of 1.5-2 in Option 2, primarily due to the 5 cm reduction in the FW/tiles thickness. The largest power density values in the magnet occur in the IB region at midplane.

Fig. 5.9.1 gives the nuclear heating distribution in the OB FW/tiles at midplane for the baseline design. Fig. 5.9.2 gives the radial variation of nuclear heating in the VV at the OB midplane. Nuclear heating in the VV drops by an order of magnitude in ~18 cm. Nuclear heating in the IB magnet drops by an order of magnitude in ~28 cm. Table 5.9.2 lists the peak nuclear heating values at the outer divertor. Relatively high nuclear heating is deposited in the W PFC. Fig. 5.9.3 shows the nuclear heating distribution in the outer divertor plate.

FIRE Engineering Report  
FY01 Update

**Table 5.9.1. Peak Nuclear Heating (W/cm<sup>3</sup>) at Midplane**

	Option 1		Option 2 (Baseline)	
	IB	OB	IB	OB
Be PFC	34.7	36.8	33.3	35.6
Cu Tiles	44.9	43.6	46.9	46.3
Gasket	19.6	11.0	40.6	40.6
Cooled Cu VV Cladding	NA	NA	40.2	40.1
H <sub>2</sub> O FW Coolant	NA	NA	27.6	30.9
SS Inner VV Wall	35.9	19.6	33.8	30.9
SS VV Filer	37.5	20.6	32.9	28.5
H <sub>2</sub> O VV Coolant	17.5	11.1	14.9	15.5
SS Outer VV Wall	35.1	0.04	30.3	0.07
Microtherm Insulator	11.4	0.01	9.8	0.02
SS Inner Coil Case	NA	0.021	NA	0.038
Cu Magnet	23.1	0.010	19.5	0.019
SS Outer Coil Case	NA	1.5x10 <sup>-5</sup>	NA	2.8x10 <sup>-5</sup>



**Fig. 5.9.1. Nuclear heating distribution in the OB FW/tiles.**

FIRE Engineering Report  
 FY01 Update

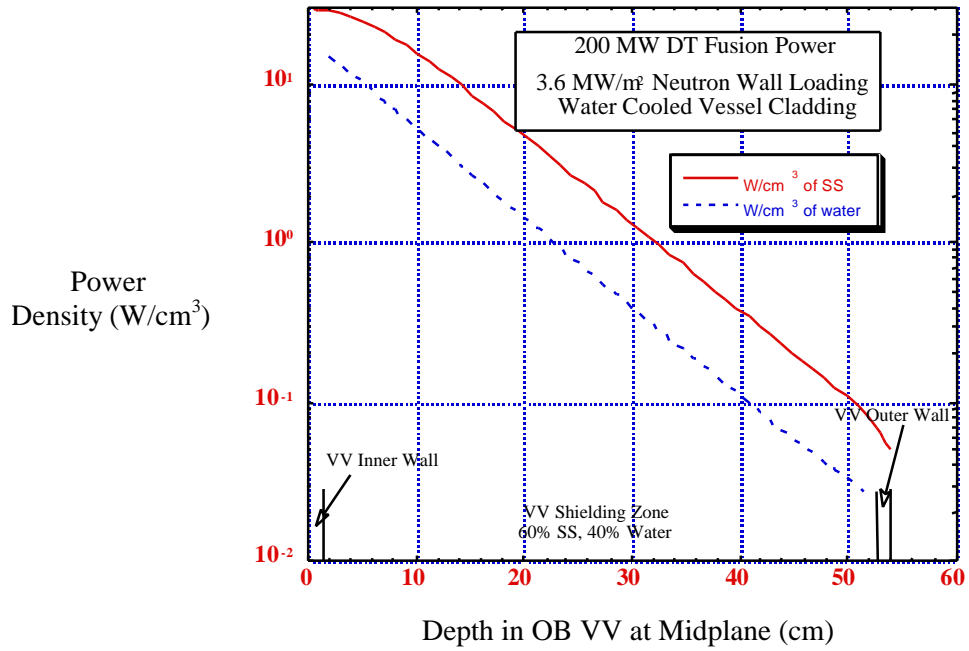


Fig. 5.9.2. Nuclear heating distribution in the OB VV

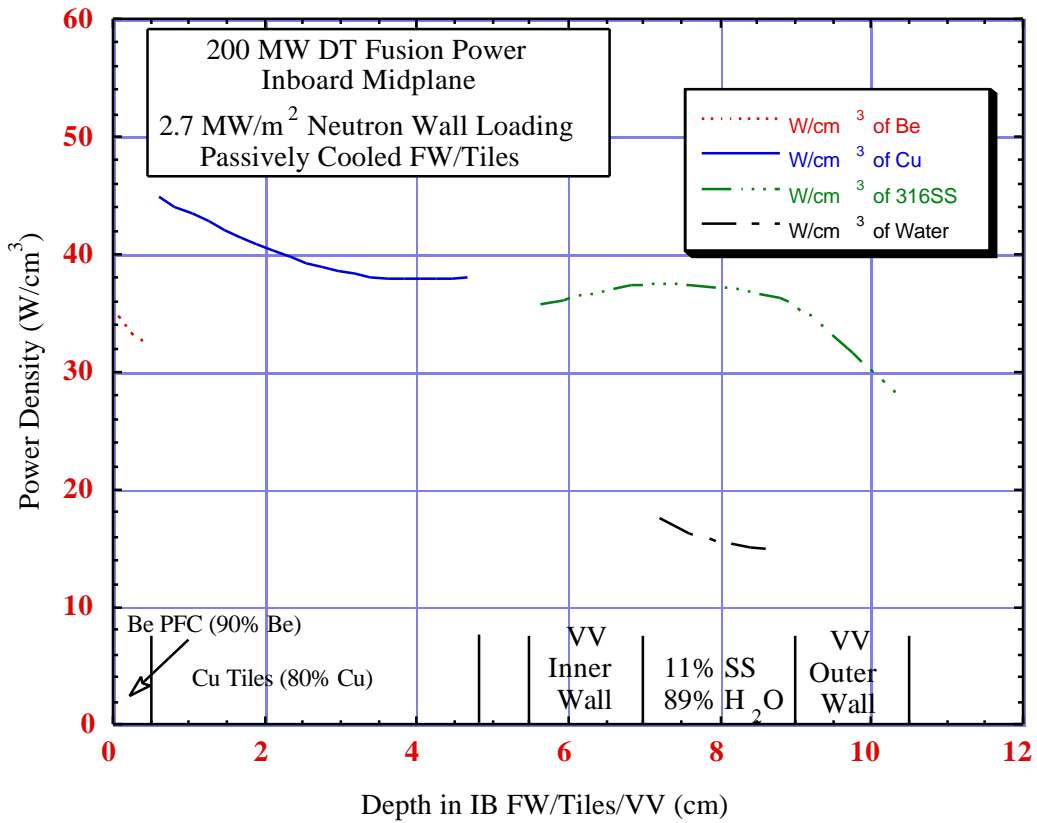


Fig 5.9.3. Nuclear heating in the outer divertor.

**Table 5.9.2.** Peak Nuclear Heating (W/cm<sup>3</sup>) at the Outer Divertor

W rods in divertor	49.0
Cu heat sink in divertor	17.2
SS structure in divertor	14.9
SS VV	6.7
Cu Magnet	1.7

The total nuclear heating in the 16 TF coils for 200 MW DT fusion power was estimated based on the results of the 1-D calculations taking into account the poloidal variation of neutron wall loading, shielding thickness, and magnet toroidal coverage. Table 5.9.3 gives the breakdown of total magnet nuclear heating for the two FW/tiles design options. The total heating is dominated by contribution from the lightly shielded IB legs. The total magnet heating decreases by 14% in the baseline design compared to Option 1 because of the added water coolant in the FW and using Cu in the gasket in place of SiC.

**Table 5.9.3.** Total Magnet Nuclear Heating

	Magnet Nuclear Heating (MW)	
	Option 1	Option 2 (Baseline)
IB region	27	22.9
OB region	0.03	0.05
Divertor region	2.1	2.1
Total	29.13	25.05

### 5.9.4 Radiation Damage

The peak cumulative end-of-life radiation damage values were calculated for the FIRE components. For the operation scenario of total DT fusion

energy of 5 TJ and total DD fusion energy of 0.5 TJ, the dpa values are very low (< 0.05 dpa). Table 5.9.4 gives the peak dpa values in the Cu tiles, vessel cladding, Cu finger plates in outer divertor, and Cu TF coils for the FIRE baseline design. Although the damage levels are very low, significant effects on physical and mechanical properties might occur. These effects are strongly dependent on irradiation temperature. This has been the subject of numerous studies in the EU, Russia and the US over the past ~8 years as part of the ITER R&D program [3].

**Table 5.9.4.** Peak end-of-life Cu dpa

	Total dpa
IB tiles	0.0327
OB tiles	0.0359
Divertor	0.0150
IB VV Cladding	0.0215
OB VV Cladding	0.0246
Magnet at IB	0.00666
Magnet at OB	7.54x10 <sup>-6</sup>
Magnet at divertor	4.55x10 <sup>-4</sup>

Radiation embrittlement for Cu alloys at T < 150 °C is a concern with reductions in tensile ductility (uniform elongation) below 5% being observed for damage levels on the order of 0.01 dpa. However, the fracture toughness is typically maintained at a sufficiently high level, at least in precipitation hardened alloys such as CuCrZr and CuNiBe. It is possible to maintain the high tensile ductility by periodically annealing the Cu at ~300 °C for ~50 hr in order to reduce the buildup of radiation damage. Irradiation to ITER doses of 1-10 dpa at higher temperatures showed pronounced increase in the uniform elongation of CuCrZr compared

FIRE Engineering Report  
FY01 Update

with irradiation at lower temperatures. However, at  $T > 300$  °C this is accompanied by significant softening. This was demonstrated by about an order of magnitude loss of yield strength at about 300 °C for 2-10 dpa.

Void swelling takes place in copper alloys irradiated in the temperature range of 180 to 530 °C. While void swelling is pronounced in copper containing oxygen impurities (~2.5%/dpa), it is only ~0.5%/dpa in pure Cu and is generally insignificant in Cu alloys up to doses of 60 dpa. Therefore, for the low dose levels in FIRE, void swelling is not a concern.

The effect of irradiation on the creep of Cu alloys is uncertain due to limited data. However, the creep behavior in Cu is comparable to that in other FCC metals. The extremely low doses expected in FIRE reduce the importance of irradiation creep. The magnitude of the irradiation creep can be estimated using the creep compliance coefficient, B. For stainless steel, B is  $\sim 3 \times 10^{-6}$  MPa<sup>-1</sup> dpa<sup>-1</sup>. Limited measurements for Cu suggest even lower B values [4]. Using the higher value of B for conservatism, and the peak cumulative dpa value in FIRE (0.036 dpa), the irradiation creep for an applied stress of 100 MPa amounts to a total deformation of only  $10^{-5}$  (0.001%) at end-of-life in FIRE.

It was recommended [3] that the operation temperature of high strength Cu alloys should be limited to  $< 300$  °C for applied stresses of 100-200 MPa to have tolerable irradiation and thermal creep at ITER conditions of 1-10 dpa. The thermal creep strength begins to decrease rapidly for temperatures  $> 300$

°C. This might cause deformation in the Cu during extended operation ( $> 100$  hr) at 300° C. Due to the low doses in FIRE, significant deformation from irradiation creep is not anticipated. Some thermal creep deformation in Cu alloys might occur if operated at elevated temperatures ( $> 300$  °C). There is a lack of detailed studies on fatigue, fracture toughness and fatigue crack growth rate behavior in high-strength, high-conductivity copper alloys [4,5].

The Cu alloys operate at different temperatures in the FIRE components. The tiles can get to temperatures over 400 °C. The tiles carry no primary stresses and should be basically unloaded except for thermal stresses and disruptions. Therefore, problems with high-temperature softening and creep should not be of concern. In addition, the tiles can be easily replaced if needed. The temperature of the vessel Cu cladding is lower than 250 °C. At this peak temperature, occurring at midplane, the low-temperature embrittlement for CuCrZr is not an issue. That will be a concern only for the lower temperature parts of the cladding at the top and bottom of the chamber. However, the dpa level will also be lower at these locations resulting in alleviating the embrittlement concern. We also have the option of annealing out the copper damage if we bake the vessel to  $> 300$  °C. The Cu in the divertor will have peak temperatures close to 500 °C. The peak damage level is only 0.015 dpa. The issue here will be mainly thermal creep. The temperature of the TF coils rises from 80 to 373 K during each pulse. The main issue here is the low-temperature embrittlement. The low temperature embrittlement data on

## FIRE Engineering Report FY01 Update

CuNiBe and OFHC Cu are limited to tensile tests between room temperature and 100 °C [6,7]. The concern is primarily at the inboard midplane where the peak damage rate is ~0.007 dpa, which is at the lower range of damage for the occurrence of radiation embrittlement. We need to check if the stresses there are in such a way that we can accommodate lower ductility at these limited locations (inboard midplane of the TF coils). Much lower damage levels occur at other locations of the TF coil.

Based on the irradiation levels and operation conditions in FIRE and the available data on Cu alloys, we can identify the R&D needs as follows:

- Data on loss of ductility of BeCu (or OFHC) at temperatures between 80 and 373 K with doses < 0.01 dpa.
- A small, relatively inexpensive irradiation program is needed to measure fatigue, fracture toughness and fatigue crack growth rate behavior in high-strength, high-conductivity copper alloys.
- Thermal creep data for CuCrZr at high temperatures up to 500 °C with doses up to 0.04 dpa. There is no need to perform irradiation creep measurements on Cu alloys for the low doses proposed in FIRE.

A concern with Cu magnet conductors in nuclear environment is the possibility of increased electric resistivity leading to increased power dissipation. Cu is transmuted producing Ni, Zn, and Co that build up as impurities with time and could significantly change the conductor resistivity. The Cu in the TF coils of FIRE is exposed to a very low fluence with peak cumulative radiation damage < 0.007 dpa. Based on previous calculations for the center post of ARIES-ST [8], the transmutation products at the FIRE fluence were determined to result in < 0.01%

resistivity increase. Another source of resistivity increase is the radiation induced resistivity resulting from the formation of vacancies and interstitials produced by atomic displacements. In FIRE, the resistivity increase due to neutron damage is expected to be self-annealed at the normal operating temperatures of the TF coils (80-373 K). In addition, the very low radiation damage per pulse ( $< 4 \times 10^{-6}$  dpa/pulse) yields less than 0.3 nΩ-cm radiation induced resistivity which is a very small fraction of the unirradiated Cu resistivity at the TF coil operating temperatures [9]. Hence, neutron-induced transmutations and radiation damage are expected to result in negligible Cu resistivity increase in FIRE.

Since the VV is protected from the fusion neutrons by the thin FW/tiles, the issue of re-weldability was addressed. The end-of-life helium production in the VV structure should be limited to 1 appm to allow for rewelding. This is the limit used in ITER [10]. Table 5.9.5 gives the results at different poloidal locations for the two FW/tiles design options. The contribution from DD shots is very small (< 0.15%). The VV helium production for Option 1 peaks in the IB region since the FW/tiles is 5 cm thinner than in the OB region. In the baseline design (Option 2), the FW/tiles thickness is the same in both regions and the higher OB neutron wall loading results in higher VV He production in the OB region. Lower VV He production occurs in the divertor region as a result of shielding by the relatively thick divertor plate. The results imply that re-weldability of the VV should not be a concern with both design options.

**Table 5.9.5.** Peak End-of-life He Production (appm) in VV

	Option 1	Option 2 (baseline)
IB midplane	0.13	0.11
OB midplane	0.07	0.15
Divertor	0.016	0.016

### 5.9.5 Magnet Insulator Dose

The insulator dose rate in the TF magnet was calculated at the front layer of the magnet winding pack. For 5 TJ of DT fusion energy and 0.5 TJ of DD fusion energy, Table 5.9.6 provides the peak cumulative magnet insulator dose for the baseline design. The peak value occurs in the lightly shielded IB side at midplane. The dose rate decreases as one moves poloidally to the OB midplane. The neutron contribution to the insulator dose varies between 50% at the front of the winding pack to 30% at the back. The relative contribution from DD shots decreases as one moves poloidally from the IB midplane to the OB midplane due to increased attenuation of low energy DD neutrons.

**Table 5.9.6.** Cumulative peak magnet insulator dose (Rads)

	Insulator Dose (Rads)	% from DD Shots
IB midplane	$1.26 \times 10^{10}$	13%
OB midplane	$1.26 \times 10^7$	1.6%
Divertor	$9.80 \times 10^8$	10%

The mechanical strength, dielectric strength, and electric resistivity are the important properties that could be affected by irradiation. The shear strength is the property most sensitive to irradiation. The commonly accepted dose limit for epoxies is  $10^9$  Rads. This is the limit used in ITER [10]. Polyimides and bismaleimides are more radiation resistant with experimental data showing only a small degradation in shear strength at dose levels in excess of  $10^{10}$  Rads. However, they are difficult to process due to their high viscosity and requirement for high temperatures to fully cure. Hybrids of polyimides or bismaleimides and epoxies could provide radiation resistant insulators with more friendly processing requirements. The availability, properties, and manufacturing impact of using these insulators will be investigated [11].

In the FIRE design with wedged coils and added compression ring, the TF inner leg insulation does not have to have significant bond shear strength, which is most sensitive to radiation. The peak torsional shear stresses occur at the top and bottom of the IB leg behind the divertor. The end-of-life insulator dose at these locations is reduced to  $\sim 10^9$  Rads due to the additional shielding provided by the divertor. The insulator dose decreases as one moves radially from the front to the back of the winding pack as shown in Figure 5.9.4. The dose decreases by an order of magnitude in  $\sim 22$  cm of the IB magnet. Based on this analysis, it is expected that insulation materials will be identified that can last for the whole device lifetime with the proposed operation scenario and load conditions.

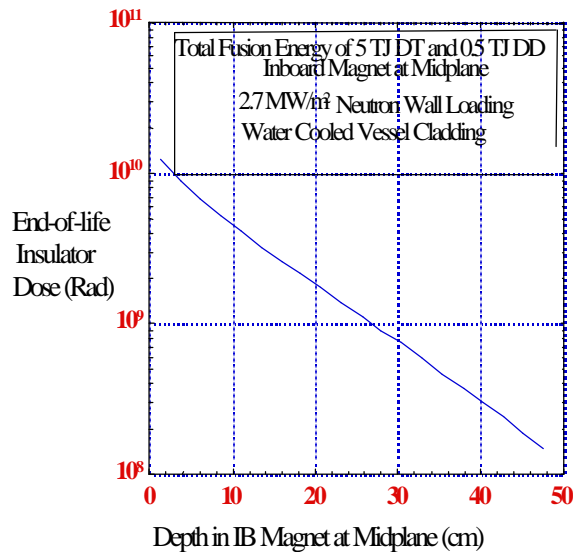


**Fig. 5.9.4.** Radial variation of insulator dose in the IB magnet.

**References for Section 5.9:**

[1] R.E. Alcouffe et al., "DANTSYS 3.0, One-, Two-, and Three-Dimensional Multigroup Discrete Ordinates Transport Code System," RSICC Computer Code Collection CCC-547, Contributed by Los Alamos National Lab, August 1995.

[2] M. Herman and H. Wienke, "FENDL/MG-2.0 and FENDL/MC-2.0, The Processed Cross-Section Libraries For Neutron-Photon Transport Calculations," Report IAEA-NDS-176, International Atomic Energy Agency (1997).

[3] S. Fabritsiev, S. Zinkle, and B. Singh, "Evaluation of Copper Alloys for Fusion Divertor and First Wall Components," *Journal of Nuclear Materials*, 233-237, 127-137 (1996).

[4] S.J. Zinkle and S.A. Fabritsiev, "Copper Alloys for High Heat Flux Structure Applications," *Atomic*

and Plasma-Material Interaction Data for Fusion, Supplement to *Nuclear Fusion*, 5 (1994) 163-192.

[5] D.J. Alexander, S.J. Zinkle and A.F. Rowcliffe, "Fracture Toughness of Copper-Base Alloys for Fusion Energy Applications," *J. Nucl. Mater.*, 271&272 (1999) 429-434.

[6] S.J. Zinkle and W.S. Eatherly, "Tensile and Electrical Properties of Unirradiated and Irradiated Hycon 3HP CuNiBe," *Fusion Materials Semiannual Progress Report for Period ending June 30, 1996*, DOE/ER-0313/20, Oak Ridge National Lab, 1996, pp. 207-216.

[7] D.J. Edwards, B.N. Singh, P. Toft and M. Eldrup, "The effect of bonding and bakeout thermal cycles on the properties of copper alloys irradiated at 100°C," *J. Nucl. Mater.* 258-263 (1998) 978-984.

[8] L. El-Guebaly and H. Khater, "Need for Inboard Shield to Protect the Center Post of ST Power Plants," *Fusion Technology*, 34, 1089 (1998).

[9] M. Sawan and P. Walstrom, "Superconducting Magnet Radiation Effects in Fusion Reactors," *Fusion Technology*, 10/3, 741 (1986).

[10] Technical Basis for the ITER Final Design Report, Cost Review and Safety Analysis, ITER EDA Documentation Series, IAEA, Vienna, December 1997.

[11] M.L. Tupper et al., "Magnet Insulation with Resistance to High Levels of Radiation," *Proceedings of the 16th International Conference on Magnet Technology*, Jacksonville, FL, September 1999.

## 5.10 Decay Heat, and Radiation Exposure

### 5.10.1 Introduction

Activation analysis was performed using toroidal cylindrical geometry with the inboard and outboard sides modeled simultaneously. Calculations assumed peak neutron wall loadings during D-T shots of 1.8 and 3.6 MW/m<sup>2</sup> for the divertor and outboard first wall, respectively. The machine is assumed to have an operation schedule of four pulses per day for one full power year (FPY). The D-T pulse burn is 20 seconds with 3 hours between pulses. Calculations were performed for D-T and D-D pulses with 200 MW and 1 MW of fusion power, respectively. The first wall is 5 cm thick and consists of 0.5 cm layer of Be coating as a plasma facing component (PFC), 1.8 cm of a CuCrZr tiles and 0.2 cm Cu gasket.

The vacuum vessel structure is made of 316 SS with inner shield made of a mixture of 304 SS and water as a vacuum vessel shield. The vacuum vessel thickness varies poloidally from 5 cm in the inboard region to 54 cm in the outboard region at the midplane. A 2.5 cm water cooled Cu cladding is attached to the plasma side of the vacuum vessel. The magnet winding pack is modeled using BeCu and OFHC in the inboard and outboard sides, respectively. The magnet uses a 316 SS coil case with 4 cm front thickness and 6 cm back thickness. The divertor consists of three layers. The front layer consists of 0.5 cm thick tungsten rods followed by 2 cm of a CuCrZr/water mixture as a heat sink, and a 3 cm thick layer of a mechanical attachment made of CuCrZr/316 SS mixture. Finally, the mechanical

attachment connects the heat sink to a 7 cm thick layer of 316 SS/water mixture which is used as a backing plate. Using of a plug (80% steel and 20% water) to stop neutrons streaming through penetrations at the midplane and using an additional shield at the top of the machine were assessed to allow for hands-on maintenance.

### 5.10.2 Activity and Decay Heat

The neutron flux used for the activation calculations was generated by the one-dimensional discrete ordinates neutron transport code DANTSYS 3.0 [1]. The activation analysis was performed using the activation code DKR-PULSAR2.0 [2]. The code combined the neutron flux with the FENDL/A-2.0 [3] cross section library to calculate the activity and decay heat as a function of time following shutdown. Figures 5.10-1 and 5.10-2 show the specific activity values for the inboard and outboard regions as a function of time following shutdown, respectively. Figures 5.10-3 and 5.10-4 show the specific decay heat values for the inboard and outboard regions as a function of time following shutdown, respectively. Finally, figures 5.10-5 and 5.10-6 show the specific activity and decay heat generated in the divertor.

As shown in figures 5.10-1 to 5.10-6, the plasma facing components, first wall on the inboard and outboard sides as well as the divertor, produce the highest levels of specific activity and decay heat. However, the favorable operational schedule allows for the decay of short-lived radionuclides between pulses resulting in low levels of activity and decay heat at shutown.

FIRE Engineering Report  
FY01 Update

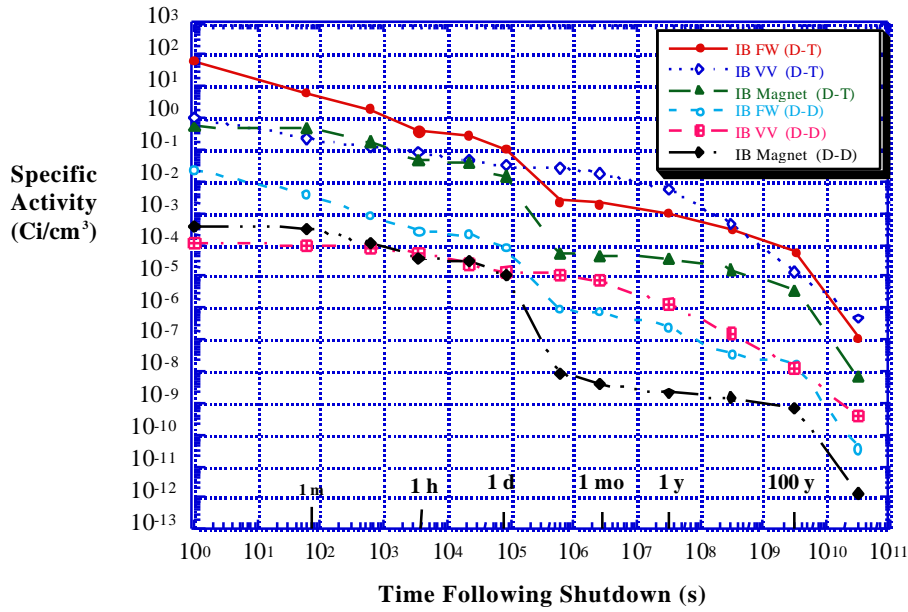


Fig. 5.10-1. Activity induced in the inboard side.

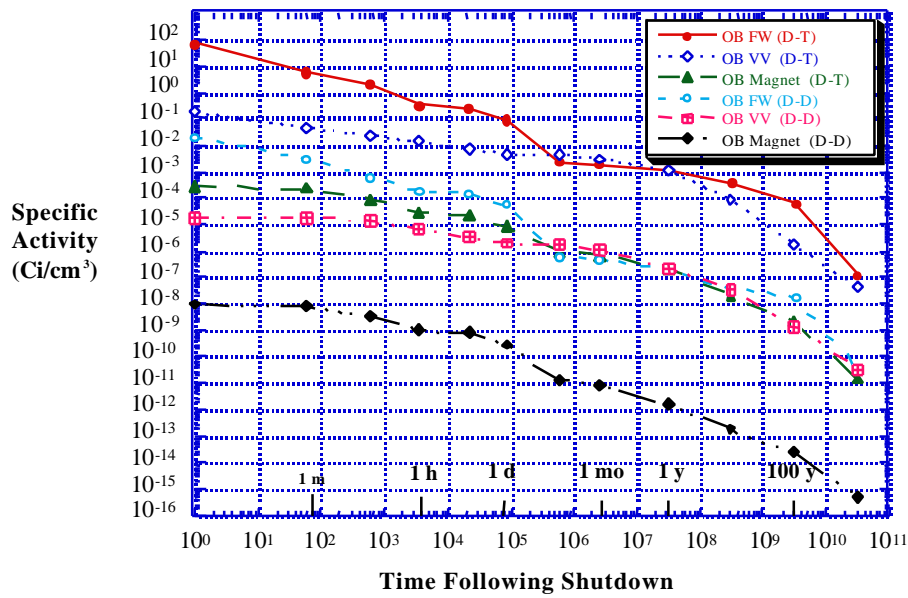


Fig. 5.10-2. Activity induced in the outboard side.

FIRE Engineering Report  
FY01 Update

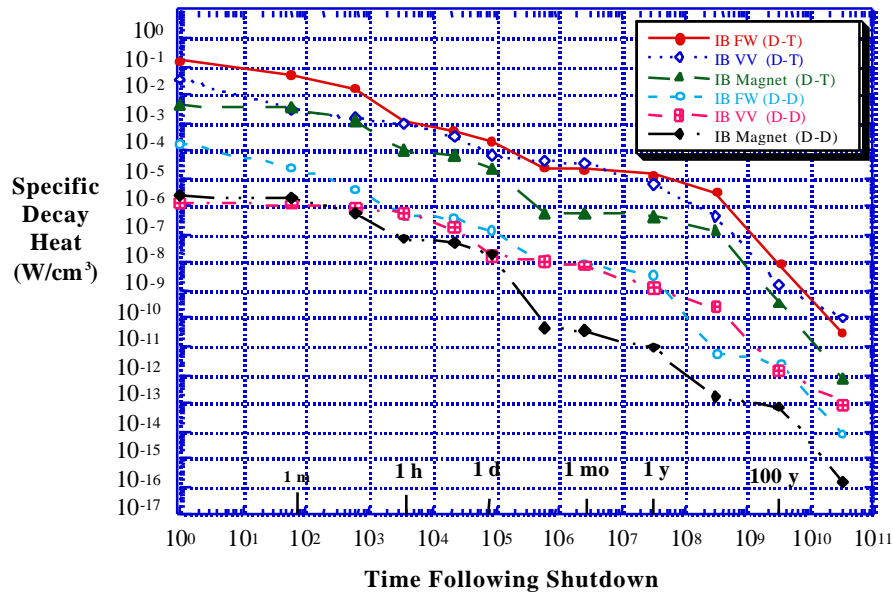


Fig. 5.10-3. Decay heat induced in the inboard side.

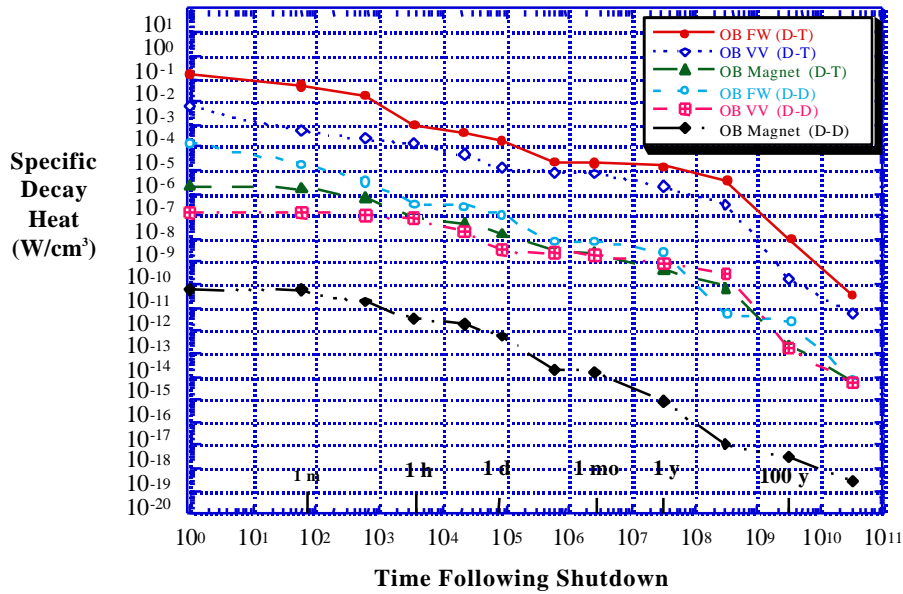


Fig. 5.10-4. Decay heat induced in the outboard side.

FIRE Engineering Report  
 FY01 Update

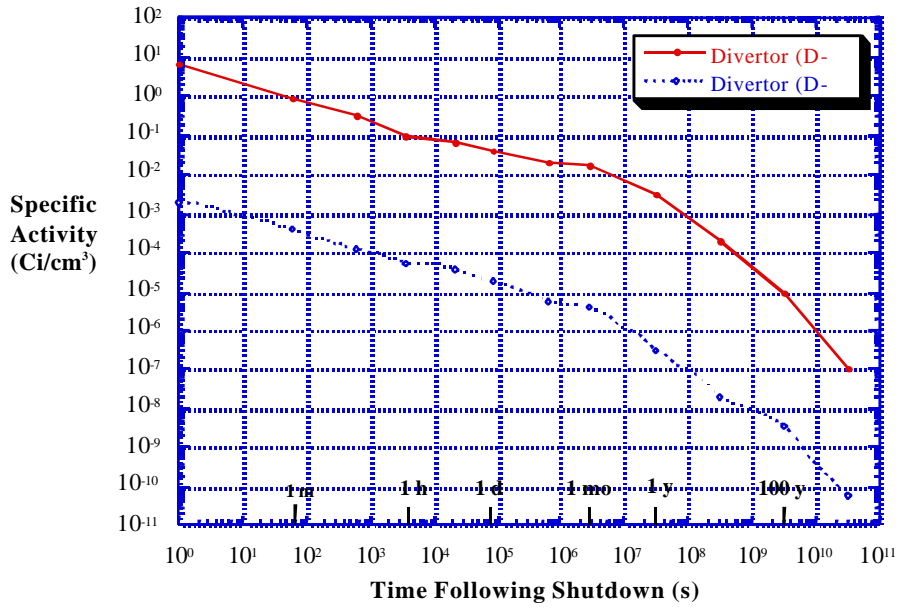


Fig. 5.10-5. Activity induced in the divertor.

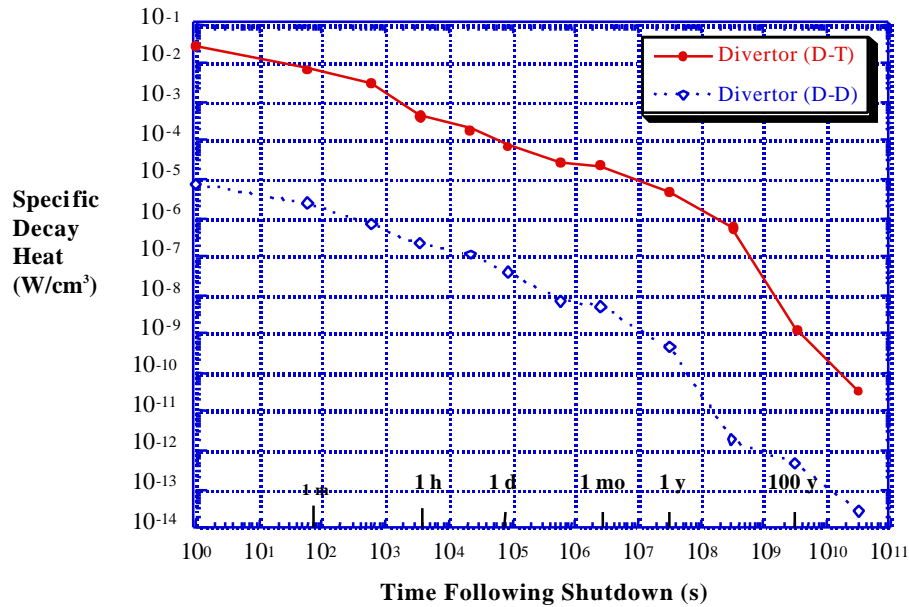


Fig. 5.10-6. Decay heat induced in the divertor.

FIRE Engineering Report  
FY01 Update

At shutdown, the decay heat induced in the first wall following D-T shots is less than 0.25% of the nuclear heating generated in the first wall during operation. In the mean time, the ratio between the shutdown decay heat and nuclear heating generated in the vacuum vessel during operation is on the order of 0.1%. The activity and decay heat generated following D-D shots are more than three orders of magnitude lower than their values following D-T shots due to the lower D-D fusion power and the significant reduction in the number of high energy neutrons.

two copper isotopes  $^{62}\text{Cu}$  ( $T_{1/2} = 9.74$  min) and  $^{66}\text{Cu}$  ( $T_{1/2} = 5.1$  min). The low decay heat induced in the first wall at shutdown is due to the fact that the short lifetimes of the  $^{62}\text{Cu}$  and  $^{66}\text{Cu}$  isotopes allow them to decay during the three hours between pulses. The decay heat induced in the vacuum vessel at shutdown is dominated by  $^{52}\text{V}$  ( $T_{1/2} = 3.76$  min) and  $^{56}\text{Mn}$  ( $T_{1/2} = 2.578$  hr) isotopes. Due to the short lifetime of  $^{52}\text{V}$ , its entire radioactivity also decays between shots, resulting in a low overall radioactivity generated in the vacuum vessel at shutdown. In general, the short-term activity and decay heat values at shutdown are almost fully dominated by activation during the last pulse. Table 5.10-I shows a list of nuclides that dominate the induced radioactivity in the different machine components.

**Table 5.10-I.** List of Dominant Nuclides.

<i>Short-term &lt; 1 day</i>		
	<b>Activity</b>	<b>Decay Heat</b>
FW	$^{62}\text{Cu}$ , $^{64}\text{Cu}$ , $^{66}\text{Cu}$	$^{62}\text{Cu}$ , $^{64}\text{Cu}$ , $^{66}\text{Cu}$
VV	$^{56}\text{Mn}$ , $^{58}\text{Co}$ , $^{51}\text{Cr}$	$^{56}\text{Mn}$ , $^{58\text{m}}\text{Co}$
Mag.	$^{62}\text{Cu}$ , $^{64}\text{Cu}$ , $^{66}\text{Cu}$	$^{62}\text{Cu}$ , $^{64}\text{Cu}$ , $^{66}\text{Cu}$
Div.	$^{187}\text{W}$ , $^{185}\text{W}$ , $^{181}\text{W}$	$^{187}\text{W}$ , $^{185}\text{W}$
<i>Intermediate-term &lt; 1 month</i>		
	<b>Activity</b>	<b>Decay Heat</b>
FW	$^{60}\text{Co}$ , $^{63}\text{Ni}$	$^{64}\text{Cu}$ , $^{60}\text{Co}$
VV	$^{55}\text{Fe}$ , $^{51}\text{Cr}$ , $^{57}\text{Co}$	$^{58}\text{Co}$ , $^{54}\text{Mn}$ , $^{58\text{m}}\text{Co}$
Mag.	$^{60}\text{Co}$ , $^{63}\text{Ni}$	$^{64}\text{Cu}$ , $^{60}\text{Co}$
Div.	$^{185}\text{W}$ , $^{181}\text{W}$	$^{185}\text{W}$ , $^{181}\text{W}$
<i>Long-term &gt; 1 year</i>		
	<b>Activity</b>	<b>Decay Heat</b>
FW	$^{63}\text{Ni}$	$^{63}\text{Ni}$
VV	$^{63}\text{Ni}$	$^{60}\text{Co}$ , $^{63}\text{Ni}$
Mag.	$^{63}\text{Ni}$	$^{63}\text{Ni}$
Div.	$^{91}\text{Nb}$ , $^{63}\text{Ni}$	$^{94}\text{Nb}$ , $^{39}\text{Ar}$

The decay heat induced in the first wall at shutdown is dominated by the

### 5.10.3 Biological Dose Rates

In order to assess the feasibility of hands-on maintenance, biological dose rates were calculated at different locations following shutdown. The gamma source from radioactive decay was determined at all mesh points and transported, using the DANTSYS 3.0 code, to calculate the dose rate at different locations following shutdown. The dose rates were calculated at the following locations:

- Behind the outboard vacuum vessel and magnet at the midplane.
- Behind the magnet at the machine top.
- Behind the additional shield at the machine top.

FIRE Engineering Report  
FY01 Update

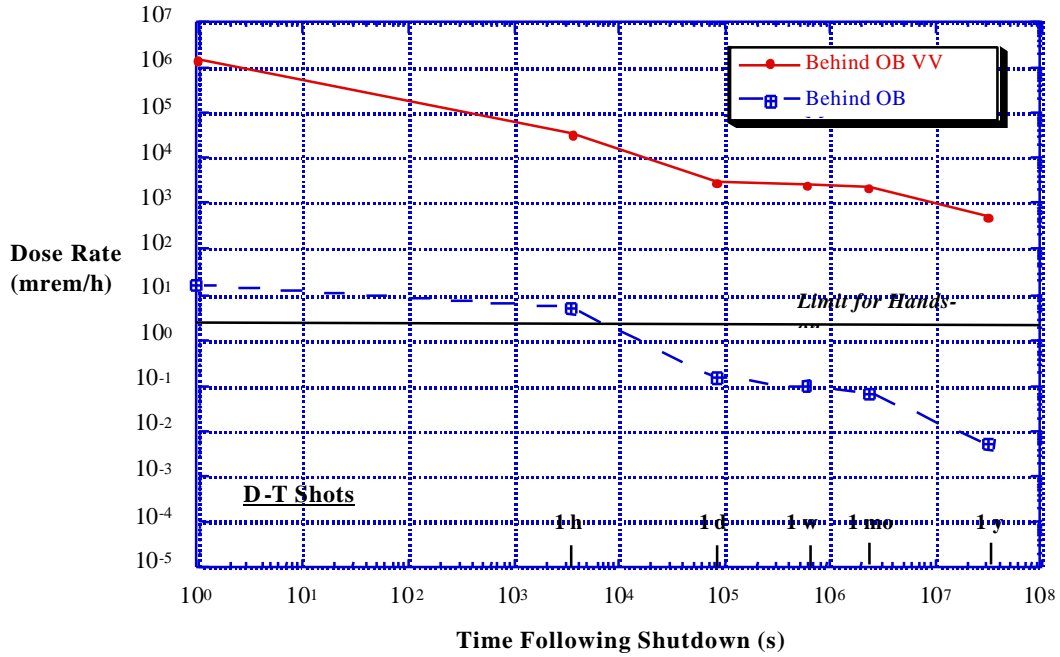


Fig. 5.10-7. Biological dose rates at the midplane following D-T shots.

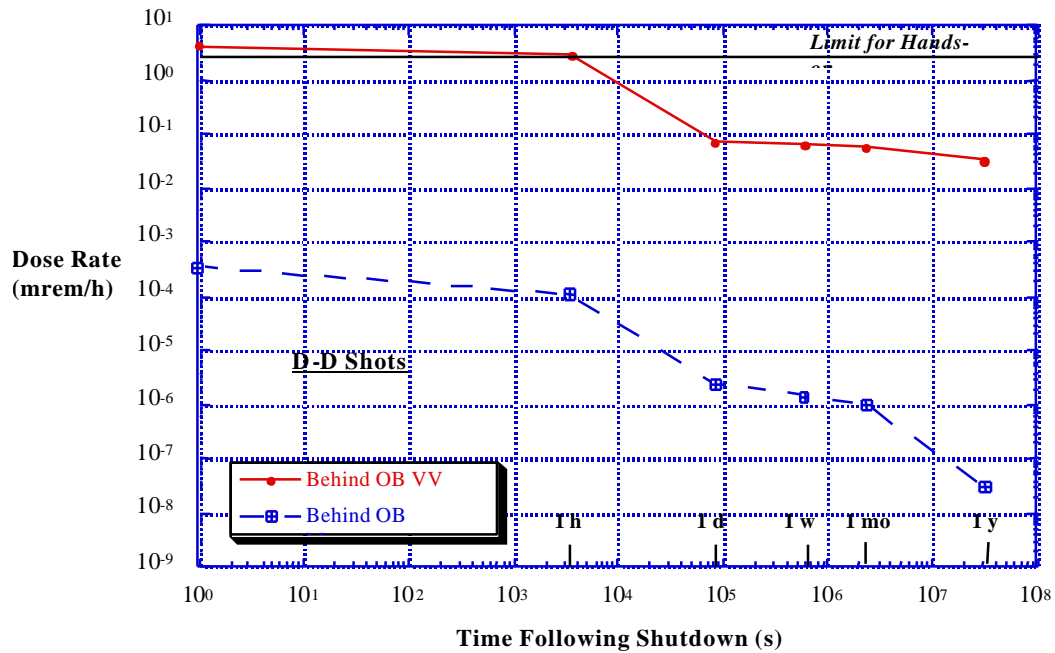


Fig. 5.10-8. Biological dose rates at the midplane following D-D shots.

FIRE Engineering Report  
 FY01 Update

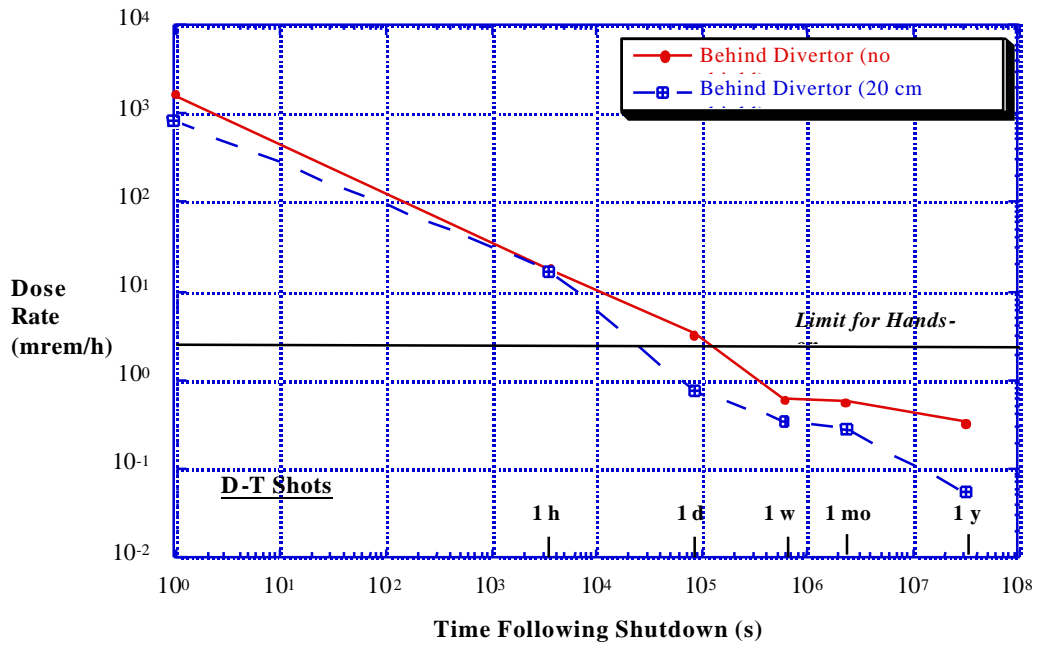


Fig. 5.10-9. Biological dose rates at the machine top following D-T shots.

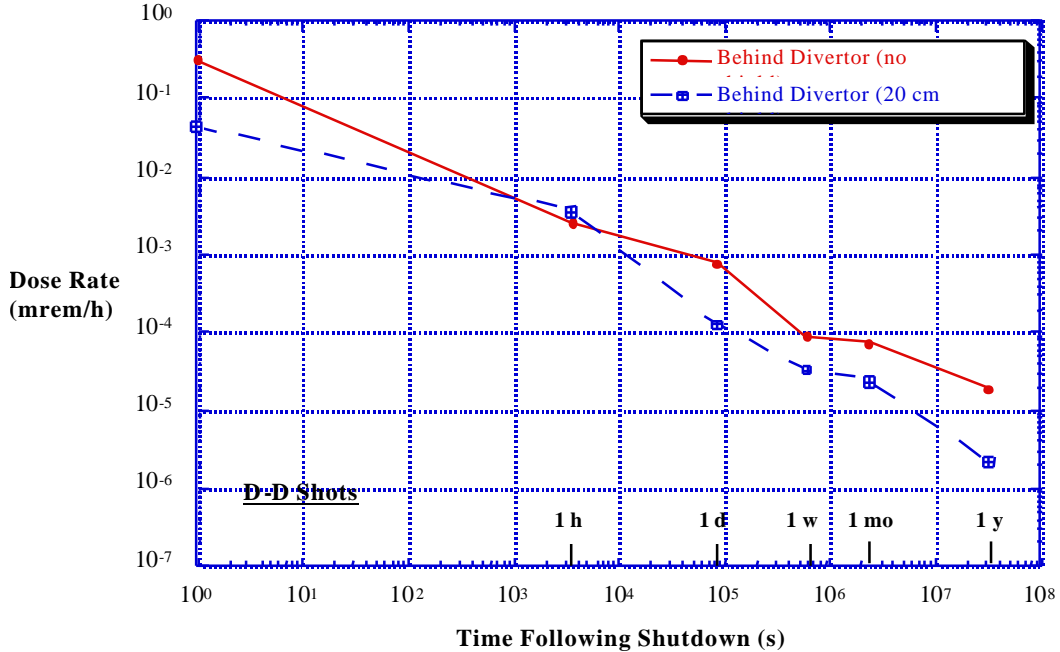


Fig. 5.10-10. Biological dose rates at the machine top following D-D shots.

## FIRE Engineering Report FY01 Update

Figures 5.10-7 and 5.10-8 show the biological dose rates at the midplane as a function of time following shutdown for D-T and D-D shots, respectively. As shown in figure 5.10-7, the biological dose rates behind the vacuum vessel remain high for several years following shutdown for D-T shots. On the other hand as shown in figure 5.10-8, in the case of D-D shots, the dose rates behind the vacuum vessel are five order of magnitudes lower than after D-T shots. The significant drop in the dose rate allows for hands on maintenance behind the vacuum vessel following D-D shots. The dose rates behind the magnet and at the midplane are acceptable for both D-D and D-T shots. Dose rates behind the magnet are caused by the  $^{62m}\text{Co}$  ( $T_{1/2} = 13.9$  min) isotope and are independent on the number of pulses due to the fact that  $^{62m}\text{Co}$  decays between pulses. One week following shutdown, the dose rates are dominated by the  $^{60}\text{Co}$  ( $T_{1/2} = 5.27$  yr) isotope. The dose rates caused by the  $^{60}\text{Co}$  isotope almost increase linearly with the increase in number of pulses. The calculations showed that using a 110 cm long steel plug in the midplane port will stop neutron streaming through penetration and provide adequate shielding that allows for hands-on maintenance.

The dose rates at the top of the machine (at the maximum divertor thickness) following D-T shots (figure 5.10-9), drops to an acceptable level within a day following shutdown. Adding a 20 cm thick POLY/CAST shield at the top of the magnet drops the dose rates on the top of the shield to acceptable levels only few hours earlier. However, since the divertor thickness is much smaller at other locations, it is essential to maintain the same shield

thickness to guarantee hands-on maintenance at all locations at the top of the machine. The shield is composed of a POLY/CAST mix placed inside a steel tank (the tank wall is 1 cm thick). The activation of the outer wall of the steel tank results in the generation of  $^{56}\text{Mn}$ . As shown in the figure, the  $^{56}\text{Mn}$  ( $T_{1/2} = 2.578$  hr) isotope results in a slightly higher dose (in comparison to the no shield case) outside the 20 cm thick shield during the first couple of hours following shutdown. As shown in figure 5.10-10, the dose rates at the top of the machine following D-D shots are very low, allowing for immediate access to that space any time following shots. Both the midplane port plug and the top shield were included in the FIRE baseline design.

### 5.10.4 Routine Release of $^{13}\text{N}$ to the Environment

Normal conducting copper magnets that are inertially cooled with LN2 are being considered in the near term ignition machines such as FIRE. In this case, liquid nitrogen is used to cool the magnets between shots. Nitrogen gas will exist inside the cryostat during the shots and will get irradiated. One radiological concern is the generation of radioactive  $^{13}\text{N}$ . The  $^{13}\text{N}$  is a major source of radioactive hazard. Activation calculations were performed for nitrogen gas at room temperature and at different locations inside the machine. The activation of nitrogen gas by D-T shots will produce  $^{13}\text{N}$  as well as a small amount of  $^{14}\text{C}$ .

Table 5.10-II gives the amount of  $^{13}\text{N}$  and  $^{14}\text{C}$  generated at different locations inside the cryostat following each D-T shot. The results indicate that

FIRE Engineering Report  
FY01 Update

the largest amount of  $^{13}\text{N}$  and  $^{14}\text{C}$  is generated in the space between the IB magnet and the IB VV. This is due to the fact that the shield thickness on the IB side is much smaller than that on the OB side. The thinner shield results in exposing the nitrogen gas in the IB region to a larger and harder neutron flux resulting in higher probabilities for the (n,2n) reaction that produces the radioisotope  $^{13}\text{N}$  from the natural  $^{14}\text{N}$  isotope and the (n,p) reaction that generates  $^{14}\text{C}$ . As a result, the specific activities in the IB side are much larger than those in the OB side. Although the gas volume in the IB side is smaller than in the OB side, the total activity is still about two orders of magnitude larger.

**Table 5.10-II.** Amount of Activity (Ci) Generated in the Nitrogen per D-T Shot.

Location of Nitrogen Gas	Activity (Ci)	
	$^{13}\text{N}$	$^{14}\text{C}$
Between IB Magnet and IB VV	1.2	$1.7 \times 10^{-6}$
Between OB Magnet and OB VV	$1.4 \times 10^{-2}$	$2.4 \times 10^{-8}$
Between OB Magnet and Cryostat	$8 \times 10^{-9}$	$7 \times 10^{-11}$

Another source of radioactive  $^{13}\text{N}$  is the activated air inside the building (outside the cryostat). Activation analysis of the large amount of air present inside the building showed that the amount of  $^{13}\text{N}$  generated per D-T shot is only  $2.5 \times 10^{-7}$  Ci. In addition, air activation results in the generation of  $8 \times 10^{-11}$  and  $2.8 \times 10^{-6}$  Ci of  $^{14}\text{C}$  and  $^{41}\text{Ar}$  per D-T shot, respectively. These are

extremely low levels of activity and should not cause any radiological concern.

### 5.10.5 Waste Disposal Ratings (WDR)

The radwaste of the different components of the machine were evaluated according to both the NRC 10CFR61 [4] and Fetter [5] waste disposal concentration limits. The 10CFR61 regulations assume that the waste disposal site will be under administrative control for 100 years. The dose at the site to an inadvertent intruder after the 100 years is limited to less than 500 mrem/year. The waste disposal rating (WDR) is defined as the sum of the ratio of the concentration of a particular isotope to the maximum allowed concentration of that isotope taken over all isotopes and for a particular class. If the calculated WDR = 1 when Class A limits are used, the radwaste should qualify for Class A segregated waste. The major hazard of this class of waste is to individuals who are responsible for handling it. Such waste is not considered to be a hazard following the loss of institutional control of the disposal site. If the WDR is  $> 1$  when Class A WDL are used but = 1 when Class C limits are used, the waste is termed Class C intruder waste. It must be packaged and buried such that it will not pose a hazard to an inadvertent intruder after the 100 years institutional period is over. Class C waste is assumed to be stable for 500 years. Using Class C limits, a WDR  $> 1$  implies that the radwaste does not qualify for shallow land burial. Fetter developed a modified version of the NRC's intruder model to calculate waste disposal limits for a wider range of long-lived radionuclides which are of interest for fusion

FIRE Engineering Report  
FY01 Update

researchers than the few that currently exist in the current 10CFR61 regulations. Fetter's model included more accurate transfer coefficients and dose conversion factors.

The waste disposal ratings for the 10CFR61 and Fetter limits are shown in Table 5.10-III. These values are at the FIRE end-of-life with total of 5TJ D-T and 0.5 TJ D-D fusion energy. Results in the table are given for compacted wastes. Compacted waste corresponds to crushing the solid waste before disposal and thus disallowing artificial dilution of activity. The dominant nuclides are given between brackets. At the end of the machine life, all components would qualify for disposal as Class C low level

waste according to the two waste disposal concentration limits used in the analysis. As shown in the table, according to Fetter limits, the WDR are dominated by the silver impurities in the CuCrZr alloy and the niobium impurities in the 316 SS and 304 SS alloys. The 10CFR61 limits indicate that the WDR of components made of the CuCrZr alloy are dominated by  $^{63}\text{Ni}$  which is produced from copper by the  $^{63}\text{Cu}(n,p)$  reaction. On the other hand, the WDR of components made of the steel alloys are dominated by their niobium impurities. Due to the reduced neutron environment following D-D shots, all components will easily qualify for disposal as Class C LLW.

**Table 5.10-III. Class C WDR.**

<b>Zone</b>	<b>Fetter</b>	<b>10CFR61</b>
IB FW	$0.2 ({}^{108m}\text{Ag})$	$2.16\text{e-}2 ({}^{63}\text{Ni})$
IB VV	$9.21\text{e-}2 ({}^{108m}\text{Ag}, {}^{94}\text{Nb})$	$3.46\text{-}2 ({}^{94}\text{Nb}, {}^{63}\text{Ni})$
IB Mag.	$1.96\text{e-}4 ({}^{108m}\text{Ag})$	$1.1\text{e-}3 ({}^{63}\text{Ni})$
OB FW	$0.21 ({}^{108m}\text{Ag})$	$2.36\text{-}2 ({}^{63}\text{Ni})$
OB VV	$1.06\text{e-}2 ({}^{108m}\text{Ag}, {}^{94}\text{Nb})$	$3.23\text{e-}3 ({}^{94}\text{Nb}, {}^{63}\text{Ni})$
OB Mag.	$2.26\text{e-}6 ({}^{94}\text{Nb})$	$2.56\text{e-}6 ({}^{94}\text{Nb}, {}^{63}\text{Ni})$
Divertor	$3.4\text{e-}2 ({}^{108m}\text{Ag})$	$1.33\text{e-}2 ({}^{94}\text{Nb})$

**References for Section 5.10:**

- [1] R.E. Alcouffe et al., "DANTSYS 3.0, One-, Two-, and Three-Dimensional Multigroup Discrete Ordinates Transport Code System," RSICC Computer Code Collection CCC-547, Contributed by Los Alamos National Lab, August 1995.
  
- [2] M. J. Sisolak, Q. Wang, H. Khater and D. Henderson, "DKR-PULSAR2.0: A Radioactivity Calculation Code that Includes Pulsed/Intermittent Operation," to be published.
  
- [3] A. Pashchenko et al., "FENDL/A-2.0: Neutron Activation Cross-Section Data Library for Fusion Applications," Report INDC(NDS)-173, IAEA Nuclear Data Section, March 1997.
  
- [4] Nuclear Regulatory Commission, 10CFR part 61, "Licensing Requirements for Land Disposal of Radioactive Waste," Federal Register, FR 47, 57446 (1982).
  
- [5] S. Fetter, E. Cheng and F. Mann, "Long Term Radioactive Waste from Fusion Reactors," Fusion Engineering and Design, 13, 239-246 (1990).

## 5.11 Remote Maintenance

### 5.11.1 Introduction

FIRE in-vessel components will become neutron activated, making it necessary to perform maintenance operations by remote techniques. Components that require remote maintenance include those mounted on the vessel interior and in the ports.

When maintenance is required, the affected components are removed from the vessel and transferred to the hot cell where they are refurbished or processed as waste. They are then replaced in the vessel by the refurbished units or a spare.

First wall (FW) and divertor modules are accessed through any of the 16 midplane ports and are handled with a cantilevered boom. Port mounted assemblies such as heating systems and cryopumps are replaced by remote handling (RH) equipment operating on the outboard end of the related port.

The strategy for FIRE ex-vessel maintenance is to employ hands-on techniques to the fullest extent possible. The FW, VV and external structures, including the magnets, are designed to provide sufficient combined shielding to allow controlled access and hands-on maintenance on the complete exterior of the machine. This includes the outboard end of the VV ports for removal of service connections in advance of removing port-mounted systems, and access to other ex-vessel areas for maintenance of services and components such as magnet current and coolant feed lines.

### 5.11.2 Remote Maintenance Requirements and Classification of Components

FIRE systems and components are designed to minimize remote maintenance requirements where possible. When remote maintenance is required, component modularity, standardization and segmentation are implemented to reduce costs, risks and maintenance time. Design features facilitating RH are standardized to minimize the number and variety of handling equipment and tools. Handling equipment is designed for ease of decontamination to allow hands-on reconditioning and repair.

Machine availability should not be compromised by maintenance operations, especially by those that are regularly required. For this reason, components that require regular remote maintenance (e.g., divertor modules and port-mounted assemblies) are designed so they can be replaced in a relatively short time period.

In-vessel component designs should be optimized towards maximum verification of component performance prior to installation in the VV. This leads to the general requirement that components are fitted and withdrawn for maintenance as much as possible in one piece, avoiding or minimizing the cutting and re-welding of functional elements.

All components are classified according to their RH requirements by the following scheme. Classification is based on the need for scheduled or unscheduled maintenance or modification, the likelihood of maintenance, and on the impact of the maintenance procedure on machine operations and availability.

Once a component's classification has been determined, the type of RH equipment required, the guidelines for component design, and the program to assure RH compatibility is established. Components that obstruct access are given at least the same classification as the component to which the access is blocked, provided they require RH.

### **Class 1**

The first category includes components that require several regularly scheduled maintenance or replacement operations (e.g., divertor). The component designs and the associated RH equipment and service procedures are optimized to ensure task completion within a specified time. All RH equipment for Class 1 components will be designed in detail during the design phase of the project. The feasibility of Class 1 maintenance tasks are to be verified during the design phase, or prior to final fabrication and may involve the use of mock-ups. Further demonstration using real components during initial assembly is highly desirable.

### **Class 2**

The second category contains components that do not require scheduled maintenance but are likely to require a few unscheduled maintenance or removal operations (e.g., FW modules). These components are designed for full remote repair or replacement, but minimization of repair and replacement time is subordinate to consideration for the component's design, such as nuclear performance and operational reliability. RH equipment for Class 2 components will be designed in detail during the design phase of the project. The feasibility of Class 2 maintenance tasks will be verified where

deemed practical and necessary and may involve the use of mock-ups. Demonstration using actual components during initial assembly of the machine is very desirable.

### **Class 3**

The third category of components are not expected to require maintenance, such as a VV segment and toroidal field coil. These components are expected to last through the operating phase, and major maintenance or upgrading is not anticipated. If major maintenance operations should be needed, they will require substantial disassembly of at least part of the tokamak and the projected maintenance time may be long. Although these components must be designed to make disassembly and replacement feasible by RH means, their design emphasizes reliability and performance optimization. The procedures for maintenance of selected Class 3 components will be defined during the design phase.

### **Class 4**

The fourth category of components do not require remote maintenance or are non-essential to continued operation. Class 4 includes components that:

- are hands-on accessible and maintained;
- are non-essential to FIRE operation and are considered expendable in the event of failure; or
- have negligible risk of failure.

The RH classification of major FIRE components is presented in Table 5.11.2-1. Auxiliary systems such as diagnostics and heating systems are not specifically listed. They are housed in standard port assemblies.

**Table 5.11.2-1 Remote Handling Classification of Major FIRE Components**

Class 1	Class 2	Class 3	Class 4
Divertor Modules	First Wall Tiles	Vacuum Vessel Octant with Toroidal Field Coils	Toroidal Field Coil Connections
Limiter Modules	Upper and Lower Horiz. Auxiliary Port Assemblies	Passive Plates and internal control coils (must be removed with vessel)	Poloidal Field Coils
Midplane Port Assemblies - RF heating - diagnostics	- cryopumps - diagnostics	In-Vessel Cooling Pipes - divertor pipes - limiter pipes	Central Solenoid Magnet Structure

Additional information regarding the anticipated frequency of component maintenance and maintenance time estimates is contained in the appendix.

### 5.11.3 Remote Maintenance Approach

In-vessel components will generally be removed as integral assemblies and transferred to the hot cell where they will be repaired or processed as waste. In-situ maintenance operations will typically be limited to inspection (viewing and metrology), vacuum window replacement and leak testing.

#### Containment and transfer of in-vessel components

In-vessel interventions are carried out with the VV cooled and vented. At least one containment barrier is required during openings to prevent the release of hazardous material (i.e., activated dust, tritium and beryllium). For this reason, in-vessel interventions will be performed from sealed transfer casks that dock to

the VV ports and that contain the required RH equipment. Cask docking interfaces at the ports and hot cell utilize “double seal doors” to keep the exterior surfaces of the port and cask doors clean.

Component transfer casks are not shielded due to the resulting excessive weight and size. When VV ports are open for extended periods, e.g., during in-vessel interventions involving the removal of several in-vessel components, a shielded enclosure will be installed at the port opening / cask location so that personnel access to other ex-vessel regions of the machine is possible.

Transfer routes between the VV and hot cell will be evacuated of personnel when a cask containing activated components is moved. This would typically be performed during off-shift hours to minimize interruptions to machine access. Casks will be moved by either the facility overhead crane or a separate vehicle such as an air cushion transporter.

### **Port-mounted system maintenance and handling**

Port-mounted systems are housed in a standard integrated assembly that includes shielding for the port opening. Auxiliary heating systems are mounted in midplane ports, diagnostics utilize all port types and cryopumps are mounted in the upper and lower auxiliary ports. Midplane port assemblies are removed to either maintain the system assembly or to gain access to the in-vessel plasma region.

Port assembly design details will vary depending on the system, but the space envelope, port attachments and handling techniques are standardized. The assembly is mechanically attached and vacuum seal welded at the vacuum closure plate located at the outboard end of the port. Prior to cask docking and removal operations, the system services (e.g., cooling water pipes, waveguides, transmission lines, etc.) feeding through the port interface in the ex-vessel region are hands-on removed. Remote operations begin with the disassembly of the VV closure plate.

Port assembly handling equipment includes a cask, double seal door and handling vehicle. A transfer cask and RH equipment are provided for each type of port (i.e., midplane port and upper & lower horizontal auxiliary port). The handling vehicle attaches to the assembly's vacuum closure plate. A manipulator is included onboard the vehicle for handling tools and performing closure plate bolting and vacuum seal cutting and welding operations. After disconnection from the port, the assembly is withdrawn to the

cask and is transferred to the hot cell for repair or replacement of any faulty components. Installation is performed by a reversal of these operations.

### **Divertor, first wall and limiter module maintenance and handling**

These components are accessed and handled through the midplane ports. At least one port assembly must first be removed using the equipment and procedures discussed in the previous section. The handling system consists of a cantilevered articulated boom operating from a transfer cask docked to the VV port as shown in Figure 5.11.3-1.

The boom reaches one-quarter of the in-vessel surfaces from a single port so localized module replacements can be performed through one or more ports and the complete in-vessel region can be accessed from 4 of the 16 midplane ports. The boom is equipped with an end-effector to position and handle either the divertor, FW or limiter modules. Different end-effectors specific to each of the module types is necessary. The end-effector envisioned for divertor module maintenance is illustrated in Figure 5.11.3-2. In addition, a general-purpose manipulator end-effector may be required to provide adaptable handling capabilities and to perform certain component maintenance operations.

Prior to removal, coolant pipes to the divertor and limiter modules must be cut. This is performed with pipe bore tooling that is hands-on deployed inside the coolant pipes where they enter the upper and lower horizontal ports. The pipes are then re-welded to the modules and leak checked during the installation process.

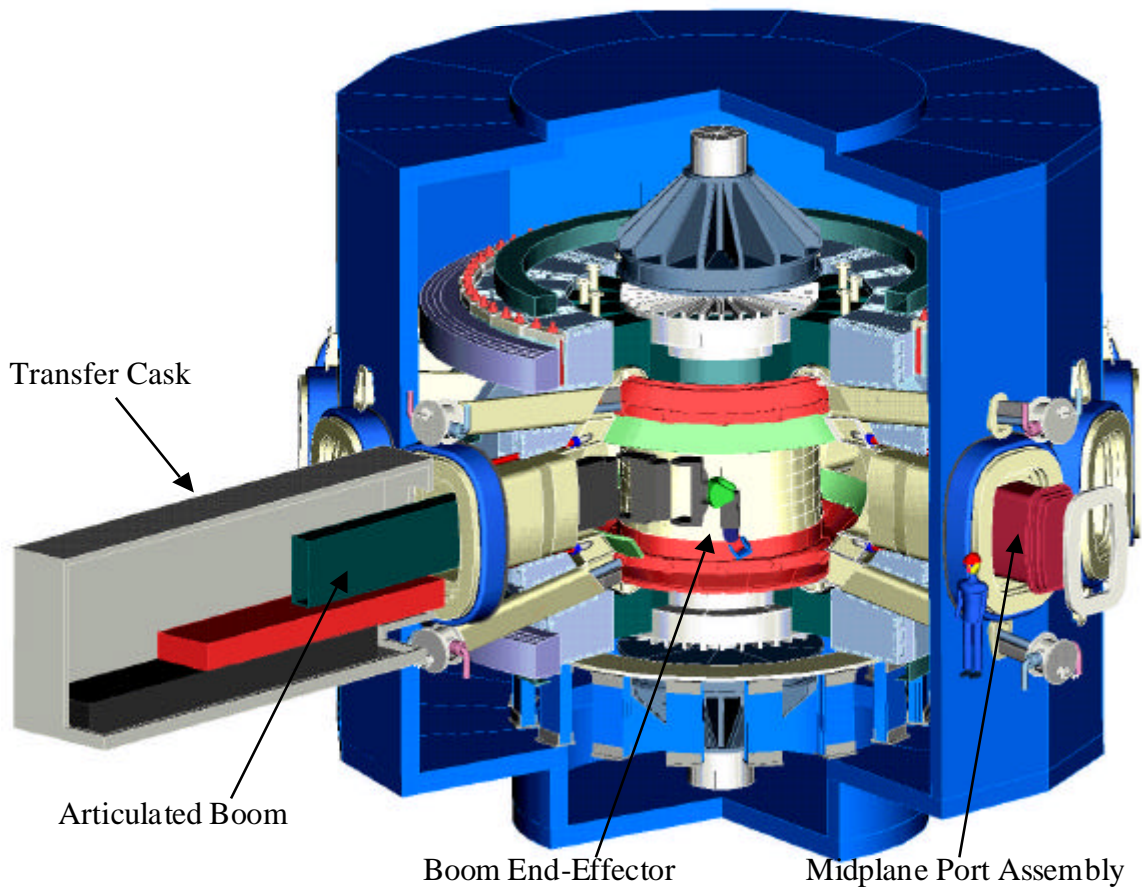
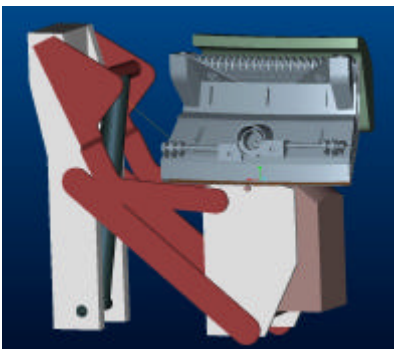


**Figure 5.11.3-1 In-vessel transporter deployed inside the vacuum vessel**

Once disconnected from the VV, a module, or modules, are removed to the

- High capacity (800 kg)
- 4 positioning degrees of freedom  
positioning accuracy ~ 2 mm required



FIRE Engineering Report  
June, 2000

cask and transferred to the hot cell for repair operations such as surface refurbishment.

**Inspection of Plasma Facing Surfaces**

Plasma facing surfaces must be periodically inspected to verify alignment, quantify erosion, and perform visual inspections. Viewing and metrology inspection is performed with vacuum compatible probes that are inserted through an upper vertical port to the plasma region of the vessel. Inspections are conducted between

plasma shots with the vessel at vacuum and bake-out temperatures, or during maintenance campaigns with the vessel cooled and vented.

Metrology measurements of sub-millimeter accuracy are required and achieved with a frequency-modulated coherent laser radar based sensor. Viewing is performed with conventional camera (video) based systems. Both inspection systems utilize a common vacuum compatible deployment probe design.

FIRE Engineering Report  
FY01 Update

**5.12 FIRE Magnet Power Supplies**

Requirements

The FIRE electrical load consists of a steady continuous load associated with the plant auxiliary systems (15MVA, 0.8 p.f., continuous duty), and a pulsed load associated with the experimental operations due to the Toroidal Field (TF), Poloidal Field (PF), and RF Heating (RF) power supply systems. The latter consists of a pulse followed by a cooling interval during which the load is zero. For the design basis scenario the pulse is on for approximately 60 seconds, then off for the assumed 2 hour

repetition period. (Presently the repetition period is set by the 3 hr. cool-down). During any 24 hour period it should be possible to perform up to 12 full power pulses, at a rate not faster than once every 2 hours. Over the lifetime of the project, a total of 3000 full power pulses, and 30000 pulses at 2/3 power (with an accelerated repetition rate within the heat load limits of the facility) are planned.

*TF System*

The FIRE TF coil system supplies a vacuum field of 10T at 2.14m. The following are the main parameters.

**Table 5.12-1 TF Coil System Parameters**

#Coils	16	
Turns/Coil	15	
Inner Leg Material	68% IACS BeCu precooled to 80K	
Inner Leg Inner Radius*	0.490	m
Inner Leg Outer Radius*	1.366	m
Inner Leg Height**	1.815	m
Inner Leg 20C Resistance	6.8	$\mu\Omega$ /turn
Inner Leg Nuclear Heating***	30	MW
Outer Leg Material	100% IACS Cu precooled to 80K	
Outer Leg Inner Radius*	3.450	m
Outer Leg Outer Radius*	4.038	m
Outer Leg 20C Resistance	4.75	$\mu\Omega$ /turn
Current per Turn	445.8	kA
Inductance	38.6	mH

\*to conductor face

\*\*above midplane, to centerline of horizontal limb

\*\*\*during flat top only

The TF current and power waveforms are given in the following figure. These are based on a simple model of the coil and power system which neglects current diffusion but accounts for coil heating and resistance variation with

temperature. The power supply is modeled as a controlled voltage source with a no-load voltage of 1.3kV, 20% regulation at full load, and a constant voltage of 66.6% of the no-load voltage during current shutdown (inversion).

FIRE Engineering Report  
FY01 Update

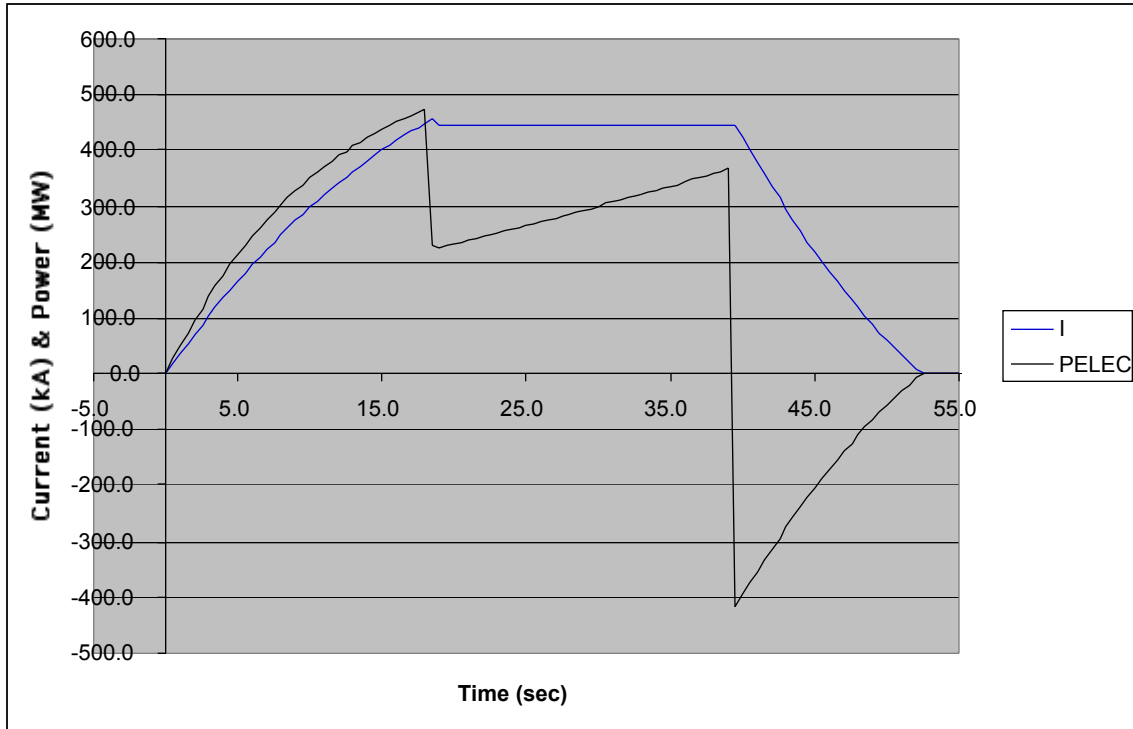


**Figure 5.12-1 TF Current and Power Waveforms**

*PF System*

The PF coils are wound from OFHC copper and are pre-cooled to 80K prior to a pulse. PF coil dimensions,

inductances, 20C resistances, and required coil currents are given in the following tables (based on C Kessel input 7/26/01).

**Table 5.12-2 PF Coil Dimensions**

	CS1	CS2	CS3	PF1	PF2	PF3	PF4
R (m)	0.68	0.68	0.68	0.8557	1.291	3.304	4.766
Z (m)	0.452	1.158	1.6668	2.2385	2.506	3.12	1.2
$\Delta R$ (m)	0.4	0.4	0.4	0.325	0.325	0.4	0.4
$\Delta Z$ (m)	0.904	0.5086	0.5086	0.38	0.38	0.4	0.4
Turns	240	120	120	96	96	72	84
Fill	0.85	0.85	0.85	0.85	0.85	0.85	0.85

FIRE Engineering Report  
FY01 Update

**Table 5.12-3 PF Coil Inductances (H) and 20C Resistances ( $\Omega$ )**

	CS1	CS2	CS3	PF1	PF2	PF3	PF4	PLASMA
CS1	1.37E-01	2.67E-02	1.03E-02	5.09E-03	6.75E-03	7.44E-03	1.40E-02	2.00E-04
CS2	2.67E-02	3.41E-02	1.59E-02	5.38E-03	5.68E-03	4.10E-03	6.67E-03	7.13E-05
CS3	1.03E-02	1.59E-02	3.36E-02	1.29E-02	9.85E-03	4.53E-03	6.26E-03	5.06E-05
PF1	5.09E-03	5.38E-03	1.29E-02	3.59E-02	2.26E-02	6.40E-03	7.20E-03	4.13E-05
PF2	6.75E-03	5.68E-03	9.85E-03	2.26E-02	6.64E-02	1.54E-02	1.55E-02	7.25E-05
PF3	7.44E-03	4.10E-03	4.53E-03	6.40E-03	1.54E-02	1.35E-01	6.32E-02	1.33E-04
PF4	1.40E-02	6.67E-03	6.26E-03	7.20E-03	1.55E-02	6.32E-02	3.59E-01	3.06E-04
PLASMA	2.00E-04	7.13E-05	5.06E-05	4.13E-05	7.25E-05	1.33E-04	3.06E-04	9.12E-06
20C Resistances	2.76E-02	1.23E-02	1.23E-02	1.63E-02	2.46E-02	2.73E-02	5.36E-02	

**Table 5.12-4 PF Coil Currents (MA-turn) for a Pulse T(sec)**

T	Ics1	Ics2	Ics3	Ipf1	Ipf2	Ipf3	Ipf4	Ip
-10	0	0	0	0	0	0	0	0
0	8.51	5.97	3.03	2.38	3.86	0.454	0.171	0
0.5	7.46	5.23	2.66	2.08	3.37	0.394	0.145	0.1
6	-11.97	1.5	1.72	4.75	4.75	-3.36	-2.81	6.44
8.5	-10.7	1.55	1.51	4.05	4.05	-1.48	-3.95	6.44
27	-11.74	0.858	0.96	3.7	3.7	-1.58	-3.96	6.44
30	-9.89	2.72	2.69	2.7	2.7	-1.19	-2.61	5
34	0.59	0.382	0.217	0.152	0.183	0.002	0.018	0.1
40	0	0	0	0	0	0	0	0

The PF coil current scenario, in Amp/turn, is depicted in the following figure.

It is noted that only CS1, PF3, and PF4 are bipolar.

FIRE Engineering Report  
FY01 Update

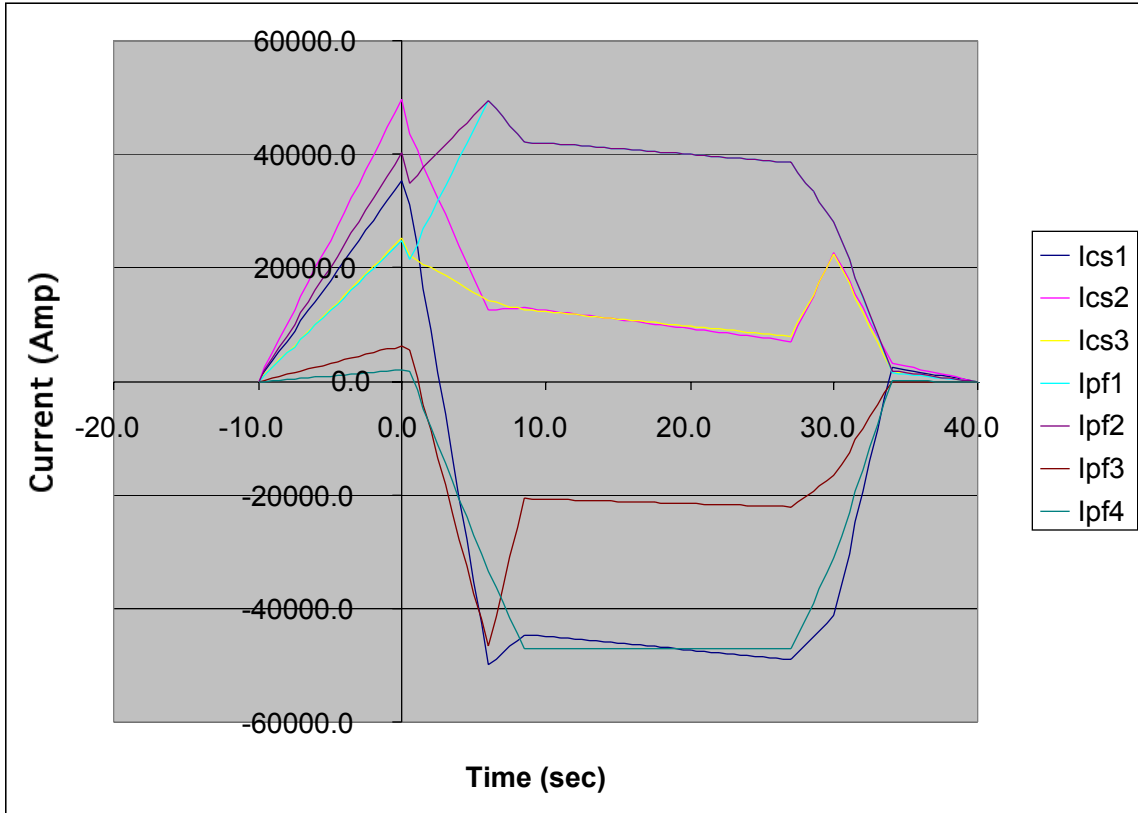


Figure 5.12-2 PF Current Scenario

*RF System*

The auxiliary heating is assumed to consist of RF with 50% efficiency from AC input to the plasma. A power level

of 20MW is assumed during Ip ramping and for the remaining interval prior to burn, and a level of 10MW is assumed during the burn.

*Overall Scenario*

Overall timing is as follows.

**Table 5.12-5 Scenario Timing**

Event	Time (sec)
Plasma Initiation	0.0
Start TF Flat Top and Start 20MW RF	6.0
Start Ip Flat Top	6.0
Start burn and 10MW RF	8.5
End Ip and TF Flat Top	27.0

The TF and Ip flat top durations are 21.0 seconds.

FIRE Engineering Report  
FY01 Update

The active power (MW) waveforms of the systems are given in the following figure. PF power is computed based on  $V \cdot I$  where  $V = R \cdot I + \sum M di/dt$ , and R is a

function of the coil temperature which increases during the pulse as the coils dissipate power.

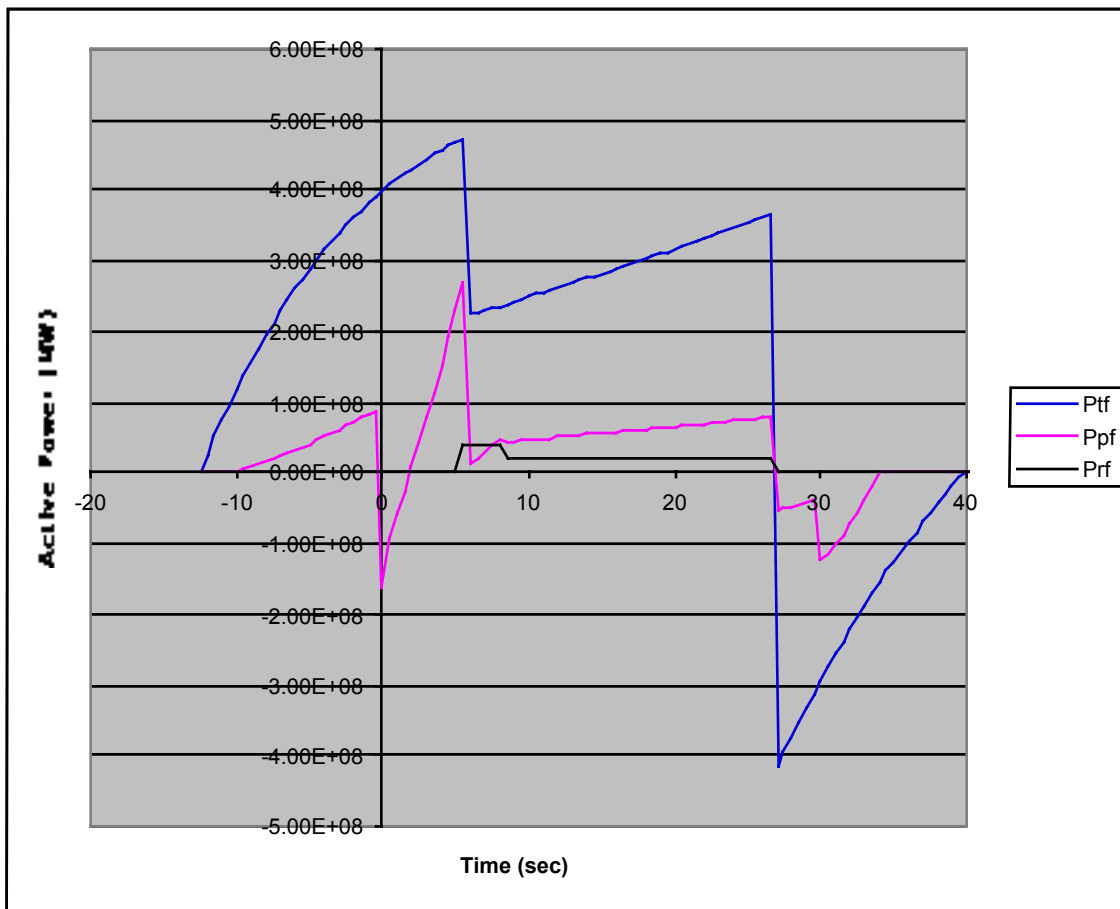


**Figure 5.12-3 TF, PF, and RF Power Waveforms**

Composition of the load is given in the following table.

**Table 5.12-6 Composition of Load**

System	Peak Power (MW)	Peak Energy (GJ)
TF	470	11.6
PF	270	2.0
RF	40	0.5
Composite Total	780	14.1

The reactive power (MVAR) waveform is highly dependent on details of the AC/DC converter system design, along

with the implementation of reactive power control and compensation schemes.

FIRE Engineering Report  
FY01 Update

Power Systems Design Concept

*TF Power Supply System*

The TF electrical power supply consists of AC/DC thyristor and/or diode converters consisting of series/parallel connected 6-pulse rectifier modules. It is noted that the 1.3kV no-load voltage rating of the TF system could be realized using two series layers of rectifiers each at 650Vdc, which corresponds to an input voltage of 480Vac. This choice lends itself to the application of common power semiconductor devices as designed and optimized for industrial usage at that voltage level.

The TF circuit operates in three successive phases namely current rise, flat top, and shutdown. Current rise time is minimized by applying the maximum available voltage. During flat top the voltage is controlled to maintain constant current. During shutdown the voltage polarity is reversed to drive the current to zero as quickly as possible and extract a large fraction of the stored magnetic energy at flat top. In case of failure of the power supplies to properly invert, they are bypassed and zero voltage is applied to the coil. In this case the coil current decays according to the L/R time constant of the circuit and most of the stored energy is dissipated in the coil resistance. An option would be to add a DC circuit breaker system and dump resistor which could be used in case the power supplies fail to invert. This would provide a means for discharging some of

the stored magnetic energy outside of the coil system in the event of a fault.

The present choice of TF power supply voltage is consistent with a 21 second flat top time at 10T, and a maximum prospective end of pulse temperature of 373K, in case the power supplies fail to invert and the coil has to absorb the full stored energy.

*PF Power Supply System*

The PF power supply system will supply controllable DC voltage to the PF coils via series/parallel connected phase controlled AC/DC thyristor converter modules. In addition, it is assumed that each PF circuit will include a DC circuit breaker and discharge resistor to provide a high loop voltage during plasma initiation. The multiple power supply modules in each circuit will be controlled in such a way that the net voltage matches the time varying demand of the load while the net reactive power demand from the AC power system is minimized.

The following table summarizes the requirements for the power supplies in each of the PF circuits. Here it is assumed that modular power supplies with a 1kV open circuit voltage are connected in series and parallel as required to provide the voltage and current described by the waveforms along with sufficient voltage margin.

FIRE Engineering Report  
FY01 Update

**Table 5.12-7 PF Power Supply Requirements**

	CS1	CS2	CS3	PF1	PF2	PF3	PF4
Max MW	95.0	22.6	8.1	8.7	21.0	78.4	88.5
Min MW	-60.3	-34.7	-15.4	-14.8	-35.5	-41.7	-69.1
Max kA	35.5	49.8	25.3	49.5	49.5	6.3	2.0
Max V(I>0)	817.5	477.9	339.0	313.9	548.5	269.4	305.0
Min V(I>0)	-2054.3	-697.9	-608.8	-598.2	-883.5	-1718.2	-2704.9
MVA(I>0)	72.8	34.7	15.4	29.6	43.7	10.8	5.5
Min kA	-49.9	0.0	0.0	0.0	0.0	-46.7	-47.1
Max V(I<0)	1090.4	0.0	0.0	0.0	0.0	964.8	2581.8
Min V(I<0)	-2234.1	0.0	0.0	0.0	0.0	-1869.3	-2925.7
MVA(I<0)	111.4	0.0	0.0	0.0	0.0	87.2	137.9
Max MVA	111.4	34.7	15.4	29.6	43.7	87.2	137.9
Regulation	0.15	0.15	0.15	0.15	0.15	0.15	0.15
VOCmin	2628.4	821.0	716.3	703.8	1039.4	2199.2	3442.0
NS	3	1	1	1	1	3	4
VOC(Volts)	3039	1013	1013	1013	1013	3039	4051
Vmargin	0.13	0.19	0.29	0.31	-0.03	0.28	0.15
Ipss(kA)	15	15	15	15	15	15	15
NP(I>0)	3	4	2	4	4	1	1
NP(I<0)	4	0	0	0	0	4	4
NPSS	21	4	2	4	4	15	20

The optimization of the design of the PF power supply system can be performed once a specific site is selected for FIRE and the range of operating scenarios and control requirements, beyond the basic scenario waveforms, is described. Some of the inter-related factors to be considered include the following:

- reactive power tolerance of local grid, or local energy storage, shall not be exceeded;
- reactive power compensation shall be implemented to the extent that it is cost effective and able to respond in the time scale of the dynamics of the load;
- sufficient voltage margin shall be included in each circuit;

- minimization of reactive power consumption of PF system favors the use of relatively small converter module ratings;
- minimization of cost of PF AC/DC converter system favors the use of a minimum number of unique converter module ratings;
- minimization of cost of PF AC/DC converter system favors the use of relatively large converter module ratings and/or ratings which are similar to those already in use in industry.

All of the above factors need to be considered to optimize the design (minimize cost) while constraining the demand for active and reactive power within the ratings of the source.

## FIRE Engineering Report FY01 Update

### *AC Power System*

It is desired to supply as high a fraction as possible of the FIRE load directly from the grid. An interface with the grid at 500kV is preferred, although 345kV might suffice if some fraction of the power is supplied from local energy storage devices. The base portion of the fire load, approximately 400MW, has a duration of order 40 seconds, which extends beyond the inertial response of the power system, into the governor response period, such that prime mover power generation will increase to supply the incremental load. Superimposed on the base portion are two transients of order 400MW which are of short duration, within the inertial response of the grid. There are large power steps associated with these transients, which will impact the generators in the grid in inverse proportion to their electrical distance from FIRE. If necessary, local energy storage can be implemented to reduce the impact of the load on the grid, in particular the transients. This would serve to reduce the amount of peak power to be transmitted to the site, and would mitigate the transients on nearby generators. The use of motor-generator-flywheel (MG or MGF) systems for this purpose remains the preferred approach. One possibility would be to power the PF systems, which cause most of the power steps, using a conventional type MG system comparable in scale to the TFTR machines, and power the other systems directly from the grid. Another possibility would be to use an AC excited MG scheme in which case all of the converters would be powered directly from the grid, but the load would be buffered. Depending upon the scheme selected for local energy storage, if any, reactive power compensation will be required to some degree, depending on the characteristics of the grid. Switched

capacitors are probably adequate for this purpose. In addition, switched resistors can be implemented on the AC or DC side to reduce the power steps, if necessary. The detailed design of the FIRE power system needs to be undertaken with the full cooperation of the host utility, and dynamic power flow studies need to be performed based on specific site conditions to assess the impact and determine what measures, if any, need to be taken by FIRE to supply active or reactive power locally.

### *Supply of FIRE at Site with Local Energy Storage*

Some sites could be considered for FIRE which do not have the capability of supplying 100% of the power via the grid. In these cases local energy storage capability will be required. As an example, a study was performed of FIRE at the PPPL site where the TFTR power supply resources already exist.

The main features of an implementation at PPPL would be:

- the two existing D-site MG sets would be dedicated to the FIRE TF system, and operated within their basic power rating except run down below 60Hz to obtain additional energy, within the 50Hz/5.7GJ level recommended in earlier “superpulse” studies by the manufacturer (GE);
- new AC/DC converter systems would be procured for the FIRE TF system, consisting of two systems connected in series. One is a diode converter which receives its AC input directly from the 138kV utility grid, and the other is a thyristor converter which receives its input from the existing D-site MG sets. Both would inject full voltage during the current rise. During flat top, the

FIRE Engineering Report  
FY01 Update

converter fed by the grid would continue to inject its full voltage, while the converter fed by the MG would be phase controlled to maintain constant flat top current;

- the grid would supply 200MW during TF flat top. Power factor correction would be required to supply 180MVAR to bring the net pulsed load to unity power factor;

- a new MG set would be procured for the FIRE PF and RF systems. The design would be identical to the existing D-site MG sets;

- the 74 existing D-site Transrex AC/DC thyristor converter sections would be

reconfigured to supply the FIRE PF systems. They are de-rated from 24kA to 15kA because of the long pulse length. For those PF circuits which require bi-directional current flow, anti-parallel configuration would be provided.

An initial configuration with flat top time limited to 12.5 seconds instead of the nominal 21.0 seconds could be supplied without the addition of a new MG set.

Distribution of load would be as summarized in the following table.

Peak power and energy requirements are summarized in the following table.

**Table 5.12-8 Example of System to Supply Power to FIRE  
with Supplemental Local Energy Storage**

	Pmax (MW)	Qmax (MVAR)	Smax (MVA)	Wmax (GJ)
TF Grid	201	180	270	6.5
TF MG	274	371	372	5.2
PF/RF MG	310	584	586	2.5

## 5.13 Cryoplant

### 5.13.1 Introduction

The FIRE cryoplant and nitrogen distribution system provides liquid nitrogen to the TF and PF magnet systems to recool the magnets after pulses and for cooldown from room temperature. The magnet system is flushed out with helium, immediately before each pulse, in order to minimize the formation of radioactive N13. This section describes the magnet cooling circuit, the overall cryoplant topology, the cryogenic loads, and the sizes of the cryoplant components.

### 5.13.2 Magnet Cooling Circuit

The magnets are cooled by circulating liquid nitrogen through cooling lines (TF), and radial flow through magnet interpancake space (CS and PF coils). Liquid nitrogen is blown out and replaced by pressurized helium, before pulses, in order to minimize the creation of N13 through neutron irradiation. A negligible amount of N13 is still formed in the shielded nitrogen atmosphere of the nuclear island, but it is sufficiently low that no nitrogen holdup system is required.

The TF inside and outside legs are cooled separately by cooling lines that are fed through adjacent holes in each of the TF coil turns. One set of lines turns inwards and cools the TF inside leg and the inner halves of the upper and lower legs, the other cools the outside leg and the outer halves. The line inlet and outlet points are located at the high and low points of the coil profile to facilitate purging of liquid nitrogen prior to a pulse.

The central solenoid and poloidal field coils are cooled radially between double pancakes. As in CIT, the flow direction is from the outside to the inside to prevent outer layer heating and turn-turn delamination. A can around the outside of the Central Solenoid acts as a distribution header. The pancakes are individually insulated, but there is no ground wrap around the entire coil, because of the need for radial flow.

### 5.13.3 Heat Load Assessment

Cryogenic heat loads, requiring the circulation of liquid nitrogen, include the following:

- 1) Radiation from the inner vacuum vessel warm surface to the inner magnet surface
- 2) Radiation from the outer magnet surface to the cryostat walls and the ducts
- 3) Radiation from the transfer lines to its cryostat walls
- 4) Conduction through cold mass supports
- 5) Joule heating of the TF and PF coils during full-power and 2/3 power pulses
- 6) Neutron and gamma heating of the TF and PF coils during pulses
- 7) Heat conduction and Joule heating in the high-current leads
- 8) Cold mass cooldown from room temperature
- 9) Removal of nuclear afterheat

The load parameters that are most relevant to assessing these loads are accumulated in Table 5.13-1.

FIRE Engineering Report  
FY01 Update

**Table 5.13-1:** Key Cryogenic Load Parameters

Parameter	Units	Value
Ediss, TF	(MJ)	16.14
Ediss, PF	(MJ)	6.84
ncircuits		8
ntransfer lines		3
L,xfer line	(m)	200
tdwell	(s)	10,800
Npulses, full-power		3000
Npulses, 2/3 current		30,000
Max pulses/storage		8
Max pulses/week		20
Max no. RT cooldowns		50
Storage tank drawdown		0.8
Storage tank boiloff		0.1
J/cooldown	(GJ)	110
J/cooldowns, lifetime	(GJ)	5,500
Pradiation, in	(kW)	59.0
Pradiation, outside	(kW)	7.48
Pconduction	(kW)	3.145
P,xfer lines	(kW)	15
Pleads, TF	(kW)	10.4
Pleads, PF	(kW)	11.1
Pdiss, TF	(MW)	1.49
Pdiss, PF	(MW)	0.633
Pdiss, total	(MW)	2.21
Pleads, total	(kW)	21.52
Pidle	(kW)	95.4
Ptotal	(MW)	2.234
IN2 flow, Total	(kg/s)	15.13
Volume, lifetime, total IN2	(gal)	8.78 x 10 <sup>8</sup>
IN2 usage/pulse	(kgal)	53.49
IN2 Storage tank requirement	(kgal)	594.4

The dominant load is the ohmic dissipation of the TF coil. All parameters have been updated to correspond to the CY2002 FIRE\* reference design at Ro=2.14 m. The increase in nitrogen cooldown requirements is roughly equivalent to the 14 % increase in the TF volume.

The nitrogen storage tanks are sized for a two-day supply of nitrogen at 4 shots/day. The energy needed for cooldown from room temperature was calculated to be equal to 12 days of idling losses. Therefore, the magnet system is kept cold over a weekend and there are only 50 room temperature cooldowns during the machine life.

### 5.13-4a Cryoplant Topology

The overall cryoplant design of FIRE was originally based on those of CIT<sup>1</sup> and BPX<sup>2</sup>. Major design features include the following:

- 1) Large liquid nitrogen storage tanks and fill stations are used, instead of a closed-cycle nitrogen refrigerator. In FY99, FIRE studies agreed with CIT, BPX, and Alcator that truck deliveries from a commercial air liquefaction plant must be the most economical option, because of the pulsed nature of the load. This was reviewed in FY00 and both BOC/AIRCO and Air Liquide recommended instead the construction of a dedicated on-site or near-site nitrogen plant. The design still includes on-site liquid nitrogen storage.
- 2) FIRE uses the Alcator C-Mod method of one pump and individual regulator valves for each flow circuit. This provides close to optimized cooldown and has proven to be very reliable.
- 3) A subcooler is used, as in the BPX and CIT designs, in order to provide 80 K liquid nitrogen to the coils. The boiling temperature of nitrogen at 10 atmospheres is 105 K.
- 4) The secondary circuit of CIT was eliminated by BPX and FIRE. One difference was that sites other than PPPL, such as ORNL, were considered with large distances to the site boundaries, so that even without holdup, the nitrogen-13 discharge could be within allowables<sup>3</sup>. The FY99 cryogenic

<sup>1</sup> R.B. Fleming and G.D. Martin, "Liquid nitrogen cooling for the Compact Ignition Tokamak," Knoxville, SOFE 13, 1989

<sup>2</sup> R.B. Fleming and G.D. Martin, "System Description, Cryogenic System, WBS Q: BPX Design Description Document," Feb 13, 1991

<sup>3</sup> H. Khater, Sec. 5.8, this report

## FIRE Engineering Report FY01 Update

system provided one day's holdup for nitrogen-13, which has a half-life of ten minutes.

The refrigerator is not sized for daily cooldown from room temperature. The magnets are kept cold overnight and weekends, and only warmed up to room temperature during maintenance periods. Despite the increase in the peak temperature to 370 K at the end of a pulse, the energy required for cooldown of the system is nearly five times higher than that for recool of the coils, and it would take 12 days for heat leakages to warm the magnets to room temperature. Heaters are used on vent lines to prevent condensation plumes of liquid nitrogen.

### 5.13-4b Design Trades

In the 1999 study, the nitrogen gas holdup system at the outlet cost several million dollars and required more space than the rest of the magnet cooling system. In the next year's design study<sup>4</sup>, it was established that the previous design, which eliminated N13 release by holding-up the outlet nitrogen vapor overnight, before release to the atmosphere, was too conservative. Four new design options were studied with the goal of further reducing or eliminating the need for N13 holdup systems at a reasonable cost or overall cost savings, as illustrated in Figure 5.13.

For siting at PPPL, it is only necessary to delay the release of N13 for somewhat over an hour. Therefore, the nitrogen can be released between shots, which are no closer than 3 hours apart for full-power

pulses, and the temporary storage system need only store the nitrogen used in one shot. Option 1 included the 1999 Reference Design and added a postpulse purge by compressed nitrogen to the 1999 Reference Design. The magnets are purged both before and after a shot, valving off a second release line, so that the nitrogen used for magnet recool that is never irradiated does not need to be held-up. This has the advantage of a large reduction in the nitrogen accumulator requirements. It has the disadvantage of a further increase in the recool time, after a pulse. The cost of the additional valve and outlet line is small compared with the savings in storage.

Option 2 has an open nitrogen loop with a helium purge before the pulse. The advantage is that essentially no radioactive gas is generated by the pulse, neglecting any imperfectly shielded nitrogen atmosphere in the cell. There is also no need to purge the magnet vapor after a shot and recool can begin immediately with no temporary storage. The disadvantage is that pressurized helium storage and a helium-nitrogen heat exchanger have to be added to the cryogenic system. There is also a modest amount of helium that is vented and has to be purchased. The study showed that the cost of the helium cooldown system was small, because the amount of helium needed to purge the magnets is tiny in comparison with the amount of nitrogen needed for cooldown.

Option 3 was a closed-loop secondary IN2 circuit, similar to that used in the original CIT/BPX cryogenic circuit<sup>5</sup>. The disadvantage is that it requires a

---

<sup>4</sup> Joel H. Schultz, "Design of the Cryoplant for specified Release of N13," Fire No WBS7\_00217, March 8, 2001

---

<sup>5</sup> R.B. Fleming and G.D. Martin, "Liquid nitrogen cooling for the Compact Ignition Tokamak," Knoxville, SOFE 13, 1989

## FIRE Engineering Report FY01 Update

primary/secondary loop heat exchanger and an emergency nitrogen holdup system in the case of a fault.

Option 4 was a closed-loop helium secondary that would eliminate the need for an emergency holdup system and would presumably have the smallest generation of N13 through parasitic effects. It would have the disadvantages of requiring a helium-IN2 heat exchanger, high-pressure helium storage, a high-pressure helium compressor. It would have the advantage over Option 2 that the helium isn't released to the atmosphere, so that the cost of helium isn't a factor. Another disadvantage is that it would be harder to recool the magnets with gaseous helium than with liquid nitrogen. The need for high pressure helium storage and pumping made this the most expensive of the options.

Option 2 was selected as the new reference design, because it had the best overall combination of low cost, radioactivity, and recool time, as shown in Table 5.13.4-I. All parameters have been updated to correspond to the CY2002 FIRE\* reference design at  $R_o=2.14$  m.

### **5.13.5 Summary**

The 1999 Reference Design has been changed so that it is less expensive and no longer generates radioactive N13. Nitrogen deliveries have been replaced by pipeline delivery from a new air liquefaction plant.

A helium purge has been added to each pulse, eliminating N13 generation and the need for an outlet gas holdup circuit.

Option 1a with nitrogen purges before and after the shot has been retained as an alternative design, because of the cost uncertainties in component and gas prices.

Nitrogen requirements for cooldown have increased almost proportionally to the 14 % increase in TF magnet volume in the CY2002 reference design.

# FIRE Engineering Report FY01 Update

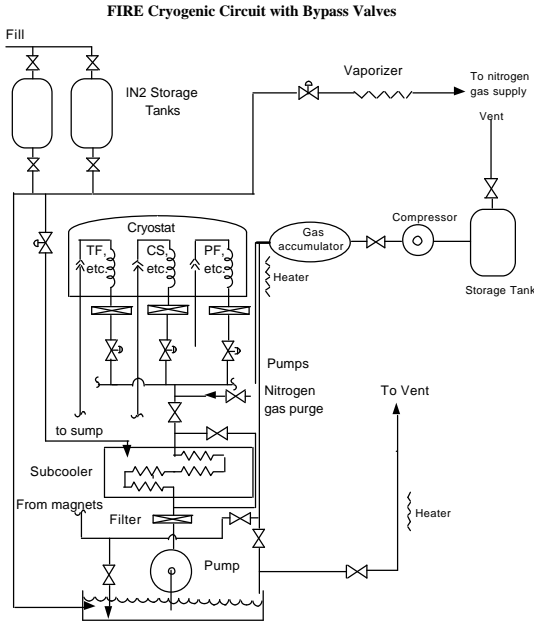


Figure 5.13.1: Option 1: Temporary Storage of Irradiated Gas after Pulse, Open secondary

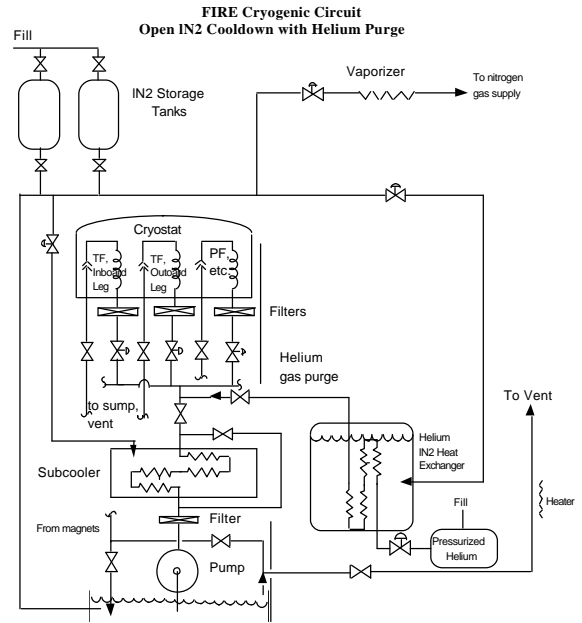


Figure 5.13.2: Option 2: Open Nitrogen Loop with Helium Purge

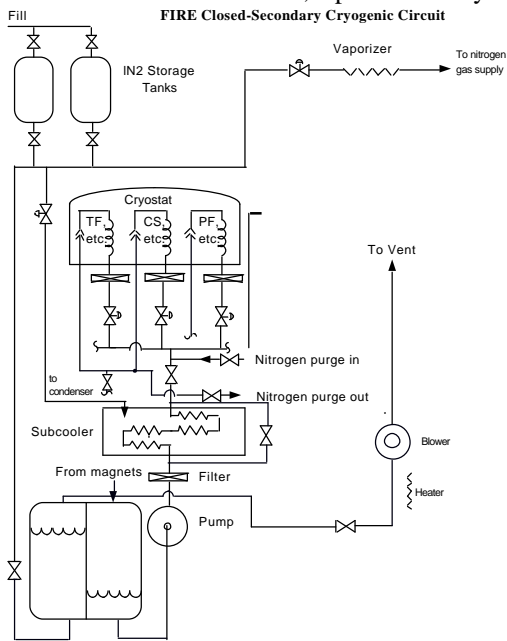


Figure 5.13.3: Option 3-Closed-loop secondary N2 Circuit (BPX/CIT)

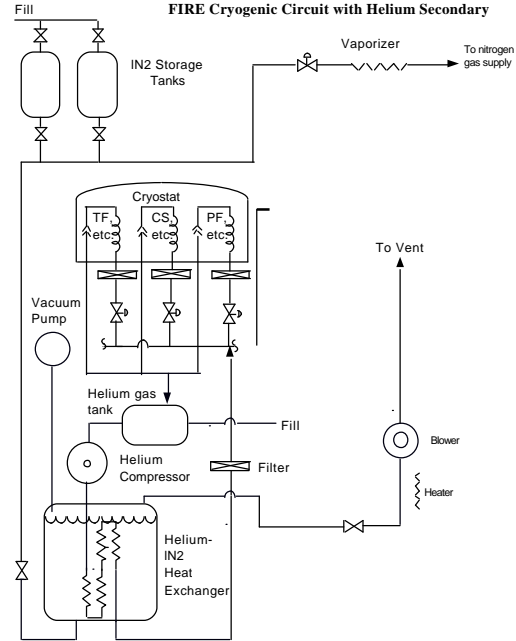


Figure 5.13.4: Option 4: Closed-Loop Helium Secondary

Figure 5.13: Four Cryogenic Refrigerator Topology Options

Table 5.13.4-I Relative Ranking of Refrigerator Options

Refrigerator Option	Cost	N13 Generated/Released	Recool time
1a Open N2, Holdup all N2	4	3	2
1b Separate holdup streams	2	4	5
2 Open N2, He purge	1	2	2
3 Closed-loop IN2 secondary	3	5	1
4 Closed-loop H3 Secondary	5	1	4

The refrigerator components required by the Option 2 design are sized in Table 5.13.4-II.

FIRE Engineering Report  
FY01 Update

Table 5.13.4-II: Component Sizes of Option 2 with an Open Nitrogen Loop, Helium Purge, and without Temporary Storage

<b>Parameter</b>	<b>Units</b>	<b>Value</b>
<b>LN<sub>2</sub> Storage tank requirement</b>	(kgal)	594.4
nstorage tank 12" shutoff valves		4
<b><i>Nitrogen Supply to Magnets</i></b>		
Lcold nitrogen piping	(m)	200
L 8" LN <sub>2</sub> vacuum-jacketed pipe	(m)	100
Average nitrogen pumping reqmnt	(kg/s)	15.13
Peak nitrogen pumping reqmnt	(kg/s)	30.26
nRegulator valves to magnets		3
Dregulator valves to magnets	(in)	10
nfilters		4
Total gpm, premagnet filters	(gpm)	594.4
no 12" shutoff valves		6
<b><i>Purge Requirements</i></b>		
Flush cycles		4
Flush length	(m)	50
Di, flushed pipes	(in)	12
V, total flushed volume	(m <sup>3</sup> )	3.65
M, He gas purges	(kg)	197.1
nshots/Pressurized He tank capacity		4
Volume, 18 atm pressure vessel, supply	(m <sup>3</sup> )	272
Di, shutoff valve, He purge stream	(in)	12
L, addit'l pipe, separate flush exhaust	(m)	100
Di, regulator valve, He purge stream	(in)	12
Total flush time	(s)	600
Average mass flow, flush stream	(kg/s)	0.328
Q, He-LN <sub>2</sub> heat exchanger	(W)	1908
Blower capacity	(kg/s)	272
Blower power	(hp)	3120
L exhaust pipes	(m)	200
Di, exhaust pipe	(in)	16
no x Di, vent valves	(in)	2 x 12
Peak mass flow through gas storage line	(kg/s)	30.3
Heater power	(kW)	6466

## **5.14 Facilities and Siting Requirements**

### **5.14.1 Introduction**

FIRE will utilize a significant on-site tritium inventory, and will be a major consumer of electrical power and liquid nitrogen. As a burning plasma experiment, FIRE will cause both direct radiation and induced radioactivity in its materials, resulting in a need to design for the safe handling of radioactive material. FIRE will therefore need to be licensed by the Nuclear Regulatory Commission, although it is expected that it will qualify as a “low hazard facility”. The design of facilities and discussion of siting requirements have been approached assuming that FIRE might be constructed at a new, undeveloped site, where there are no constraints on the orientation and interaction between buildings and systems.

### **5.14.2 Functional Requirements**

Generally, the various buildings and site infrastructure comprising the FIRE facilities must be designed to enclose, protect, support, and provide key services to the systems and components which are located within each building or structure. The facilities are also assigned the functional requirements to protect workers and the public from radiation or toxic hazards associated with FIRE operation. Spatial and geometric requirements include space for the tokamak itself, and space to perform assembly, operation, maintenance, and future decommissioning functions. Because of containment and shielding needs, some FIRE maintenance activities will involve the use of robotic remote handling equipment. The FIRE test cell, hot cells, and remote maintenance systems facilities must be large enough to house and shield the remote handling equipment that performs these functions.

FIRE is designed to provide sufficient self-shielding so that the exposed parts of the machine can be approached during shutdown by maintenance workers. However, when operating, the tokamak cannot be approached, and a suitable shielding boundary must be established around the machine. This boundary must include labyrinths and access control features to prevent unplanned worker exposure. In addition, FIRE must be

designed against certain accident events (see Section 5.15). To prevent the uncontrolled spread of radioactive material, the tokamak building must include a confinement boundary. This boundary must include features such as airlocks, depressurization, exhaust filters, and perhaps water removal systems to capture tritium, so as to mitigate the consequence of any accidental releases. When radiation sources are enclosed inside the tokamak vacuum vessel, it provides their containment. Whenever objects or materials are removed from the tokamak, the confinement function must be maintained. However, it is not desirable to permit radioactive materials to contaminate the test cell. To deal with radioactive materials and components, the facilities must include one or more hot cells where objects can be maintained or processed as waste. The remote handling system must be configured so that it can transport objects between the tokamak and the hot cell without losing the containment function.

The buildings and structures must be designed to resist all appropriate forces, including gravity, seismic events, wind and extreme weather loads, maintenance loads, and any dynamic loads imposed by operating systems. The various buildings are categorized as either safety related, or non-safety related, depending on the systems and materials they contain, and the functions they are assigned. Safety related buildings are designed and constructed so that they will not lose their functionality during any event included within the design basis. Non-safety-related buildings are designed so that they might fail to perform all their functions during extreme events, however, they are always designed to protect the health and safety of workers.

Figure 5.14.2-1 shows a generic site plan and includes a legend indicating conceptual buildings and structures.

### **5.14.3 Design Descriptions**

#### **5.14.3.1 Tokamak and Hot Cell Building**

The tokamak and hot cell building is a two-level reinforced concrete structure. The building outside dimensions are 39 m wide at the south end, 59 m wide at the north end, and 98 m long. An overhead bridge crane serves the tokamak test cell and an

# FIRE Engineering Report FY01 Update

adjacent space on the north side of the test cell  
(used for remote handling cask operations).

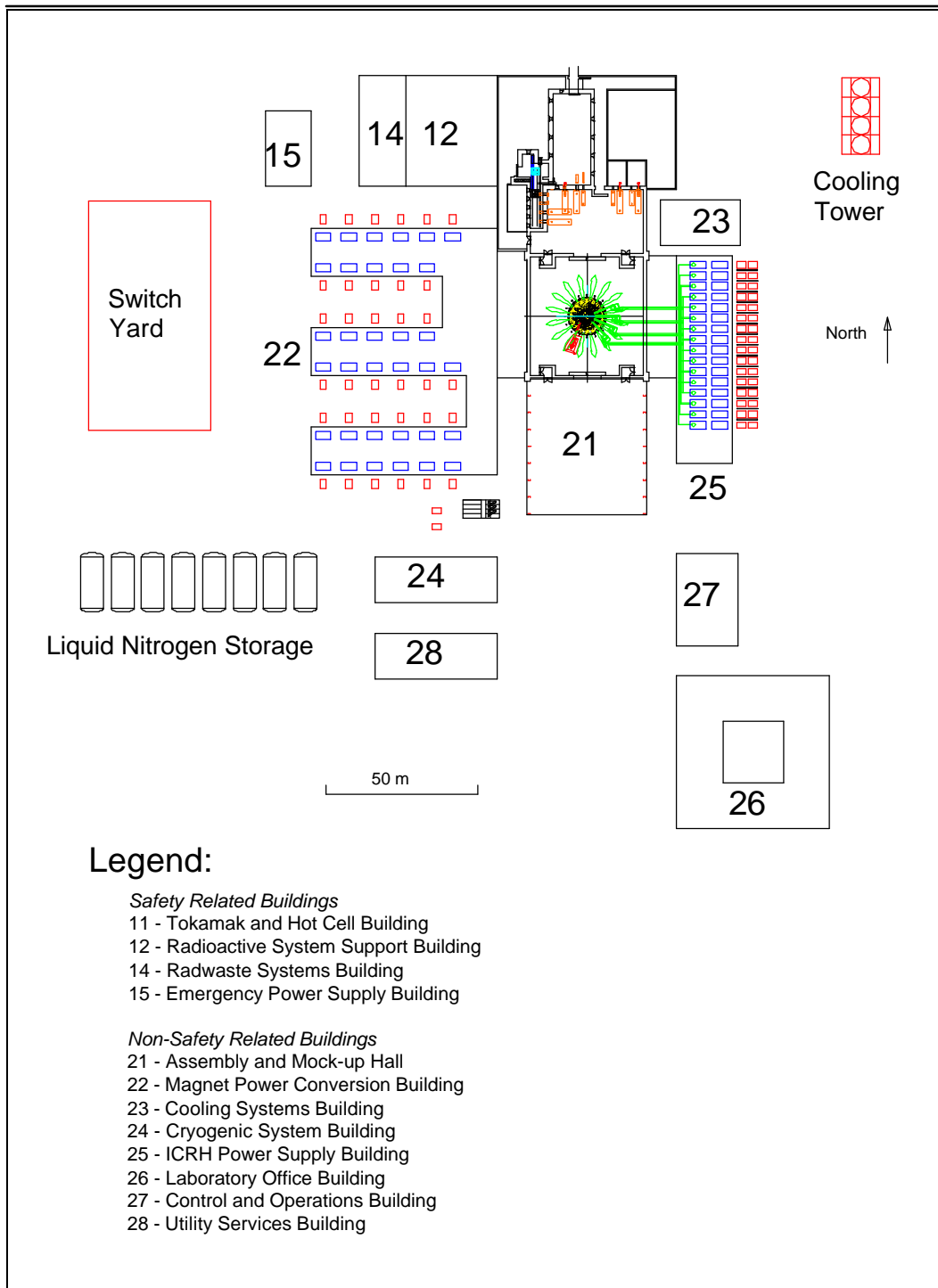


Figure 5.14.2-1 – FIRE Conceptual Site Plan

## FIRE Engineering Report FY01 Update

The rails for this crane also continue over the assembly and mockup building at the south end of the test cell. The tokamak test cell and remote maintenance area are enclosed by 1 m thick concrete walls and a 60 cm thick roof. These structural elements form a shielding and confinement envelope around the tokamak and some of the remote handling operations. The crane bay is approximately 20 m high. Other parts of the building, which wrap around the remote handling area, contain hot cells and remote handling tools service areas. These parts of the building are approximately 10 m high. The below grade basement level of the building has an internal height of 5 m, and the basemat is 3 m thick. The building is arbitrarily oriented on the site with the longest side of the building in the north-south direction.

The wall at the south end of the test cell is equipped with a large movable section that can be raised to allow the crane to also serve the assembly and mockup building. A similar movable shield wall is provided at the north wall of the test cell. Both the north and south walls of the test cell also have large door sections that can be moved horizontally to allow the crane to carry loads from the assembly and mockup area to any point in the test cell or remote maintenance operating area. The horizontal and vertical shield wall sections at the south end of the test cell are also equipped with inflatable seals, since they form part of the confinement boundary.

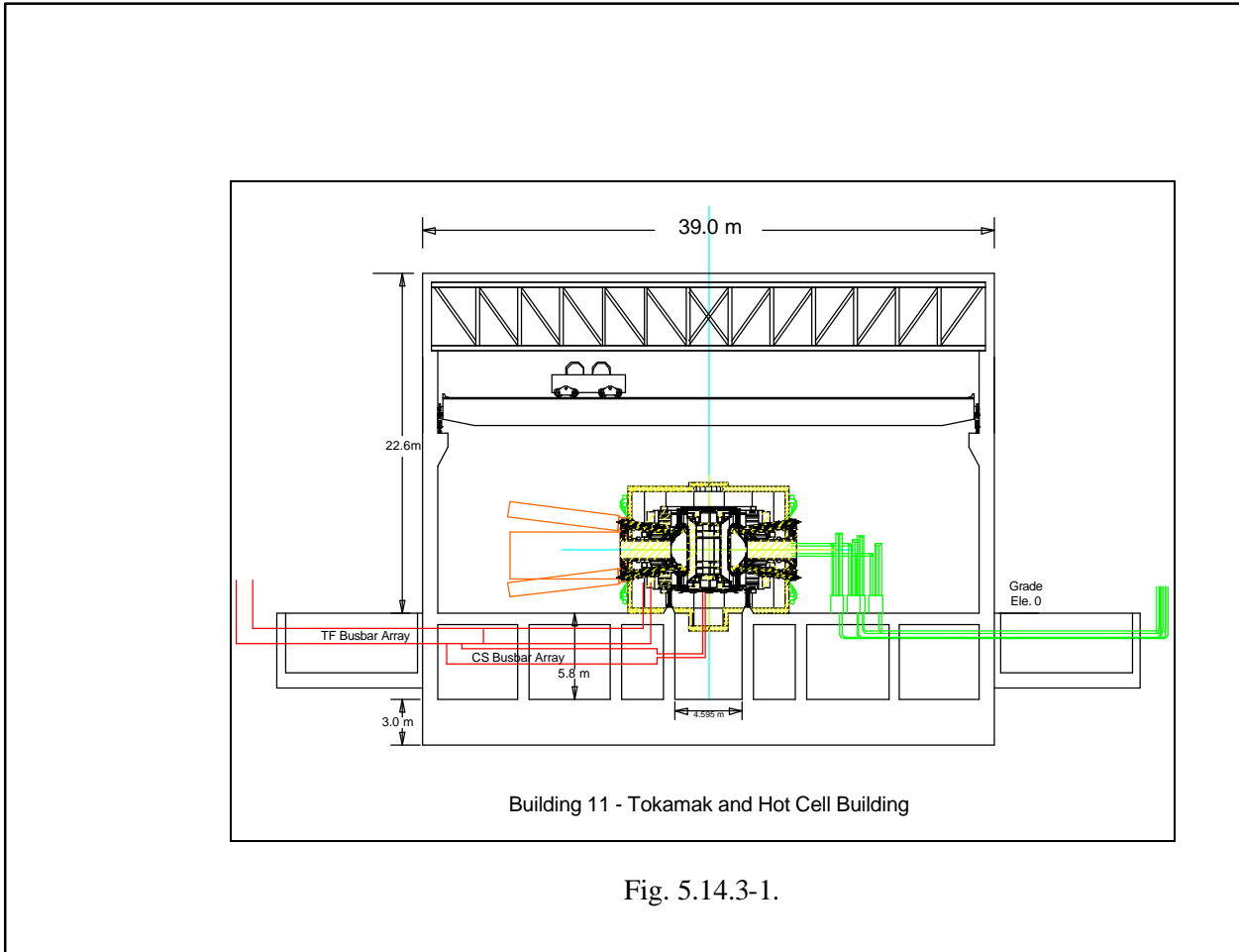
Figure 5.14.3-1 shows an east-west elevation view, or cross-section of the tokamak building. The tokamak is located so that its vertical centerline is in the center of the test cell, and its horizontal centerline is 4.2 m above the operating floor. This elevation is chosen to allow space around the tokamak for the operation of remote handling casks. This view also shows the approximate location of waveguides for the ICRF system, magnet busbars, and the minor structures located east and west of the test cell to facilitate horizontal entry to the test cell basement from the adjacent buildings. Services such as ICRF waveguides, cryopumping, diagnostics, and divertor cooling will connect to the tokamak via vacuum vessel ports. The current test cell layout strategy calls for services that will connect to ports to be routed

through the test cell basement and penetrate the test cell through the operating floor. Because port closure assemblies (except one blocked by a diagnostic neutral beam) are designed to be replaceable, the space immediately in front of each port must be kept clear of permanent installations. Penetrations through the floor must be located in areas aligned with the magnet centerlines, and demountable sections of piping, waveguides, or other systems used to complete the connection to the ports.

Other services, such as magnet power leads, magnet pre-cooling and vacuum vessel cooling, will connect to the tokamak at locations other than the ports. The current layout strategy calls for these connections to be made through the test cell basement and to penetrate the tokamak pedestal or test cell floor in the space below the cryostat. This area will be congested because of the tokamak support system. The current concept for these supports is a ring of flexing columns located below each TF coil. Because of space constraints, the tokamak support system must be integrated with the clamps for PF coil 3L.

Figure 5.14.3-2 shows an above grade plan view and North-South elevation view of the assembly, tokamak and hot cell buildings. The test cell size is determined by the space required to maneuver and dock remote handling casks at ports. Because of the length of the port closure assemblies, remote handling casks are expected to be approximately 8 m in length and about 1.9 m in width. There are several strategies under consideration for the design of remote handling cask vehicles. Casks could be transported between the tokamak and the hot cell using the building overhead crane, or they could be designed to move on the building floor using either wheels or air cushion supports. Because of the expected weight of these objects, it is likely that air cushions will be superior to wheels. A strategy for cask access to the inclined upper and lower horizontal ports has not yet been determined, however, the facilities layout assumes that casks for each of the three horizontal locations will be mated with a vehicle designed to support the cask at the correct level from the floor. A floor-supported vehicle will move the cask to a pre-determined position in front of the port established by guide pins or stops. The vehicle

FIRE Engineering Report  
FY01 Update



frame system will provide the final motion along the axis of the port.

When port inserts are removed from the tokamak they need to be transported to and transferred into one of the hot cells. It is expected that the radioactivity level of these components will require enough dose attenuation to make it impractical for the casks and remote handling vehicles to include shielding. Therefore, object transfer operations are planned as remote handling activities. When radioactive sources are being moved between the tokamak and the hot cells, the test cell and remote handling vehicle areas must be made inaccessible to workers. The test cell will also be inaccessible whenever a port insert is removed and not replaced by a new insert or a dummy shield. It should be possible to restrict all transfer operations to night shifts.

It will also be necessary to maintain the divertor and first wall. To access these components, an in-

vessel manipulator is proposed. This device should be capable of being inserted through any port (except the port blocked by the DNBI cell) and able to reach one eighth of the vessel in either direction. The in-vessel manipulator may be mounted at a port for an extended time, and there are several potential strategies for re-closing the tokamak shield to make the test cell accessible. These include movable shield walls that could be erected around the manipulator cask, or shielding within the manipulator or cask that prevent radiation streaming from reaching unacceptable levels. Figure 5.14.3-3 is a plan view in the basement of the complete building. Space is available for the roughing vacuum pumping system and for the tritium processing systems. In earlier FIRE reports, these systems were located in a dedicated Vacuum Pumping and Tritium Building, which has now been eliminated.

FIRE Engineering Report  
FY01 Update

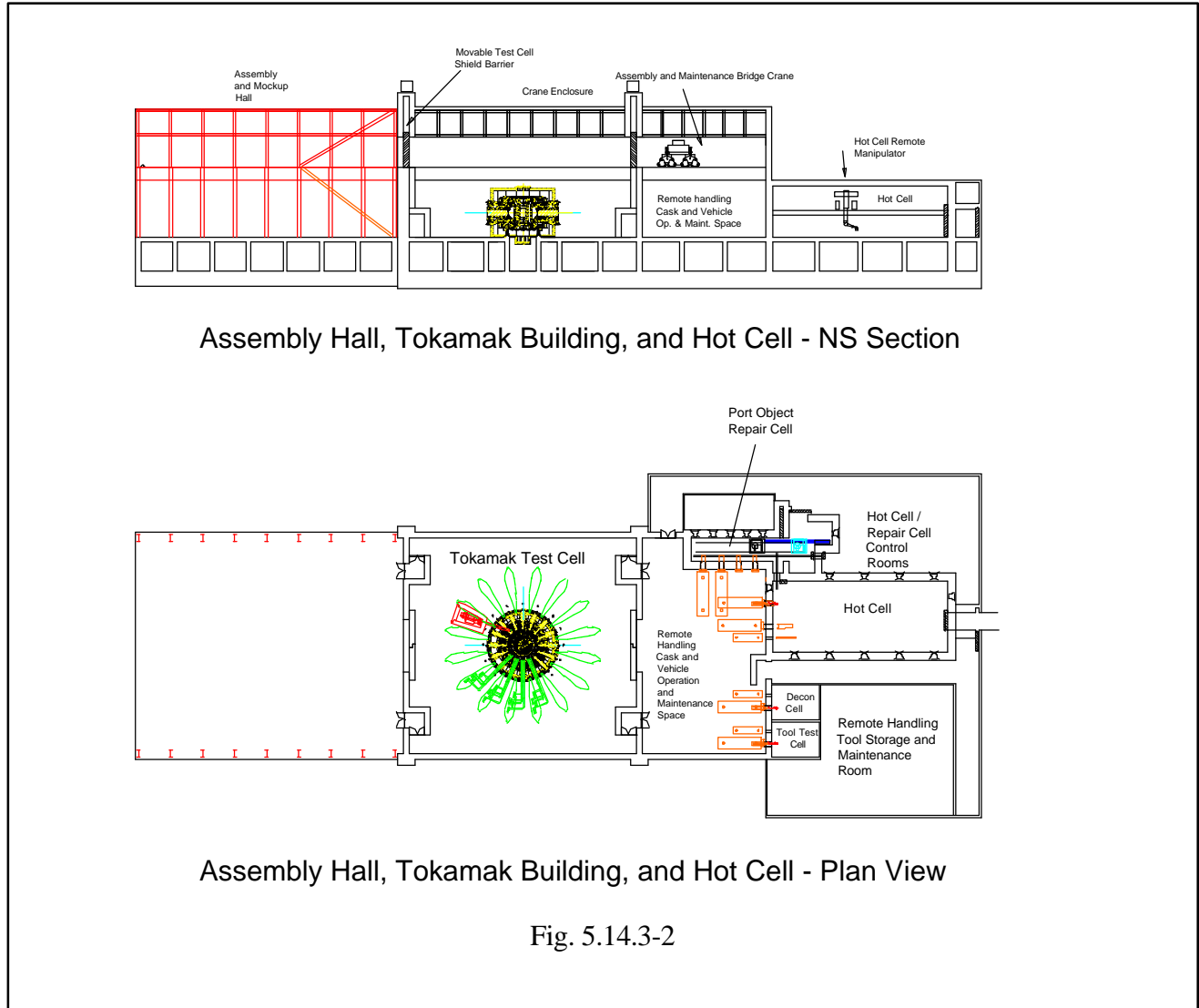


Figure 5.14.3-2. It is expected that cryopumps located in upper and lower horizontal ports will operate during tokamak pulsing. Between pulses (three hours), cryopumps will be warmed and regenerated back to the vacuum vessel, which will be pumped using mechanical vacuum pumps located in the outer part of some of the mid-plane ports. Because of the high magnetic field, these mechanical pumps will only operate between pulses. The mechanical pumps will exhaust to roughing pumps located in the tokamak building basement. This area will also contain fuel gas purification systems and isotopic separation systems. Tritium and D-T mixtures recovered from the fuel gas will be stored on hydride beds in a secure vault. All tritium processing equipment will be housed in glove boxes. The hot cell

concept is based on the expectation that some port mounted objects can be repaired and returned to the tokamak. To facilitate this, part of the hot cell system will allow port objects to be placed into a cell wall penetration that is physically identical to the tokamak port. Inside the cell, which provides shielding and containment, a remotely controlled work center will be provided, which can perform repair operations on plasma facing components. Meanwhile, the outboard end of the port assembly remains accessible for hands-on work. Divertors and plasma facing objects that cannot be repaired will be transferred through a docking port into a second, larger hot cell. This hot cell will house remotely controlled equipment and workstations used to remove and replace the

# FIRE Engineering Report FY01 Update

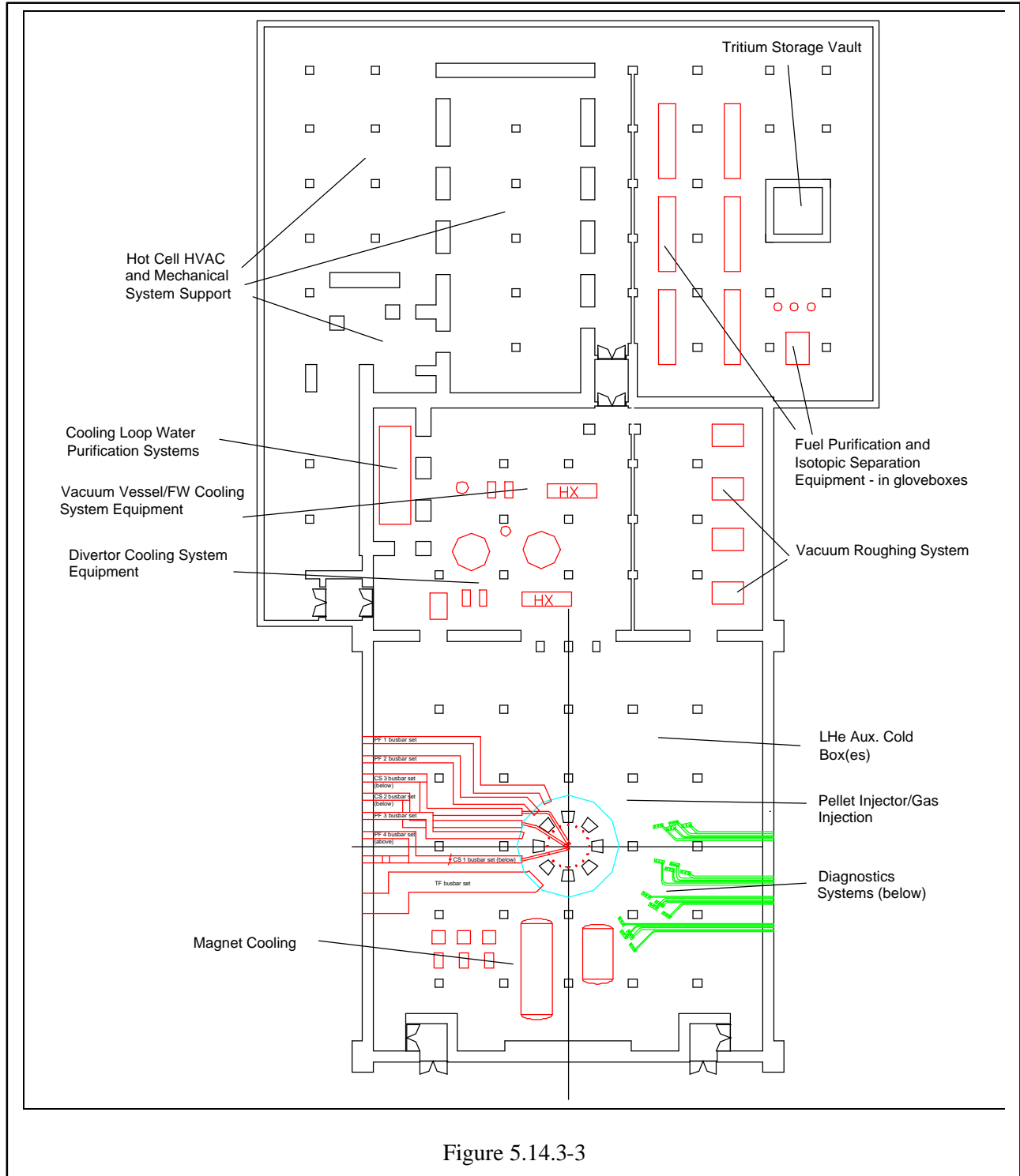


Figure 5.14.3-3

finger elements on divertor modules, which will then be returned to service in the tokamak. Discarded divertor fingers and other irradiated components will be stored and eventually processed for disposal. The extent and nature of

these hot cell processes are not yet well developed, but it is expected that they will include divertor repair (replacement of individual finger-tiles), tritium recovery from beryllium, size reduction by sawing or cutting, and encapsulation of radioactive

## FIRE Engineering Report FY01 Update

material for subsequent shipment to a waste repository.

The tools that operate within the remote handling casks are likely to become contaminated with tritium or radioactive dust, but are unlikely to become radioactive sources. They will need development and periodic maintenance and testing. To serve these functions, facilities are provided where remote handling casks can dock and discharge tools to a decontamination facility. Tools are subsequently moved to a storage and repair facility.

### 5.14.3.2 Other Safety Related Buildings

The tokamak and hot cell building, and other safety related buildings will generally be constructed using cast-in-place reinforced concrete. They will be designed to resist seismic forces and extreme weather hazards such as tornado missiles. For the tokamak and hot cell building, which is also assigned a shielding function; the thickness required for shielding is generally more than the thickness required to resist tornado missiles.

The radioactive system support building (Building 12) will be used to provide locker and change facilities for workers entering radiation controlled areas and to support systems used in remote repair and processing in the hot cell. This building will also provide space to store materials and supplies used by radwaste encapsulation systems, tritium recovery systems, and waste shipping to offsite disposal locations.

The radwaste systems building (Building 14) will be used to house treatment systems for water which has become contaminated with tritium or activated corrosion products. All floor drains and other intentional drainage from cooling systems which could be contaminated will be processed in this building to remove particulate and ionic activity. Water which is contaminated with tritium or which is recovered from atmospheric detritiation units in the plant HVAC systems will be treated in a water detritiation system. This system will use established technology including vapor phase catalytic exchangers and a tall distillation column.

The emergency power supply building (Building 15) will be used to house a backup power generating system. Presently, the need for safety related backup power is not well known, but the loads are likely to include the HVAC systems and any other loads associated with maintenance of the confinement function. If these loads are small, the safety related power supply system could consist of two small auto-start diesel generators. Some systems will require battery powered uninterruptible power supplies, which could also be located in this building, or which could be distributed on the site.

### 5.14.3.3 Non-Safety Related Buildings

Non-safety related buildings will generally be constructed using the lowest cost building technology that is suitable for their purpose. This usually means a steel-framed structure built on a concrete slab foundation at grade. The assembly and mock-up hall (Building 21) is provided to facilitate assembly and maintenance functions. The width of this building is set so that the overhead crane used in the test cell and remote handling staging area can also operate here. The assembly and mockup hall will have a below grade level dedicated to diagnostic signal acquisition and processing, and will be built from reinforced concrete below grade. The floor loading capability of the assembly hall will be the same as the tokamak and hot cell building, tentatively 20 tons/m<sup>2</sup>. The above grade portions of the building will be steel framing with architectural siding and roofing.

The magnet power conversion building (Building 22) will be used to house the indoor portions of the magnet power supplies. Transformers will be kept outdoors as a safety measure, and rectifier sets and power conditioning and switching apparatus located indoors. This building will be a single floor, steel frame on concrete slab structure. To minimize the length of busbars and cables, the shape proposed for this building uses a main corridor and three transformer-rectifier bays.

The cooling system building (Building 23) will be used to house the indoor parts of the heat rejection system, which provides secondary coolant to the divertor and vacuum vessel cooling systems.

## FIRE Engineering Report FY01 Update

Under present site assumptions, secondary coolant is pumped to cooling towers and rejects heat to the atmosphere. This building will also house the plant component cooling water system, which provides water cooling to many of the plant's power supply and plasma heating systems.

The cryogenics systems building (Building 24) is used to house indoor parts of the liquid nitrogen system used to pre-cool FIRE magnets. Liquid nitrogen storage tanks are located outdoors. Because FIRE will consume large amounts of liquid nitrogen for magnet pre-cooling, it has been proposed that FIRE should be co-located with a commercial air liquefaction plant. Under ideal circumstances, the liquid nitrogen system could be filled by pipeline. Building 24 also houses a liquid helium refrigerator that provides liquid helium to the vacuum vessel cryopumps. Other liquid helium users will be the diagnostic neutral beam, and the isotopic separation system in the fuel process. These systems are not yet well developed, and the size of the system components and building are very preliminary.

The ion cyclotron heating system power supply building (Building 25) will be similar in design and construction to the magnet power supply building. It will house the indoor portions of the ICRH system, including power supply cubicles, and tetrode signal generator modules. The ICRH system will deliver 30 MW to the plasma via 16 trains; hence each train will be sized for about 2 MW. Waveguides from the ICRH building and busbars from the power supply building will be routed through access structures on the east and west sides of the tokamak building, so that they can enter the tokamak building below grade.

The laboratory office building (Building 26) and the control and operations building (Building 27) will be designed and constructed to conventional office building standards. The laboratory office building will be sized for 500 to 700 scientists, engineers, administrators, and other site workers. The LOB will be located near the perimeter of the FIRE site, to permit relative freedom of public access. The control and operations building, on the other hand, will be located as close to the tokamak buildings as reasonably possible, to facilitate easy physical access to FIRE facilities. The control and

operations building will include facilities for operator interface with all FIRE control systems, and will include space dedicated to management of abnormal events.

The utility systems building (Building 28) will be dedicated to necessary site infrastructure, and will house compressed air systems, potable and demineralized water treatment systems, site central heating and chilled water systems, and storage of clean parts and supplies.

### **5.14.3.4 Site Improvements and General Arrangement**

In addition to safety and non-safety-related buildings, the FIRE site will include improvement needed to meet the functional requirements of outdoor equipment. The switchyard to receive grid power and step it down to voltages suitable for FIRE systems must be capable of handling approximately 1000 MW. Cooling towers will be required to reject heat from the divertor and vacuum vessel cooling systems. If the heat rejection system is able to average the heat load, the total capacity of the cooling towers could be quite small. Magnet pre-cooling will use liquid nitrogen, supplied by pipeline from a commercial on-site plant or a nearby offsite plant. Because FIRE will be a licensed nuclear facility, perimeter fencing and multiple levels of access control will be required. These features will be further developed in future work.

### **5.14.5 Site Selection Process**

The FIRE design process has been based on the assumption that the experiment will be sited at a new, undeveloped location - a "greenfield" site. This assumption presents the minimum set of design constraints. However, it is likely that several current experimental sites could also provide a good basis for design. The following key criteria are expected to be important to the process of selecting a site for FIRE:

- *Availability of land.* Since FIRE will be a licensed nuclear facility, it will be necessary for the operating organization to be able to control land use within a distance of 500 to 1000 meters from the tokamak building. This exclusion distance is related to the analysis of

## FIRE Engineering Report FY01 Update

radiation release events, and suitability of the site for a nuclear facility.

- *Access to electrical power* FIRE will require input power on the order of 1000 megawatts for periods at least as long as the plasma pulse plus the ramp-up time. If an otherwise good site does not have a sufficient electrical supply, some form of energy storage could be considered. However, the high power demand and relatively long pulse could require total energy storage on the order of 20 gigajoules.
- *Access to industrial infrastructure.* Supply of construction labor and material, transportation for the delivery of tokamak and other large components, and the availability of industrial commodities such as liquid nitrogen will be factors which could effect the cost and schedule.
- *Ability to transport radioactive materials.* It *must* be acceptable to the surrounding community that the FIRE facility receives shipments of tritium and issue shipments of encapsulated radioactive waste.
- *Access to amenities for FIRE staff .* The scientists, engineers, and technicians who build and operate FIRE will require adequate schools, health care, and community infrastructure.

In the future, candidate sites will be identified and evaluated for their technical acceptability and their influence on the cost and schedule of the project.

# FIRE Engineering Report FY01 Update

## 5.15 Safety

### 5.15.1 Safety Philosophy and Requirements

The safety philosophy for FIRE is to use a graded approach to the mitigation of hazards. Since FIRE will utilize deuterium-tritium shots to fulfill part of its operating mission; hazards associated with the use of tritium and activation of materials from the 14 MeV fusion neutrons must be considered. In addition, the toxicity of beryllium, used as a plasma-facing component in FIRE, must also be addressed.

The DOE Fusion Safety Standard<sup>1</sup> was developed in 1996 to enumerate the safety requirements and to provide corresponding safety guidance related to the hazards associated with next step D-T magnetic fusion devices like FIRE. Furthermore, from a regulatory perspective, the standard also establishes the design and operational envelopes for next step fusion facilities. Given the pre-conceptual stage of FIRE design, we have focused our efforts on implementing the safety-related design requirements in the DOE Fusion Safety Standard that have the greatest impact on public safety.

The highest level requirements in the Fusion Safety Standard stem from DOE policy, namely:

- The public shall be protected such that no individual bears significant additional risk to health and safety from the operation of those facilities above the risks to which members of the general population are normally exposed.
- Fusion facility workers shall be protected such that the risks to which they are exposed at a fusion facility are no greater than those to which they would be exposed at a comparable industrial facility.
- Risks both to the public and the workers shall be maintained as low as reasonably achievable (ALARA).

In addition to these requirements, two additional fusion-specific requirements were developed:

- The need for an off-site evacuation plan shall be avoided

- Wastes, especially high-level radioactive wastes, shall be minimized

Radiological release targets for tritium, activated tungsten (e.g. tokamak dust) and activated air and nitrogen have been established to meet regulatory dose limits in the DOE fusion safety standard taking into account the ALARA principal. The design targets are presented in **Table 5.15-1**.

**Table 5.15-1.** Radiological Release Targets for FIRE

	Normal Operation <sup>a</sup>	No-evacuation Limit	
Dose Limit	0.1 mSv/yr (10 mrem/yr)	10 mSv (1 rem) per off normal event	
Meteorology	Yearly average	Best-estimate or Average Weather	
Site Boundary	1 km	1 km	1 km
Release Point	Elevated via 100 m stack	Ground	Elevated via 100 m stack
Tritium as HTO	8 g/a	150 g	1.3 kg
Activated W dust	5 kg/a	5 Mg	53 Mg
Ar-41	5 Ci/hr	b	b
N-13	8 Ci/hr	b	b
C-14	0.1 Ci/hr	b	b

- a. Release targets have been reduced by a factor of ~ 10 relative to regulatory limits as an implementation of the ALARA principle.
- b. Not considered an accident hazard because of low inventory in FIRE

Radiological confinement is implemented as a key safety function to ensure that the release targets are met and that the overall high-level safety requirements are satisfied. Following the approach of the fusion safety standard, potential safety concerns that could affect the radiological confinement safety function are also examined to determine events that could lead to releases in excess of the targets. In Section 5.15.2, the methodology used to

## FIRE Engineering Report FY01 Update

implement radiological confinement is discussed. The potential safety concerns that could threaten radiological confinement are addressed in Section 5.15.3. An interim safety assessment is provided in Section 5.15.4.

### 5.15.2 Radiological Confinement

Because of the use of tritium and the presence of activated materials in FIRE, some degree of radiological confinement is needed to protect the public and the workers at the facility. Our philosophy is to minimize inventories of tritium and activated material where possible and to use a graded approach in establishing the number of confinement barriers needed for each system/component.

FIRE has as its goal to keep the total on-site tritium inventory below 30 g, so that it can be classified as a low hazard nuclear facility based on current DOE hazard classification rules.<sup>2</sup> Such a classification allows the greatest flexibility in applying the graded approach methodology in the management of hazards at the facility. We propose to use the graded safety approach for confinement implementation developed for ITER.<sup>3</sup> Thus, mobilizable inventories in excess of 100 g of tritium require at least two highly reliable (typical failure rate less than  $10^{-3}$  per demand) confinement barriers. Mobilizable inventories, less than 1 g of tritium, require two barriers of moderate reliability (typical failure rate less than  $10^{-1}$  per demand). Inventories between these extremes require at least one highly reliable barrier and one barrier of moderate reliability. The confinement barriers should be independent and as passive as possible with minimal dependence on new components that cannot practically be tested in the appropriate service environment before construction.

Table 5.15-2 provides a preliminary estimate of the radiological inventories in the FIRE facility. Based on these values, the vacuum vessel will be a highly reliable primary confinement barrier for the in-vessel inventories. The thermal shield will serve as a moderately reliable secondary barrier. Double confinement (e.g., a combination of

valves, windows or other barriers of moderate reliability) will be implemented in all penetrations attached to the FIRE vacuum vessel. In terms of the ex-vessel inventories, two moderately reliable barriers (e.g., the vessel, process piping, or component containing the inventory and a glovebox or other secondary boundary) will be used. Acceptable leak rates for these boundaries will be established as the design progresses.

**Table 5.15.2. Radionuclide Inventories in FIRE Facility**

Location	Tritium Inventory
In-vessel	
• Bred in Be	0.02 g
• Cryopumps	~ 10 g (TBD)
Ex-vessel	
• Pellet injector	TBD
• Tritium Cleanup	TBD
Location	Activated Material Inventory
Torus	TBD kg of W dust
Inside cryostat	<b>5 pCi C-14/pulse<sup>a</sup></b> <b>2.4 Ci N-13</b>
Air outside cryostat	<b>0.16 pCi C-14/pulse<sup>a</sup></b> <b>0.5 μCi N-13</b> <b>5.3 μCi Ar-41</b>

a. Even with 10000 pulses, the inventories would be only on the order of tens of microcuries

### 5.15.3 Potential Safety Concerns

The DOE Fusion Safety Standard<sup>1</sup> identified five potential energy sources that could threaten the confinement safety function:

- a. decay heat
- b. coolant internal energy
- c. plasma energy
- d. chemical energy and combustible gas generation, and
- e. magnet energy.

We are in the process of examining each of these potential energy sources and their impact on the FIRE design. The MELCOR code was used to analyze the consequences of loss of control of these energy sources. These calculations are scoping in nature and detailed

## FIRE Engineering Report FY01 Update

accident event sequences with estimated probabilities have not yet been developed.

MELCOR is being developed at the Sandia National Laboratory (SNLA) to analyze severe accidents in fission reactors.<sup>4</sup> MELCOR tracks the flow of two-phase water during such accidents, as well as any radioactive aerosols that may exist in either water phase. Structure temperatures are determined by one-dimensional heat conduction equation solutions. Heat transfer to both phases is considered. External (walls) or internal (pipes) flow configurations are considered during forced, natural, boiling, and condensation heat transfer modes. Modifications have been made to MELCOR at the INEEL for fusion specific analyses.<sup>5,6,7,8</sup>

To analyze these events, a MELCOR model was developed that includes the in-vessel PFC components, the vacuum vessel, the toroidal field (TF) magnets, and the thermal shield. A detailed description of this model appears in the Appendix to this report. Cooling systems characteristics for the divertor and VV were assumed for these analyses, because design information for these cooling systems is not yet available. Plasma heating of the PFCs (particle, nuclear and decay heating) was included in this model as presented in Section 5.7. Heat transfer from the back of the FW, baffles, and inboard divertors is by radiative heat transfer to the VV. The outboard divertor cooling system has a water inventory of 31 m<sup>3</sup>, pressure of 10 MPa, temperature of 50°C, and a pump head of 0.8 MPa. This system provides coolant through the divertor tubes at a velocity of 10 m/s.

The VV walls, shielding, and Solimide insulation were included in this model. The nuclear heating of this structure is that given in Section 5.7. The VV cooling system model has an inventory of 24 m<sup>3</sup>, pressure of 10 MPa, temperature of 100°C, and pump head of 0.27 MPa. This system is a scaled down version (based on VV water inventory) of the model developed for ITER, and provides a loop coolant inventory transit time of about 250 s. In addition to this cooling, thermal radiation and natural convection to the TF magnets was modeled.

If no heat were added to the water jetting into the vacuum vessel during an in-vessel LOCA, the pressure would rise to that of the saturation pressure at the divertor coolant temperature. For 50°C water this pressure is only 0.0123 MPa. However, the PFC's of the vacuum vessel will superheat this water, resulting in higher pressures. Based on tests performed in the Japanese Ingress-of-Coolant (ICE) Experiments, it was estimated that for FIRE the water impingement heat transfer coefficient would be 20,000 W/m<sup>2</sup>-K over an area of 0.8 m<sup>2</sup>.<sup>9</sup> This area was assumed to be part of the inboard top divertor and outboard FW surface areas. To simulate the temperature rise following a plasma disruption produced by the injected water, 16 MJ of thermal energy was deposited on the PFCs over a 100 ms period. The partitioning of this energy among the PFCs was the same as that during a normal pulse.

We have examined the long-term thermal response of FIRE and the passive decay heat removal capability of the design under a complete loss of coolant condition. The safety concern is the mobilization of activated PFC material by oxidation in air. It is assumed that following a FIRE plasma pulse the coolant in the divertor and VV cooling systems is completely lost. The only means of heat removal that remains is the radial conduction and radiation of the decay heat to the environment. Figure 5.15.3-1 contains temperatures from different radial locations in FIRE for this event. The maximum temperature (inboard divertor) drops from 600°C to 350°C within 15 minutes after the pulse, and then steadily drops to nearly ambient temperature by ten days. By ten days, the magnet and thermal shield temperatures are still below 0°C. Since the decay heat burden has dropped to about 0.5 kW by this time, these temperatures are not likely to dramatically change beyond this time. Given these results, decay heat is not a serious concern in FIRE and oxidation of the activated PFC surfaces will not be significant.

## FIRE Engineering Report FY01 Update

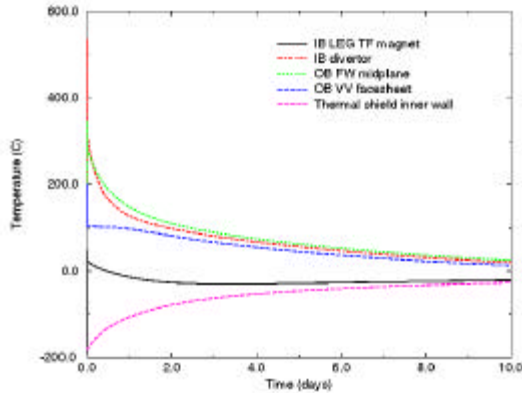


**Figure 5.15.3-1** Thermal response of FIRE due to decay heating under complete loss of cooling.

The internal energy of the divertor and vacuum vessel coolants pose a potential pressurization threat to the vacuum vessel (the primary confinement boundary) if an in-vessel leak develops in these systems, either because of thermal fatigue, disruption erosion, and disruption forces. Thus, in-vessel loss-of-coolant accident (LOCA) calculations have been performed for the FIRE design. These accidents involve a break in the divertor or vacuum vessel cooling systems inside of the vacuum vessel, allowing coolant to jet into the vacuum vessel. This coolant impinges on hot plasma facing component (PFC) surfaces, producing vacuum vessel pressurization in excess of the coolant saturation pressure. The safety concerns are the possible over-pressurization of the vacuum vessel, and the production and possible combustion of hydrogen produced by the chemical reaction of first wall (FW) beryllium with the injected steam.

For divertor system breaks, the LOCA was assumed to occur at the end of a plasma pulse when PFC temperatures were at a maximum. In addition, this LOCA was assumed to induce a plasma disruption. The coolant was allowed to impinge on the inboard divertor surface (a radiatively cooled PFC) and on a portion of the outboard FW. Three different break sizes were assumed: a single cooling tube, 10 cooling tubes, and 100 cooling tubes. Figure 5.15.3-2 contains VV pressure for these events. As can be seen, the VV pressure resulting from a single tube break

gradually rises to 0.044 MPa in 60 seconds. The larger breaks give a more rapid initial pressure rises, but result in lower pressures by 60 seconds (0.025 MPa). This initial rise is primarily due to the rapid steam generation produced by coolant impingement heat transfer, that is eventually offset by VV steam condensation as additional water is injected from the divertor cooling system and PFC surfaces begin to quench. These breaks do not result in a near-term pressure that could fail the vacuum vessel. As such they do not represent safety hazards as long the long-term cooling of PFCs is provided by the VV cooling system, which operates at a temperature of 100°C. Thus, breaks in the divertor coolant system do not seriously threaten the radiological confinement integrity of the vacuum vessel.

The VV cooling system LOCA was assumed to occur at the time of maximum VV coolant temperature, and the coolant to impinge on the back of the FW (a radiatively cooled PFC) at the reactor mid-plane. An in-vessel LOCA from a 0.01 m<sup>2</sup> break in the vacuum vessel cooling system was analyzed for FIRE. This break size is arbitrary, but is about the same size as the 100-tube divertor break. The time of the break was established to be approximately 100 seconds, which is the time of peak VV coolant temperature for the adopted VV cooling system design. Because the FW is radiatively cooled, the temperatures of these PFCs do not change much from those at the end of the pulse. The results of VV pressure for this event is given in Figure 5.15.3-3. The maximum pressure in the VV is slightly above 0.15 MPa. This pressure is below the 0.2 MPa design pressure for the VV and is not expected to cause a failure of this structure.

In all of the events examined thus far, because of the low VV steam pressures and low FW temperatures (below 350°C), insignificant amounts of hydrogen are generated from Be-steam and W-steam interactions. Thus, the chemical energy from these reactions does not threaten the radiological confinement function of the vacuum vessel.

## FIRE Engineering Report FY01 Update

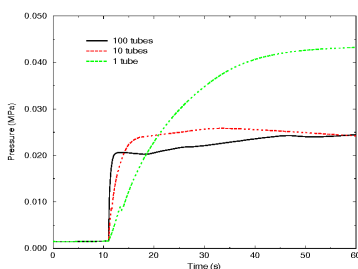


**Figure 5.15.3-2** Pressure in FIRE plasma chamber for different levels of tube rupture in the divertor

Another concern with hydrogen production is deflagration and/or detonation upon mixing with air. Keeping the inventory of all hydrogenic species below the deflagration limit for the FIRE plasma chamber and extensions would reduce the threat to the radiological confinement barrier. For the 35 m<sup>3</sup> FIRE vacuum vessel, the deflagration limit is 60 gmols of hydrogenic species. From the accident perspective, hydrogen from Be/steam and W/steam reactions is not the concern, however the tritium on the cryopumps must be controlled. The 30 gmols translates into a deflagration limit of ~ 300 g DT. Regeneration will be scheduled frequently enough to stay well below this limit.

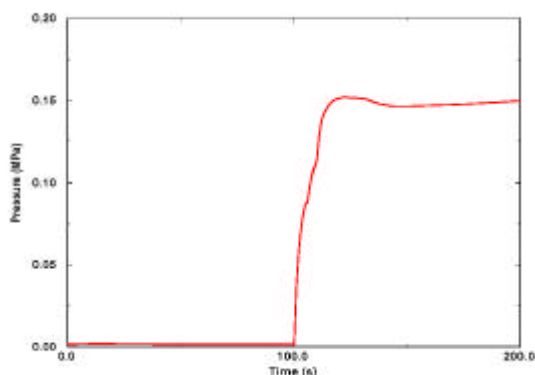


**Figure 5.15.3-3** Pressure in FIRE plasma chamber resulting from an in-vessel break of the vacuum vessel cooling system

We have not yet examined the control of plasma energy, magnet energy, loss of vacuum events, or potential cryogen/water interactions as means of challenging the radiological confinement of the

vacuum vessel. These events will be examined as the design evolves.

### 5.15.4 Interim Safety Assessment

An interim assessment of the safety of FIRE has been made relative to the project's release targets and the overall safety requirements of the DOE Fusion Safety Standard.

Examination of the inventories in Table 5.15-2 and the release targets in Table 5.15-1 indicates that none of the inventories in FIRE pose a serious concern for normal/routine effluents from the facility. Activated material inventories are orders of magnitude below the release targets. For tritium, the yearly release limit of 8 g/a is easily achievable given the modest inventories involved in FIRE and the current state of the art in tritium technology.

For off-normal events, as long as the total facility tritium inventory remains below 100 g, then complete release of that inventory would not threaten the ability of FIRE to meet the no-evacuation objective.

Implementation of the radiological confinement safety function is consistent with the overall graded approach philosophy of the Fusion Safety Standard. The use of multiple barriers improves the overall ability of FIRE to ensure that the confinement safety function is maintained over a broad range of conditions and is a good implementation of the defense-in-depth nuclear safety philosophy.

Examination of the potential safety concerns associated with the different energy sources in FIRE has not yet revealed any events that pose a serious challenge to the radiological confinement function

In terms of radioactive waste generation, the low fluence of the FIRE machine would allow all components to either be disposed of as low level waste or recycled for other fusion experiments.

# FIRE Engineering Report FY01 Update

## REFERENCES

---

- <sup>1</sup> DOE STD 6003-96, The Safety of Magnetic Fusion Facilities, May 1996
- <sup>2</sup> DOE STD 1027, "Hazard Categorization and Accident Analysis Techniques for Compliance with DOE Order 5480.23, Nuclear Safety Analysis Reports," DOE-STD-1027, December 1992.
- <sup>3</sup> Technical Basis for the ITER Final Design Report, Cost Review and Safety Analysis (FDR), ITER EDA Documentation Series No. 16, IAEA, Vienna, 1998.
- <sup>4</sup> R. M. Summers, et al., "MELCOR 1.8.0: A Computer Code for Severe Nuclear Reactor Accident Source Term and Risk Assessment Analyses," NUREG/CR-5531, Sandia National Laboratories report SAND-90-0364, January 1991.
- <sup>5</sup> Merrill, B. J. "Initial Modifications to the MELCOR Code," ITER/US/95/TE/SA-18, US Home Team, June 30, 1995.
- <sup>6</sup> B. J. Merrill and D. L. Hagrman, "MELCOR Aerosol Transport Module Modifications for NSSR-1," ITER/US/96/TE/SA-03, US Home Team, February 21, 1996.
- <sup>7</sup> R. L. Moore, "Documentation of New MELCOR Flow Boiling, EOS, and Diffusion Coefficient Subroutines" ITER/US/97/TE/SA-6, US Home Team, April 24, 1997.
- <sup>8</sup> B. J. Merrill, "An Enclosure Thermal Radiation Heat Transport Model for the MELCOR code," ITER/US/97/TE/SA-04, January 31, 1997.
- <sup>9</sup> H.-W. Bartels, editor, "Accident Analysis Specifications for NSSR-2 (AAS)," version 2, S 81 RI 19 97-05-04 W1.1, SEHD 8.1.C-1, May 6, 1997.

## 5.16 Diagnostics

### 5.16.1 Introduction

The success of FIRE's physics mission is dependent on there being a comprehensive set of plasma diagnostics. This set must be capable of providing the same quality of data available in present-day devices, in addition to providing new information about the alpha-particles, the new feature of a burning plasma experiment. The set must provide high quality, reliable information on many plasma parameters, including data on profiles, to be used as input to plasma control. The set must operate with good space and time resolutions in an extreme radiation environment.

At this point in the design process, it has only been possible to begin to consider some conceptual aspects of the integration of diagnostics with the tokamak, its internal hardware and the necessary radiation shielding. There are many diagnostics requiring optical sightlines to the core plasma and to the divertor, which will require labyrinthine paths through thick shielding "plugs" in the access ducts. Magnetic diagnostics, for measuring parameters such as the plasma current and position and high-frequency instabilities, will necessarily be mounted immediately behind first-wall tiles and must be integrated with the structures planned for these areas. For access to the divertor, and to gain sightlines for the x-points and separatrix legs into the divertor and their contact points, significant design integration with the divertor and first wall components is required.

FIRE diagnostic design, at least at the concept stage, can benefit from the much, much greater design effort put into conceiving access routes for diagnostics for ITER [1]. Very similar measurement requirements apply for FIRE and ITER with similar spatial resolution requirements (as a fraction of minor radius) and temporal resolutions. The higher toroidal magnetic field and higher expected plasma density may affect the diagnostic technique chosen to make the measurement. Also since FIRE's mission is more exploratory in terms of plasma scenarios and in

investigating alpha-particle physics than ITER's, higher priority for some particular measurements may be found. So far, the measurements have only been considered in terms of full-scale operation in deuterium-tritium (D-T), and little consideration has been given to optimizing the timing of instrumentation to different phases of the operational program.

### 5.16.2 Aspects of Diagnostic Design

The measurements required and the diagnostic techniques proposed to carry them out are shown in table 5.16.2-1. In this table, there is indication, by a tick, of which measurements would provide data to the control systems. During the construction phase of FIRE, it is likely that some of these systems will be dropped while new techniques will be adopted as the physics and diagnostic technology evolve. Twelve large radial ports are presently available for diagnostics, one of which may be shared with vacuum pumping of the vessel. There are also upper and lower outer ports aligned with the x-points which provide access to the divertor plasma regions. Of these half of each of the upper and lower ports are available for diagnostic use, but the access is shared with water cooling to the internal divertor hardware. There are sixteen small vertical ports, at the top and bottom of the vacuum vessel. All of these ports have been provisionally allocated to different diagnostics and this plan is shown in fig. 5.16.2-1.

Detailed design of all of the components to be installed in the ports, including the necessary shielding to limit radiation doses to the coils and the facility, will be necessary before it can be shown that the planned installation is possible. Hence, while a relatively simple set of diagnostics will be installed initially for start-up and early device demonstration, planning of the final set is required *ab initio*. Rather detailed designs of individual diagnostic, with the necessary first labyrinths and first mirrors - refractive optical components will not survive the first wall flux levels - will be required to determine whether the required spatial

resolutions are achievable. In some cases, such as techniques using measurement of plasma x-rays, it may not be possible to implement the diagnostic because of the radiation environment.

The magnetic diagnostics have to be mounted in the high-radiation ( $\sim 1.2$  Gy/s) and high temperature environment experienced near the first wall. There are design issues with their size and the ability to integrate them with the copper stabilizer and tiles so that they can function and be sufficiently cooled. Their design and placing should limit the detrimental effect caused by radiation-induced conductivity (RIC) in the ceramic insulation, but the small size and mineral insulated (MI) cable connections make this challenging. Success in this implementation is critical to the tokamak's operation, because of the role magnetic signals play in plasma control and physics understanding.

For the premier operating tokamaks, a number of measurements of key plasma parameters, and obviously their profiles, have been made using spectroscopic techniques dependent on a relatively high neutral particle density at the plasma core provided by heating neutral beams. Such beams will not be available on FIRE with its narrow radial ports. Unfortunately, there are not good alternative methods, in terms of spatial resolution, to the spectroscopic techniques so that a diagnostic neutral beam is necessary. The beam energy is optimal for most measurement at  $\sim 125$  keV/amu (atomic mass unit), but very high current density is required to provide a sufficient density at the center of the plasma despite the beam attenuation. This beam should operate in short pulses so as not to affect the plasma and will require special development.

The measurement of the alpha-particles, the internal energy source for the burning plasma, and determination of their behavior under different plasma operational scenarios, is a major goal of this program. While some success was achieved on TFTR [2], and hopefully more will be attained during the upcoming JET-EP program, significant improvements are necessary to provide reliable measurement throughout the

high-yield neutron part of the discharges. Radiation-hard detectors are needed for determining the energy and source region of the escaping high-energy alpha-particles. Reduction of radiation-induced fluorescence and absorption in optical components, full testing of collective scattering techniques with lasers or microwaves, and developing methods for measuring the high-energy neutron tail created by collisions of the alpha-particles with the fuel ions, are all necessary elements in developing an understanding of the confined alpha-particles. A high-energy lithium-impurity pellet is desirable to provide a source of particles with which the alpha-particles can interact so that their spatial distribution can be determined. At the same time a full complement of measurements of high-frequency instabilities is essential for understanding the impact of this new component of high-energy ions in the plasma.

### **5.16.3 Research and Development Necessary for Diagnostic Implementation**

There are three main areas in which research and development (R&D) of diagnostic systems is necessary. Much of the work parallels the requirements of ITER diagnostics [3], so that hopefully there can be some sharing of the expense of this effort. Some examples of scope in the three areas are:

i) Irradiation Tests of Materials;

Studies of RIC in selected ceramics and MI cable to define the materials to be used;

Investigations of the cause of radiation-induced electromotive force (RIEMF) with MI cables to prevent signal pollution;

Evaluation of electrical connection techniques for MI cable for remote-handling and insulation properties;

Testing of selected optical fibers for performance in realistic radiation environments at relatively low light-signal levels.

ii) Development of New or Improved Diagnostic Techniques:

FIRE Engineering Report  
FY01 Update

Development of an intense pulsed diagnostic neutral beam with  $\sim 125$  keV/amu,  $1 \times 10^6$  A/m<sup>2</sup> for 1  $\mu$ sec at 30 Hz repetition rate;

Demonstration of fast-wave reflectometry for measuring hydrogen isotope ratios in the plasma core;

Extension of the range of Faraday-cup based and scintillator-based detectors for lost alpha-particles to the higher temperatures and radiation levels at FIRE conditions.

iii) Development of New Components and Techniques:

Continuation of development of small radiation-hard high-temperature magnetic probes;

Development of a prototype shielding "plug" containing diagnostic components for a radial port to incorporate required tolerances, alignments, assurance of ground isolation, actuation of shutters, etc., while maintaining sufficient shielding.

Evaluation of metallic mirror performance and the effects on reflectivity of neutral particle bombardments and nearby erosion sources.

This R&D program is critical to demonstrating performance of the measurements and should be carried out in parallel with the design.

#### 5.16.4 Summary

The determination of the capability for measuring the necessary plasma parameters both for understanding the behavior and for feeding back control signals is in its infancy. Some of the key issues have been indicated and the initial design efforts must be applied to these. The supporting R&D must move ahead in parallel with the design. Fortunately there has been a strong ongoing effort on diagnostic implementation on ITER and this effort is leading the way to a number of solutions.

[1] ITER Physics Basis, chapter 7, Nucl. Fusion, **39**, 2541 (1999) and the ITER Final Design Report.

[2] S.J. Zweben et al., Nucl. Fusion, **40**, 91 (2000).

[3] A.E. Costley et al., Fus. Engg. & Des., **55**, 331 (2001).

FIRE Engineering Report  
FY01 Update

Table 5.16.2-1: Diagnostics Proposed for FIRE

Physics Parameter	Control	Diagnostic Set	Physics Parameter	Control	Diagnostic Set
<b>Magnetic Measurements</b>			<b>Radiation (continued)</b>		
Plasma current		Rogowski Coils	Divertor low-Z imps. and detachment		Multichord visible spectrometer
Plasma shape and Shape, position & MHD		Flux/voltage loops Saddle coils (inc. locked-mode)	High-Z impurities		X-ray pulse height
Plasma pressure		Discrete Br, Bz coils	Divertor impurities		UV spectrometer
Disrupt.-induced currents		Diamagnetic loops	Total radiation profile		Bolometer arrays
<b>Current Density</b>		Halo current sensors	Total light image		Visible TV imaging
Current density for most of profile		Motional Stark effect	<b>MHD and Fluctuations</b>		
		FIR polarimetry	Low-frequency MHD		Discrete Br, Bz coils
Current density in edge		Li-beam polarimetry	High-frequency MHD, TAE, etc.		Saddle coil for locked-mode
<b>Electron Density</b>			Core density fluctuations		Neutron fluctuation dets.
Core elect. density		Thomson scattering	Core electron temperature fluctuations.		High-frequency Mirnov coils
X-point/div. dens.		FIR multichannel interferometer/polarimeter	<b>Neutron Measurements</b>		Mm-wave reflectometers
Edge, transp. boundary profile		Thomson scattering	Calibrated neutron flux		Beam emission spectr.
Edge density profile		mm-wave reflectometer	Neutron energy spectra		ECE grating
Divertor density variation along		Li-polarimetry	<b>Alpha-particle Measurements</b>		polychromators
Divertor plate density		Fast-moving probe	Escaping $\alpha$ -particles/fast-ions		
<b>Electron Temperature</b>		Multichannel interferometer	Confined thermalizing alphas/spatial		Epithermal neutron dets.
Core electron temperature profile		Fixed probes	Confined $\alpha$ -particles' energy distribution		Neutron camera spect.
			Spatial distribution of alphas		Faraday cups/scintillators at first wall
X-point/divertor		Thomson scattering	Volume-average $\alpha$ -particle energy spectrum		IR TV imaging
Edge elect. temp. profile		Fast-moving probe	<b>Runaway Electrons</b>		$\alpha$ -CHERS
Div. plate elect. temp.		Fixed probes	Start-up runaways		Collective scattering
<b>Ion Temperature</b>			Disruption-induced runaways		Li-Pellet charge exchange
Core ion temperature		Charge exchange spect.	<b>Divertor Pumping</b>		Knock-on bubble-chamber neutron detectors
Divertor ion temperature		Imaging x-ray crystal	Pressure in div. gas-box		Neutron spectrometer
<b>Plasma Rotation</b>		Neutron camera spect.	Helium removed to div.		
Core rotation profile		UV spectroscopy	<b>Machine Operation Support</b>		ASDEX-type press. gauges
			Vacuum base pressure		Penning spectroscopy
<b>Relative Isotope Concentration</b>			Vacuum quality		
Density of D and T		Charge-exchange spect.	Vac. vessel illumination		Torus ion gauges
		Neutron spectroscopy	<b>Surface Temperature</b>		Residual gas analyzer
<b>Radiation</b>			First-wall/RF antenna		Insertable lamps
Zeff, visible bremsstrahlung		Visible bremsstrahlung array	Divertor plate temps. and detachment		
Core hydrogen isotopes, low-Z impurities		Visible filterscopes			IR TV imaging
Divertor isotopes and low-Z impurities		Divertor filterscopes	<b>Neutral Particle Sources</b>		IR TV imaging
Core low-Z impurities		Visible survey spectrometer	Neutral particle source for core spectroscopy	indirect	Thermocouples
		UV survey spectrometer	Lithium source for polarimetry		Diagnostic neutral beam
			Li-pellet target for confined- $\alpha$ spatial dist.		High current lithium beam
					High velocity lithium pellet injector

# FIRE Engineering Report FY01 Update

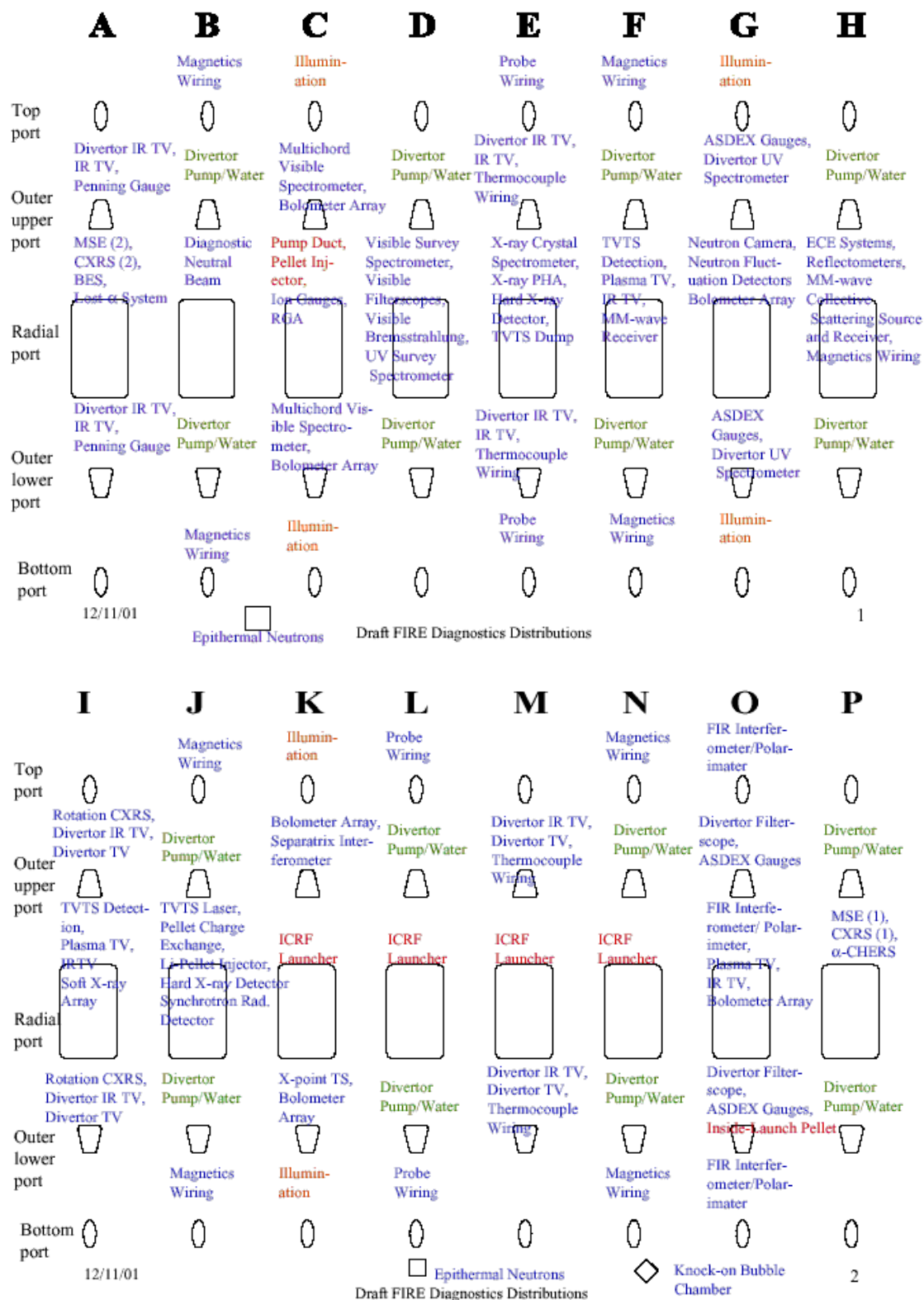


Figure 5.16.2-1 Provisional FIRE Diagnostic Port Occupancy

## 6.0 Evaluation of the FY 01 Design

In the previous studies, FIRE considered a range of machine and operating parameters. A bucked/wedged TF design was considered in FY01 as an alternative to the baseline wedged design. *One of the major accomplishments this year was the selection of a single set of parameters and design options from the several which were being considered.* This set of parameters will permit engineering to proceed more efficiently as the project progresses towards and begins the Conceptual Design Phase in FY 03. This selection evolved from feedback gained from the fusion community and from tradeoff studies performed by the FIRE project. The basic parameters and features of FIRE that were chosen for FY02 work are presented in Table 3.0-1. The most significant choices made and the background on these choices are discussed below:

- **The machine size parameters were adjusted to permit increased plasma current.** The major radius,  $R$ , was increased from 2.0 to 2.14, the minor radius,  $a$ , was increased from 0.525 to 0.595, and  $I_p$  increased from 6.5 MA to 7.7 to improve FIRE's margin to the global plasma energy confinement scaling provided by ITER  $H_{98}(y,2)$ . This is provided by the increase in the plasma current and results in a slight decrease in the plasma aspect ratio from 3.8 to 3.6. The fusion power is determined by the operating  $\beta$ ; the  $\beta_N$  decreased from 2.4 to 1.6
- **A wedged TF configuration was chosen.** Although the

bucked/wedged design study indicated a number of potential advantages, the most significant being a possible 45% reduction of peak power, the wedged design was selected in October to be the baseline TF design structural configuration. The major factors which led to this choice are:

- *Experience with Wedged Machines:* There is great deal of worldwide operating experience with wedged machines and none yet with bucked / wedged machines. IGNITOR is a bucked / wedged machine, and has done an impressive job of design and engineering analysis. However, it has not yet been constructed and operated. Since FIRE is a fairly large burning plasma experiment and will quickly become activated, it was determined that FIRE is a poor candidate to be the first bucked/wedged demonstration.
- *Robustness of the Wedged TF Coil Design:* FIRE must have a robust design to routinely operate at its design rating and achieve its physics mission. The wedged design is judged to be more robust against manufacturing uncertainties and variations in operational conditions. The bucked / wedged design requires a fit-up tolerance of +2/-0 mm for the TF / CS interface. If these clearances

FIRE Engineering Report  
FY01 Update

are not achieved, the load sharing will not be as projected by the analysis. Another concern of the bucked / wedged design is the potential limitations on operational flexibility. In the bucked/wedged design, a portion of the "excess" centering force (ie, the portion not needed to generate wedge friction between the TF inner legs to react the overturning loads) is reacted (bucked) against the CS coil. A portion of the expansive stress generated in the CS by its self-field is reacted by the pressure on its OD by the TF legs. This mutual support requires synchronization of the TF and CS, and therefore will limit operating flexibility.

- *BeCu Copper plate availability* - Another major factor that led to the choice of the wedged design is the availability of the C17510 "Hycon 3" plate made by Brush-Wellman that is needed for the inner legs. Discussions with Brush-Wellman indicate that BeCu could be produced with the mechanical properties required. They indicated that there is also a high probability that the electrical conductivity would be a minimum of 70% IACS (compared to the 68% assumed in calculations).
- **The maximum operating field of the machine is set at 10T.** 12T was previously

considered as a potential upgrade operating mode because it would provide margin for advanced tokamak performance or the achievement of the desired Q at 10T. However, since the forces scale as  $B^2$ , the forces would be 1.44 times higher. Providing this 12T capability results in a fairly high cost, in both the engineering and monetary sense.

Results of the design work continue to be very encouraging. The design meets or exceeds all of the major performance objectives that were set for FIRE at the beginning of the study in FY 99:  $B_T=10$  T;  $I_p=6.4$  MA; minimum flat top time=10 s; minimum full power pulses=3000. The new baseline FIRE design can operate at 10T with a plasma current of 7.7 MA and a flat-top time of 20 s for a minimum of 3000 full power pulses.

The main features of the FIRE design are:

- Sixteen LN<sub>2</sub> pre-cooled, wedged TF coils with C17510 beryllium copper inner legs and C10200 OFHC copper for the balance of the TF coils
- LN<sub>2</sub> pre-cooled, C10200 OFHC copper, free standing, 5 section, modular central solenoid
- Four LN<sub>2</sub> cooled, C10200 copper PF coils
- A double walled vacuum vessel with integral shielding, passive stabilization system and active control coils
- Shielding with water and steel within the double walled vacuum vessel to reduce activation to allow

## FIRE Engineering Report FY01 Update

hands-on maintenance outside the TF coils.

- Plasma Facing Components using Be for the First Wall and W for the Divertor.
- Double null radiative divertors.

The status and assessment of specific systems is as follows:

### 6.1 TF Coils and Global Structure

The TF coil peak conductor membrane plus bending stresses are 529 MPa. This is within the static 724 MPa allowable stress for C17510 beryllium copper. Stress limits for a mission lifetime of 3000 cycles at full field and 30000 cycles at 2/3 field are expected to be acceptable for the TF coil since the loading in the peak stress areas is primarily compressive, which inhibits crack growth. **Factor of Safety (peak stress /allowable) = 1.4**

The TF coil temperature excursion for a 10 T, 18.5 s DT pulse or for a 26 s DD pulse is from 80K to 370K. The excursion is the same for a 12 T, 12 s DT pulse or 15 s DD pulse. The peak temperature allowable is 373K. **(TF conductor temperature rise is at the allowable).**

One of the design issues for tokamaks with highly shaped plasmas and “external” PF coils is the support for the overturning moment on the inner TF coil leg. This moment is due to the fields from the central solenoid and PF coils crossing the legs of the TF coil. This moment causes shearing stresses in the insulation between the turns in the inner leg. In FIRE, the maximum calculated shear in the inner leg of the TF coil, at the mid-plane, is ~50 MPa. Using a

conservative coefficient of friction of 0.3 and the calculated wedging pressure of ~200 MPa, the allowable stress would be 60 MPa. **(Insulation shear stress in the throat region is at 83% of allowable).**

In wedged TF coils, the wedging pressure has a tendency to decrease at the top and bottom of the inner leg so the allowable shear stress on insulation decreases. However, the large compression rings in FIRE compensate for this effect by providing a preload and load augmentation as the TF coil temperature increases during a pulse.

Cool down analyses indicate that cooling on the inside edge of the inboard leg of the TF coil is sufficient to achieve a pulse repetition rate of 3 hours. The space required for manifolds and cooling have been incorporated into the design, but detailed stress analyses have not been done. Consideration will be given to adding cooling to the inboard edge of the TF coil so as to decrease the time needed between pulses.

### 6.2 Central Solenoid and PF Coils

Work has begun on the CS and PF coils for the 2.14 m baseline design. As with the 2.0 m design, stress and thermal analyses indicate that all of the CS and PF coils can use liquid nitrogen cooled OFHC copper conductor. The maximum von Mises stress in CS1 is 322 MPa has been calculated for one scenario; the factor of safety is 1.07. Current studies to optimize the design are considering the allocation of radial space between the CS, vacuum vessel, diagnostics, and PFCs. OH biasing is also being adjusted to find the optimum stress and thermal profiles for the coils. If necessary, consideration will be given to the use of

## FIRE Engineering Report FY01 Update

a CuCrZr (Elbrodur) alloy to raise the allowable stress for the CS.

### 6.3 Vacuum Vessel

The double walled Vacuum Vessel has 16 sets of ports including large mid-plane ports, angled ports above and below the mid-plane, and vertical ports. The combined water and steel shielding allows hands-on maintenance outside the TF coils. Port plug shielding concepts, passive stabilization plates and active control coils have been incorporated into the vacuum vessel. Seismic and VDE loads have been estimated to allow vertical and lateral supports to be sized for the VV. Support and cooling concepts are being analyzed for the passive stabilization plates, active control coils, and PFC's. This will continue in FY02. Since the use of carbon inside the vessel is avoided, high temperature bakeout and operation is not needed. The vessel will operate at 100 C.

The vessel is fabricated in octants from Type 316 LN stainless steel. When all the octants are in place within the TF coils, they are welded together from the plasma side of the torus. The field joint for the double wall structure uses splice plates to accommodate assembly tolerances. It also allows accessing the coil-side, face-sheet from the plasma side of the torus. This type of joint has undergone significant, full scale testing using remote welding equipment as part of the ITER R&D program.

### 6.4 Divertor and Plasma Facing Components

The divertor design is required to be open to accommodate the short distances

from the x-point to the plate and the spreading of the field lines. The connection lengths are short and the scrape-off layer (SOL) thickness is small.

The actively-cooled, outer divertor module design is based on fabrication technologies developed for the ITER divertor and consists of 24, modular, copper-alloy "finger" plates that are mechanically attached to a stainless-steel support structure that spans the toroidal width of the module. The support structure includes machined distribution and collection pathways and manifolds that route coolant to the individual finger plates. Concepts for remotely attaching the modules to the vacuum vessel have been developed.

Passive cooling of the inner divertor plate and baffle components is sufficient for the baseline pulse lengths of 20 s at 10 T. To accommodate longer pulses, the baffle now uses active cooling and the inner divertor is conduction cooled to the baffle. Passive cooling is adequate for the first wall for pulse lengths of about 2 minutes at full power.

Analyses of the PFC designs have begun based on initial specifications for projected disruption and thermal loading conditions to assure that the structures and attachments are sufficient. Work to date has considered halo current loads and disruption eddy current loads on the inner and outer divertor modules. Further analyses are underway to develop the attachment requirements and details of interface conditions.

In general, reliable, yet easily detachable electrical contact must be provided between the plasma facing components

## FIRE Engineering Report FY01 Update

and / or plasma facing components and the vacuum vessel. Grounding straps and Multilam® contacts were proposed for this in ITER, since each can accommodate thermal cycling and relative motion. Similar design concepts are being considered for FIRE.

### 6.5 Thermal Shield

The thermal shield or cryostat provides the insulating environment for the liquid nitrogen cooled coils. The cryostat consists of a stainless steel structure with a thin shell of stainless steel covered by insulating panels and sprayed-on insulation. Penetrations will be sealed with rubber or fabric bellows that accommodate the relative motion between the VV and thermal shield. The result is a cost-effective concept that is relatively easy to maintain and modify.

### 6.6 Ion Cyclotron Heating

The ICH system requirements were updated to match the needs of the new baseline. The ICH system is designed to support heating at 10T for full burning plasma operation and 7T operation for setup shots. It operates at 80-120 MHz, delivering 20 MW at 90-110 MHz, with modest falloff allowed at the high and low frequency ends of the operating ends. Four adjacent ports with 2 straps in each port will be used. Each strap will have 2 feed points, giving a total of 16 feeds. 20 RF sources will be used, with each having the capability to deliver ~1.25 MW to the plasma.

### 6.7 Fueling and Vacuum Pumping

Pellet injection is used in FIRE from the outside mid-plane, vertically and also from the inside lower quadrant aimed

towards the plasma center. This will be accomplished by three sets of injectors. The initial sizing and integration of the pellet injector components into the vessel has been done.

A tritium-rich pellet source will be used for core fueling and a deuterium-rich gas source for edge fueling. The fueling system includes: a conventional gas puffing system, using all-metal electromagnetic valves, (four toroidal stations at two poloidal locations at each divertor level), and a pellet injection system using two identical (redundant) injectors. The technology to deliver intact pellets at the highest possible speeds around curved surfaces (guide tubes) is under development.

The design vacuum pumping speed is 200 torr-liter/s for a 20 s pulse length. The base pressure prior to discharge is  $10^{-7}$  torr for fuel gases (H, D, T) and  $10^{-9}$  torr for impurities; operating pressure is  $\sim 10^{-4}$  to  $10^{-3}$  torr. There will be a total of 16 cryopumps with 8 each on the top and bottom (at alternate divertor ports), close coupled to the torus in the pumping duct directly from the double null divertor. The interface issues for these elements will continue to be addressed together with the impact on the requirements for other possible operating scenarios. Sufficient pumping speed will be assured by providing additional pumping capacity through a section of one of the midplane ports.

### 6.8 Tritium System

The on-site tritium inventory has been set at 30 g to allow sufficient operational flexibility without introducing additional restrictions. However, the inventory can be reduced if a tritium reprocessing

## FIRE Engineering Report FY01 Update

system is added to recycle the tritium daily.

### 6.9 Neutronics and Shielding

Nuclear heating has been computed for the major components (e.g., magnets and PFC's) as input to the cooling design. The largest nuclear heating values in the different components were calculated for the 200 MW fusion power DT pulses. During these pulses the average neutron wall loading is 3 MW/m<sup>2</sup> with values at the outboard (OB) midplane, inboard (IB) midplane, and divertor being 3.6 MW/m<sup>2</sup>, 2.7 MW/m<sup>2</sup>, and 1.8 MW/m<sup>2</sup>, respectively. Radiation damage estimates have also been done to size shields and estimate lifetime for sensitive components. Evaluations are underway to determine the impact of radiation on the electrical resistivity and, in turn, on the electrical and thermal performance of the TF coil materials.

The insulation dose is computed to be 1.3-1.5 x 10<sup>10</sup> rads for 3000 full power DT pulses (fusion energy of 5 TJ) and 30,000 DD pulses (fusion energy of 0.5 TJ). This is the peak, end of life, value and occurs at the magnet surface at the inboard mid-plane. This value drops to 9.8x10<sup>8</sup> rads in the divertor region and 7-12.6 x 10<sup>6</sup> rads in the outboard region at mid-plane.

The commonly accepted dose limit for epoxies is 10<sup>9</sup> rads. Polyimides and bismaleimides are more radiation resistant with experimental data showing only a small degradation in shear strength at dose levels in excess of 10<sup>10</sup> rads. However, they are difficult to process due to their high viscosity and requirement for high temperatures to fully cure. Newly developed insulations,

such as cyanate esters, should provide radiation resistance with easier processing requirements.

The vacuum vessel jacket/shield thickness has been sized so that it, in conjunction with the shielding provided by the TF coils and port plugs, will permit "hands on" ex-vessel maintenance. This will require further consideration of shielding details.

### 6.10 Activation, Decay Heat and Radiation Exposure

The plasma facing components, first wall on the inboard and outboard sides and the divertor, experience the highest levels of specific activity and decay heat. However, the operational schedule allows short-lived radio nuclides to decay between pulses resulting in low levels of activity and decay heat at shutdown.

The biological dose rates behind the vacuum vessel and the divertor remain for several years following shutdown, however, the dose rates outside the magnet and at the mid-plane are acceptable for hands on maintenance within a few hours after shutdown. At the top of the machine the dose rate drops to an acceptable level within one day after shutdown.

Dose rate calculations have indicated that port plugs 1.1 m long would provide adequate shielding and have led to the addition of shielding outside the magnets on the top and bottom of the machine.

At the end of the machine life, calculations indicate that all components would qualify for disposal as Class C low level waste.

## FIRE Engineering Report FY01 Update

### 6.11 Remote Maintenance

The strategy is to employ hands-on maintenance to the fullest extent possible in order to minimize remote handling operations and equipment while achieving acceptable machine availability. Activation levels outside the vacuum vessel are low enough to permit hands-on maintenance in the ex-vessel region. Remote handling (RH) is required for in-vessel components including the divertor, FW and limiter modules, and the port mounted systems including heating, diagnostics and cryopumping systems.

When in-vessel maintenance or modification is required, the affected components are removed from the vessel and transferred to the hot cell where they are refurbished or processed as waste. Divertor, FW and limiter modules are accessed through the midplane ports and are handled with an articulated boom equipped with a specialized end-effector. The boom can access the complete in-vessel region from 4 of the 16 midplane ports. Port mounted system assemblies are located in both the mid-plane ports and the upper and lower auxiliary ports and are removed by a vehicle and manipulator system operating at the closure plate of the related port. A boom and manipulator built for RH R&D and demonstrations will serve as a back-up for the single boom built for machine service.

RH operations are performed from sealed transfer casks that dock to the ports via a double door system to contain and prevent the spread of in-vessel contamination. Casks carry components between the reactor and the hot cell and

are transported by a vehicle or the facility overhead

Components have been classified according to their required maintenance frequency and their designs will be standardized and optimized for RH. Preliminary time estimates to complete the more frequent maintenance tasks are consistent with the required machine availability. Replacement of a port assembly requires approximately 3 weeks of maintenance operations. A complete divertor changeout, 32 modules, is completed in about 6 months. Individual divertor, limiter and first wall modules can be replaced in about one month. The time target to perform a complete changeout of the divertor and FW components is 1 year

Studies have begun and will continue in FY02 on kinematics and end-effector design for the in-vessel manipulator to assure that sufficient space has been allocated in ports and around the machine. Analysis shows that the 800 kg combined divertor module (32 module configuration) can be supported and transported through the vessel and ports. Studies will also continue in FY02 on the port assembly and handling equipment design, cell layout and cask design to assure adequate building size and layout for component transport for repair or disposal.

### 6.12 Power Supplies

The conceptual design of power supplies for FIRE magnet systems seeks to minimize capital cost by leveraging existing capabilities of the local electric utility, which are assumed to be robust. Therefore, all of the FIRE device's time-varying power (peak demand of

## FIRE Engineering Report FY01 Update

800MW) for TF and PF magnets as well as the RF systems are provided directly by the utility's "stiff grid" without requiring any power demand ramp rate limiting equipment, or energy storage equipment, at the FIRE device site. However, provision for reactive power (MVA) support up to 300MVA is included in the design baseline. The grid's ability to supply the required time varying active and reactive power demand will be evaluated when a specific FIRE site is chosen and the above assumptions adjusted as necessary.

If the local electric utility is not capable of powering the pulsed load directly from its ac power line, MG energy storage devices could still be installed, but at additional cost.

We plan to survey grid capabilities to determine if direct pulsing from the grid would seriously restrict site selection options before choosing between direct grid powering or combined grid/MG set powering.

Power equipment for TF and CS/PF magnets includes thyristor rectifiers, resistor banks, and switching/interrupter circuits. The required total pulse rating of the rectifier complement is approximately 1000 MVA for the 10 T pulse. For the DD long-pulse scenario at 4 T, 2 MA the total 243 second long-pulse rectifier rating required is 345 MVA. By way of comparison, these total rectifier MVA ratings are similar to the total ratings of existing rectifiers, that were used to operate the TFTR magnets. Resistor banks and interrupter switching circuits are used in FIRE for plasma initiation in a fashion similar to TFTR and JET. Some of the magnets require current reversal during a pulse

and therefore incorporate dc polarity switching in their rectifier circuits, as done for TFTR.

### 6.13 Cryoplant

The FIRE cryoplant and nitrogen distribution system is a modified form of the design developed for CIT and BPX.

Major design features of the cryoplant:

- Large liquid nitrogen storage tanks are used on site. The FY99 concept for nitrogen deliveries by truck has been replaced by pipeline delivery from a new on-site or near site air liquefaction plant. Commercial suppliers recommended the latter.
- The amount of radioactive  $N^{13}$  generated in FIRE is small and would be within allowables for most site boundaries. A helium purge has been added before each pulse to displace any remaining nitrogen in the passage prior to the pulse, thus eliminating  $N^{13}$  generation and the need for a gas holdup circuit.
- FIRE uses the Alcator C-Mod method of one pump and cool down and which has proven to be very reliable.
- A subcooler is used to provide 80 K liquid nitrogen to the coils.

The magnets are kept cold overnight and weekends, and only warmed up to room temperature during maintenance periods. This provides considerable flexibility for adjusting shot scenarios.

## FIRE Engineering Report FY01 Update

### 6.14 Facilities and Siting

A conceptual layout and building design has been developed for a “green field” site. For example, the deletion of the central tie rod system from the tokamak has allowed a decrease in the test cell height. In the future, candidate sites should be identified and evaluated for their technical acceptability and their influence on the cost and schedule of the project since significant savings may be available in the form of “site credits”.

The test cell size is determined by space required to maneuver and dock remote handling casks at ports. Because of the length of the port inserts, remote handling casks are expected to be approximately 8 m in length and about 1.9 m in width. There are several strategies under consideration for the design of remote handling cask vehicles. A tentative routing for the vehicles to other parts of the facility has been selected.

Some components, for example port inserts (“plugs”), will require enough shielding to make it impractical for the casks and remote handling vehicles to include shielding. Therefore, transfer of objects of this type are planned as remote handling activities. The special requirements on the facility for routing and storage of these items are being evaluated.

The hot cell concept is based on the expectation that some port mounted objects can be repaired and returned to the tokamak. The extent and nature of these hot cell processes are not yet well developed, but it is expected that they will include divertor repair, tritium recovery from beryllium, size reduction

by sawing or cutting, and encapsulation of radioactive material for subsequent shipment to a waste repository.

Some building requirements are not yet well developed, but a preliminary allowance has been made. For example, the cryogenics systems building is used to house indoor parts of the liquid nitrogen system for the FIRE magnets. It also houses a liquid helium refrigerator that provides liquid helium to cryopumps in the tokamak vacuum vessel and in the diagnostic neutral beam, and to the isotopic separation system in the fuel process.

### 6.15 Safety

Radiological release targets for tritium, activated tungsten (e.g. tokamak dust) and activated air and nitrogen have been established to meet regulatory dose limits in the DOE fusion safety standard taking account of the ALARA principle.

A goal for the FIRE design is to keep the total on-site tritium inventory below 30 g, so that it can be classified as a low hazard nuclear facility based on current DOE hazard classification rules. For off-normal events, as long as the total facility tritium inventory remains below 100 g, then complete release of that inventory would not threaten the ability of FIRE to meet the no-evacuation objective.

The vacuum vessel will be a highly reliable primary confinement barrier for the in-vessel inventories. The thermal shield will serve as a moderately reliable secondary barrier. Double confinement (e.g. a combination of valves, windows or other barriers of moderate reliability) will be implemented in all penetrations attached to the FIRE vacuum vessel.

FIRE Engineering Report  
FY01 Update

Acceptable leak rates for these boundaries will be established as the design progresses.

Examination of the potential safety concerns associated with the different energy sources in FIRE has not yet revealed any events that pose a serious challenge to the radiological confinement function. A preliminary analysis has been done for:

- Long term thermal response and passive decay heat removal capability under a complete loss of coolant condition for the divertor and VV following a pulse-- Results indicate that decay heat is not a serious concern and that oxidation of the activated PFC surfaces will not be significant.
- Break in the divertor or VV cooling lines inside of the VV—Results indicate that pressure within the VV does not rise to a level expected to compromise its radiological confinement integrity. Further-more, because of the low VV steam pressures and low FW temperatures (below 350°C), insignificant amounts of hydrogen are generated from Be-steam and W-steam interactions. Thus, the chemical energy from these reactions does not threaten the radiological confinement function of the vacuum vessel.
- Deflagration and/or detonation of hydrogen upon mixing with air. From the accident perspective,

hydrogen from Be/steam and W/steam reactions was not of concern, however the tritium on the cryopumps must be controlled. The deflagration limit of 30 g-moles translates into a deflagration limit of ~ 300 g DT. Regeneration will be scheduled frequently enough to stay well below this limit.

The control of plasma energy, magnet energy, loss of vacuum events, and potential cryogen/water interactions has not yet been analyzed. As the design matures, this examination will continue such that confinement is adequately ensured in FIRE.

In summary, all of the major subsystems for FIRE have been addressed to a level that provides confidence that the mission requirements can be achieved. Several design improvements have been incorporated to produce greater physics flexibility or resolve engineering issues. First round cost estimates have been completed and are being reviewed to determine design changes, which can reduce costs. Modest changes to machine parameters were specified at the end of FY01 and work has started to modify the design as required for the selected baseline of a wedged TF system. This work will continue in FY02.

## **7.0 FIRE Engineering Peer Review**

An engineering review was held June 5-7, 2001 at PPPL, in which independent reviewers provided comments on the following areas: TF coils, PF coils, Structures, Vacuum Vessel, Divertor, Plasma Facing Components, and Fueling and Pumping. In parallel with the review at PPPL, a review of the Neutronics area and Facilities were performed by mail and phone. The reviewers represented a cross-section of expertise in the community as indicated below.

### **Review at PPPL:**

C. Bushnell, Chairman,  
Independent Consultant  
J. Irby, MIT  
S. Majumdar, ANL  
P. Mioduszewski, ORNL  
R. Parker, MIT  
A. Pizzuto, ENEA  
F. Puhn, GA

**Review of Neutronics:** Y. Gohar, ANL

**Review of Facilities:** J. Commander, INEL

A copy of the reviewers report to Charles Baker, VLT Director, is available on the FIRE web site. The reviewers had very favorable comments on the depth of analyses performed at this stage of design and also provided written comments on specific areas that will be determined by the project for disposition in the near to moderate term, consistent with availability of resources. The review committee recommended an increase in team resources to continue design development and to expeditiously engage in the R&D necessary to support the design effort.

During the review process, the reviewers were asked to submit written comments and suggestions. About 65 "chits" were received and numbered. They were then divided into specific technical areas and some were grouped into "superchits" because they were closely related to the same issue/comment. The chits are summarized in the following Table 7.0-1. It is organized by area and gives the reviewers name and comment. The FIRE Team response is given in a row for a specific "chit" or in a wide format following several chits that form a "superchit."p

A scan of the table indicates the depth of the review and of the analyses performed at this stage of the design process.

FIRE Engineering Report  
FY01 Update

<b>Table 7.0-1. FIRE Engineering Peer Review Chit Summary</b>					
<b>DESIGN PT - PHYSICS &amp; TRADE STUDIES</b>					
<b>Schit #</b>	<b>chit #</b>	<b>Reviewer</b>	<b>Reviewer Comment or Suggestion</b>	<b>FIRE Team Comment</b>	<b>FIRE Team Action by</b>
PTS1	1	R. Parker	The baseline design fails to reach the $Q>5$ objective with $H98(y,z) = 1.0$ , even with optimistic assumptions about $Z_{eff}$ ( $Z_{eff} = 1.4$ including Helium). With more realistic assumptions about the level of Be and W, the performance would degrade well below the	FIRE has worked closely with the International Confinement Data Base Group to determine the correct methodology for applying empirical scaling to FIRE. As documented in the FIRE 2000 IAEA paper and FIRE 2001 EPS paper, FIRE uses ITER98IPB(y,2) scaling wi	Meade,Schultz
PTS2	4	C.Bushnell	Too many options being looked at. Choose one and focus! Focus next immediate efforts on points or discontinuity (learn) tubes, cutouts, keys, etc.	In October, 01, the wedged configuration was selected for the baseline. A comparative overview may be found in the FY01 Engineering Report.	Meade, Thome, Heitzenroeder
PTS3	14	R. Parker	The number of full power shots is limited by radiation damage of insulators. More shielding between plasma and inner base.	see Schit PTS3	Meade, Thome, Heitzenroeder
PTS3	30	J. Irby & A. Pizzuto	Too few full performance shots. <ul style="list-style-type: none"> <li>• Increase shielding in critical areas</li> <li>• Improve insulation operation</li> <li>• consider more DD</li> </ul>	see Schit PTS3	Meade, Wesley
SChit PTS3 - A meeting was held with CTD, Inc to discuss their high radiation resistant resin which is under development. This may provide more full power shots. Nevertheless, we feel that 3000 full power D-T shots are adequate for FIRE's mission.					
<b>R&amp;D</b>					
RD1	2	R. Parker	More R&D needs to be earmarked for diagnostics.	see Schit RD1	Young
RD1	29	P.Mioduszewski	There should be some R&D funding for diagnostics, especially due to the harsh neutron environment and unique geometry. It is generic, but who will do it if not F.I.R.E.?	see Schit RD1	Young
SChit RD1: An R&D plan has been outlined by K. Young in a memo, "FIRE Diagnostics Research & Development Plan", Aug 15, 2001					
RD2	9	F.Puhn	R&D is required to verify the design concept. Cost of R&D is a serious concern. Perform a complete survey of previous R&D to identify data and design solutions that can cut cost of FIRE R&D. ITER and Ignitor R&D seem most applicable to FIRE. Other fusion	see Schit RD2	Heitzenroeder, Thome
RD2	12	C.Bushnell	The use of all OFHC copper is a simplifying move for R&D and downstream power and cooling costs etc. etc. - The allowable implies 50=% cold work - Concern is this possible for plates this thick and this size? Get on with immediate R&D to demonstrate! - F	see Schit RD2	Thome, Heitzenroeder, Titus
RD2	28	C.Bushnell	Will the copper (101-102) embrittle with radiation, will it creep at the stress levels indicated? Put these problems behind with immediate investigation / R&D!	see Schit RD2	Driemeyer, Titus, Zinkel
SChit RD2: The wedged configuration has been selected for the baseline. A comparative overview may be found in the FY01 Engineering Report. R&D plans are being evaluated to verify the availability of plates with the properties required in the sizes need					

FIRE Engineering Report  
FY01 Update

<b>R&amp;D (Continued)</b>					
RD3	7	A. Pizzuto	It is urgent to confirm the design assumptions. CuBe and insulator properties not yet well assessed. Radiation resistance of insulator the main issue. Tests of: - Cu creep at R.T. -- Qualification of the impregnation process compatible with copper prope	see Schit RD3	Action: Thome, Heitzenroeder
RD3	15	C.Bushnell	The R&D level requires materials for insulation on the forefront of development. Get on with immediate R&D of available materials.	see Schit RD3	Meade, Thome, Heitzenroeder,Sawan
RD3	27	F.Puhn	Radiation damage to insulator seems to limit total useful operating life. Selection of suitable insulation material is critical to getting full value from machine. Presently no insulation with supporting radiation damage data has been identified. As high	see Schit RD3	Schultz, Titus
SChit RD3: R&D plans are being developed for FY 02. Review of the design and experimental literature indicates that existing polyimide sheets may have adequate compressive strength and radiation-resistance. Promising new organic insulations are being					
RD4	24	C.Bushnell	The choice of castings could be a major cost driver if found not to be appropriate! Immediate R&D to prove one way or the other!	Information on castings being considered for NCSX should provide initial information. R&D is probably not possible this FY due to budget limitations.	Heitzenroeder, Thome
<b>PFC's</b>					
PFC1	3	Irby	Tiles are to be replaced 2-3 times during lifetime of machine. How will you know when to replace them. Will machine performance degrade slowly before changes are made. Make sure you have the diagnostics needed to monitor erosion.	Not critical to the conceptual design process. There are at least two good ideas of how to monitor the erosion without access to the vessel (IR and markers). In-vessel inspection may be enough also.	Ulrickson
PFC2	46	Pizzuto	Divertor max. temperature in CuCrZr seems to exceed 550	see Schit PFC2	Ulrickson, Driemeyer
PFC2	47	C.Bushnell	Baffle plates, first wall and inner divertor are in the minimal stage of P.C. design. Work on design immediately!	Work on the baffle and inner divertor design is part of FY02 effort. This will be completed by Spring 2002. The first wall design is not as high priority and will be done after the baffle and inner divertor work.	Ulrickson, Driemeyer
PFC2	50	F.Puhn,GA	Thermal gradient in divertor modules can cause excessive stress, distortion, and creep. These effects have not been assessed. Continue analysis to superimpose thermal loads with electromagnetic loads. Investigate creep behavior in copper.	see Schit PFC2	Ulrickson, Driemeyer
PFC2	51	S. Majumdar	Thermal stress analysis of divertor structure is incomplete. Conduct thermal stress analysis and fatigue evaluation including creep effect. Also, need to satisfy design criteria for combined load effect, e.g., gravity + thermal + disruption etc.	see Schit PFC2	Ulrickson, Driemeyer
PFC2	52	A. Pizzuto	Divertor thermal stresses: Divertor fingers are highly constrained so thermal stress could be very high.	see Schity PFC2	Ulrickson, Driemeyer
PFC2	54	C.Bushnell	Outer divertor module needs much more work - on disruption loads/material and on copper finish that has high thermal stress. Work this soon with design effort and R&D as required!	Disruption analysis is in progress. This is a high priority activity for FY02. We will complete the analysis for the VDE, Radial inward and stationary disruption by Spring 2002.	Ulrickson, Driemeyer
SChit PFC2:The temperatures presented at the review did not exceed the allowables to CuCrZr. Iteration 2 of thermal stress analysis is examining the possibility of modifying the mounting pins to allow expansion of the fingers along their length. If this					

FIRE Engineering Report  
FY01 Update

PFC3	48	J. Irby	Can the disruptions really be predicted 30-50 ms ahead of time in FIRE? I don't think any engineering decisions should be made that depend on predictions. Reduce forces on plates by reducing size.	FIRE just has to keep up with current activities - DIII-D's massive gas puffs show promise that they can control energy deposition and current decay. This is not a conceptual design issue.	Ulrickson
PFC4	49	J. Irby	Several kA/cm <sup>2</sup> vacuum contacts are very risky. I suggest some other approach be found to deal with the toroidal disruption currents.	Only a backup if disruption forces prove to be too high; highly likely this will not be necessary.	Ulrickson, Driemeyer
PFC5	53	A. Pizzuto	R.H. - Module to be refurbished is too heavy. Boom with limited operations area. Very long operation and complex out of vessel maintenance (3 full divertor plate refurbishments)	see Schit PFC5	Ulrickson, Driemeyer, Burgess
PFC5	57	J. Irby	Size of divertor plates should be reduced.	see Schit PFC5	Ulrickson, Driemeyer
PFC5	55	F.Puhn	Size of divertor module drives the design in several critical areas: •Weight of module impacts boom design and R&D requirements. •Size of module requires cut-outs in TF coil which creates critical section in coil and restricted space for leads. •Disrup	see Schit PFC5; Disruption loads are being assessed. If they are too high, other options exist.	Ulrickson, Driemeyer
SChit PFC5: No compelling need to change. Present module size OK for remote handling and divertor mounting. Water connections would be much more complex with a change to more, but smaller modules.					
PFC6	56	A. Pizzuto	Divertor - The use of inconel back plates for fingers could have a big impact for waste and activation points of view.	Not expected to be a problem with our low fluence. However, if future stress analyses indicate SS can be used, Inconel will be eliminated.	Ulrickson, Driemeyer, Sawan
PFC7	58	P. Mioduszewski	Need comparative study of single-versus double null configuration with respect to: connection length, temperature gradient, power disposition pattern.	see Schit PFC7	Ulrickson, Rognlien
PFC7	59	P. Mioduszewski	Detached divertor operation needs to be studied with respect to: — plasma performance —He exhaust —Zeff —neutrals control	see Schit PFC7	Ulrickson - Rognlien, Brooks
PFC7	60	P. Mioduszewski	It is not obvious that the short connection lengths in the SOL can support the need temperature gradients between divertor and separatrix/pedestal. What pedestal temperature is needed to achieve the desired H-mode confinement?	see Schit PFC7; Pedestal temperature required must be specified by physics.	Meade
PFC7	61	P. Mioduszewski	CX - fluxes at the divertor entrance are usually fairly large. Sputtering of Be from the passive plate could lead to tungsten sputtering from the divertor surface and lead to unacceptable W-concentration in the plasma. Need plasma edge/neutrals modeling	see Schit PFC7	Ulrickson/Brooks
PFC7	62	P. Mioduszewski	Need to evaluate ranges for divertor loads; discussed was 80/20, should also look at performance of e.g. 70/30, 90/10 etc. The given loads are already at the limit. Partially detached.	see Schit PFC7	Ulrickson, Wesley, Rognlien
SChit PFC7: These issues will be addressed by T. Rognlien in FY 02, priorities are being developed. In addition, ELMS studies must be done and such studies are probably more important than some of these variation studies. A proposed work plan will b					

FIRE Engineering Report  
FY01 Update

<b>TF/PF/STRUCTURES</b>					
<b>•Stress Analysis</b>					
TPS1	5	A. Pizzuto	Out of plane loads during disruption not yet considered. Could be the determining stress as far as shear is concerned	As measured in C-Mod and based on a transient electromagnetic disruption analysis of FIRE, the vessel shields the coils from any significant loading. See Memo NSO N0: WBS1.3.5_100501_TF_Disrupt_PHT.doc	Titus
TPS2	17	J. Irby	Compression ring needs more R&D. Allow time for study of non-metallic structure. Increase R&D in this activity.	see Schit TPS2	Titus
TPS2	18	C.Bushnell	The loading rings (stiffness) and jack design need to be settled. Apply immediate design R&D as required.	see Schit TPS2	Titus
TPS2	19	F.Puhn	Preload ring requires high strength and insulating breaks. To carry hoop load across insulating break requires special features, presently not defined. Consider use of a non-metallic filament wound preload ring. Stiffness is 5 to 10 times lower than meta	see Schit TPS2	Titus
SChit TPS2: The compliance of non-metallics would probably make the opposed jack wedge system inadequate in terms of the displacement they could supply. The thermal contraction properties of non-metallics would have to be simulated and creep of the non-metal					
<b>•Design Criteria</b>					
TPS3	13	R. Parker	Copper embrittles at very low dpa and could lead to degradation of performance at or near end-of-life fluence. Carefully check data on Cu and BeCu if data exists. If data is inadequate or inconclusive, plan to explore in R&D program.	see Schit TPS3	Sawan,Nelson,Zinkle
TPS3	32	S. Majumdar	(1) Treatment of low ductility material in the FIRE design criteria is absent. (2) Treatment of fatigue, creep/fatigue in the FIRE design criteria is incomplete. (1) First, conduct literature survey on low fluence embrittlement of copper/copper alloys. I	see Schit TPS3	Titus, Zatz
SChit TPS3: The peak cumulative end-of-life dpa values in the Cu components were calculated for the FIRE baseline design. The dpa values are very low (< 0.04 dpa). Although the damage levels are very low, some effects on physical and mechanical properties					
TPS4	6	A. Pizzuto	12 T Operation. Baseline solution must have sufficient engineering margin to allow operation at maximum performance. ME=1.5 should be achieved.		Titus
TPS4	25	S.Majumdar	Safety factors for Sm in FIRE design criteria are unconservative compared to ASME Code. Magnet allowables should be separate from those for vacuum vessel and in-vessel components for which ASME Code or ISDC safety factors should be maintained.		Zatz, Titus Section in FY01 rpt
TPS4	31	S. Majumdar	Inelastic analysis rules in FIRE design criteria at present. If elastic analysis rules cannot be satisfied use either limit analysis rule (with flat top stress-strain curve with 1.5 SM as yield) of ISDC and show collapse load >3/2 design load or use inel		Zatz, Titus
Chit TPS4: The FIRE magnet design criteria is directly descended from CIT,BPX TPX and ITER magnet criteria. The issue of the non-conservative derivation of Sm being the lesser of 2/3 yield and 1/2 ult - rather than the ASME 1/3 Ult,has been discussed many					

FIRE Engineering Report  
FY01 Update

TPS5	33	S. Majumdar	Bucked & wedged design is justified by highly complex, nonlinear, contact stress analysis. Need to benchmark analysis technique by tests.	Both the Wedged and Bucked and Wedged configurations use the same non-linear analysis tools - gaps, plasticity etc. The predictive value of large, complex analysis models has been an issue and probably will remain an issue as long as we use state of the art	Titus
<b>•Configuration</b>					
TPS6	16	J. Irby	B&W design: can you take it apart? Bucking arrangement should allow removal of CS w/o difficulty. Failure scenarios should be carefully considered.	The CS for both Wedged and B&W concepts needs to disconnect the case assembly for PF1 and 2 lower for the CS to be removed without disassembly of the TF. Passing LN2 through the CS cooling channels with the TF at room temp allows removal of the CS for the	Titus, Brown
TPS7	21	R. Parker	Cooling of TF is too slow. Improve cooling by adding cooling of inner base of magnet.	see Schit TPS7	Titus, Meade, Wesley, Brown
TPS7	37	J. Irby	Between shot time too long @ 400 shots/year -- 7-8 years to get through the 3000 shots. Look at cooling both sides of TF. Look at cooling between TF & CS	see Schit TPS7	Titus, Meade
Schit TPS7: We are investigating cooling from both sides. Estimates indicate that we will lose about 1 sec from the 20 sec FIRE* flat-top time if we give up 1 cm to the tube. With cooling from only one side, most shots will have cooldown times substantial					
TPS8	20	R. Parker	Cooling tube manifold presents a tricky design problem -- Tubes must be insulated from each other and no leak can be tolerated. Requires some R&D!	see Schit TPS8	Thome, Heitzenroeder; develop R&D Plan; Brown, Config. Study
TPS8	22	J. Irby	Connections to magnets need to be analyzed/designed with high priority. Material - work hardened. Focus on these issues as soon as possible.	see Schit TPS8	Titus, Brown
TPS8	23	F. Puhn	TF Coil lead is located in congested position next to midplane ports. Carrying TF coil load may require a thicker section adjacent to lead. Consider relocating TF coil leads to a position between ports to allow more space for structure.	see Schit TPS8	Brown, Titus See 22
Schit TPS8: The manifolds are an issue, but a leak can be tolerated since it will contribute to the gaseous nitrogen atmosphere within the cryostat. Our plan is to focus first on CS leads and terminals as these are in a high field region.					
<b>Remote Maintenance</b>					
RM1	8	R. Parker	A single boom is risky since it could malfunction in machine or be unavailable when needed. Also, maintenance time (e.g., to replace divertor or substantial fraction of FW) would be needlessly long. Two booms should be part of baseline design.	see Schit RM1	Burgess
RM1	35	F. Puhn	No rescue capability is identified for remote handling boom. Suggest requiring a second boom which has rescue capability. The training boom might be used in an emergency if another training boom can be obtained in a reasonable time.	see Schit RM1	Burgess

FIRE Engineering Report  
FY01 Update

<b>Schedule &amp; Costs</b>					
SC1	10	C.Bushnell	In manufacturing, time is money! Could \$\$ be reduced by building it faster? By front loading in program more R&D and/or prototype? Trade offs or ....\$\$ need to be looked at -- soon.	Project costs could, indeed, be reduced by front loading R&D and compressing the construction schedule. The present strategy is based on an assumption for the fastest implementation schedule based on likely fiscal limitations. Our plan is to obtain f	Simmons, Thome, Heitzenroeder
<b>VV &amp; Cryostat</b>					
VVC1	11	C.Bushnell	The purpose of the cryostat needs a crisp definition! Then we will know if the costs are correct. Define - Design - and Cost.	The requirements for the cryostat have been updated and can be found in the FY01 report.	Nelson,Petti
VVC2	34	J. Irby	What happens if the vacuum vessel goes down to LN2 temps? What happens to outer cooling lines?	see Schit VVC4	Nelson
VVC3	38	J. Irby	What are the vacuum properties of the Cu-Ss wall composite? •trapped volume •impurities. Inspection techniques. Prototype tests	see Schit VVC4	Nelson, Driemeyer
VVC4	39	J. Irby	Pumping speed of cryopump @ 20 u\pT much too low for density control (Base p). Look at relocation of pump. Larger ports.	see Schit VVC4	Fisher, Gouge, Ulrickson
SChit VVC4: Consideration is being given to using one of the main horizontal ports for pumping, in addition to the auxiliary ports.					
VVC5	40	S. Majumdar	Vacuum vessel stress analyses have been conducted for thermal, gravity, etc. Disruption analysis is incomplete. Design criteria limits for combined loading effects have to be satisfied. Fatigue evaluation needed for regions of stress concentration. What a	see Schit VVC5	Nelson
VVC5	41	A. Pizzuto	Vacuum Vessel - The stress analysis has to be also considering coherent disruption scenario.	see Schit VVC5	Nelson
VVC5	42	F.Puhn	Vacuum Vessel and divertor design/analysis not complete. Stresses exceed allowables in some regions. Complete redesign and stress analysis. Include thermal stress and all loading conditions. Include thermal stress on divertor. Apply electromagnetic load	see Schit VVC5	Ulrickson, Nelson
VVC5	43	F.Puhn	Eddy current analysis does not include cut-outs for ports. Thus the poloidal current flow in port edges is not calculated. This current crosses toroidal field and produces loads on port walls. Perform more detailed eddy current analysis to include ports	see Schit VVC5	Nelson, Ulrickson
SChit VVC5: Disruption analyses have begun and are considered appropriate for a pre-conceptual design phase. Further analyses are essential as indicated. This will be pursued further in FY02 and FY03.					
VVC6	44	F.Puhn	Vacuum vessel supports not fully analyzed for side loads. Load path relies on bending of slender tie rod. Shock loads or maldistribution will occur unless precise fit-up is ensured. Space and access is very restricted. Complete VV support design and ana	Support analyses have begun and are considered appropriate for a pre-conceptual design phase. Further analyses are essential as indicated. This will be pursued further in FY02 and FY03.	Nelson

FIRE Engineering Report  
FY01 Update

VVC7	45	F.Puhn	No obvious means to access fasteners connecting baffle modules to vacuum vessel. Remote handling requires large access holes and visibility. Design concept for remote assembly/disassembly of baffle modules. Analyze impact of cut-outs when subjected to p	Access and remote handling analyses have begun and are considered appropriate for a pre-conceptual design phase. Further analyses are essential as indicated. This will be pursued further in FY02 and FY03.	Ulrickson, Driemeyer, Burgess
<b>Neutronics</b>					
N1	36	F.Puhn	Safety implications of activated nitrogen inside the cryostat is not addressed. This may be a problem due to neutron streaming. Perform 3D neutronics analysis. Address safety implications. Include off-normal events.	The issue is addressed in the FY01 Engineering report. Based on 1-D calculations, total <sup>13</sup> N production after each D-T pulse is only 1.2 Ci with only 1 micro Ci of <sup>14</sup> C. These are generated mostly in the space between the IB magnet and the IB VV. Due to lar	Sawan
N2		Y.Gohar	All the analyses and the results are produced with a one-dimensional toroidal model without including safety factors to account for engineering details, model assumptions, and other uncertainties.	Past comparison between toroidal 1-D calculations and 3-D calculations showed that peak nuclear parameters at midplane close to FW are overestimated by up to a factor of 1.6 when 1-D calculations are used. Since worst conditions in FIRE occur at midplane	Sawan
N3		Y.Gohar	The performance of the TF coils is sensitive to the nuclear heating load which impacts the operating pulse length. In addition, the peak IB insulator dose determines the allowable number of pulses based on the acceptable limit. Careful neutronics analys	The largest nuclear heating and insulator dose in TF coils occur in the IB leg on plasma side at midplane. 1-D calculations tend to overestimate results there compared to 3-D results with proper modeling of source distribution and geometry. In addition, s	Sawan
N4		Y. Gohar	Biological dose during operation needs to be determined to define the shielding requirements for the building and to check the compliance with the site dose requirements.	These calculations will be planned in the conceptual design phase.	Sawan
N5		Y. Gohar	Nuclear heating loads in the divertor ports based on the device geometry are required to provide input for sizing the cryoplant to achieve the operating scenario.	This requires detailed 3-D calculations with details of geometrical configuration and arrangement of components and material in the divertor port. Due to current limited funding and lack of design details, these calculations will be postponed until design	Sawan

## 8.0 Research and Development (R&D)

### Introduction:

FIRE has relatively modest R&D requirements since it is a cryo-cooled copper magnet tokamak and can draw upon a great deal of existing data from CIT/BPX, ALCATOR C-Mod, IGNITOR, and other high field, copper magnet tokamaks. The planned areas of R&D described below concentrate on items which fill in gaps in the existing data, permit higher performance, higher reliability, and help to keep costs as low as possible.

### 8.0-1 Copper Conductor and Design Criteria

#### Background:

The available data base requires assessment and extension for plates of the size to be procured for the full scale TF and PF conductor. The properties assumed require validation.

#### For Inner TF Coil Legs

C17510 BeCu (68% IACS) in thick plate (36mm) form is used in the inner leg. The principal stresses are primarily axial tension and azimuthal compression. Required: Ultimate Tensile Strength 800 MPa; min. yield: 724 MPa.

#### For Outer TF Coil Legs

C10200 (OFHC) 36 mm thick is required. This task will verify that the plate properties can be obtained in the thicknesses required. Required: 0.2% min. yield strength 200 Mpa ; minimum elongation of 12%, and a room temperature conductivity of >100% IACS.

#### For Central Solenoid Coil

Uses cold worked C10200 copper in thick plate (38mm) form. Required: Ultimate Tensile Strength 350 Mpa; Yield Strength 300 Mpa (43,350 psi).

Min. 15% elongation at RT.

### R&D Tasks:

Obtain samples from full size plate stock and carry out a mechanical testing program to assure that static and crack growth properties at room and LN2 temperatures are adequate. The design criteria will be peer reviewed.



**Fig. 8.0-1. C17510 Copper Plate Produced for BPX.** Its size and properties are similar to that required by FIRE.

### 8.0-2 Conductor Joint Development

Background: The TF and PF coil conductors require a high strength joining process which does not result in an annealed zone. The conductors of the TF and PF coils are much different in size and strength requirements and therefore they may or may not employ the same technique. Three areas of investigation are:

(1) The baseline design uses C17510

## FIRE Engineering Report FY01 Update

BeCu for the inboard leg of the TF coils and C10200 copper for the balance of the coils. A cost effective, reliable high strength method for joining C15520 to C10200 copper is required.

(2) The C-shaped outer portions of the TF coil, consisting of the horizontal legs and the outer leg vertical section, will be manufactured from three plates to reduce costs. A practical, high strength reliable joining process is required.

(3) A joining process is required for the outer PF coil conductors. The same joining processes developed for the TF coil may possibly be applicable, but the smaller size of the PF conductor may make it possible to consider methods which would not be applicable to the larger TF conductors.

### R&D Tasks:

Develop manufacturing processes and carry out a mechanical testing program to assure adequate mechanical properties and to validate design criteria for the joints. Potential candidate processes include friction stir welding and e-beam welding. In addition, electroform welding, which was successfully developed and used for Alcator C-Mod, will be considered for use in the PF coils.

### **8.0-3 Radiation Resistant Insulating Materials**

Background: Data from the BPX insulation test program indicates that there are several glass/epoxy formulations (CTD-101; Shikazima) which can meet FIRE's requirement for radiation exposure capability of  $1.5 \times 10^{10}$  rads. This is a high leverage R&D item, since it has the potential to permit a greater number of full power D-T shots and may permit the experimental

program to be expanded with possibly only a minor impact on costs.

### R&D Task:

The plan is to collaborate with an SBIR which is underway at Composite Technology Development (CTD) to develop high radiation resistant insulating materials with good processing characteristics.

### **8.0-4 Insulation Frictional Requirements**

Criteria used in the design of the TF and CS coil systems require that selected interface areas retain a desired level of either low or high friction during operation.

#### 8.0-4.1 Low Friction Insulation Characterization

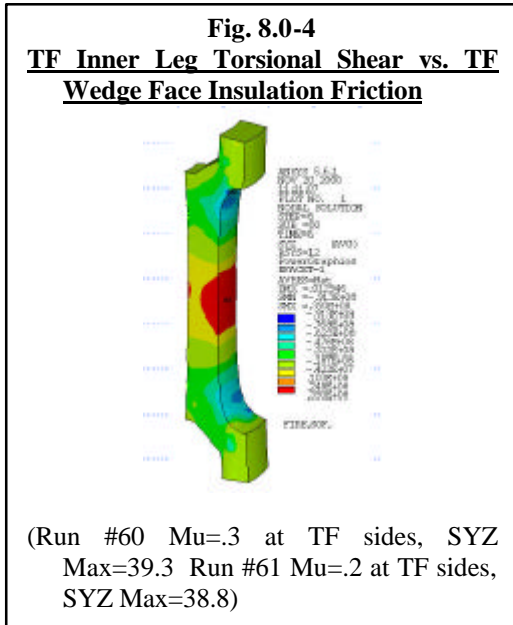
Background: FIRE employs a segmented CS with a variation of currents among the 5 coils in the stack during a pulse. Adjacent coils in the CS operate with different temperature and electromagnetic load profiles during a pulse. Adjacent coils will strain differently and relative radial motion between coils in the CS will occur. Interface must lock the coils azimuthally, maintain the coils co-axial, and allow relative radial motion with low friction.

### R&D Tasks:

- ♦ Prototypes of the interface areas will be fabricated and tested under simulated operating conditions to verify operation and adequate life.
- ♦ Apply low friction materials to substrates on a scale consistent with fabrication methods for FIRE.
- ♦ Perform mechanical tests to assure

that expected surface friction performance is consistent with design criteria and reliable for the lifetime of the machine.

- ♦ Plans are to survey the significant work done in this area by CIT, IGNITOR, and ITER. We may only have to downselect from materials already identified.



- ♦ Torsional Shear Stress Distribution in the Inner Leg shown in Fig. 8.0-4 Indicates Amount of slippage / fretting.
  - Continuous Axisymmetric Contours Indicates No Slippage; "Spots" Mid Build Indicate Bending Shear and some Slippage at the Wedge Surface.

Background: Overturning moments on the TF coils are reacted by wedging action at the inboard legs and by shear between interfaces of the outer intercoil structures on the TF cases.

A friction coefficient of ~0.3 is needed

between TF inboard legs, and also to limit torsional motions between cases on the outboard side to reduce shear pin and bolting requirements

R&D Task: Testing is required to verify friction coefficients and adequate life.

### 8.0-5 Ring Preload Jacking System

Background: A pair of large steel rings encircle the TF coils. The rings are preloaded at assembly using radial jacks to augment the wedge compression at the inboard faces of the TF coils and provide compression between the faces of the outboard intercoil structures during operation. The space available is very limited. Three jack concepts have been identified:

1. A mechanical system (proposed by IGNITOR) consisting of opposing wedges
2. Stainless steel bladders with hydraulic fluid
3. Commercial "Enerpac" jacks

R&D Task: Select one primary concept plus one back-up. Mock-up and test under expected operating conditions simulating assembly, cooldown, operational pressures, and temperatures.

### 8.0-6 Fueling

Background: A new, twin screw, extruder concept has the potential to run steady state with reduced hydrogen ice inventories compared to existing linear piston extruders. In parallel, a cooling concept based on a Gifford-McMahon cryocooler could be developed to simplify operation of the pellet injector by removing the need for liquid helium.

## FIRE Engineering Report FY01 Update

R&D: Design, build and test a prototype twin screw extruder with the goal of minimizing tritium inventory for safety and siting flexibility. Demonstrate extruder cooling without LHe by using a G-M cryocooler.

### **8.0-7 Pumping**

Background: The design of cryopumps for the divertor relies on the level of helium compression in the pump entrance region to allow a compact, in-vessel system.

R&D: Design, build and test a single cryopump module to validate the expected inlet He compression which permits a compact in-vessel pumping system.

### **8.0-8 ICRF System**

Background: R&D is needed to develop and validate the design choices for the ICRF system.

#### R&D Tasks:

1. Develop and test RF sources.
2. Fabricate and test antenna prototypes.
3. Fabricate mock ups for remote handling development.

### **8.0-9 Remote Handling**

Background: Verification of designs and component maintenance tasks should start in the design phase and be completed, where possible, prior to final design completion, or at least prior to fabrication of components. Six areas have been identified for remote handling R&D:

1. In-vessel transporter (articulated boom) and component handling end effectors
2. In-vessel inspection systems (laser metrology and video systems and deployment mechanisms)
3. Midplane and auxiliary port handling vehicles and dexterous manipulator
4. YAG laser based divertor pipe and port lip seal cutting, welding, and inspection tools, and power fastener wrench
5. Midplane port cask and air cushion transport vehicle
6. Hot cell remote repair stations and fixtures for midplane port assembly, divertor modules, and cryopump

R&D Task: Develop remote handling system prototypes and use in mock-up facilities to verify designs and to demonstrate maintenance and task times. The goal should be to reduce cost and times for replacement, repair and maintenance tasks.

### **8.0-10 First Wall and Divertor**

Background: The first wall and divertor components are subjected to radiation, high heat flux, and high electromagnetic loads during disruption events. Substantial development has occurred and progress has been made in past programs, for example, ITER. However, testing to validate design criteria and fabrication processes are required for the specific performance requirements for FIRE. Fabrication processes also need optimization to reduce cost because of the large number of components involved. Areas identified for R&D are:

1. Heat transfer enhancement techniques (swirl tubes, hypervaportrons,...)

## FIRE Engineering Report FY01 Update

2. Development of an effective, passive, heat transfer layer for the first wall (e.g. copper foam metals).
3. Optimization of joining methods (e.g. tungsten rods to copper) to improve reliability and reduce cost
4. Optimization of a Be plasma spray technique to coat the first wall

### R&D Tasks:

Review status of heat transfer enhancement techniques and passive heat transfer layers. Down select to one concept suitable for the FIRE requirement plus one back-up then carry out a testing program to validate the design features.

Develop an improved, cost effective joining method for tungsten rods to Cu backing plates. Investigate methods for Be plasma spray coatings for the first wall.

### **8.0-11 Vacuum Vessel**

Background: The double wall vacuum vessel (VV) includes a passive stabilization structure and internal, active control coils. Fabrication processes are complex and the vessel is assembled from octants. Field welds must be capable of remote maintenance.

R&D Tasks: Fabricate prototypes and mockups to develop fabrication and assembly processes (Wherever possible, mockups should be suitable for RM studies). Areas to be investigated are:

- Passive stabilizer bonding to the vv wall;
- Octant fabrication;
- Octant field joint remote welding and cutting demonstration;
- Port extension fabrication;
- Docking flange prototype and remote operation demonstrations;

- Gravity support link prototypes and testing.

### **8.0-12 Power Supplies**

Background: There are no feasibility issues with the power supplies for the TF or PF coils since existing technology can be used. There may, however, be opportunities for cost savings, particularly for the TF power supplies. The latter are very high power, low voltage, and have minimal control requirements compared to the PF coils.

Two areas may offer significant benefits:

1. Semiconductor device optimization for high current switching, including consideration of cryo cooled switches.
2. Methodology optimization for control on the AC side rather than on the DC side.

### R&D Task:

Perform computer simulations to investigate candidate switching and control configurations. Select and/or develop candidates and perform tests on subsections of the circuitry.